Bench-Scale Development of a Hot Carbonate Absorption Process with Crystallization-Enabled High-Pressure Stripping for Post-Combustion CO_2 Capture

Final Scientific/Technical Report

Project Period: January 1, 2011 to March 31, 2014

Report Authors: **Yongqi Lu* (PI)**

Nicholas DeVries*,†, David Ruhter*, Manoranjan Sahu*, Qing Ye*,†, Xinhuai Ye*, Shihan Zhang*

Scott Chen#, Zhiwei Li#, Kevin O'Brien#

***Illinois State Geological Survey, Prairie Research Institute, University of Illinois at Urbana-Champaign**

†Department of Agricultural & Biological Engineering, University of Illinois at Urbana-Champaign

#Carbon Capture Scientific, LLC, Pittsburgh, Pennsylvania

Date of Report: April 2014

DOE Award No.: DE-FE0004360

Submitted by: Illinois State Geological Survey
Prairie Research Institute
University of Illinois at Urbana-Champaign
615 E. Peabody Drive
Champaign, IL 61820

ACKNOWLEDGMENTS

This report is an account of research sponsored by the U.S. Department of Energy/National Energy Technology Laboratory (DOE/NETL) through Cooperative Agreement No. DE-FE0004360. The research is also supported as a cost share by the Illinois Department of Commerce and Economic Opportunity (IDCEO) through the Office of Coal Development (OCD) and the Illinois Clean Coal Institute (ICCI) under Contract No. 11/US-6. We are indebted to Mr. Andrew Jones, project manager at the DOE/NETL, for the time and effort he dedicated to all aspects of this project over the last three years. Dr. Joseph Hirschi at the ICCI contributed to project management in many valuable ways. The investigators thank Ms. Susan Krusemark at the Illinois State Geological Survey for her great assistance in editing and review of the report.

ABSTRACT

A novel Hot Carbonate Absorption Process with Crystallization-Enabled High-Pressure Stripping (Hot-CAP) has been developed by the University of Illinois at Urbana-Champaign and Carbon Capture Scientific, LLC in this three-year, bench-scale project. The Hot-CAP features a concentrated carbonate solution (e.g., K_2CO_3) for CO_2 absorption and a bicarbonate slurry (e.g., $KHCO_3$) for high-pressure CO_2 stripping to overcome the energy use and other disadvantages associated with the benchmark monoethanolamine (MEA) process. The project was aimed at performing laboratory- and bench-scale experiments to prove its technical feasibility and generate process engineering and scale-up data, and conducting a techno-economic analysis (TEA) to demonstrate its energy use and cost competitiveness over MEA.

To meet project goals and objectives, a combination of experimental, modeling, process simulation, and economic analysis studies were applied. Carefully designed and intensive experiments were conducted to measure thermodynamic and reaction engineering data relevant to four major unit operations in the Hot-CAP (i.e., CO_2 absorption, CO_2 stripping, bicarbonate crystallization, and sulfate reclamation). The rate promoters that could accelerate the CO_2 absorption rate into the potassium carbonate/bicarbonate (PCB) solution to a level greater than that into the 5 M MEA solution were identified, and the superior performance of CO_2 absorption into PCB was demonstrated in a bench-scale packed-bed column. Kinetic data on bicarbonate crystallization were developed and applied for crystallizer design and sizing. Parametric testing of high-pressure CO_2 stripping with concentrated bicarbonate-dominant slurries at high temperatures (≥140°C) in a bench-scale stripping column demonstrated lower heat use than with MEA. The feasibility of a modified process for combining SO_2 removal with CO_2 capture was preliminarily demonstrated.

In addition to the experimental studies, the technical challenges pertinent to fouling of slurry-handling equipment and the design of the crystallizer and stripper were addressed through consultation with vendors and engineering analyses. A process flow diagram of the Hot-CAP was then developed and a TEA was performed to compare the energy use and cost performance of a nominal 550-MWe subcritical pulverized coal (PC)-fired power plant without CO_2 capture (DOE/NETL Case 9) with the benchmark MEA-based post-combustion CO_2 capture (PCC; DOE/NETL Case 10) and the Hot-CAP-based PCC. The results revealed that the net power produced in the PC + Hot-CAP is 609 MWe, greater than the PC + MEA (550 MWe). The 20-year levelized cost of electricity (LCOE) for the PC + Hot-CAP, including CO_2 transportation and storage, is 120.3 mills/kWh, a 60% increase over the base PC plant without CO_2 capture. The LCOE increase for the Hot-CAP is 29% lower than that for MEA. TEA results demonstrated that the Hot-CAP is energy-efficient and cost-effective compared with the benchmark MEA process.

TABLE OF CONTENTS

LIST OF FIGURES

LIST OF TABLES

ACRONYMS AND ABBREVIATIONS

AMP	2-amino-2-methyl-1-propanol
AR	as-received
Ar	argon
BOP	balance of plant
BPTG	back pressure turbine generator;
CCS	carbon capture and storage
CCS LLC	Carbon Capture Scientific, LLC
CO_2	carbon dioxide
COE	cost of electricity
CT	cooling tower
CTB	carbonate-to-bicarbonate conversion
CW	cooling water
DEA	diethanolamine
DOE	U.S. Department of Energy
FGD	flue gas desulfurization
H_2O	water
HDA	hexamethylenediamine
Hg	mercury
HHV	higher heating value
Hot-CAP	hot carbonate absorption process with crystallization-enabled high-pressure stripping
HP	high pressure
Hr, hr, h	hour
HRSG	heat recovery steam generator
IEP	innovations for existing plants
ILP	intermediate low pressure
IP	intermediate pressure
K_2CO_3	potassium carbonate
KPa	kilopascal (for pressure)
kWe	kilowatt electric
kWh	kilowatt hour
lb	pound mass
LCOE	levelized cost of electricity
LP	low pressure
ME	major equipment
MEA	monoethanolamine
mm	millimeter
MM	million

MPa	megapascal (for pressure)
MSMPR	mixed suspension - mix product removal
MWe	megawatt electric
N_2	nitrogen
Na_2CO_3	sodium carbonate
NETL	National Energy Technology Laboratory
Nm^3	Normal cubic meter under standard conitions
NO	nitric oxide
NO_2	nitrogen dioxide
NO_x	oxides of nitrogen
O&M	operating and maintenance
O_2	oxygen
PC	pulverized coal
PCB	potassium carbonate and bicarbonate solution
PCC	post-combustion capture
ppmv	parts per million by volume
psia	pounds per square inch, absolute
psig	pounds per square inch, gauge
PZ	piperazine
Sat	saturated
SCB	sodium carbonate and bicarbonate solution
sccm	standard cubic center meter
SCR	selective catalytic reduction
SH	superheat
SO_2	sulfur dioxide
ST or ton	short ton
STG	steam turbine generator
STR	stirred tank reactor
TBD	to be determined
TDC	total direct cost
TEA	techno-economic analysis
TFC	total field cost
TG	turbine generator
tonne or t	metric ton
TPC	total plant cost
TS&M	transport, storage, and monitoring
UIUC	University of Illinois at Urbana-Champaign
vol%	percentage by volume

Executive Summary

The proposed Hot Carbonate Absorption Process with Crystallization-Enabled High-Pressure Stripping (Hot-CAP) is an absorption-based, post-combustion CO_2 capture (PCC) technology that uses a carbonate salt (e.g., potassium carbonate) as a solvent. The process integrates four major unit operations: CO_2 absorption at an elevated temperature, high-pressure CO_2 stripping, crystallization of a bicarbonate, and reclamation of a sulfate from SO_2 removal. The process is unique in using a concentrated carbonate solution for CO_2 absorption and a bicarbonate slurry for high-pressure CO_2 stripping to overcome the energy use and other disadvantages associated with the benchmark monoethanolamine (MEA) process.

Project objectives include performing a proof-of-concept study aimed at generating process engineering and scale-up data to help advance the Hot-CAP technology to the pilot-scale demonstration level. The project uses laboratory- and bench-scale test facilities to measure thermodynamic and reaction engineering data related to those four unit operations in the Hot-CAP. The results were used to analyze the technical feasibility and cost-effectiveness of the Hot-CAP for PCC.

To meet these project objectives, a combination of experimental, modeling, process simulation, and technical and economic analysis studies were applied. A team of engineers and scientists from the University of Illinois at Urbana-Champaign (UIUC) and Carbon Capture Scientific, LLC (CCS LLC) conducted the project. UIUC oversaw the project as the primary contractor and was responsible for laboratory- and bench-scale experiments to generate engineering and process data. CCS LLC applied the experimental results and conducted a techno-economic analysis (TEA) for the Hot-CAP integrated with a full-scale pulverized coal (PC)-fired power plant for PCC.

The major work activities and the results of these studies are summarized below.

1. Identification of promoters/catalysts for CO_2 absorption into PCB

Three Lewis base inorganic catalysts, five amines, and five amino acid salts were evaluated as promoters to accelerate the CO_2 absorption rate into a concentrated 40 wt% potassium carbonate/bicarbonate (PCB) solution at 60 to 80°C. A batch stirred tank reactor (STR), made of a Plexiglas vessel 7 in. (17.8 cm) in height and 4 in. (10.2 cm) in internal diameter (I.D.), was used in this study.

The addition of 4 wt% CAT1 or CAT2 Lewis base catalyst into a 40 wt% PCB with 20% carbonate-to-carbonate (CTB) conversion (PCB40-20, and so forth thereafter) approximately doubled the rates at 60, 70, and 80°C. However, the rates into PCB40-20 in the presence of 4 to 6 wt% of these inorganic catalysts in the STR were still several times (2.5 to 4.8 times) slower than those into a 3 M MEA solution at 50°C.

The five amine promoters increased the absorption rate into the PCB solution by 3.5 to 50 times at 70°C. Rates promoted with piperazine (PZ) and aminomethyl propanol (AMP) were the highest, followed by hexamethylenediamine (HDA). The rates into the lean PCB40-20 promoted

with 1 M PZ, AMP, or HDA at 70°C were greater than, or comparable to, a lean 5 M MEA solution loaded with 0.2 mol of CO_2/mol of MEA at 50°C.

All the amino acid salt solutions at a concentration of 3 M exhibited rates at 70°C higher than, or comparable to, the 5 M MEA at 50°C. The three highest performing amino acid salts were further evaluated as promoters; the rates into both PCB40-20 and PCB40-40 promoted by K-sacrosine and K-glycine were more substantial than those promoted by K-proline. Compared with the lean 5 M MEA, the promoted rates into the PCB40-20 were significantly lower. However, the rate difference between the promoted lean and rich PCB was much less substantial than that for MEA.

2. Testing of CO_2 absorption in a packed-bed column

A 3-m-high, 10-cm-diameter bench-scale packed-bed column was fabricated to test the kinetic performance of CO_2 absorption into the 40 wt% PCB solution without or with a promoter. Results confirmed that in the column, the CO_2 removal rate into PCB increased as the liquid-to-gas (L/G) ratio increased, as the promoter dosage increased, as the CO_2 loading decreased, or as the inlet CO_2 concentration decreased. Potassium bicarbonate ($KHCO_3$) precipitation occurred when the CTB conversion in the feed PCB solution reached 40 to 45%. However, the accumulation of precipitates in the solution did not result in a pronounced decrease in CO_2 removal efficiency.

Results revealed that the use of PZ, AMP, or diethanolamine (DEA) as a promoter greatly increased the rate of CO_2 removal into the PCB solution. Among the promoters tested, the addition of PZ was the most effective in accelerating the rate. The 40 wt% PCB solution promoted with 0.5 M PZ at 70°C performed one-to-three times better than 5 M MEA at 50°C at the representative lean loading levels, and performed three-to-five times better at the rich CO_2 loading levels when all other conditions were the same.

If desired, a sodium carbonate/bicarbonate (SCB) or a PCB/SCB mixture solution can potentially be used as an alternative to a PCB solution as the solvent. Sodium bicarbonate ($NaHCO_3$) may be crystallized more easily than $KHCO_3$ from the CO_2-rich solution via cooling crystallization to form a $NaHCO_3$-based slurry that can be used for CO_2 stripping at a higher pressure than the $KHCO_3$ slurry. A 15 wt% SCB solution (limited to its solubility) promoted with 0.5 M PZ exhibited a higher CO_2 removal efficiency at 70°C than did 5 M MEA solution at 50°C within the corresponding CO_2 loading range. Promoted mixtures with similar total PCB/SCB concentrations revealed comparable CO_2 removal efficiencies, whereas at the same total concentration, the solution with a higher PCB concentration showed slightly higher CO_2 removal efficiency. A mixture of 25 wt% PCB and 10 wt% SCB promoted with 0.5 M PZ had a CO_2 removal efficiency at 70°C comparable with that of the promoted 40 wt% PCB and a removal efficiency significantly higher than that of 5 M MEA at 50°C.

3. Kinetic study of bicarbonate crystallization

A kinetic study of the crystallization of $KHCO_3$ from the CO_2-rich PCB solution was performed using a continuous STR system under the mixed-suspension–mixed-product-removal (MSMPR)

mode. The reactor is a 1-L round-bottomed glass vessel double-jacketed for precise temperature control and equipped with an in-situ turbidity sensor. Parametric experiments were conducted to investigate the crystal size distribution and the crystal growth and nucleation rates of $KHCO_3$ crystallization under simulated process conditions.

The MSMPR tests revealed that the rate of $KHCO_3$ crystal growth was size-dependent, increasing with increasing particle size and then leveling off when a certain critical size was reached (~600 μm). The crystallization of $KHCO_3$ was kinetically fast and could be completed within a residence time of as little as 15 min. A longer residence time decreased the overall rates of both nucleation and crystal growth, but resulted in larger crystal particles. An increase in agitation speed enhanced the nucleation process, but slowed crystal growth, which resulted in an overall reduction in crystal size. A higher level of supersaturation favored crystal growth and the formation of larger particles. The presence of PZ in the PCB solution accelerated crystallization.

A three-parameter, size-dependent crystal growth model was developed to describe the rates of $KHCO_3$ crystal growth and nucleation and to predict the mean crystal size in the PCB system. The model was applied to perform a crystallizer sizing analysis based on a configuration of five crystallization units operating in sequence for the Hot-CAP equipped in a 609-MWe (net) power plant. A total crystallizer volume of approximately 3,200 m^3 (equivalent to a total residence time of 11 min) was found to be sufficient.

When a PCB/SCB mixture is used as a solvent, $NaHCO_3$ is preferentially crystallized out and used for CO_2 stripping. The feasibility of two process concepts for $NaHCO_3$ crystallization was investigated. The first process involves mixing the PCB-dominant mixture exiting the absorber with the SCB solution regenerated from the stripper to crystalize $NaHCO_3$ via cooling. X-ray diffraction (XRD) analyses indicated that the composition of crystal particles depended on the composition of the PCB/SCB solution: the higher the total SCB concentration in the feed PCB/SCB mixture, the higher the content of nahcolite ($NaHCO_3$) in the crystal solids. The mass mean size of $NaHCO_3$ crystal particles (80 to 130 μm) was several times smaller than that of $KHCO_3$ particles (~400 μm). The second process involves the reactive crystallization of $NaHCO_3$ in the regenerated SCB solution with the addition of $KHCO_3$ solids (which can be formed from the cooling crystallization of the PCB-dominant mixture solution exiting the absorber). XRD analyses revealed that the crystal samples contained three crystallite phases: nahcolite, kalicinite, and trona. In all the crystal products, nahcolite was dominant (>81 wt%) and kalicinite was insignificant (<5 wt%), indicating that it is feasible to crystalize $NaHCO_3$ through the reaction between solid $KHCO_3$ and aqueous Na_2CO_3 under the test conditions.

In addition, solubility data for the PCB, SCB, and PCB/SCB mixture solutions at various concentrations, CO_2 loading levels in solution, and temperatures were measured using a turbidity-based approach. Such data are either unavailable or incomplete in the literature, but are required for identifying the design and operating conditions desired for the crystallization process. Empirical models were developed based on the measured results to predict solubility limits for these systems.

4. Measurement of phase equilibrium behavior of PCB systems at high temperatures

The vapor–liquid equilibrium (VLE) data were measured for the 40, 50, and 60 wt% PCB solutions with CTB conversion levels ranging from approximately 20 to 85% at 140 to 200°C. These data cover a full range of operating conditions for CO_2 stripping in the Hot-CAP.

The VLE data demonstrated that the partial pressure of CO_2 increased substantially with increasing temperature and CTB conversion in the PCB solution; whereas the partial pressure of water vapor increased moderately with increasing temperature, but decreased slightly with increasing CTB conversion. The concentration of the PCB solution (40 to 60 wt%) did not substantially affect the partial pressure of CO_2, but remarkably reduced the partial pressure of water vapor. A higher operating temperature, high PCB concentration, and higher CTB conversion level in solution were thus favored to obtain a higher total pressure and lower H_2O/CO_2 partial pressure ratio. For example, over the 60 wt% PCB with 83% CTB conversion at 200°C, the total pressure reached 507 psia (34.5 atm) and the ratio of H_2O/CO_2 partial pressure was 0.11:1. A high stripping pressure and a lower H_2O/CO_2 pressure ratio can result in a significant reduction in energy use, and the results demonstrated the energy use advantage of the Hot-CAP when using a concentrated bicarbonate-dominant slurry for CO_2 stripping.

5. Testing of CO_2 stripping in a bench-scale stripping column

A bench-scale, packed-bed stripping column system with an I.D. of 1 in. (2.54 cm) and a height of 7 ft (2.1 m) rated at 200°C and 500 psia (34.0 atm) was fabricated in this study. Parametric tests revealed that a higher stripping temperature favored a deeper level of $KHCO_3$ regeneration from the PCB solution/slurry. The change in CTB conversion through the 7-ft (2.1-m) column varied from 1 to 20 percentage points. As the stripping temperature was increased from 120 to 160°C, both the partial pressure of CO_2 in the product gas stream and the total stripping pressure increased, whereas the CO_2/H_2O pressure ratio in the product gas decreased only slightly. A high CTB conversion in the feed or a high concentration of PCB, which is unique to the Hot-CAP, increased both the total stripping pressure and the CO_2/H_2O pressure ratio in the product gas. For example, the stripping pressure attained with a PCB60-40 feed solution, which is not even high in CO_2 loading, was 180 psia (12.2 atm) at 200°C.

The heat duty required for CO_2 stripping under different conditions was determined based on heat usage for CO_2 desorption, water vaporization, and heating of the PCB solution. Increasing either the PCB concentration or CTB conversion in the PCB feed solution could significantly decrease the heat use for CO_2 stripping. Increasing the temperature was found to be beneficial for reducing the total stripping heat per unit of CO_2 stripped from the PCB system because more CO_2 was generated. For comparison purposes, a rich 5 M MEA feed solution (loaded with 0.475 mol of CO_2/mol of MEA) was tested in the same column, and the total heat use for CO_2 stripping varied from 4,300 to 6,200 kJ/kg of CO_2 when the obtained lean CO_2 loading varied from 0.37 to 0.2 mol of CO_2/mol of MEA. Compared with the 5 M MEA solution, the heat duty for CO_2 stripping from the 30 to 50 wt% PCB feed solutions with 80% CTB conversion was two-to-three times lower. Note that a leaner regenerated MEA solution was obtained compared with the PCB solution in those tests.

Experiments also demonstrated that the presence of K_2SO_4 (1 wt%) and PZ (0.2 M) in the PCB solution did not noticeably affect CO_2 stripping performance. In comparison, a deeper level of $KHCO_3$ regeneration and a higher pressure were achieved in the presence of 0.5 M methyldiethanolamine (MDEA). Accordingly, it was observed that the addition of MDEA in the PCB solution decreased the heat use for CO_2 stripping. For example, the heat use was reduced by 69% for the PCB30-60 feed solution when 0.5 M MDEA was present. MDEA is regarded as a favorable additive for CO_2 stripping from the hot PCB solution.

6. Feasibility study of sulfate reclamation for combining SO_2 removal with CO_2 capture

A process concept involving two reaction steps was initially proposed to reclaim the desulfurization product, K_2SO_4, from the PCB solution. The first step is to reduce the CO_3^{2-} concentration by using a high-pressure CO_2 gas stream, and the second is to selectively precipitate $CaSO_4$ over $CaCO_3$ by using lime.

Batch and semi-continuous tests were performed to study the feasibility of K_2SO_4 reclamation. When the PCB concentration was above 0.2 M (2.7 wt%) or the reaction temperature was greater than 50°C, no $CaSO_4$, but rather $CaCO_3$ crystallite phases were formed. Improving the gas–liquid interface and mixing via CO_2 gas bubbling increased the $CaSO_4$ content from 1.5% gypsum + 42.3% syngenite to 8.6% gypsum + 91.4% syngenite in the precipitate particles obtained from the reaction of 0.2 M Ca^{2+} in 0.2 M PCB + 0.4 M K_2SO_4 solution for 1 hr at room temperature.

A reaction mechanism was suggested to explain the competitive precipitation of $CaSO_4$ over $CaCO_3$. $CaCO_3$ was first precipitated by the reaction between CO_3^{2-} and the added Ca^{2+}. The produced $CaCO_3$ precipitates then reacted with high-pressure CO_2 to form $Ca(HCO_3)_2$. $Ca(HCO_3)_2$ has higher solubility and is dissociated into Ca^{2+} and HCO_3^-. Ca^{2+} ions further react with SO_4^{2-} to precipitate out $CaSO_4$. The composition of precipitates was controlled by the kinetics of $CaCO_3$ conversion to $Ca(HCO_3)_2$ and $Ca(HCO_3)_2$ dissociation.

The precipitate particles obtained from the reaction of 0.4 M Ca^{2+} in either a 0.2 M $NaHCO_3$ + 0.4 M Na_2SO_4, or a 0.1 M $KHCO_3$ + 0.1 M $NaHCO_3$ + 0.2 M Na_2SO_4 + 0.2 M K_2SO_4 solution contained almost 100% gypsum phase, whereas those in a 0.2 M $KHCO_3$ + 0.4 M K_2SO_4 solution contained 8.6% gypsum and 91.4% syngenite under comparable operating conditions. This result suggests that the presence of sodium instead of potassium ions favored the competitive precipitation of $CaSO_4$ over $CaCO_3$ by prohibiting the formation of syngenite.

To overcome the limitations associated with low-concentration PCB and low operating temperature and thus improve the compatibility of SO_2 removal with CO_2 capture, a modified process was proposed. The new process consists of SO_2 scrubbing using the CO_2-rich PCB solution from the Hot-CAP absorber, the oxidation of K_2SO_3 into K_2SO_4 in a forced-air unit, and the precipitation and separation of K_2SO_4 (because of its low solubility compared with other potassium salts) from the solution.

Precipitate solids containing 100% K_2SO_4 were obtained from the oxidation of 10 wt% K_2SO_3 in PCB20-40 at 70°C, which was desirable for the modified process. Precipitate solids obtained

from PCB40-40 contained approximately 70 wt% K_2SO_4 and 30 wt% $KHCO_3$, indicating that solvent loss might occur when the CO_2 loading in the 40 wt% PCB for SO_2 removal is too high. The rates of sulfite oxidation ranged from 10^{-6} to 10^{-5} mol/m^2·s under the investigated conditions (1 to 10 wt% sulfite concentrations, 50 to 70°C, and 3 to 13 psia (20.7 to 89.6 kPa) of O_2 pressure). The rate depended considerably on the temperature and oxygen pressure, but did not vary appreciably with the sulfite concentration. The oxidation of sulfite was almost zero-order with the sulfite concentration and first-order with the oxygen pressure. These preliminary results of equilibrium composition and rate of K_2SO_3 oxidation indicated the feasibility of the modified process.

7. Techno-economic analysis of the Hot-CAP

In addition to the experimental studies, a technology-focused risk mitigation analysis was conducted to address the related technical questions. Discussions with vendors indicated that fouling of the cross-flow heat exchangers and of the cooler inside the crystallizer, owing to possible $KHCO_3$ scaling on equipment surfaces, can be solved by a variety of available engineering solutions, such as pre-seeding and reducing the temperature difference between the inlet and outlet streams. The conventional crystallizer design requires a large temperature difference between the inlet solution (solution entering the crystallizer) and the mother liquor (solution leaving the crystallizer), jeopardizing the heat recovery from the incoming solution from the absorber. Thus, a configuration of five consecutive continuous STR-type crystallization tanks is used instead of a single crystallizer. This new configuration reduces the temperature difference between the inlet and outlet streams in each crystallizer to approximately 5°C, thereby facilitating the heat recovery desired in the Hot-CAP. Another challenge of the Hot-CAP is the need to modify the conventional stripper to handle slurry and operate at high pressure. To attain a high stripping pressure, a combination of a high-concentration slurry and high CO_2 loading in the regenerated lean solution is required. However, a high lean CO_2 loading will cause the risk of recrystallization in the cooling process downstream of the stripper. Thus, a reasonably high stripping pressure (e.g., 6 bar/5.92 atm) is selected as a trade-off between the high-pressure requirement and the stripper design concern.

A TEA was performed to compare the energy use and cost performance of a nominal 550-MWe subcritical PC power plant without CO_2 capture (DOE/NETL Case 9) with the benchmark MEA-based PCC (DOE/NETL Case 10) and the Hot-CAP-based PCC. The results showed that the net power produced in the PC power plant equipped with the baseline Hot-CAP is 609 MWe, greater than that with MEA (550 MWe) owing to the reduced steam demand for CO_2 stripping.

The baseline Hot-CAP has a slightly lower capital cost ($48 million) for CO_2 compression compared with the MEA-based PCC ($50 million), because the stripped product gas is at a higher pressure (6 bar/5.92 atm vs. 1.6 bar/1.58 atm). The baseline Hot-CAP also has a lower capital cost in the CO_2 capture section ($362 million) compared with the MEA-based PCC ($443 million), because it requires a smaller stripping column and does not use an upstream polishing unit for deep sulfur removal prior to CO_2 capture. Operating & maintenance (O&M) costs for the PC plant equipped with Hot-CAP are estimated to be $175 million annually, less than that for the PC plant with MEA ($178 million).

The 20-year levelized COE (LCOE) for the PC plant with the baseline Hot-CAP, including CO_2 transportation and storage, is 120.3 mills/kWh, a 60% increase over the base PC plant without CO_2 capture. The LCOE increase caused by the Hot-CAP is 29% lower than that of the benchmark MEA-based process.

Results of the sensitivity analysis indicate that the PC plant LCOE is quite sensitive to the capital cost of the absorber, the use of a new polishing scrubber for deep desulfurization, and the power consumption for crystallization. However, the LCOE is not markedly affected by the price of the PCB solvent, the crystallization equipment cost, or the stripping pressure increase.

8. Major conclusions

The major conclusions of the project are as follows: (1) major reactions and individual unit options involved in the Hot-CAP are thermodynamically- and kinetically-feasible, and (2) the Hot-CAP is energy-efficient (26% lower in parasitic power loss) and cost-effective (29% lower in COE increase) compared with MEA.

For future work, a scale-up study of an integrated Hot-CAP system using a slipstream of actual flue gas is recommended to investigate operating issues, such as slurry handling and integration of individual unit operations.

Chapter 1. Introduction

1.1 Background

Post-combustion CO_2 capture (PCC) from coal power plant flue gas is the most expensive step in an integrated carbon capture and storage (CCS) process. According to a recent DOE/NETL Baseline Study, the total cost of electricity (COE) for a pulverized coal (PC)-fired power plant equipped with a benchmark monoethanolamine (MEA) process is as high as 110 mills/kWh, equivalent to a CO_2 capture cost of $57/tonne.[1]

A breakdown of the incremental COE increase attributable to MEA-based CO_2 capture is displayed in Figure 1-1. The largest contributor to the cost is the energy use (61% of the total COE increase), comprising steam extraction, compression work, and auxiliary power uses. The capital cost of the CO_2 capture system is the second largest, responsible for 23% of the total COE increase. Clearly, reducing energy consumption of the MEA process is the key to lowering the total CO_2 capture cost.

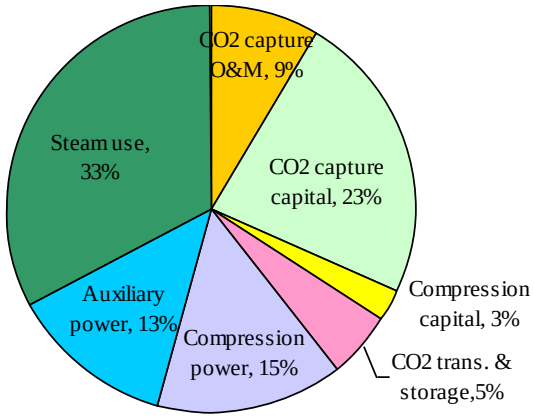

Figure 1-1. Breakdown of the COE increase for the benchmark MEA process.

Among the energy required for CO_2 capture, compression work is the energy required to compress CO_2 from the operating pressure in the stripper (1.5 to 2 atm in the benchmark MEA process) to the sequestration-ready pressure (2,250 psia/153.1 atm). Auxiliary power uses include electricity consumption by pumps and fans. In the stripper, steam is required to supply the heat demand by three components of heat, as shown in Figure 1-2:

$$Q_{Total} = Q_{Sensible} + Q_{Reaction} + Q_{Stripping}, \quad (1\text{-}1)$$

where $Q_{Reaction}$ is the heat of reaction, which is required to desorb the CO_2 from the CO_2-rich solvent; $Q_{Sensible}$ is the sensible heat, required to heat the CO_2-rich solution entering the stripper to the temperature of the CO_2-lean solution leaving the reboiler; and $Q_{Stripping}$ is the stripping heat, consumed to generate the amount of water vapor leaving the top of the stripper (per unit mass or mole of CO_2). For the benchmark MEA process, $Q_{Reaction}$, $Q_{Sensible}$, and $Q_{Stripping}$ are approximately 825, 450, and 275 Btu/lb /1,917, 1,046, 639 kJ/kg of CO_2 (1,550 Btu/lb/3,602 kJ/kg) of CO_2 in total), respectively.[1]

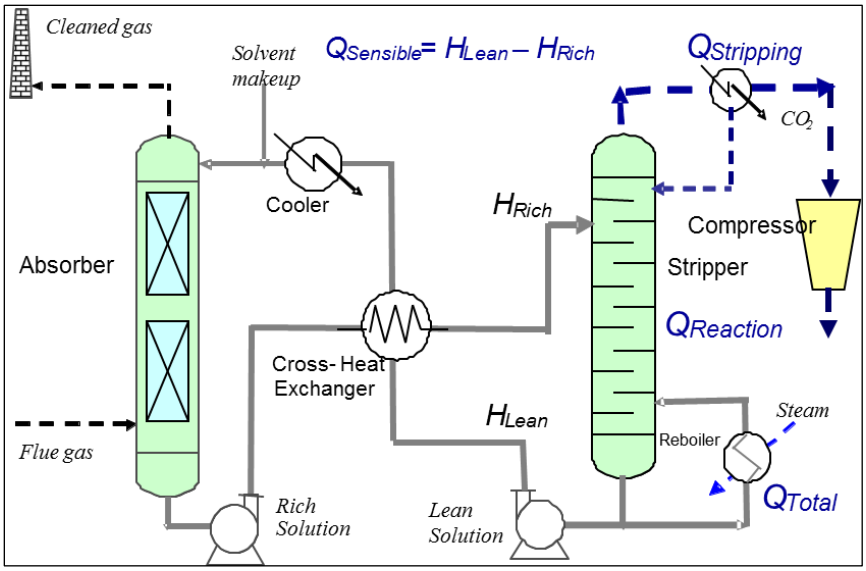

Figure 1-2. Schematic diagram showing the three components of heat required in a CO_2 stripping column.

The steam required for CO_2 stripping is extracted from the steam turbine system of the power plant. Steam extraction affects the availability of steam remaining in the turbine system and thus reduces the plant's electricity output. The resultant electricity loss depends not only on the amount, but also on the quality of steam extracted. The stripper in the MEA process typically withdraws steam at approximately 60 psia (4.1 atm) and 295°F/146°C (after power recovery of the steam), resulting in a parasitic power loss of 0.20 kWh/kg of CO_2 captured.[2] The total parasitic power loss of the benchmark MEA process amounts to 0.32 kWh/kg of CO_2 captured (i.e., 0.20 attributed to steam extraction, 0.09 to CO_2 compression, and 0.03 to auxiliary power use), which is almost 30% of the total electric output of the power plant without CO_2 capture. Steam extraction to the stripper is the main cause of the total parasitic power loss.

The large energy requirement in the MEA process results mainly from the following four factors. First, the $Q_{Reaction}$ is high. Second, a high solvent recirculation rate increases the sensible heat ($Q_{Sensible}$) and electricity consumption by the circulation pump. Third, the operation of the stripper at near atmospheric pressure results in higher CO_2 compression work. Fourth, the low operating pressure of the stripper results in a high $Q_{Stripping}$ value per unit of CO_2 regeneration, because the water vapor pressure in the gas stream leaving the stripper accounts for a significant portion of the total pressure at the top of the stripper.

In this regard, new absorption technologies focusing on developing new solvents and processes are emerging to reduce the solvent regeneration energy and capital cost, and/or to mitigate solvent degradation and emissions associated with amine-based processes. Carbonate salt (potassium or sodium carbonate)-based absorption technologies are of increasing interest at present since carbonates have a number of advantages over amine-based solvents, such as a low solvent cost, low volatility, less corrosion, lack of degradation, and allowance for desorption at high temperatures. A research group at the University of Texas–Austin has tested CO_2 capture in a pilot plant using an amine-promoted K_2CO_3 solvent; however, the results did not show a significant improvement in energy performance compared with MEA-based processes.[3] The use

of carbonates for PCC is currently being studied by the Cooperative Research Centre for Greenhouse Gas Technologies (CO_2CRC) in Australia.[4] The group is testing the CO_2 capture performance of an un-promoted 30 wt% K_2CO_3 solution as a baseline in their pilot unit (25 tonne of CO_2/day-equivalent of gas flow) at the Hazelwood Power Station. The baseline solvent was reported to absorb only 20 to 25% of CO_2 in the flue gas. Shell reported a slipstream test (25 kg of CO_2/day) on a precipitating carbonate technology and concluded that energy consumption was at the lower end of the 2,500 to 4,000 kJ/kg of CO_2 range.[5] Akermin Inc. has completed a bench-scale test of a capture process using an enzyme-catalyzed K_2CO_3 solvent on actual coal-derived flue gas, and demonstrated about 80% CO_2 capture, a 16% reduction in equivalent work, a low accumulation of heat-stable salts, low solvent aerosol emissions, and negligible corrosion on stainless steel.[6]

Different from the carbonate-based absorption processes, the Hot-CAP presents a unique technical option to overcome the energy use and other disadvantages associated with the benchmark MEA process. This process is described in the next section.

1.2 Description of the Hot-CAP technology

Figure 1-3 is a schematic diagram of the Hot-CAP. In this process, the warm flue gas (~60°C) from a flue gas desulfurization (FGD) unit, or the hot flue gas (~150°C) exiting from an electrostatic precipitator (ESP) or baghouse of the power plant, is introduced into an absorption column operating at an elevated temperature (60 to 80°C) and atmospheric pressure where CO_2 is absorbed into a concentrated potassium carbonate/bicarbonate (K_2CO_3/$KHCO_3$, or PCB) solution, e.g., 40 wt% PCB. The CO_2-rich PCB solution exiting the absorption column is cooled in a heat exchanger by the CO_2-lean PCB solution circulating to the column before entering a crystallization reactor. In the crystallizer, $KHCO_3$ crystals precipitate out from the rich PCB solution owing to its low solubility at low temperatures (30 to 35°C). Solid crystals are filtered, which produces a bicarbonate slurry that is fed to the stripper after it is preheated by the hot regenerated lean solution coming from the stripper. The slurry has a much higher CO_2 loading than a traditional CO_2-rich PCB solution, thus enabling high-pressure CO_2 stripping (≥6 atm) at temperatures ranging from 140 to 200°C. The CO_2 gas stream exiting the top of the stripper is further cooled, dehydrated, and compressed to a sequestration-ready pressure. The CO_2-lean solution exiting the stripper enters the crystallizer after exchanging heat with the feed slurry.

In addition, SO_2 removal from the flue gas may potentially be combined with CO_2 capture in the Hot-CAP. During CO_2 absorption, SO_2 as a more acidic gas will react more favorably with PCB to form potassium sulfate (K_2SO_4). A small slipstream of the rich PCB solution can be extracted from the system and fed to a sulfate reclamation unit, where lime or hydrated lime is added to convert SO_4^{2-} in the solution to $CaSO_4$. The pH of the solution in the reclaimer can be controlled using a small amount of high-pressure CO_2 gas. A filtration unit then separates the $CaSO_4$ (gypsum) solids from the liquid. The reclaimed solution will finally return to the Hot-CAP (not shown in Figure 1-3).

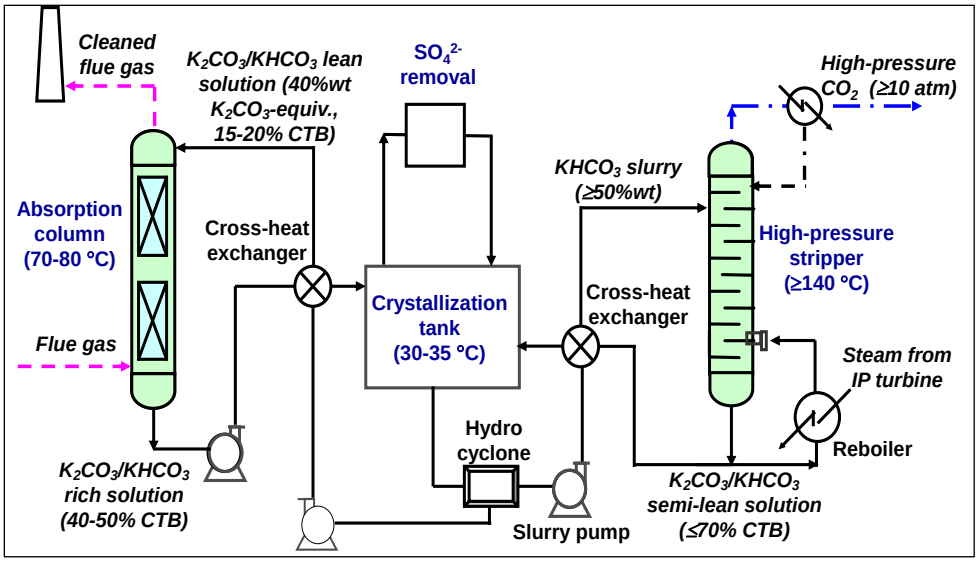

Figure 1-3. Schematic diagram of the Hot-CAP.

The chemistry involved in the Hot-CAP, namely CO_2 absorption, crystallization of bicarbonate, and CO_2 stripping, is shown in Figure 1-4. During the absorption process, CO_2 is mainly absorbed by carbonate to form bicarbonate. In the cooling crystallization process, the absorbed CO_2 in the rich PCB solution from the absorber is concentrated in the form of bicarbonate crystal particles. In the stripping process, the bicarbonate decomposes to release CO_2 and regenerate carbonate subjected to the heat supplied.

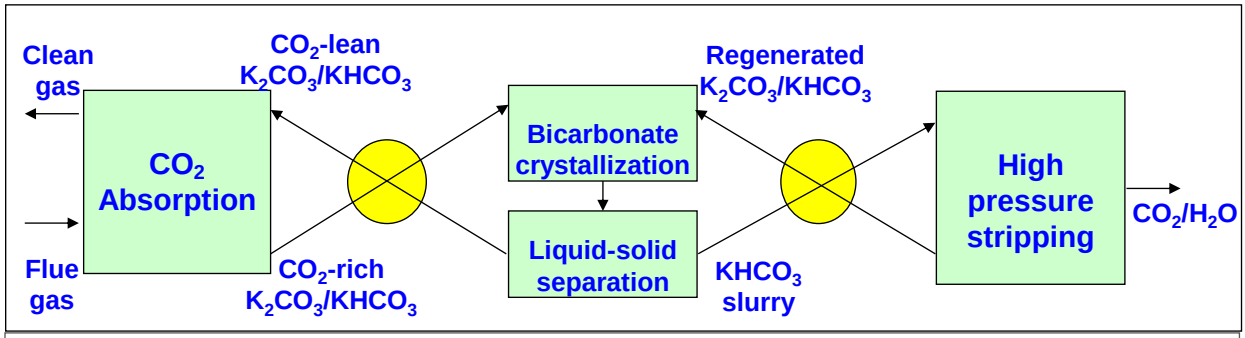

CO_2 absorption at 60 to 80 °C:

$$CO_2 + H_2O + K_2CO_3 = 2KHCO_3$$

Crystallization at 35 °C:

$$KHCO_3 = KHCO_3(s)\downarrow$$

CO_2 desorption at ≥140 °C:

$$KHCO_3 = CO_2(g)\uparrow + H_2O + K_2CO_3$$

Figure 1-4. Conceptual schematic for the chemical reactions involved in CO_2 absorption into PCB, the crystallization of bicarbonate, and CO_2 stripping in the Hot-CAP.

The Hot-CAP reduces all three heat components ($Q_{reaction}$, $Q_{sensible}$, and $Q_{stripping}$) in the stripper and the required work of CO_2 compression. The PCB solution has a lower heat of reaction (7 kcal/mol of CO_2) than MEA. With the inclusion of the heat of crystallization, depending on the

desired concentration of bicarbonate slurry, the overall heat of reaction, $Q_{reaction}$ (absorption + crystallization), ranges between 7 and 17 kcal/mol of CO_2. In comparison, the heat of absorption in the MEA solution amounts to 21 kcal/mol of CO_2.

Since a bicarbonate slurry is used for CO_2 stripping, the CO_2 working capacity of the solvent can be significantly increased. For example, for a 50 wt% bicarbonate slurry, its working capacity throughout the stripper is 1.5-to-3 times higher than the benchmark MEA process. Furthermore, the working capacity of the bicarbonate slurry can be optimized according to the process requirement, because the bicarbonate concentration can be adjusted as needed. A higher working capacity of the bicarbonate slurry, together with its lower specific heat capacity than MEA, reduces the energy required to heat the slurry, i.e., the sensible heat, $Q_{sensible}$.

The stripping process with a bicarbonate slurry in the Hot-CAP can be operated at a higher pressure (6 to 40 bar/5.92 to 39.48 atm). An increase in stripping pressure, mostly contributed by the CO_2 partial pressure, lowers not only the stripping heat, $Q_{stripping}$ [see Equation (1-1)], but also the CO_2 compression work. In theory, if the stripping pressure is high enough, the compression work may be eliminated.

It should be noted that because the bicarbonate slurry comes from the crystallizer, the stripping process is decoupled with, and thus independent of, the absorption process. Additionally, compared with MEA, a PCB solvent does not degrade at high regeneration temperatures, has little corrosion tendency, is not expensive, and has potential to combine SO_2 removal with CO_2 capture to eliminate or downsize an FGD and/or a SO_2 polisher unit. Therefore, the Hot-CAP has potential to remedy the major shortcomings of the benchmark MEA process.

1.3 Technical challenges to be addressed

As summarized in Table 1-1, five major technical risks have been identified for the Hot-CAP. The first risk relates to the slow rate of CO_2 absorption into the PCB solution. Although the rate into PCB at an elevated temperature (60 to 80°C) and PCB concentration (~40 wt%) used by the Hot-CAP is estimated to be improved compared with those by other carbonate-based processes, it could still be slower than those of aqueous amines. If this is the case, research would be aimed at identifying a rate catalyst or promoter, or developing a different absorber design to increase the absorption rate to a level comparable with that into MEA. Note that because absorption and stripping in the Hot-CAP are decoupled, the risk associated with the absorption process, if any, does not directly affect the design and operation of the stripper.

The second risk relates to whether a desired stripping pressure, which will directly affect the overall energy performance of the Hot-CAP, can be obtained. Stripping pressures up to 40 bar (39.48 atm) are predicted for the Hot-CAP. However, the predictions had been based on an extrapolation from literature data. If an achievable maximum pressure is much lower than 10 bar (9.87 atm), a sodium bicarbonate ($NaHCO_3$) slurry would be considered to replace the use of $KHCO_3$ for CO_2 stripping and, accordingly, a sodium carbonate/bicarbonate (SCB) or a PCB/SCB mixture solution would be used for CO_2 absorption. The equilibrium pressure of CO_2 over the SCB system is several-fold higher than that of the PCB system.

The third risk is associated with potential fouling in the heat exchangers. Two cross-heat exchangers, one between the absorber and crystallizer and the other between the stripper and crystallizer, involve slurry streams (Figure 1-3). Fouling on heat exchanger surfaces will reduce heat transfer efficiency and create problems for continuous operation. Therefore, a literature search and data analysis, along with consultation from equipment venders, will be followed to assess the available means to prevent fouling through the optimal design of heat exchangers and selection of desirable operating conditions.

The fourth risk is associated with the design of the crystallizer. Two relevant issues need to be addressed. One is the requirement for fast rates of crystallization and cooling in the crystallizer. The desired process design and operating conditions are required to be determined experimentally. If the rates are not favorable, technical approaches, such as the addition of seeds and the improvement of heat transfer, would be assessed. The other issue is the requirement for heat recovery from the inflow solution to the mother solution. Equipment vendors will be consulted and the crystallization process will be reviewed and configured to address this issue.

The fifth risk relates to the design of the stripping column and its accessories. The stripper is required to operate at high pressure while processing a bicarbonate slurry. The risk will be mitigated by conducting a literature search, consulting with equipment vendors and design companies, and comparing and assessing different column configurations.

Table 1-1. Major technical risks of Hot-CAP and strategies to be considered for risk mitigation

Risk	Mitigation option	Location in the process
1. Rate of CO_2 absorption at a temperature (60 to 80°C) and concentration of PCB solution (40 wt%) insufficient to achieve process economics	Develop absorption promoters or catalysts, reconfigure absorption column design, or both	Absorber
2. Stripping pressure of potassium bicarbonate slurry is <10 atm, thereby unfavorably affecting process economics	Develop a sodium bicarbonate-based slurry to obtain stripping pressures ≥10 atm.	Stripper
3. Heat exchanger fouled by slurry streams	Literature search, vender consultation, and engineering analysis to identify means to prevent fouling	Heat exchanger
4. Crystallizer must be quickly cooled to achieve process economics	Literature search, vender consultation, and engineering analysis to identify means to achieve fast cooling in large systems	Crystallizer
5. Commercially-available strippers require modifications to handle slurry and operate at high pressure	Literature search, vender consultation, and engineering analysis to determine means to modify standard stripper design	Stripper

1.4 Primary goals and technical objectives

The primary goals of the project are to perform a proof-of-concept study that will generate process engineering and scale-up data to optimize the Hot-CAP technology and demonstrate its capability to achieve the DOE goals of at least 90% CO_2 removal from coal-fired power plant flue gas with less than a 35% increase in the COE, and that will help advance the process to a pilot-scale level within three years.

The technical objectives include: (1) performing laboratory- and bench-scale experiments to obtain kinetics and phase equilibrium data associated with the major reactions and unit operations in the Hot-CAP, including CO_2 absorption, bicarbonate salt crystallization, CO_2 stripping, and sulfate reclamation; (2) applying the results from the experimental studies to help create a process flow diagram, perform equipment sizing and process simulations, and conduct a TEA for a conceptual 550 MWe high-sulfur PC-fired power plant retrofitted with the Hot-CAP; and (3) using the results from the experimental and process simulation studies to identify optimal Hot-CAP process conditions to meet or exceed the DOE technical and cost goals.

1.5 Technical approach

To meet the project goals and objectives, a combination of experimental, modeling, process simulation, and technical and economic analysis studies will be applied. The project will first investigate the kinetic and thermodynamic data relevant to the four-unit operation of the Hot-CAP (CO_2 absorption, bicarbonate crystallization, CO_2 stripping, and sulfate recovery) using laboratory and bench-scale test facilities. The absorption tests will be conducted using both a stirred tank reactor (STR) for the kinetics measurement and a bench-scale absorption column for the overall performance evaluation. An autoclave reactor and a continuous high-pressure distillation column will be used to measure the equilibrium behavior and stripping kinetics of the bicarbonate slurry system at elevated temperatures and pressures. A modeling study will further evaluate the overall performance of the stripping unit. The bicarbonate crystallization kinetics will be evaluated at various process conditions (e.g., temperature, concentration, loading of CO_2 in the feed solution, and presence of impurities) using a STR with in-situ turbidity measurement. A similar approach will be used to investigate the feasibility and kinetics of K_2SO_4 reclamation for SO_2 removal combined with CO_2 capture. The experimental and modeling studies will determine optimal operating conditions in each of the unit operations for CO_2 removal and regeneration. The experimental results will be used as a basis for performing process simulations and a TEA to evaluate the overall performance, commercial feasibility, and cost-effectiveness of the Hot-CAP as a PCC process integrated with coal-fired power plants.

A team of engineers and scientists with expertise in process development, technology assessment, and economic analyses from the University of Illinois at Urbana-Champaign (UIUC) and Carbon Capture Scientific, LLC (CCS LLC) will perform the project. UIUC will oversee the project as the primary contractor and will be responsible for laboratory- and bench-scale experiments to generate engineering and process data. By interacting with the UIUC team, CCS LLC will apply the results from the experimental studies to perform a TEA of the Hot-CAP for a full-scale CO_2 capture application.

1.6 Scope of the work

The goals and objectives of the project will be achieved through execution of six primary tasks: (1) project planning and management, (2) kinetics of CO_2 absorption, (3) crystallization kinetics and solubility of bicarbonate, (4) phase equilibrium and desorption kinetics of high-pressure stripping, (5) kinetics of sulfate reclamation, and (6) techno-economic and process evaluation.

In Task 1, a test plan will be developed to defined the objectives and specify all the tasks to be carried out. A Project Management Plan will be formulated, and will then be followed and modified throughout the project to track the technical, schedule, and budget status. Progressive results of the project will be updated in quarterly reports, topical reports, annual contractors' meetings, and other reports or meetings required by DOE/NETL.

Task 2 is aimed at evaluating the kinetics of CO_2 absorption into high-concentration PCB or PCB/SCB mixture solutions with and without the addition of a promoter at elevated temperatures. First, the selected inorganic and organic catalysts or promoters that can accelerate the rate of CO_2 absorption into PCB will be screened using a laboratory stirred tank reactor, and the best performing promoters will be identified. The effect of major impurities on the promoted absorption reaction will also be investigated.

Next, a bench-scale packed-bed absorption column operated in continuous mode at atmospheric pressure will be designed and fabricated. Parametric tests of CO_2 absorption into un-promoted and promoted PCB, PCB/SCB mixture solutions, or both will be conducted, and results will be compared with those of the benchmark MEA.

Task 3 is aimed at determining the crystallization kinetics of bicarbonate (potassium and sodium) crystals formed from PCB or PCB/SCB mixture solutions at various operating conditions, because such data are critical for the design and scale-up of crystallization tanks. Parametric tests with respect to various process variables, including temperature, composition of the feed solution, agitation speed, residence time, and presence of additives (promoter and sulfate), will be conducted in continuous mode and/or batch mode to determine the nucleation and crystal growth rates of bicarbonate crystallization. Crystal samples will be characterized using various techniques, such as X-ray diffraction (XRD), scanning electron microscope (SEM), and crystal particle sizing.

In addition, a solubility measurement method will be developed in this task. The solubility data for bicarbonates (potassium and sodium) in PCB, SCB, and PCB/SCB solutions will then be measured to obtain the data under conditions typical of the Hot-CAP that are either incomplete, or unavailable in the literature.

Task 4 has two main objectives. One is to measure the vapor–liquid equilibrium (VLE) data of CO_2-H_2O-K_2CO_3-$KHCO_3$ slurry systems with high PCB concentrations (≥40 wt%) at elevated pressures (1 to 40 atm) and temperatures (120 to 200°C) typical of the Hot-CAP stripping process. The impacts of impurities (e.g., sulfate) on the VLE behavior of the PCB system will also be assessed. The VLE data will be measured using a high-pressure autoclave reactor.

The other objective of Task 4 is to test the performance of the PCB slurry in a bench-scale stripping column. For this purpose, a high-pressure, packed-bed stripping column will be

designed and fabricated. Parametric tests will be performed to investigate the CO_2 stripping performance at varying concentrations of PCB slurry, CO_2 loading levels, and reboiler temperatures. Experimental results will be analyzed to evaluate the attainable pressure, water vapor-to-CO_2 pressure ratio, and energy use performance under different operating conditions. In addition, the effects of impurities (e.g, sulfate) and additives on the performance of CO_2 stripping over PCB slurry will be tested in the stripping column. The optimal stripping pressure and temperature will be determined from the experimental measurements as well as the process simulations.

In Task 5, the feasibility of a proposed process to reclaim K_2SO_4 from the PCB solution for combined SO_2 removal and CO_2 capture will be investigated. The process is intended to reclaim the sulfate via a reaction with added lime reagent in high-pressure CO_2 to preferentially form and precipitate $CaSO_4$. An existing high-pressure autoclave experimental system will be modified or assembled in this study, and semi-continuous tests and/or batch tests will be performed to investigate competitive precipitation reactions at different compositions of PCB solution, sulfate concentrations, temperatures, CO_2 pressures (up to 60 atm), presence of additives, and types of carbonate/bicarbonate solutions (PCB, SCB, or PCB/SCB). Liquid and precipitate samples will be analyzed using different analytical methods. In addition, as required for the process design and evaluation, the solubility data for the $K_2CO_3/KHCO_3/K_2SO_4$ system will be measured.

In Task 6, process simulation, equipment sizing, and TEA studies will be conducted to evaluate the energy efficiency and cost-effectiveness of the Hot-CAP integrated with a full-scale power plant. Several subtasks are included in Task 6. First, through a literature search, discussions with equipment vendors, and the evaluation of potential equipment options, a risk analysis study on the identified technical risks will be performed to develop related mitigation strategies. Second, a detailed process flow diagram will be developed for the Hot-CAP, and thermo-chemical modeling simulations will be conducted with data input from experimental studies in the tasks above and from the literature. Third, on the basis of the results for equipment sizing and process simulation, the capital cost, operating & maintenance cost, cost of electricity, and so forth of the Hot-CAP installed in a conceptual 550-MWe (net) high-sulfur bituminous (Illinois No. 6) coal-fired power plant for CO_2 capture will be estimated following the standard cost analysis methodology. Finally, a sensitivity analysis of the economic performance in relation to a few important process and cost variables will be examined.

A detailed description of the research activities is available in the Statement of Project Objectives (SOPO) attached in Appendix A.

References

1. USDOE/NETL. *Cost and Performance Baseline for Fossil Energy Plants*, Report, DOE/NETL- 2010/1397, Novermber 2010.
2. Singh D., Croiset E., Douglas P.L., Douglas, M.A. Techno-economic study of CO_2 capture from an existing coal-fired power plant: MEA scrubbing vs. O_2/CO_2 recycle combustion. *Energy Conversion and Management* 2003, 44: 3073–3091.
3. Rochelle G., *CO_2 Capture by Absorption with Potassium Carbonate*, Final Report, DE-FC26-02NT41440, December 2007.

4. Mumford K. A., Smith K.H., Anderson, Shen S., Tao W., Suryaputradinata Y.A., Qader A., Hooper B., Innocenzi R.A., Kentish S.E., Stevens G.W. Post-combustion capture of CO_2: Results from the solvent absorption capture plant at Hazelwood Power Station using potassium carbonate solvent, *Energy & Fuels* 2012, 26(1):138–146.

5. Schoon L., van Straelen J. *Development of a precipitating carbonate technology for post-combustion CO_2 capture*, 6th Trondheim CCS Conference, Trondheim, Norway, June 16, 2011.

6. Zaks A. *Advanced low-energy enzyme-catalyzed solvent for CO_2 capture*, Project Close-Out Meeting Presentation, DE-FE0004228, DOE/NETL, November 2013.

Chapter 2. Kinetics Study of CO_2 Absorption into a Concentrated K_2CO_3/$KHCO_3$ Solution

Part 2A. Screening of Promoters to Accelerate CO_2 Absorption

2A.1 Introduction

Absorption of CO_2 into a potassium carbonate/bicarbonate (PCB) solution is based on the following overall reaction:

$$K_2CO_3 + CO_2 + H_2O \leftrightarrow 2KHCO_3 \quad \text{(2A-R1)}$$

Two elementary reactions take place during CO_2 absorption. The first involves the hydration of dissolved CO_2 with water (2A-R2), and the second involves the hydration of dissolved CO_2 with hydroxyl ions in solution (2A-R3):

$$CO_2 + H_2O \leftrightarrow HCO_3 + H^+ \quad \text{(2A-R2)}$$

$$CO_2 + OH^- \leftrightarrow HCO_3 \quad \text{(2A-R3)}$$

The rate of reaction 2A-R2 is negligible and reaction 2A-R3 becomes important only at high values of pH (>>10). Therefore, a key technical issue of the Hot-CAP, which uses a carbonate salt-based solution as a solvent for CO_2 absorption, is that the rate of CO_2 absorption is much slower compared with that into a monoethanolamine (MEA) solution. A promoter or catalyst able to substantially accelerate the absorption rate into the carbonate solution is necessary for the Hot-CAP.

Several inorganic catalysts, such as arsenite, sulfide, hypochlorite, and formaldehyde, can accelerate the rate of CO_2 hydration by two-to-five times, as reported in the literature.[1-4] However, drawbacks associated with their low catalytic activity, toxicity, instability, and/or corrosion have limited their practical application. In this project, three Lewis bases were selected as rate promoters. Lewis bases have a lone pair of electrons on their anions that can serve to neutralize the Lewis acidity of CO_2. For a "base" to act as a promoter, it must possess certain required properties. A base that is too strong may form a very stable CO_2·base complex, or simply react with water to generate more OH^-; on the other hand, a very weak base may not interact efficiently with the CO_2. Lewis bases are also thermally-stable, highly-soluble, and not volatile.

Several types of organic compounds were also considered as potential promoters or catalysts to enhance the rate of absorption into carbonate solutions. Amine promoters have been widely studied and applied in industry. However, most of the studies have been limited to applications at low temperatures ($\leqslant$50 °C) and with low concentrations of carbonate solution. Amino acid salts are also potential promoters, because they contain functional amino groups similar to amines that can undergo rapid reactions with CO_2. It has been reported in the literature that the rates of CO_2 absorption into amino acid salts are comparable with those of primary amines.[5,6] Amino acid salts have the advantages of high thermal stability, low volatility, a low environmental impact, and high biodegradability. However, few studies have been conducted on amino acid salts as rate promoters.

When an amine-type of organic promoter is added to the carbonate solution, the absorption involves a sequence of elementary reactions as follows:

$$2ORG + CO_2 = ORG \cdot COO^- + ORG \cdot H^+ \quad \text{(2A-R4)}$$

$$ORG + CO_2 + H_2O = ORG \cdot H^+ + HCO_3^- \quad \text{(2A-R5)}$$

$$CO_2 + H_2O + CO_3^{2-} = 2HCO_3^- \quad \text{(2A-R6)}$$

$$ORG \cdot H^+ + CO_3^{2-} = ORG + HCO_3^- \quad \text{(2A-R7)}$$

In the presence of a promoter, CO_2 is absorbed into the liquid quickly near the gas–liquid interface through reactions 2A-R4 and 2A-R5. In comparison, reaction 2A-R6 is very slow under low-alkaline conditions. In the bulk of the solution, the organic promoter can be regenerated by the reaction with carbonate (2A-R7). Thus, carbonate in the bulk serves as a CO_2 sink.

For this purpose, three inorganic salts, five amines, and five amino acid salts were selected as promoters or catalysts, and their performance in enhancing the rate of CO_2 absorption into a concentrated PCB solution (40 wt% K_2CO_3-equivalent) at elevated temperatures (60 to 80°C) was investigated and compared with a benchmark MEA solution.

2A.2 Experimental methods

2A.2.1 Experimental system

Rates of CO_2 absorption into PCB solutions promoted with various catalysts or promoters were measured using a stirred tank reactor (STR) system. The experimental setup consisted of an STR, a gas supply/control unit, and data acquisition instrumentation. The reactor was a Plexiglas vessel 7 in. (17.8 cm) in height with a 4-in. (10.2 cm) internal diameter. Four symmetrical baffles, each 0.5 in. (1.3 cm) wide, were attached inside the vessel to prevent vortex formation in the liquid phase. A magnetic stirrer (VWR Scientific, Series 400 HPS) with a 2-in. (5.1 cm) Teflon stir bar provided mixing for the liquid phase at the desired speed. A stirrer driven by an external motor (Caframo, Model BCD2002) via a magnetic coupling (MMC Magnetics, FCM-1) provided mixing for the gas phase up to 3,000 rpm. Temperature control of the reactor was achieved by water circulation through a stainless steel coil (0.6 cm outside diameter) inside the reactor. The temperature of this water was controlled by a thermostatic water bath (VWR Scientific, Model 1140A). The pressure of the gas stream into the reactor was controlled and measured by a pressure transducer (Alicat Scientific, PC-30PSIA-D/5P). The temperature inside the reactor was measured by a thermocouple (Omega, Type K, Model KMQSS-125-G-6). A vacuum pump (Dekker, RVL002H-01) was used to achieve the required initial vacuum level for the system. The pressure and temperature readings were monitored and recorded by a computer through a National Instrument Digital Data Acquisition System (NI USB 6009). A schematic diagram and picture of the system are shown in Figure 2A-1.

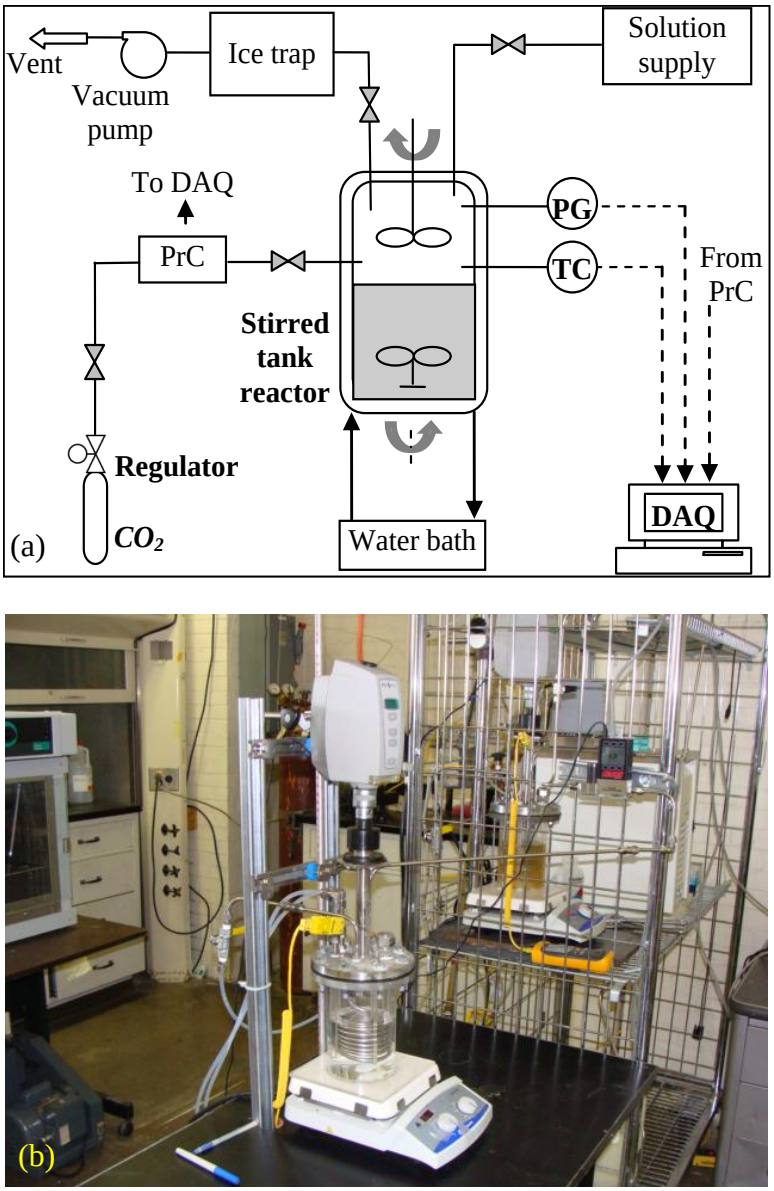

Figure 2A-1. (a) Schematic and (b) Photograph of a STR experimental system.
(PrC: pressure controller, PG: pressure gauge, TC: thermocouple, DAQ: data acquisition)

2A.2.2 Test procedure and conditions

The measurement operated under a batch mode. In a typical test, 800 mL of solution was used to absorb pure CO_2 gas (<15 psia/1 atm). First, the system was evacuated by the vacuum pump. A gas stream of pure CO_2 was then introduced into the reactor to a desired pressure in a short burst. The change in total gas pressure with respect to time was recorded, from which, the CO_2 partial pressure was obtained by subtracting the water vapor pressure. Because pure CO_2 was used under vacuum conditions, the mass transfer resistance in the gas phase was minimal and could be neglected during kinetic calculations.

For CO_2 absorption in the STR, equation 2A-1 could be derived based on the conservation of mass, the ideal gas law, and Henry's law. The mass transfer resistance in the gas phase was minimal and could be neglected. The instantaneous rate of CO_2 absorption into the liquid phase could be determined from the change in CO_2 partial pressure over time:

$$R = -\frac{V_G}{A*R_{gas}*T}\frac{dP_i}{dt} \quad (2A\text{-}1)$$

where R is the absorption flux of CO_2, V_G is the volume of the gas phase, A is the gas–liquid interfacial area, R_{gas} is the universal gas constant, T is the temperature, P_i is the CO_2 partial pressure, and t is time. This absorption rate was used to compare the performance of different solutions.

In the tests, different parameters were investigated to determine their effect on the rate of CO_2 absorption into the PCB solution. First, baseline tests were performed with the 40 wt% PCB (PCB40) at elevated temperatures of 60 to 80°C. The 40 wt% PCB solutions with 20% (PCB20-40) and 40% (PCB40-40) carbonate-to-bicarbonate (CTB) conversion were used to simulate the lean and rich conditions in the Hot-CAP absorption process. The full test matrix is provided in Table 2A-1.

Table 2A-1. Test matrix for CO_2 absorption into an un-promoted PCB solution

Test	PCB solution	Temperature (°C)
1	PCB40-20	60
2	PCB40-20	70
3	PCB40-20	80
4	PCB40-40	80

After the baseline of the un-promoted PCB solutions was established, three Lewis base catalysts were tested, CAT1, CAT2, and CAT3. These catalysts are commercially-available, and the as-received materials were in the form of a powder and had a purity of >99%. The tested dosage of the catalysts ranged between 2 and 5 wt%. The individual catalyst was mixed into the PCB40-20 solution, and the tests were performed at 60, 70, and 80°C. The test matrix is shown in Table 2A-2.

Table 2A-2. Matrix for testing inorganic catalysts to promote CO_2 absorption into PCB

Test	PCB solution/promoter	Dosage level of promoters, wt%	Temperature (°C)
1	PCB40-20 + CAT1	4	60, 70, and 80
2	PCB40-20 + CAT2	2	
3		4	
4		6	
5	PCB40-20 + CAT3	5	

Five primary and secondary amines, including diethanolamine (DEA), aminomethyl propanol (AMP), piperazine (PZ), hexamethylenediamine (HDA), and hexylamine (HA), were selected as promoters in the tests. The dosage of the amine promoters ranged from 0.5 to 1 M, and the absorption temperature was maintained at 70°C. Rates of CO_2 absorption into PCB40-20 and PCB40-20 were compared in the presence of these promoters. Along with the promoted PCB

solutions, 3 and 5 M MEA solutions at varying levels of CO_2 loading were tested at 50°C for comparison as an accepted industry standard. The full test matrix is shown in Table 2A-3.

Table 2A-3. Matrix for testing amine promoters to promote CO_2 absorption into PCB

Test	PCB solution/catalyst	Temperature (°C)	Promoter dosage
1	MEA (reference)	50	5 M loaded with 0, 0.1, or 0.2 mol of CO_2/mol of MEA
		50	3 M loaded with 0.2 mol of CO_2/mol of MEA
2	DEA in PCB40-20	70	0.6 M DEA
		70	1.2 M DEA
3	AMP in PCB40-20	70	0.5 M AMP
		70	1 M AMP
4	PZ in PCB40-20	70	0.5 M PZ
		70	1 M PZ
5	HDA in PCB40-20	70	0.5 M HAD
		70	1 M HDA
6	HA in PCB40-20	70	1 M HA
7	AMP in PCB40-40	70	1 M AMP
8	PZ in PCB40-40	70	1 M PZ
9	HDA in PCB40-40	70	1 M HDA

Amino acids were tested both as rate promoters for the PCB solution and as stand-alone absorbents. To absorb CO_2, amino acids need to be activated in water by adding an equimolar quantity of base. The salt form of amino acid provides stability to the solvent at high temperature and pressure conditions and reduces its volatility. In these experiments, the potassium salts of amino acids were prepared by neutralizing the dissolved amino acids with an equimolar quantity of potassium hydroxide in solution. The absorption capacity was initially evaluated by using a 3 M solution, and then the three amino acid salts with the highest absorption were further tested as promoters of the PCB solution. The full test matrix for amino acid screening is shown in Table 2A-4.

Table 2A-4. Matrix for testing amino acid salts to absorb CO_2 or promote absorption into PCB

Test	PCB solution/catalysts	Temperature (°C)	Promoter dosage
1	K-glycine	70	3 M
2	K-sacrosine	70	3 M
3	K-proline	70	3 M
4	K-taurine	70	3 M
5	K-alanine	70	3 M
6	K-glycine in PCB40-20	70	1 M
7	K-sacrosine in PCB40-20	70	1 M
8	K-proline in PCB40-20	70	1 M
9	K-glycine in PCB40-40	70	1 M
10	K-sacrosine in PCB40-40	70	1 M

In addition, during CO_2 absorption, the SO_2 in the flue gas will react with PCB to form K_2SO_4. To investigate the effect of SO_2 on the absorption rate, small, representative amounts (0.05 and

0.08 M) of K_2SO_4 were added to the un-promoted PCB, or the PCB promoted with AMP as a representative promoter. The test matrix is given in Table 2A-5.

Table 2A-5. Matrix for testing the effect of K_2SO_4 on CO_2 absorption into PCB solutions

Test	PCB solution/promoter	Temperature (°C)	K_2SO_4 dose (M)
1	PCB40-20	70	0.05
2	PCB40-20	70	0.08
3	PCB40-20 + 1 M AMP	70	0.05
4	PCB40-20 + 1 M AMP	70	0.08

2A.3 Results and discussion

2A.3.1 CO_2 absorption into PCB

Figure 2A-2 shows the rate of CO_2 absorption into the PCB40-20 solution at 60, 70, and 80°C. The rate increased remarkably as the reaction temperature was increased from 60 to 80°C. Henry's law constant, which indicates CO_2 solubility, and reaction kinetics both strongly depend on the temperature. As the temperature increases, reaction kinetics are accelerated and the CO_2 solubility decreases. The net effect of the temperature on the CO_2 absorption rate depends on which property undergoes a greater change. Results showed that increasing the reaction temperature from 60 to 80°C greatly improved the CO_2 absorption rates, which indicates that an increase in temperature was beneficial for promoting the rates of CO_2 absorption into the PCB.

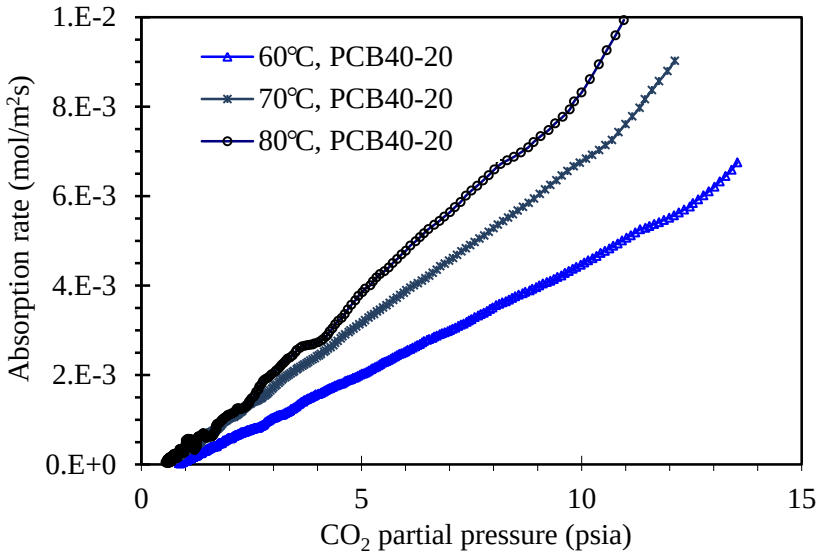

Figure 2A-2. Absorption of CO_2 into the PCB40-20 solution at 60, 70, and 80°C.

Figure 2A-3 shows the absorption of CO_2 into PCB40-20 and PCB40-40 at 80°C, and into PCB20-20 and PCB20-40 at 60°C. It is apparent that the higher the CTB conversion level, the lower the CO_2 absorption rate for the PCB with the same concentration and temperature. This tendency was more substantial for the 40 wt% PCB solution tested at 80°C. The rate of CO_2 absorption into PCB40-40 at 80°C was the slowest among the solutions tested, which could be because the equilibrium pressure of CO_2 over PCB40-40 at 80°C was much higher than over the

PCB40-20 solution at the same temperature, and over the 20 wt% PCB solutions (PCB20-20 and PCB20-40) at 60°C. As a result, at the same CO_2 partial pressure, the driving force for CO_2 absorption into PCB40-40 was significantly reduced compared with the other solutions.

Increasing the PCB concentration increases the ionic strength and viscosity and lowers the CO_2 solubility of the solution. These factors are important to the CO_2 reaction kinetics, physical mixing, and mass transfer in the liquid phase during the absorption process. However, there is potential for the reduced absorption rate into a high-concentration PCB solution (40 wt% vs. 20 wt%) to be overcome by increasing the reaction temperature, as shown above, where the PCB40-20 at 80°C had a an absorption rate comparable with that of PCB20-20 at 60°C.

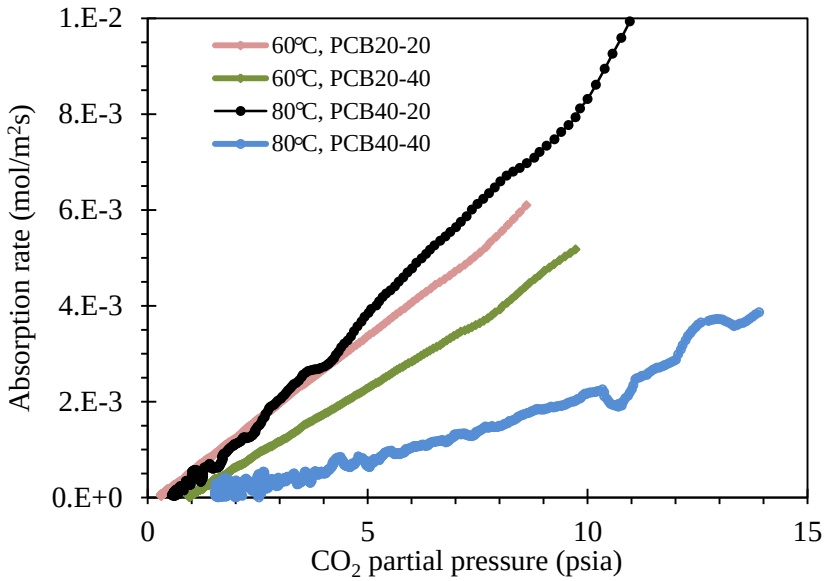

Figure 2A-3. Absorption of CO_2 into PCB solutions at varying PCB concentrations and CTB conversions at 60 and 80°C.

2A.3.2 CO_2 absorption into PCB with an inorganic catalyst

In the initial screening tests, the doses of CAT1, CAT2, and CAT3 in PCB40-20 were 4, 4, and 5 wt%, respectively. Figure 2A-4 shows the rates of CO_2 absorption into the promoted PCB40-20 at 60, 70, and 80°C. The addition of 4 wt% CAT1 or CAT2 almost doubled the CO_2 absorption rates. In contrast, the addition of 5 wt% CAT3 slightly reduced the rates of CO_2 absorption. That might have been caused by some adverse change in the physical property of the solution after the CAT3 was added.

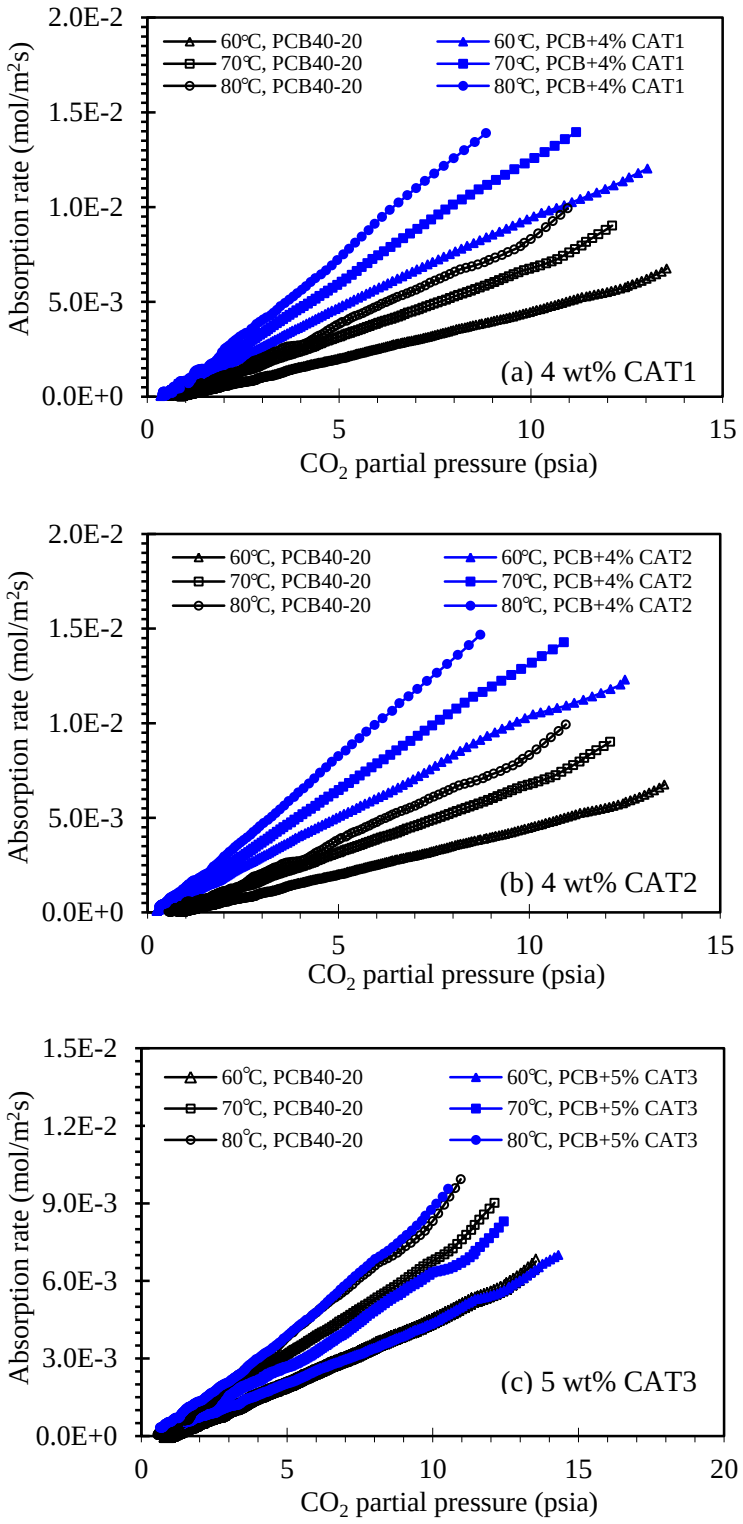

Figure 2A-4. Absorption of CO_2 into PCB40-20 promoted by three inorganic catalysts at 60, 70, and 80°C.

The apparent enhancement factor (*E*), defined as the ratio of the rate of CO_2 absorption into the PCB solution with a catalyst to that without a catalyst, was used to evaluate the catalytic efficiency quantitatively. The *E* values for the CAT1 and CAT2 catalysts at 60, 70, and 80°C are shown in Figure 2A-5. Results indicate that the catalytic activity of either CAT1 or CAT2 was slightly higher at 60°C than at 70 or 80°C. The addition of CAT2 showed slightly higher *E* values. Thus, CAT2 was selected for further evaluation tests with varying doses, i.e., 2, 4, and 6 wt%.

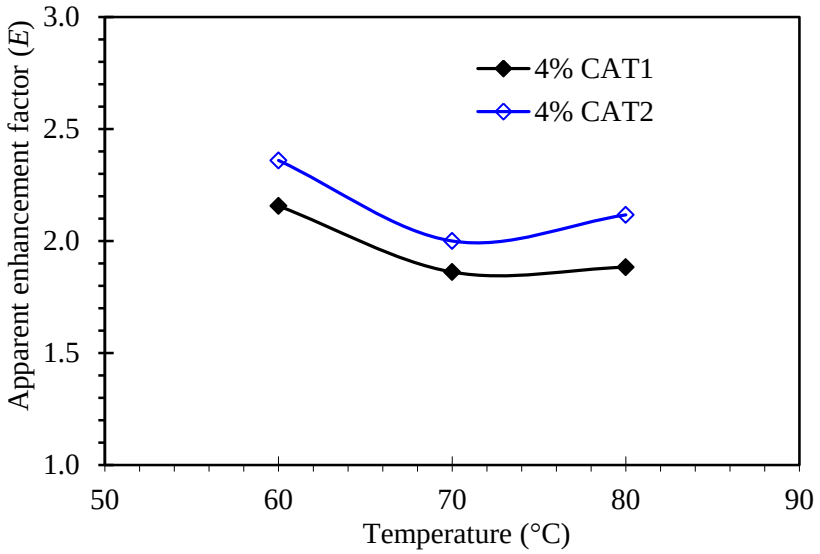

Figure 2A-5. Apparent enhancement factors of the CAT1 and CAT2 catalysts for CO_2 absorption into PCB40-20 at 60 to 80°C.

Figure 2A-6 shows the rates of CO_2 absorption into the PCB40-20 solution in the presence of 2, 4, and 6 wt% CAT2 catalyst at 60, 70, and 80°C. The rate increased as the CAT2 dose was increased from 2 to 6 wt%. The difference in the promoted rate was small between using 4 and 6 wt% CAT2 at 60 and 70°C, but it became more substantial at 80°C.

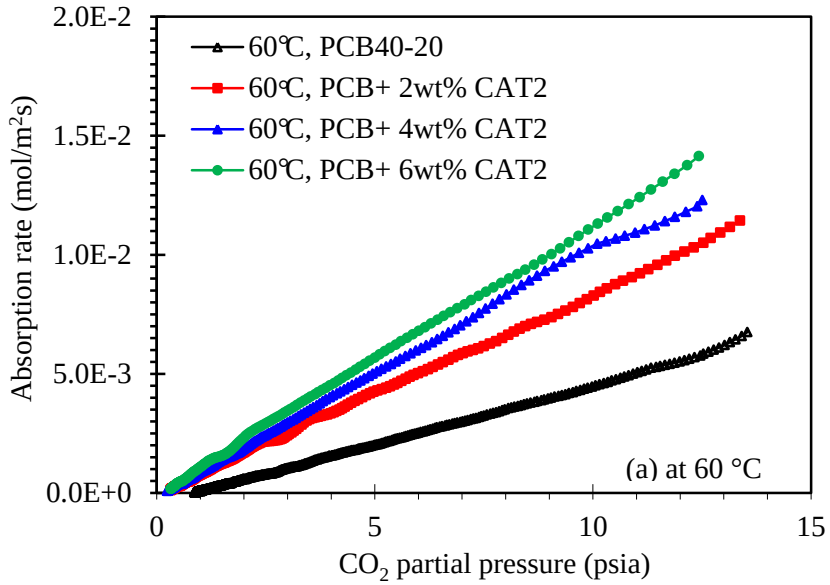
2.0E-2
1.5E-2
1.0E-2
5.0E-3
0.0E+0
Absorption rate (mol/m²s)
60℃, PCB40-20
60℃, PCB+ 2wt% CAT2
60℃, PCB+ 4wt% CAT2
60℃, PCB+ 6wt% CAT2
(a) at 60 °C
0
5
10
15
CO2 partial pressure (psia)

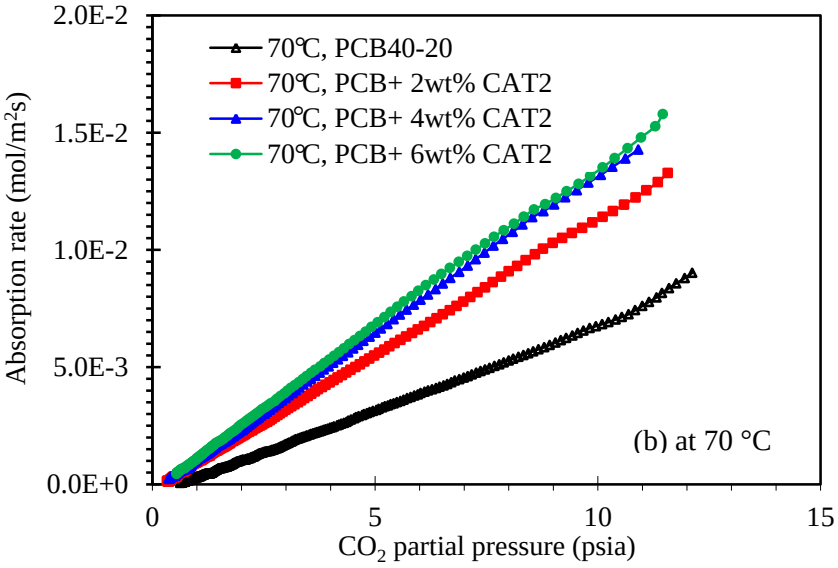
2.0E-2
1.5E-2
1.0E-2
5.0E-3
0.0E+0
Absorption rate (mol/m²s)
70℃, PCB40-20
70℃, PCB+ 2wt% CAT2
70℃, PCB+ 4wt% CAT2
70℃, PCB+ 6wt% CAT2
(b) at 70 °C
0
5
10
15
CO2 partial pressure (psia)

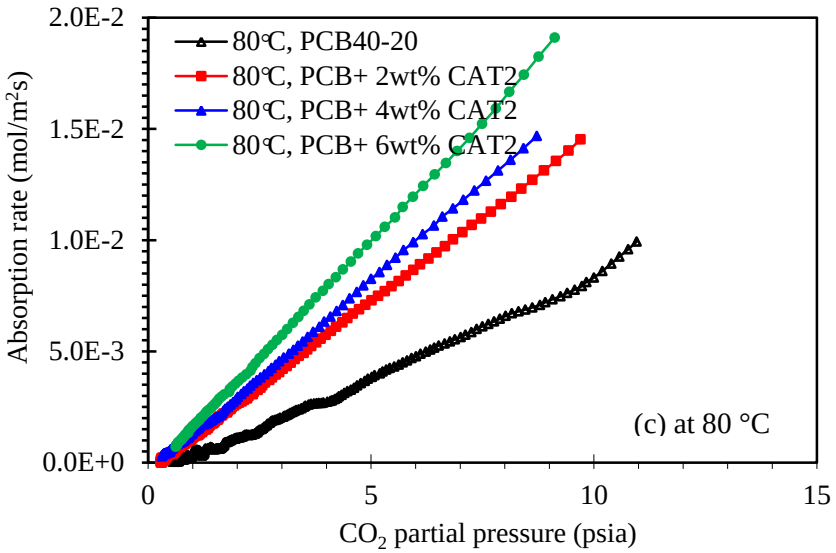

Figure 2A-6. Rates of CO_2 absorption into PCB40-20 promoted by 2, 4, and 6 wt% CAT2 catalyst at 60, 70, and 80°C.

The *E* values for using different doses of CAT2 catalyst at 60, 70, and 80°C are shown in Figure 2A-7. As expected, *E* increased with an increase in the CAT2 dose. This tendency was more substantial at 60 or 80°C than at 70°C. At 70°C, the enhancement factor reached the minimum at the three catalyst doses. This result can be explained by the impact of temperature on both the kinetics and CO_2 solubility. When the temperature was increased, the kinetics was enhanced and CO_2 solubility decreased. The net effect on the absorption rate was a combination of these two terms. The lower *E* values observed at 70°C might represent the fact that the reduced solubility had a more substantial impact than did the increased kinetics at this temperature.

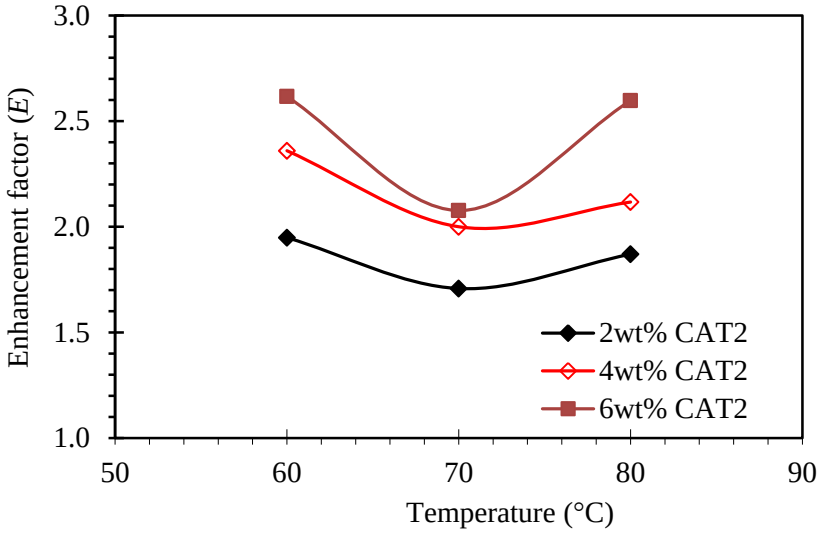

Figure 2A-7. Enhancement factors of the CAT2 catalyst for CO_2 absorption into PCB40-20 at varying doses at 60, 70, and 80°C.

Rates of CO_2 absorption into PCB40-20 with and without an inorganic catalyst were also compared with those into a 3 M MEA solution with a 40% conversion rate (MEA3-40, equivalent to a CO_2 loading of 0.2 mol/mol of MEA; Figure 2A-8). The PCB40-20 and MEA3-40 were selected to represent their respective CO_2 lean conditions. Testing with MEA was performed at 25 and 50°C. Because CAT1 and CAT2 exhibited similar activities, only CAT2 was used for comparison with MEA3-40. Rates of CO_2 absorption into the 3 M MEA at 50°C were 7.1-to-17.9 times greater than those into the PCB40-20 without a catalyst at 80°C, depending on the CO_2 partial pressure. Although adding 4 wt% CAT2 to PCB40-20 substantially promoted the absorption of CO_2, the rate was still much lower than that into MEA. For example, under CO_2 partial pressures ranging between 1 and 3 psia (6.9 and 20.7 kPa), the rates into the CAT2-promoted PCB40-20 solution at 80°C were 3.1-to-4.8 times slower than those into 3 M MEA at 50°C.

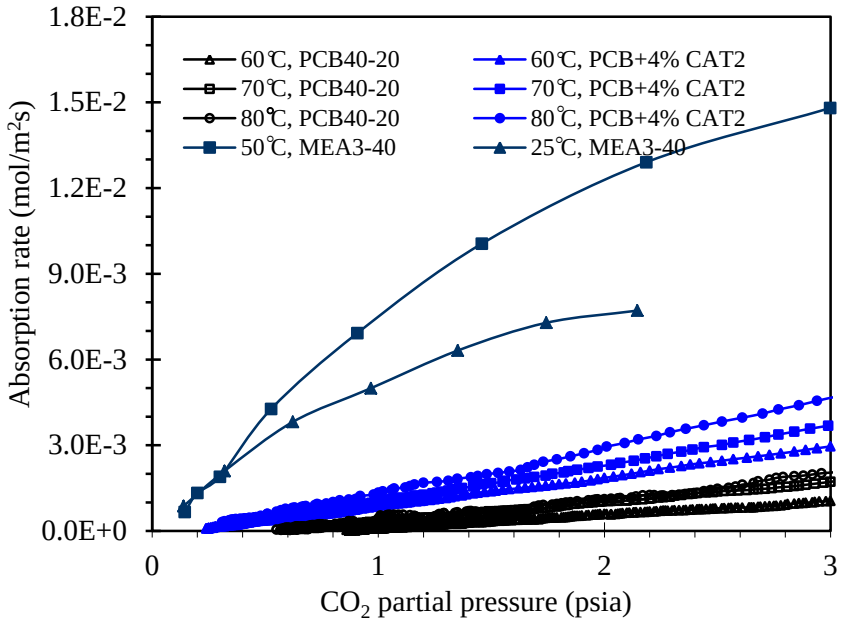

Figure 2A-8. Comparison of CO_2 absorption rates into CAT2-promoted PCB40-20 and MEA3-40 solutions.

2A.3.3 CO_2 absorption into PCB with an organic promoter

2A.3.3.1 Amine promoters

Screening of amine promoters. Figure 2A-9 shows rates of CO_2 absorption into PCB40-20 solutions promoted with five amine promoters at 70°C. The rate into the un-promoted PCB40-20 is also included for comparison. All five amine promoters enhanced the rate of CO_2 absorption to various extents, depending on the amine type and dosage. Absorption rates were promoted by 3.5-to-50 times compared with the un-promoted PCB solution when the CO_2 partial pressure was between 1 and 5 psia (6.9 and 34.5 kPa). Among the five amines, at the same dosage (1 or 0.5 M), PZ and AMP had the highest rate of promotion, followed by HDA. The 1 M HDA was less effective for rate promotion than were 1 M AMP and PZ at higher CO_2 partial pressures, but the difference was less substantial at lower partial pressures (<1.5 psia/10.3 kPa).

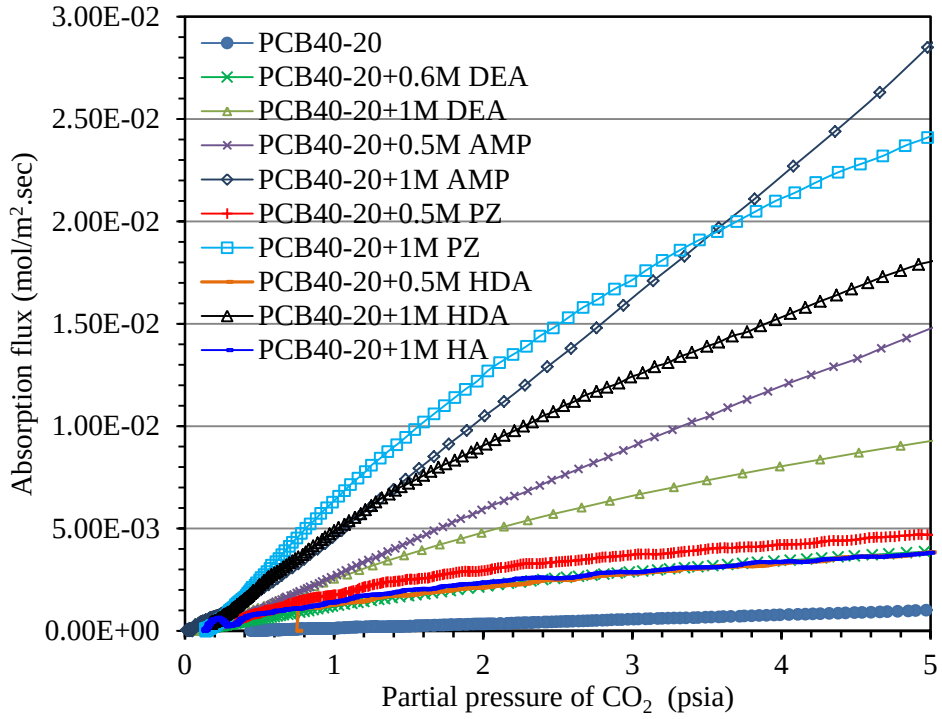

Figure 2A-9. CO_2 absorption rates into PCB40-20 solutions promoted with selected amines at 70°C.

AMP is a hindered amine and absorbs CO_2 at a 1:1 molar ratio. It promoted the absorption rate into PCB because of its relatively high CO_2-carrying capacity. The reaction between AMP and CO_2 is fast and does not form a stable carbamate, which is a reaction intermediate hydrolyzed immediately into bicarbonate ions, resulting in less amine consumption per mole of CO_2 absorption. PZ enhanced the absorption rate because it is highly active with CO_2 (e.g., more reactive than MEA) to form carbamate and dicarbamate products according to the following reactions:[7]

$$PZ + H^+ \leftrightarrow PZH^+ \quad \text{(2A-R8)}$$

$$PZ - CO_2 + H_2O \leftrightarrow PZH^+ + HCO_3^- \quad \text{(2A-R9)}$$

$$PZ + CO_2 + H_2O \leftrightarrow PZCOO^- + H_3O^+ \quad \text{(2A-R10)}$$

$$PZCOOH + H_2O \leftrightarrow PZCOO^- + H_3O^+, \quad \text{(2A-R11)}$$

$$PZCOO^- + CO_2 + H_2O \leftrightarrow PZ(COO^-)_2 + H_3O^+ \quad \text{(2A-R12)}$$

$$PZH^+ + H_2O \leftrightarrow PZ + H_3O^+ \quad \text{(2A-R13)}$$

The good rate promotion performance of HDA might be due to its high reactivity with CO_2 and the high capacity related to its molecular structure. These results indicate that using amine or similar promoters is a promising means of substantially increasing the rate of CO_2 adsorption into PCB.

To examine the performance of promoters in the PCB40 solution with a high CO_2 loading, the rates of CO_2 absorption into PCB40-40 in the presence of 1 M PZ, AMP, or HDA were also measured. The results of these tests are compared with those by promoted PCB40-20 (Figure 2A-10). The rates of CO_2 absorption into PCB40-40 with the addition of 1 M AMP were 2-to-3 times lower than those for the PCB40-20 with the same promoter; however, for the 1 M PZ and HDA promoters in the PCB40-40 and PCB40-20 solutions, the difference between absorption rates was 5-to-6 times lower under the same conditions. The decrease in absorption rate as the CTB conversion increased from 20 to 40% was expected, because the driving force of CO_2 absorption into PCB40-40 was smaller.

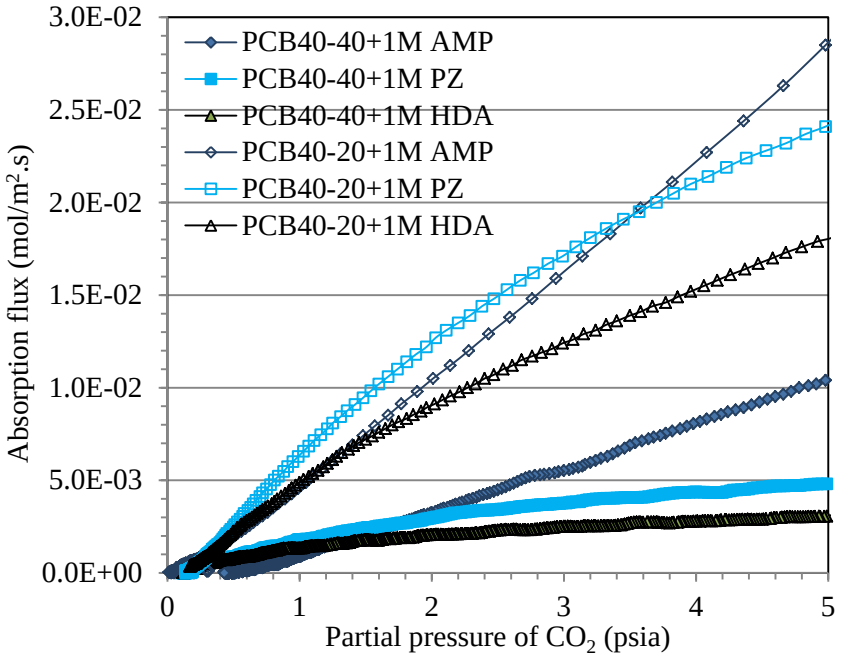

Figure 2A-10. CO_2 absorption rates into promoted PCB40-20 and PCB40-40 solutions at 70°C.

Comparison of amine-promoted PCB with MEA. In Figure 2A-11, the rates of CO_2 absorption into the PCB40-20 solution without and with an amine promoter at 70°C were compared with those into 3 and 5 M MEA solutions at 50°C. Only the data for the promoter dosage of 1 or 1.2 M are included in the figure. Two 3 M MEA solutions, fresh and loaded with 0.2 mol of CO_2/mol of MEA, and three 5 M MEA solutions, fresh and loaded with 0.1 and 0.2 mol of CO_2/mol of MEA, were selected for the comparison at 50°C.

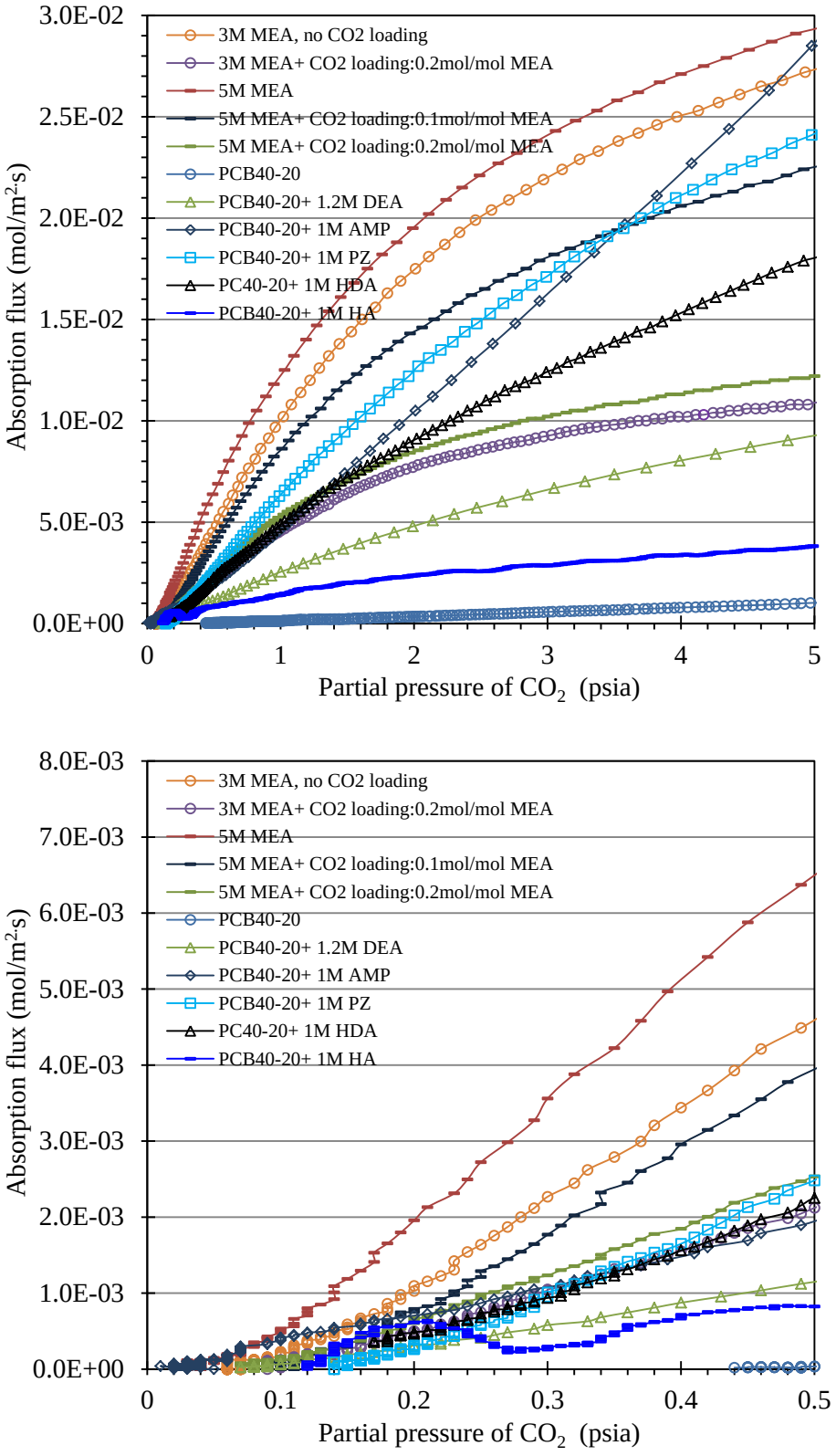

Figure 2A-11. CO_2 absorption rates into amine-promoted PCB40-20 solutions at 70°C and MEA solutions at 50°C. The figure at the bottom zooms in on the low end of CO_2 partial pressures.

It appeared that the absorption rates into 5 M MEA were not substantially higher than those into 3 M MEA with the same CO_2 loading levels. For example, the rate into 5 M MEA loaded with 0.2 mol CO_2/mol MEA was only about 10% higher than that into its 3 M MEA counterpart on average. Note that all the CO_2 absorption rates were measured in an STR reactor using pure CO_2 gas with minimal gas phase diffusion resistance during CO_2 absorption. However, when the absorption rate was sufficiently fast, the CO_2 diffusion resistance in the gas phase in the presence of water vapor might have imposed some impact on the overall rate. As also shown in Figure 2A-11, the 5 M MEA solutions exhibited a similar trend with respect to the effect of CO_2 loading on the absorption rate. For example, compared with fresh 5 M MEA, absorption rates into 5 M MEA loaded with 0.1 and 0.2 mol/mol decreased by about 25 and 60% on average, respectively.

Compared with 5 M MEA solution with 0.2 mol/mol CO_2 loading at 50°C (a lean condition typical of the benchmark MEA process), absorption rates into the PCB40-20 (a lean condition typical of Hot-CAP) promoted with 1 M PZ, 1 M AMP, and 1 M HDA at 70°C were higher at CO_2 partial pressures greater than 2 psia (13.8 kPa) and comparable at lower partial pressures down to approximately 0.15 psia (1.0 kPa). However, lower absorption rates were observed for the PCB promoted by DEA or HA. The results above indicate that the CO_2 absorption rate into a PCB solution can be enhanced to levels comparable to that of 5 M MEA with the use of amine promoters.

2A.3.3.2 Amino acid salt promoter

Absorption into a pure amino acid salt solution. Figure 2A-12 shows the absorption rates into five 3 M amino acid salt solutions. The K-glycine solution demonstrated the highest absorption rate, followed by K-sacrosine and K-proline. At 70°C, the 3 M K-glycine, K-sacrosine, and K-proline salt solutions exhibited absorption rates higher than (at higher CO_2 partial pressures), or comparable with or slightly lower than (at CO_2 partial pressures lower than about 0.7 psia (4.8 kPa) those into 5 M MEA at 50°C.

The difference in absorption rates into these amino acid salt solutions was mainly caused by the different molecular structures and locations of the amino groups. Glycine is similar in structure to primary amines, whereas proline and sacrosine are secondary amine group acids. The K-taurine and K-alanine salt solutions showed the lowest rates for CO_2 absorption. The reaction mechanism of CO_2 with amino acid salts can be described by the formation of carbamates followed by the hydrolysis of carbamates to produce bicarbonate ions, which is similar to the mechanism for alkanolamines.[6]

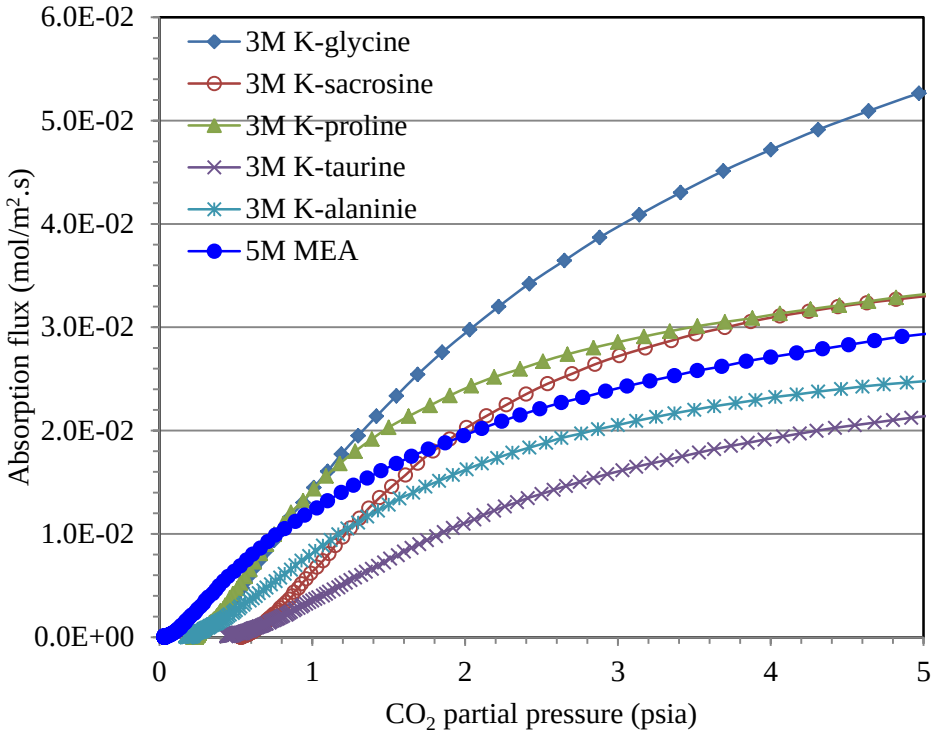

Figure 2A-12. CO_2 absorption rates into amino acid salt solutions at 70°C.

Absorption into an amino acid salt-promoted PCB solution. The three best performing amino acids - glycine, sacrosine, and proline - were selected as promoters to test CO_2 absorption into PCB at 70°C. Rates of CO_2 absorption into un-promoted PCB40-20 and PCB40-20 promoted with the amino acid salts (1 M) were compared with those into 5 M MEA with a CO_2 loading of 0.2 mol/mol at 50°C, as shown in Figure 2A-13.

The absorption rates into MEA solution at 50°C were 10-to-40 times greater than the rate into PCB40-20 at 70°C for CO_2 partial pressures between 1 and 5 psia (6.9 and 34.5 kPa). Adding 1 M amino acid salt promoters substantially improved the absorption rates in the PCB40-20. The addition of K-glycine and K-sacrosine increased the rates by 3-to-11 times for the CO_2 partial pressure range tested. However, the promoted rates were still lower than those into MEA solution. It was observed that the equilibrium vapor pressures over the amino acid salt solution were higher than those over MEA, which could have reduced the driving force for CO_2 absorption.

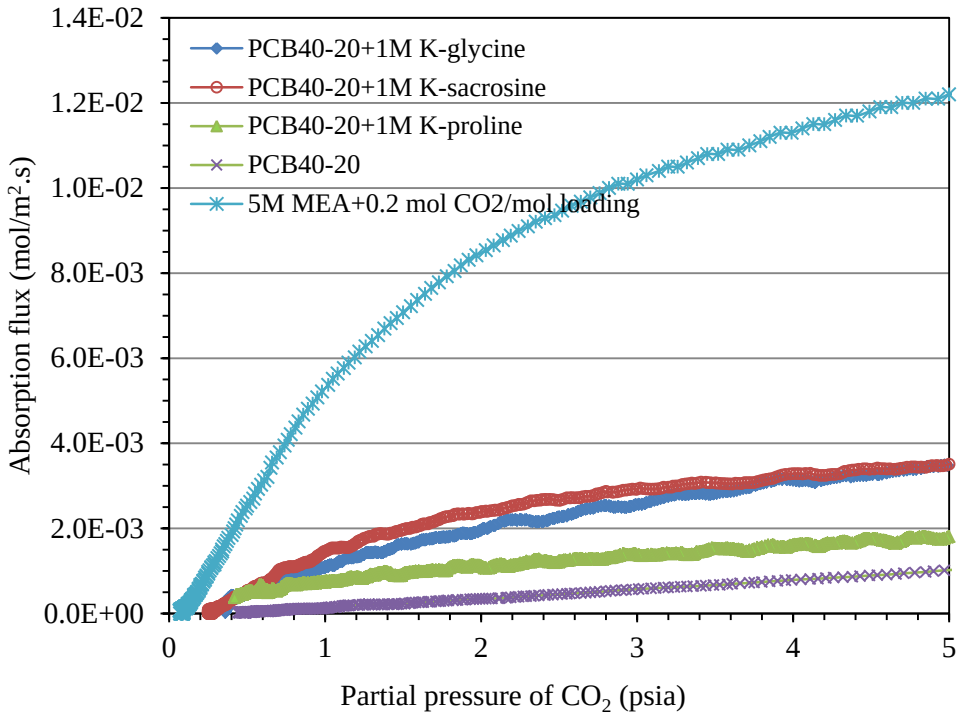

Figure 2A-13. Comparison of CO_2 absorption rates into amino acid salt-promoted PCB40-20 at 70°C and 5 M MEA at 50°C.

The rates of CO_2 absorption promoted by K-glycine and K-sacrosine in the PCB solutions with different CTB conversion levels are shown in Figure 2A-14. As expected, the absorption rates into the promoted PCB40-40 were lower than those into the PCB40-20 counterparts. The addition of 1 M K-sacrosine in PCB40-20 and PCB40-40 was more effective at accelerating CO_2 absorption compared with 1 M K-glycine in the same solutions. The difference in absorption rates into PCB40-20 + 1 M K-sacrosine and into PCB40-40 + 1 M K-sacrosine was minimal (~20%), considering the large change in CTB conversion. In comparison, in the presence of 1 M AMP, the rates into PCB40-40 were up to 2-to-3 times lower than those into PCB40-20. In 5 M MEA solution, when the CO_2 loading was increased by merely 0.1 mol/mol, the absorption rate decreased significantly (~50% reduction), as shown in Figure 2A-11. It suggests that increasing CO_2 loading could result in a less reduction in rate into 40 wt% PCB promoted with an amino acid salt than that into 5M MEA.

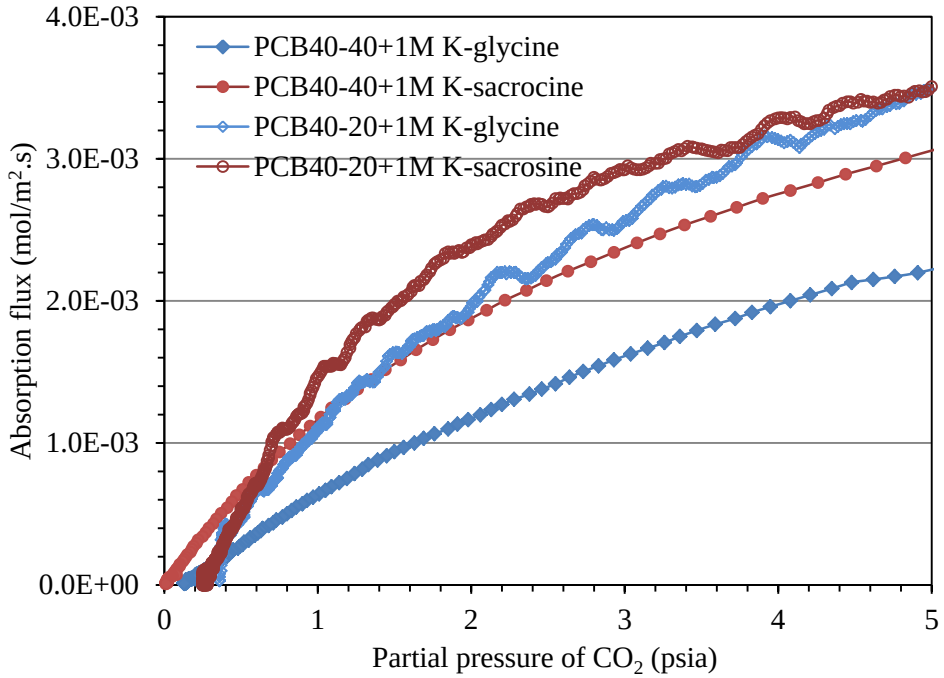

Figure 2A-14. Comparison of CO_2 absorption rates into PCB40-40 and PCB40-20 at 70°C promoted by amino acid salts.

2A.3.3.4 Effect of the presence of K_2SO_4

Figure 2A-15 compares the rates of CO_2 absorption into the un-promoted PCB40-20 solution with and without the addition of K_2SO_4. No substantial difference in absorption rate was observed in the presence of either 0.05 or 0.08 M K_2SO_4 for the un-promoted solution.

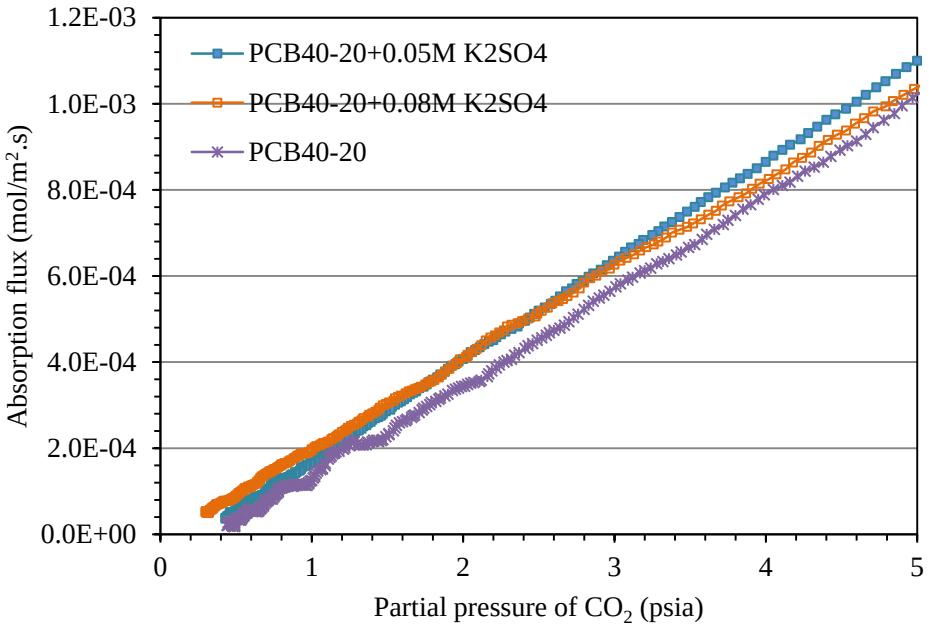

Figure 2A-15. Effect of the presence of K_2SO_4 on absorption rates into the un-promoted PCB40-20 solution at 70°C.

Figure 2A-16 displays the rates of CO_2 absorption into the AMP-promoted PCB20-40 solution with and without the addition of either 0.05 or 0.08 M K_2SO_4. Similar to the un-promoted PCB, the presence of K_2SO_4 did not noticeably affect the CO_2 absorption rate. Note that the solubility of K_2SO_4 in the 40 wt% PCB solution is low (<0.2 M) at 70°C. In practice, if an excess amount of SO_2 is absorbed into the PCB solution, K_2SO_4 may precipitate from the solution. Therefore, the tested K_2SO_4 concentrations are deemed representative.

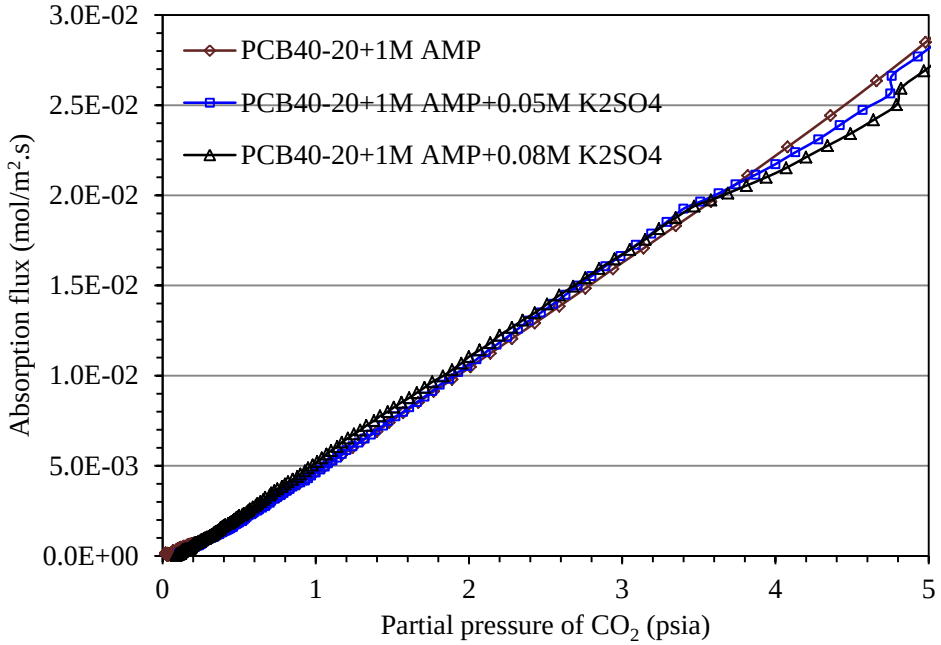

Figure 2A-16. Effect of the presence of K_2SO_4 on absorption rates into the PCB40-20 promoted with 1 M AMP at 70°C.

2A.4 Summary

Three Lewis base inorganic catalysts, five primary and secondary amines, and five amino acid salts were evaluated as promoters for accelerating the CO_2 absorption rates into a concentrated 40 wt% PCB solution at elevated temperatures using a batch STR.

The addition of 4 wt% CAT1 or CAT2 into PCB40-20 approximately doubled the rates at 60, 70, and 80°C, whereas the addition of 5 wt% CAT3 did not present any significant effect. Increasing the CAT1 or CAT2 dosage increased the rates into the 40 wt% PCB. In comparison to MEA3-40 solution at 50°C, the rates into PCB40-20 with 4 and 6 wt% CAT2 were 3.1-to-4.8 and 2.5-to-3.9 times slower at 80 °C, respectively; depending on the CO_2 partial pressure, which ranged between 1 and 3 psia (6.9 and 20.7 kPa). The rate difference between the promoted PCB and MEA will be smaller in a packed-bed column where gas phase mass transfer resistance is present.

All five amine promoters improved the rate of CO_2 absorption into the 40 wt% PCB solution. Results showed that these amine promoters increased the absorption rates into the PCB solution by 3.5-to-50 times at 70°C, depending on the amine type and dosage, CTB conversion, and CO_2

partial pressure. Among the promoters, the rates promoted with PZ and AMP were the highest, followed by HDA. Compared with 5 M MEA solution loaded with 0.2 mol of CO_2/mol of MEA (typical CO_2-lean condition in the benchmark MEA process at 50°C), the absorption rates of PCB40-20 promoted with 1 M PZ, 1 M AMP, and 1 M HDA at 70°C were comparable. This indicates that amine promoters are promising for significantly accelerating the CO_2 absorption into PCB solution. The best performing promoters, PZ and AMP, and an industrial benchmark promoter (DEA) were selected for investigation in the bench-scale packed-bed column described in Chapter 2B.

All the tested amino acid salt aqueous solutions, including K-glycine, K-sacrosine, K-proline, K-taurine, and K-alanine, showed high rates of CO_2 absorption, especially 3 M K-glycine, K-sacrosine, and K-proline. At 70°C, these solutions exhibited rates higher than or comparable with those of 5 M MEA at 50°C. The three highest performing amino acid salts - K-glycine, K-sacrosine, and K-proline - were further evaluated as promoters for CO_2 absorption into 40 wt% PCB at 70°C. The rates into both PCB40-20 and PCB40-40 were accelerated by these promoters, but K-sacrosine and K-glycine improved the absorption rates more significantly than K-proline. Compared with the rate into a lean 5 M MEA (loaded with 0.2 mol/mol), the rates into PCB40-20 promoted by these amino acid salts were significantly lower. However, the rate difference between the promoted lean and rich PCB was much less substantial than that for MEA. For example, the rates into PCB40-20 and PCB40-40 promoted by 1 M K-sacrosine differed by about 20%.

The impact of potassium sulfate, a product of the reaction of SO_2 in flue gas with PCB during CO_2 absorption, was investigated in the STR. The presence of K_2SO_4 at either 0.05 or 0.08 M did not substantially affect the rates of CO_2 absorption into the un-promoted 40 wt% PCB, or PCB with an amine promoter.

References

1. Sharma M.M., Danckwerts P.V. Fast reactions of CO_2 in alkaline solutions—(a) Carbonate buffers with arsenite, formaldehyde and hypochlorite as catalysts (b) Aqueous monoisopropanolamine (1-amino-2-propanol) solutions. *Chemical Engineering Science* 1963, 18: 729–735.
2. Pohoreck R. The absorption of CO_2 in carbonate-bicarbonate buffer solutions containing hypochlorite catalyst on a sieve plate. *Chemical Engineering Science* 1968, 23: 1447–1451.
3. Augugliaro V., Rizzuti L. Kinetics of carbon dioxide absorption into catalysed potassium carbonate solutions. *Chemical Engineering Science* 1987, 42: 2339–2343.
4. Kohl A.S., Nielsen R.B. Gas Purification, 5th edition, Houston: Gulf Publishing, 1997.
5. Hook R.J. An investigation of some sterically hindered amines as potential carbon dioxide scrubbing compounds, *Industrial & Engineering Chemistry Research* 1997, 36(5): 1779–1790.
6. Kumar P.S., Hogendoorn J.A., Versteeg G.F. Kinetics of the reaction of CO_2 with aqueous potassium salt of taurine and glycine, *AIChE Journal* 2003, 49: 203–213.

7. Cullinane J.T. *Thermodynamics and kinetics of aqueous piperazine with potassium carbonate for carbon dioxide absorption*, Ph.D. thesis, 2005.

Part 2B. Testing in a Bench-Scale Packed-Bed Column

2B.1 Introduction

After screening and selecting promoters with the greatest potential for boosting rates of CO_2 absorption in concentrated $K_2CO_3/KHCO_3$ (PCB) solutions, a bench-scale, packed-bed column was fabricated to further test the performance of CO_2 absorption into PCB, $Na_2CO_3/NaHCO_3$ (SCB), and PCB/SCB mixture solutions with the selected promoters.

2B.2 Experimental Method

2B.2.1 Packed-bed column system

A bench-scale, packed-bed absorption column was designed and fabricated for the CO_2 absorption study. The column was constructed of cast acrylic so the flow through the column could be observed during tests. The acrylic material was tested by immersing it into a 40 wt% PCB solution for a month, after which, no signs of corrosion or degradation were seen. This demonstrated that the material would be suitable for this application. The column was constructed to be 3 m tall and have a 10-cm inner diameter, and was packed with a corrugated stainless steel packing material (Hai-Yan New Century Petrochemical Device Co., Ltd., Model 500) 2 m in height. The structured packing has a specific surface area of approximately 800 m^2/m^3. Specifications of the packing material are given in Table 2B.1.

Table 2B-1. Geometric specifications of the structured packing material

Property	Specification
Height of packing element, mm	100
Diameter of packing element, mm	100
Specific surface area (a), m^2/m^3	800
Angle of inclined corrugation to the horizontal (θ), degree	45
Corrugation crimp height, mm	5
Side dimension of corrugation, mm	10
Void fraction (ε)	0.66

A schematic diagram of the system is shown in Figure 2B-1, and photographs are displayed in Figure 2B-2. The gas stream is a simulated flue gas mixture made up of air, CO_2, and water vapor. Air is supplied from an air compressor, CO_2 from a compressed gas cylinder, and steam from a steam generator (Chromalox/CMB-3). The flow rates of CO_2 and air are controlled by valves and monitored by flow meters (Dwyer, GFM). The amount of steam added is valve-adjusted and metered to provide the required temperature and humidity of the gas mixture inlet (60 to 80°C). The PCB feed solution was pumped from a 10-gallon stirred tank using a peristaltic pump (MasterFlex). The liquid flow rate was controlled by setting the speed (rpm) of the pump, and was consistently monitored. An electric heater with temperature control was mounted inside the tank to maintain the solution at the desired temperature. The inlet and outlet CO_2 concentrations were measured by a CO_2 analyzer (Quantek Instruments, Model 906) after any moisture was removed from the gas streams by a diffusion dryer. Five thermal couples were mounted along the height of the column to measure the temperate profile. The pressure drop across the column was measured using a U-tube. A humidity analyzer (Vaisala) measured the

moisture contents of the inlet and outlet gas streams. All the flow meters and control valves that regulated the CO_2, steam, and air flows were precisely calibrated. The liquid flow rate was calibrated for both water and hot PCB solutions.

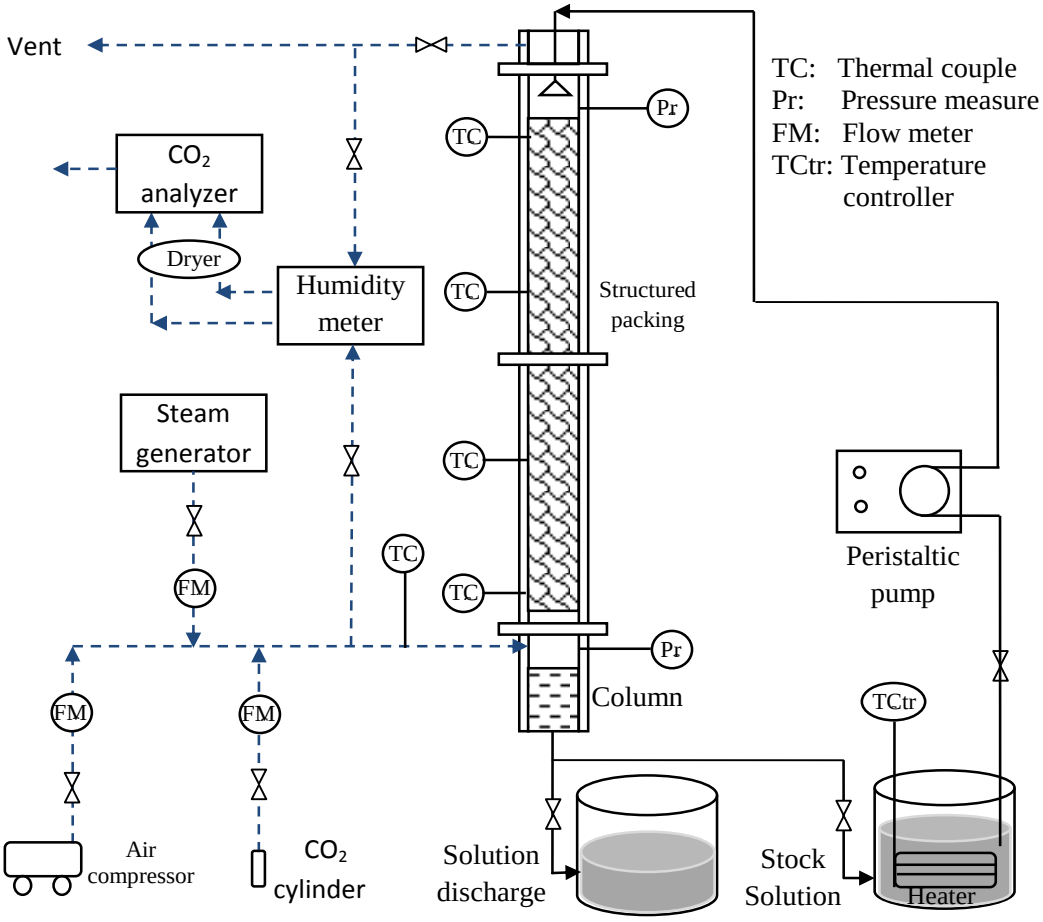

Figure 2B-1. Schematic diagram of the bench-scale packed-bed absorption column.

Figure 2B-2. Photographs of the bench-scale packed-bed absorption column: (a) overview of the column setup; (b) solution supply tank with stirrer and temperature-controlled heater; (3) packing unit (10 cm in diameter by 10 cm high).

2B.2.2 Method of CO_2 absorption testing

The absorber operated counter-currently; the liquid was pumped to the top of the column and flowed downward, while the gas flowed upward from the bottom. The CO_2-rich solution exiting the column returned to the tank and was recycled in the system for continuous use. Because the volume of feed solution in the liquid tank was large (≥15 L) and the amount of CO_2 absorbed during each cycle was relatively small, the composition of feed solution did not change significantly in a short period of time (e.g., 10 min). This allowed a pseudo-steady operation under a preset condition, as well as enough time for liquid sampling and CO_2 concentration measurements during the continuous test.

On the basis of the CO_2 concentrations measured in the dried inlet and outlet streams, the CO_2 removal efficiency of the solution at a given CTB conversion level was determined using the following equation:

$$CO_2\ Removal\ Efficiency = \frac{CO_2\ Inlet\ Volume\ \% - CO_2\ Outlet\ Volume\ \%}{CO_2\ Inlet\ Volume\ \%} \qquad (2B\text{-}1)$$

This removal efficiency was used for comparison, or to identify the molar flow rate or other variables that depend on the CO_2 absorption rate.

Tests were carried out in three stages. First, un-promoted PCB was tested at various conditions to establish baseline removal rates to compare later with the promoted solutions. The concentration of PCB was varied from 20 to 40 wt%, and a large range of CTB conversions were tested, ranging from lean to rich CO_2 loading. Because a PCB concentration of 40 wt% was considered the standard, multiple liquid-to-gas (L/G) ratios were tested to see their effect. The baseline temperature was 70°C, but tests were also performed at 80°C to evaluate the effect of temperature on CO_2 absorption. The full test matrix for these solutions is shown in Table 2B-2.

Table 2B-2. Test matrix for CO_2 absorption into un-promoted PCB solutions

No.	Initial solvent	Temp (°C)	L/G with 0.56 LPM liquid flow rate (L/m^3, under actual conditions)	CO_2 inlet concentration (vol%)
1	PCB40-20*	70	2, 4, 8, 12	14
2	PCB40-30	70	2, 4, 8, 12	14
3	PCB40-40	70	2, 4, 8, 12	14
4	PCB20-20	70	4	14
5	PCB20-30	70	4	14
6	PCB20-40	70	4	14
7	PCB30-20	70	4	14
8	PCB30-30	70	4	14
9	PCB30-40	70	4	14

*PCB40-20: 40 wt% (K_2CO_3-equivalent) PCB solution with 20% CTB conversion, and so forth thereafter.

Table 2B-3. Test matrix for CO_2 absorption into promoted PCB and 5 M MEA solutions

No.	Initial solvent	Temp (°C)	L/G with 0.56 LPM liquid flow rate (L/m^3, under actual conditions)	CO_2 inlet concentration (vol%)
1	PCB40-20 + 1 M DEA*	70	4	14
2	PCB40-20 + 0.5 M DEA	70	2, 4, 8	14
3	PCB40-20 + 0.5 M DEA	70	4	8
4	PCB40-20 + 1 M AMP	70	4	14
5	PCB40-20 + 0.5 M AMP	70	2, 4, 8	14
6	PCB40-20 + 0.5 M AMP	70	4	8
7	PCB40-20 + 0.75 M PZ	70	4	14
8	PCB40-20 + 0.5 M PZ	70	2, 4, 8	14
9	PCB40-20 + 0.5 M PZ	70	4	8
10	PCB30-20 + 0.5 M PZ	70	4	14
11	PCB20-20 + 0.5 M PZ	70	4	14
12	5 M MEA	50	4	14

*PCB40-20 + 1 M DEA: PCB40-20 promoted with 1 M MEA promoter, and so forth thereafter.

Once a baseline removal was established for PCB at the desired PCB concentrations and CTB conversions, testing was done to evaluate the effectiveness of various rate promoters. This involved testing multiple amine promoters with differing dosages, as well as evaluating the effect of the L/G ratio and CO_2 inlet concentration on CO_2 removal effectiveness. The test matrix was set up such that only one variable at a time was changed from the predetermined baseline conditions so that the deviation could be measured easily. These tests were performed at 70°C.

As a reference, 5 M MEA was also tested, with the temperature set point at 50°C. The full test matrix for these solutions is shown in Table 2B-3.

After these tests were completed, other solvents were investigated for their absorption potential, including an SCB solution and PCB/SCB mixture solutions. These solutions were investigated in a fashion similar to PCB, whereby only one variable at a time was changed to see the effect of different variables, such as promoters, L/G ratios, SCB and PCB/SCB concentrations, and CO_2 inlet concentrations. The full test matrix is shown in Table 2B-4.

Table 2B-4. Test matrix for CO_2 absorption into SCB and PCB/SCB solutions

No.	Initial solvent*	Temp (°C)	L/G with 0.56 LPM liquid flow rate (L/m^3) under actual conditions	CO_2 inlet concentration (vol%)
1	SCB15-15	70	4, 12	14
2	SCB15-15 + 0.5 M PZ	70	4, 12	14
3	PCB25/SCB10-20 + 0.5 M PZ	70	4, 8, 12	14
4	PCB25/SCB10-20 + 0.5 M PZ	70	4	8
5	PCB25/SCB10-20 + 1 M DEA	70	4	14
6	PCB20/SCB15-20 + 0.5 M PZ	70	4	14
7	PCB12.5/SCB5-20 + 0.5 M PZ	70	4	14

*SCB15-15: 15 wt% (Na_2CO_3-equivalent) SCB solution with 15% CTB conversion; PCB25/SCB10-20: 25 wt% (K_2CO_3-equivalent) PCB and 10 wt% SCB (Na_2CO_3-equivalent) mixture solution with 20% CTB conversion, and so forth thereafter.

2B.2.3 Analysis of CO_2 loading

The CO_2 loading of a carbonate solution is a very important measure affecting CO_2 removal rates. As the solution flows down the column, it absorbs CO_2 in the form of bicarbonate, which increases the CTB conversion.

A Chittick apparatus, as shown in Figure 2B-3, was used to measure the CO_2 loading in the solution. During analysis, 1 mL of CO_2-laden sample was added to a 50-mL flask placed on a magnetic stirrer. The flask was connected to an adjustable graduated tube and a fluid reservoir, which contained a 1 M HCl solution and an acid solution. The 1 M HCl solution was introduced into the sample flask using a titration burette. When excess HCl acid was added to the sample, the CO_2 in solution was released by the following reactions:

$$CO_3^{2-} + 2H^+ \rightarrow CO_2 \uparrow + H_2O \quad \text{(2B-R1)}$$

$$HCO_3^- + H^+ \rightarrow CO_2 \uparrow + H_2O \quad \text{(2B-R2)}$$

$$RNHCOO^- + 2H^+ \rightarrow CO_2 \uparrow + RNH_3^+ \quad \text{(2B-R3)}$$

where RNH_3^+ is the protonated amine, $RNHCOO^-$ is the carbamate, and R is the hydrocarbon substitutes in an amine promoter.

As CO_2 was released from the PCB sample in the flask, the liquid in the graduated tube was displaced. The CO_2 loading in the sample was then calculated from the displaced liquid volume

(equal to the volume of CO_2 released). This technique was also used for measuring the loading of MEA solutions using exactly the same process, with slightly different reactions.

Figure 2B-3. Photograph of the Chittick apparatus used for the CO_2 loading measurement.

Although using the Chittick apparatus was accurate, it proved to be somewhat time consuming. Therefore, a different approach was also adopted as an alternative. During a test, CO_2 loading in the solution increased over time as the absorption of CO_2 continued. CO_2 loading was estimated from the measured CO_2 removal efficiency and the gas and liquid flow rates based on the mass balance principle using the initial CTB conversion (e.g., 20%). Because any CO_2 that was removed from the gas stream had to be absorbed into the liquid solution, with known reactions, the CTB conversion level could be estimated at a given time and could be related to the CO_2 absorption efficiency.

2B.2.4 Measurement of mass transfer coefficients

To determine the impact of mass transfer on the overall rate of CO_2 absorption, it was important to quantify the gas and liquid phase mass transfer coefficients of the bench-scale absorption column. These coefficients are directly related to the mass transfer resistance in the column and are important parameters in evaluating the CO_2 absorption performance. Literature data are available for packed-bed columns; however, a small difference in the setup can cause great variance in these correlations, thus measuring mass transfer in the current column was essential.

To determine the liquid phase mass transfer coefficient of the packed-bed column, the physical absorption of oxygen from air into water was studied. The solubility of oxygen in water is low and can be used sparingly as a soluble gas in the absorption. In this scenario, the overall mass transfer is dominated by the liquid phase, making it possible to calculate the liquid side mass transfer coefficient. This was done by introducing air from a cylinder into the bottom of the absorption column. The air flow rate was measured by the same calibrated mass flow meter as

was used in the CO_2 absorption tests. The water used in the experiment was deionized (DI) water sparged with nitrogen to minimize initial dissolved oxygen. The N_2-treated water was pumped to the top of the column and allowed to flow down through the column for O_2 absorption. Unlike in the CO_2 absorption tests, the spent water exiting the column was not recirculated in the system. The flow rate of water was varied along with the flow of air to cover the full operating range of the column. When the column reached a steady state at each preset condition, as indicated by a stable temperature profile along the column as well as a stable O_2 concentration in the liquid outlet, liquid samples were taken at the inlet and outlet. The liquid samples were analyzed for dissolved oxygen concentration using a dissolved oxygen meter (Hach, Model HQ30d).

Since the main resistance to mass transfer during physical absorption of oxygen into water is localized in the liquid phase, the individual liquid mass transfer coefficient could be approximated as the overall liquid phase coefficient:[1]

$$\frac{1}{K_L a_e} = \frac{1}{k_L a_e}, \tag{2B-2}$$

where $K_L a_e$ (s^{-1}) is the overall liquid phase mass transfer coefficient, $k_L a_e$ (s^{-1}) is the individual liquid phase mass transfer coefficient, and a_e (m^2/m^3) is the effective surface area of the packing material.

The following equation can thus be derived to calculate the individual liquid mass transfer coefficient based on the measurement of dissolved O_2 in water during absorption:[2]

$$k_L a_e = \frac{u_L}{Z} \times \ln\left(\frac{C^* - C_{L,in}}{C^* - C_{L,out}}\right), \tag{2B-3}$$

where C^* (mg/L) is the physical solubility of oxygen at the interface, $C_{L,in}$ and $C_{L,out}$ (mg/L) are the inlet and outlet concentrations of dissolved oxygen in the water, u_L (m/s) is the specific liquid flow rate, and Z (m) is the column packing height. The value of C^*, estimated based on Henry's law, is approximated as a constant because the change in O_2 concentration in air (21 vol%) during absorption is negligible.

To measure the gas phase mass transfer coefficient, the CO_2 absorption into a 1.0 M NaOH solution was measured. In the measurement, the inlet gas contained 4% CO_2 and the test was run at ambient temperature (~20°C). When absorption reached steady state, as indicated by a stable outlet CO_2 concentration and a stable temperature profile in the column, the inlet and outlet gas compositions were analyzed by the CO_2 analyzer. The NaOH solution was not recirculated to maintain high alkalinity of the solution.

The overall gas phase mass transfer coefficient ($K_G a_e$) is measured by the absorption of CO_2 into the NaOH solution at ambient temperature according to the following equation:[2]

$$K_G a_e = \frac{u_G}{Z} \times \ln\left(\frac{[CO_2]_{in}}{[CO_2]_{out}}\right), \tag{2B-4}$$

where $K_G a_e$ (s^{-1}) is the overall liquid phase mass transfer coefficient, u_G (m/s) is the gas velocity, and $[CO_2]_{in}$ and $[CO_2]_{out}$ (mol/L) are the CO_2 concentrations at the gas inlet and outlet, respectively. The relationship between the overall gas phase mass transfer coefficient and individual liquid and gas mass transfer coefficients is shown in the following equation:[1]

$$\frac{1}{K_G a_e} = \frac{1}{k_L a_e EH} + \frac{1}{k_G a_e}, \quad \text{(2B-5)}$$

where $k_G a_e$ (s^{-1}) is the individual gas phase mass transfer coefficient, E is the enhancement factor attributable to the chemical reaction, and H is the dimensionless Henry's constant. The value of E can be calculated as follows:[3,4]

$$E \approx Ha = \frac{\sqrt{D_{CO_2} k_{OH^-} [OH^-]}}{k_L}, \quad \text{(2B-6)}$$

where D_{CO_2} (m^2/s) is the diffusivity of CO_2 into NaOH solution, k_{OH^-} (L/mol·s) is the kinetic rate constant, and $[OH^-]$ (mol/L) is the OH^- concentration in the bulk solution. Using Eq. (2B-6) requires the absorption of CO_2 into NaOH solution to undergo a pseudo first-order reaction and the value of the Hatta number (*Ha*) to be greater than 3.

Once the overall gas phase mass transfer is determined by the CO_2 absorption measurement in NaOH solution [Eq. (2B-4)] and the individual liquid phase mass transfer coefficient by the O_2 absorption measurement [Eq. (2B-3)], the individual gas phase mass transfer coefficient of the column can be calculated from Eq. (2B-5).

It should be noted that, different from the CO_2 absorption tests, half of the structured packing (1 m high) in the column was removed in the measurements of mass transfer coefficients. This was done to ensure that both absorption processes were not completed throughout the packing in the column. The test matrix for the mass transfer coefficient measurements is presented in Table 2B-5. Different gas and liquid flow rates were selected to cover the typical design conditions of the absorption column.

Table 2B-5. Test matrix for the measurement of mass transfer coefficients of the packed-bed column

Test no.	Solvent used	Superficial gas velocity (m/s)	Superficial liquid velocity (cm/s)		
1	1 M NaOH	0.23	0.12	0.3	0.5
		0.34	0.12	0.3	0.5
		0.47	0.12	0.3	0.5
2	DI water	0.23	0.12	0.3	0.5
		0.34	0.12	0.3	0.5
		0.47	0.12	0.3	0.5

To validate the above-mentioned test methods, the mass transfer measurements were also conducted with 1-m stainless steel pall rings (with a specific surface area of 500 m^2/m^3) since data on random Pall rings is widely available in the literature. For this purpose, the mass transfer coefficients measured for the Pall ring packing were compared with those predicted by correlations developed by Onda *et al*.[5] because these correlations are well accepted for such columns.[6-8]

2B.4 Results and Discussion

2B.4.1 Determination of the mass transfer coefficients

2B.4.1.1 Liquid phase mass transfer coefficients

The measured individual liquid phase mass transfer coefficients (k_La_e) for the random Pall ring packing are shown in Figure 2B-4a. For each condition tested, the experimental values are very close to the correlations predicted by Onda *et al*.[5] The value of k_La_e was almost independent of the gas velocity. In comparison, changes in liquid velocity did have a considerable effect on the mass transfer. As the liquid flow rate was increased, the rate of liquid phase mass transfer also increased, which was due to a higher Reynolds number and thus better mixing in the liquid phase, and an increase in the effective area for gas–liquid absorption caused by greater wetting of the packing. Since these results for the Pall ring packing were consistent with the literature data,[2,9] the measurement methods were considered validated.

In comparison with the random packing, structured packing provides better mass transfer performance (Figure 2B-4b). The measured values of k_La_e for structured packing ranged between 0.0055 and 0.017 s^{-1}, 20-to-40% higher than those for random packing. This was expected because the structured packing is designed to have better mass transfer properties than the random packing, such as a higher specific surface area and improved wettability.

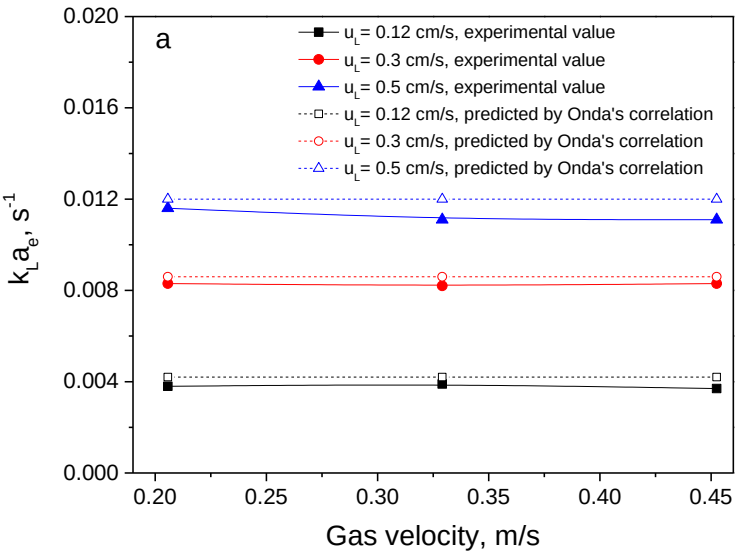

(a) Random packing

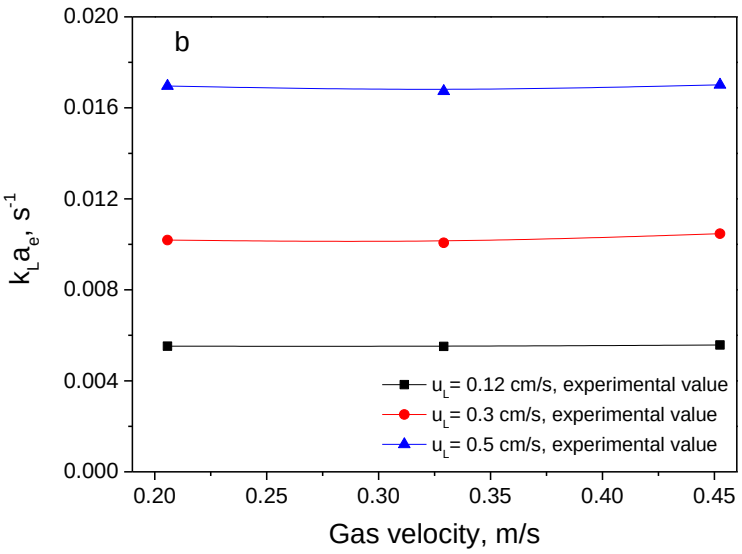

(b) Structured packing

Figure 2B-4. Liquid phase mass transfer coefficients in the packed-bed column with (a) random and (b) structured packing at varying gas flow rates at 20°C. (u_L: superficial liquid velocity).

2B.4.1.2 Gas phase mass transfer coefficients

The obtained values for the overall gas phase mass transfer coefficients ($K_G a_e$) for the random Pall ring packing tests are shown in Figure 2B-5. It is apparent that the $K_G a_e$ was nearly independent of the gas velocity, indicating that the liquid phase mass transfer might have been dominant under the test conditions. A comparison of the predicted and experimental values indicated they were in good agreement.

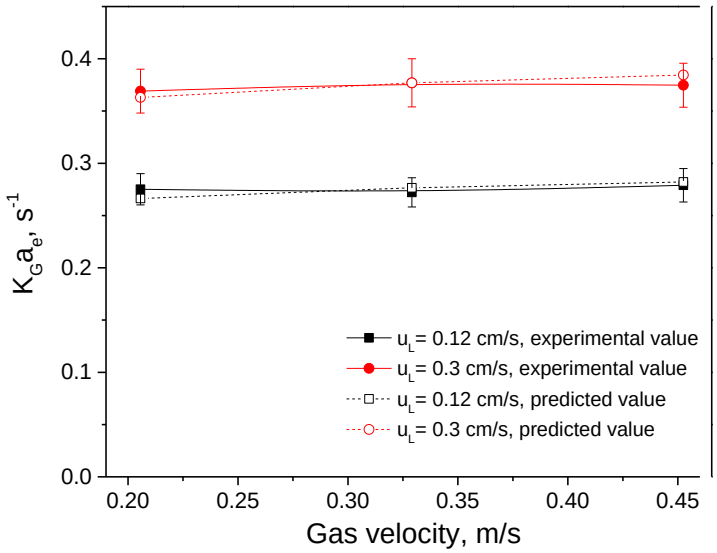

Figure 2B-5. Overall gas phase mass transfer coefficients in a packed-bed column with random packing at varying gas flow rates at room temperature. (u_L: superficial liquid velocity).

The $K_G a_e$ values increased as the liquid flow rate increased. This may be because a higher liquid velocity leads to a larger individual liquid mass transfer coefficient ($k_L a_e$), as well as a greater effective surface area from the improved liquid wetting. The measured $K_G a_e$ values for the random packing closely matched those calculated using Eq. (2B-5) when the experimental $k_L a_e$ values shown in Figure 2B-4 and the $k_G a_e$ values from the correlations by Onda *et al.* were used.

For the structured packing, the absorption of CO_2 into NaOH solution was controlled by the liquid phase, so it was not necessary to measure the overall gas phase mass transfer coefficients ($K_G a_e$). Instead, these coefficients were determined based on the fact that they are nearly equal to $k_L a_e EH$, according to Eq. (2B-5). The overall mass transfer coefficients were obtained by calculating the enhancement factor, E, and the individual liquid mass transfer coefficient, k_L, in NaOH solution, which could be estimated from $k_{L,water}$ by using the following correlation:[4]

$$k_{L,NaOH} = k_{L,water}\left(\frac{D_{CO2,NaOH}}{D_{CO2,water}}\right)^{0.6} \qquad \text{(2B-7)}$$

The values for $K_G a_e$ calculated using this alternative method in the column packed with the structured packing are shown in Figure 2B-6.

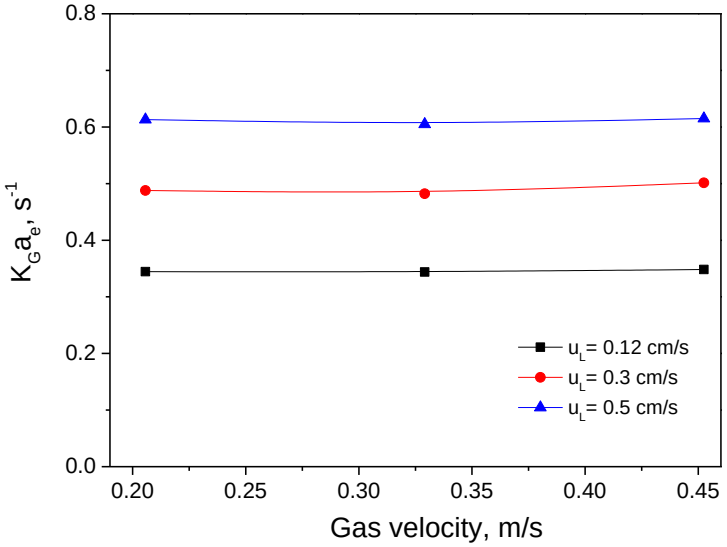

Figure 2B-6. Overall gas phase mass transfer coefficients in a packed-bed column with structured packing at varying gas flow rates at room temperature. (u_L: superficial liquid velocity).

2B.4.2 CO_2 absorption into PCB solutions without a promoter

Several tests were run on the 40 wt% PCB (PCB40) at CTB conversion rates of 20, 30, and 40%. The temperature in the column was held constant at 70°C (±5°C). The CO_2 concentration of the mixture gas at the inlet was 14 vol%. In these tests, the liquid flow was held constant at 0.56 LPM and the gas flow was varied from 47 to 280 L/min (LPM, at actual conditions). This led to a full range of the L/G ratios from 2 to 12 L/m^3, which were chosen based on the theoretical minimum L/G ratio (3.3 L/m^3) for PCB40 to achieve 90% CO_2 removal from flue gas in a full-scale column. Results of these tests are shown in Figure 2B-7. As the L/G ratio increased, greater

CO_2 removal was observed because of the increased gas residence time. The effect of solvent CO_2 loading on the CO_2 removal rate was also significant. As the CTB conversion increased, the CO_2 removal efficiency decreased, because of a reduced driving force for mass transfer. Note that to measure the removal efficiency of lean and rich solutions and all points in between, the solution was recycled back through the column. Therefore, over a long test period, the CO_2 loading in the inlet solution increased over time, simulating the complete working height of a full-sized absorption column. In general, depending on the L/G ratio and CTB conversion in the inlet solution, the efficiency of CO_2 removal using the un-promoted 40 wt% PCB solution varied between 3 and 25%.

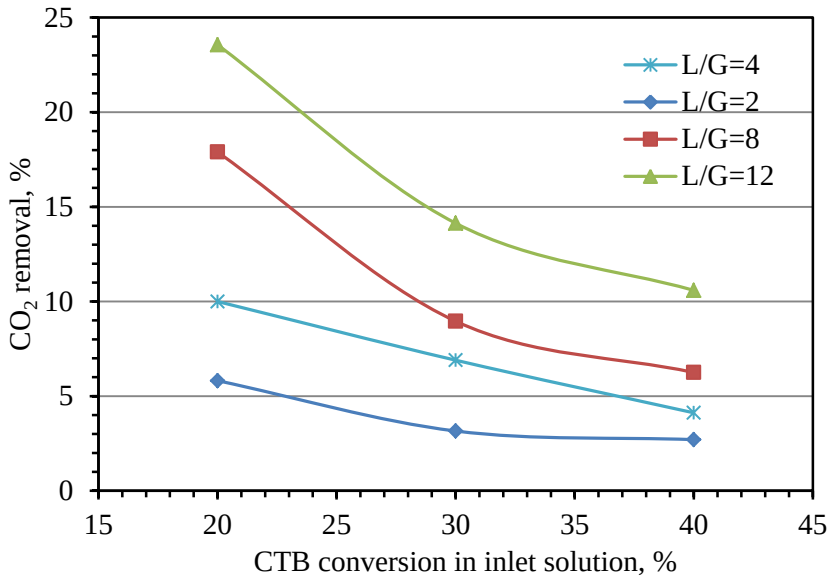

Figure 2B-7. CO_2 removal efficiency of un-promoted PCB40 solutions with varying L/G ratios and CTB conversions at 70°C, a liquid flow rate of 0.56 LPM, and a CO_2 inlet concentration of 14 vol%.

As mentioned, the 40 wt% PCB solution was adopted as a baseline in the Hot-CAP. However, for comparison purposes, PCB solutions at lower concentrations, i.e., 20 wt% (PCB20) and 30 wt% PCB (PCB30), were also tested. Results showed that the higher PCB concentration resulted in a slightly higher absorption of CO_2, especially under lean conditions (Figure 2B-8). However, such a difference was not great, and as the CO_2 loading increased, the difference caused by the different PCB concentrations was almost negligible. It was expected that there would not be much change in the removal efficiency, because it was limited by a slow reaction rate, rather than the lack of capacity of the PCB solution, which was being varied in the tests.

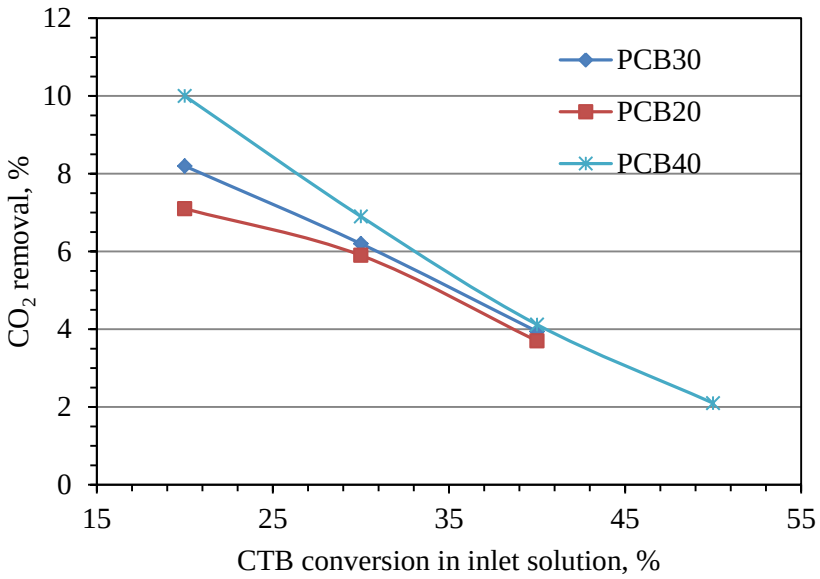

Figure 2B-8. CO_2 removal efficiency in PCB solutions with varying concentrations at 70°C absorption, a liquid flow rate of 0.56 LPM, an L/G ratio of 4 L/m^3, and a CO_2 inlet concentration of 14 vol%.

CO_2 removal rates for un-promoted PCB solutions were tested at both a baseline temperature of 70°C and an increased temperature of 80°C. From these tests (data not shown), it can be seen that CO_2 removal efficiency values in both the PCB40-20 and PCB40-30 solutions were slightly higher at 80°C. As the temperature was increased, the kinetic rate of CO_2 absorption increased, whereas the solubility of CO_2 in the solution (i.e., the mass transfer driving force) decreased. The results thus indicate that the effect of temperature on CO_2 solubility was smaller than that on the kinetics of CO_2 absorption.

2B.4.3 CO_2 absorption into the PCB solution with a promoter

Effects of L/G ratio and CO_2 loading. Tests were conducted on PCB40 with the addition of 0.5 M promoter to investigate the effects of L/G ratio and CO_2 loading on the efficiency of CO_2 removal. The inlet CO_2 concentration was kept at 14 vol% and the absorber operated at 70°C. The L/G ratio was varied at 2, 4, and 8 L/m^3, equivalent to 0.61, 1.21, and 2.42 times the theoretical minimum L/G for PCB40. The L/G ratios were varied by varying the gas rate while keeping the liquid flow rate constant (0.56 LPM).

As shown in Figure 2B-9, all three promoters showed similar behavior. Results revealed that the CO_2 absorption rate increased with increasing L/G ratios for all the promoters. In the PCB40 + 0.5 M PZ solution, increasing the L/G ratio from 2 to 4 increased the CO_2 removal efficiency by 20 to 30%, depending on the solvent CO_2 loading. The performance at higher L/G ratios was improved because of the enhanced gas–liquid contact and increased gas residence time. It was also observed that the CO_2 removal efficiency decreased significantly with increasing CO_2 loading, mirroring the results in the un-promoted solution. For the PCB40 + 0.5 M DEA, the CO_2 removal efficiency decreased from 50 to 15% at an L/G ratio of 4 when the CTB conversion at the inlet increased from 20 to 40%. This was caused by the reduced mass transfer driving force

for CO_2 absorption as the CO_2 loading in the solution increased. It is worth noting that the addition of 0.5 M PZ most effectively promoted CO_2 absorption into PCB40, followed by the addition of 0.5 M AMP and 0.5 M DEA. The better performance for the PZ promoter was mainly due to its higher reactivity with CO_2 to form carbamate and dicarbamate species.

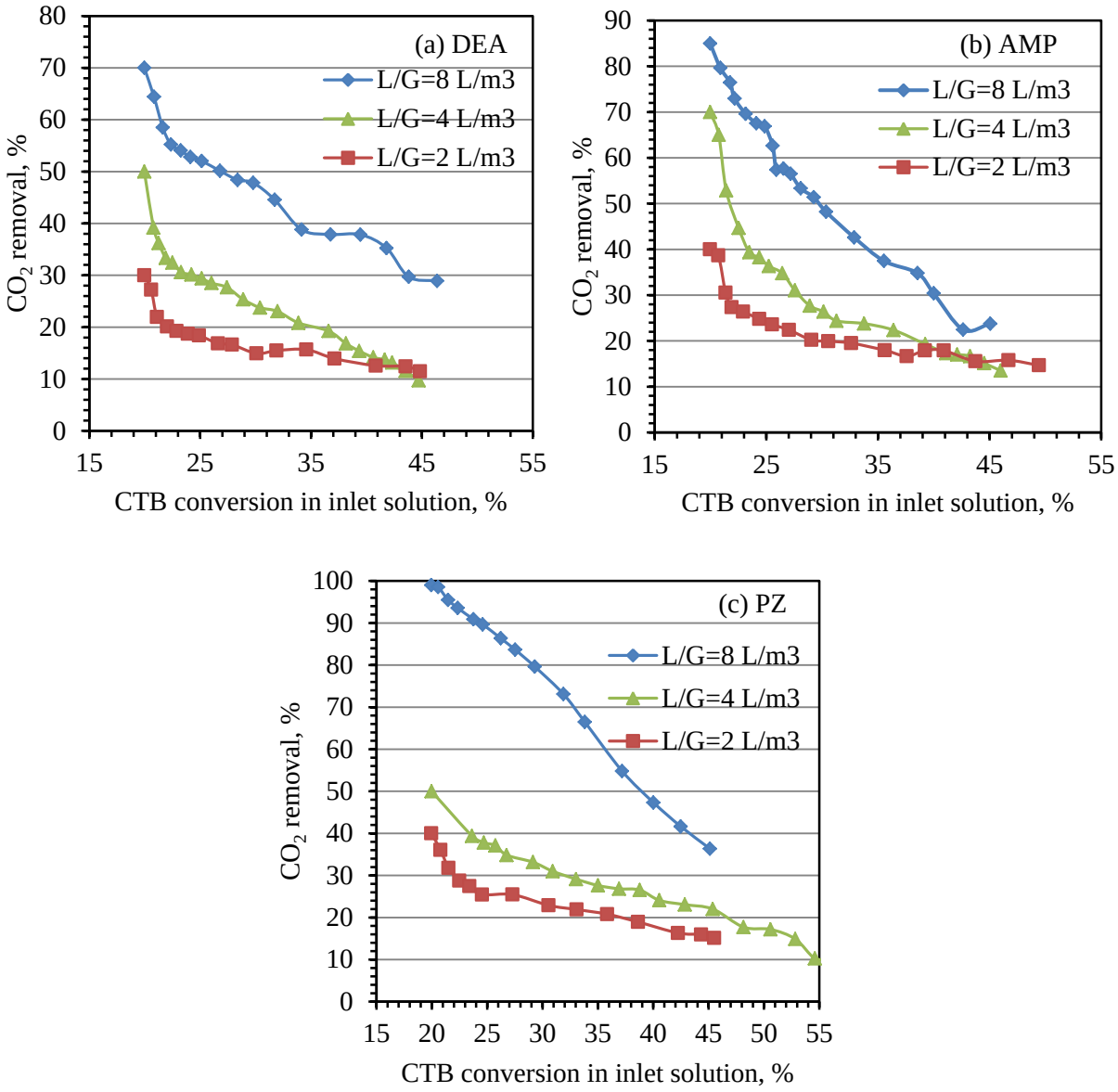

Figure 2B-9. CO_2 removal in the 40 wt% PCB solution promoted with (a) 0.5 M DEA, (b) 0.5 M AMP, and (c) 0.5 M PZ with varying L/G ratios and CO_2 conversions at 70°C absorption, a liquid flow rate of 0.56 LPM, and an inlet CO_2 concentration of 14 vol%.

Effect of inlet CO_2 concentration. The inlet CO_2 concentration was varied from 14 to 8 vol% to investigate its effect on the efficiency of CO_2 removal. Results for the two CO_2 inlet concentrations are shown in Figure 2B-10 for each of the three promoters.

It can be seen that a higher inlet CO_2 concentration resulted in lower CO_2 removal efficiency under the same conditions. At a higher inlet CO_2 concentration, a larger amount of CO_2 needed to be removed to achieve the same removal efficiency. At the same time, a higher inlet CO_2 concentration led to a larger driving force for CO_2 absorption. The reduction in CO_2 removal efficiency at a higher inlet CO_2 concentration indicates that the increase in the CO_2 removal rate was less than the increase in the rate of CO_2 inflow. Among the three solutions, the effect of inlet CO_2 concentration was more significant for the PCB + PZ than the PCB + AMP or PCB + DEA solutions.

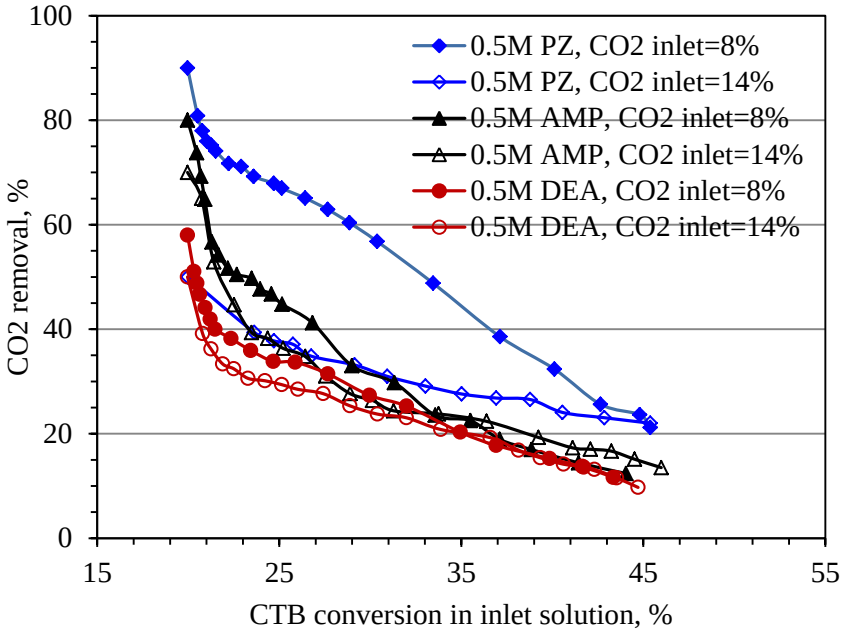

Figure 2B-10. CO_2 removal efficiency in the 40 wt% PCB solution promoted with 0.5 M DEA, AMP, or PZ at two different inlet CO_2 concentrations (absorption at L/G = 4 L/m^3 and 70°C).

Effect of promoter dosage. The dosage of the promoters in the PCB40 solution was increased to 1 M for DEA and AMP, and 0.75 M for PZ to investigate the impact on CO_2 removal efficiency. The higher PZ dosage of 0.75 M was selected due to solubility and precipitation concerns for the PCB + PZ solution. The results shown in Figure 2B-11 compare this higher dosage with the 0.5 M baseline dosage. All three promoters showed that the CO_2 removal efficiency increased with increasing promoter dosage when all other test conditions were the same. This increase in removal efficiency was mainly due to the faster CO_2 absorption reactions in the presence of a larger amount of amine promoter, according to a "shuttle" mechanism.[10]

The PCB solution promoted with 0.75 M PZ compared with 0.5 M PZ showed the greatest increase in removal efficiency. As a result of the solubility issue with the PCB40 + 0.75 M PZ, there was precipitation in the column from the very beginning of the test, and the longer the solution was circulated, the more precipitation accumulated on the packing. Since some of the promoter or $KHCO_3$ was immobilized in the packing during this test, it is difficult to compare it directly with other tests, because the hydrodynamic performance of the packing column might be different. When the 1 M dosage of AMP was used, it improved the removal rate by 18% at the lean loading (20% CTB conversion) and by 48% at the rich loading (45% CTB conversion) over

the 0.5 M dosage in PCB40. Similar behavior was seen with the addition of 1 M DEA in PCB40: at the lean loading, the removal efficiency was 23% better than with the addition of the 0.5 M dosage, and at the rich loading, the efficiency was 50% better.

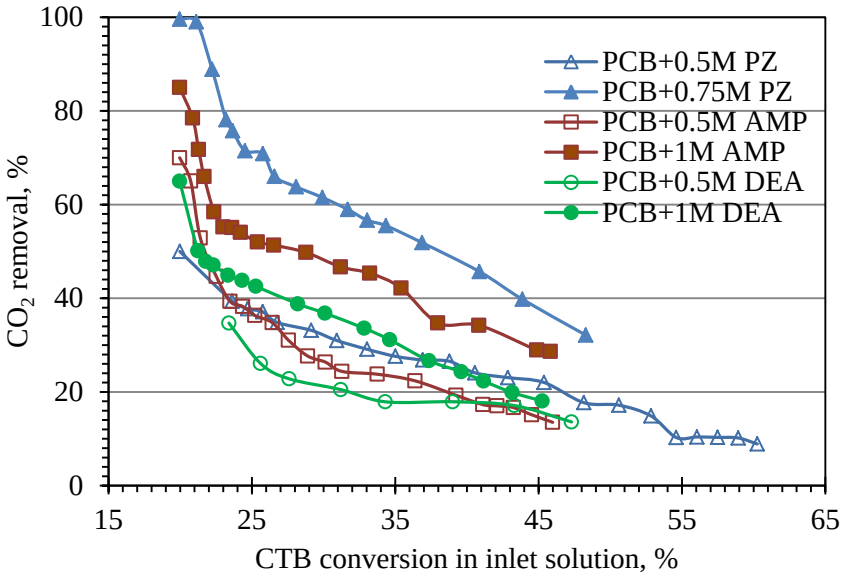

Figure 2B-11. CO_2 removal efficiency in the 40 wt% PCB solution at two promoter dosage levels (CO_2 absorption at L/G = 4 L/m^3, an inlet CO_2 concentration of 14 vol%, and 70°C).

Effect of PCB concentration. Lower PCB concentrations (20 and 30 wt%) were also tested to examine the impact on CO_2 removal rate. The results of tests with PCB concentrations varying from 20 to 40 wt% are shown in Figure 2B-12. All solutions were promoted with 0.5 M PZ.

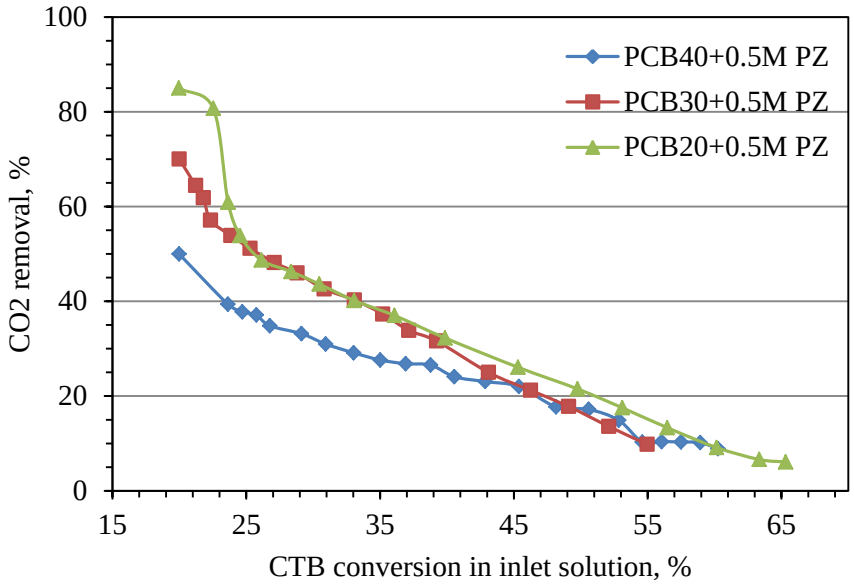

Figure 2B-12. Effect of PCB concentration on CO_2 removal, promoted with 0.5 M PZ (CO_2 absorption at L/G = 4 L/m^3, an inlet CO_2 concentration of 14 vol%, and 70°C).

Results revealed that PCB20 had the highest CO_2 removal efficiency, followed by PCB30 and finally PCB40 at the same CTB conversion. According to the literature, absorption rates of PCB solutions first increase with increasing concentration and then pass through a maximum on the Kuznets curve. This might be accounted for by increases in viscosity and ionic strength, and changes in VLE behavior as the concentration increases. Although PCB20 featured the highest CO_2 removal rate among the tested PCB solutions, it had the lowest working capacity at the same variation in CTB conversion. The PCB concentration should thus be selected based on the trade-off between CO_2 removal rate and working capacity.

Effect of $KHCO_3$ precipitation on CO_2 absorption. To investigate the impact of $KHCO_3$ precipitation, the rates of CO_2 absorption into the promoted PCB40 solutions were tested for an extended period of time even after precipitates occurred. The solubility limit of $KHCO_3$ in PCB40 solution is equivalent to approximately 50% CTB conversion at 70°C. This corresponds to precipitation occurring at approximately 40% inlet CTB conversion, because at a CO_2 removal efficiency of 30%, for example, the CTB conversion changes by approximately 11% as the solution runs through the packed column. Precipitation of $KHCO_3$ would be expected to result in a decrease in total PCB concentration. However, as shown in Figure 2B-13, the data for high CTB conversion levels show that the CO_2 removal efficiency remained relatively stable and no sharp decline was seen after $KHCO_3$ precipitates were present and accumulated in the PCB solution over time. No plugging associated with precipitation in the structured packing was observed during the tests. Similar results for CO_2 absorption in the presence of precipitates were seen in the PCB40 solution promoted with PZ, AMP, or DEA. These results suggest that it is possible for CO_2 absorption to operate in the presence of $KHCO_3$ precipitation without adversely affecting the rate of absorption, provided the equipment can handle slurry operation.

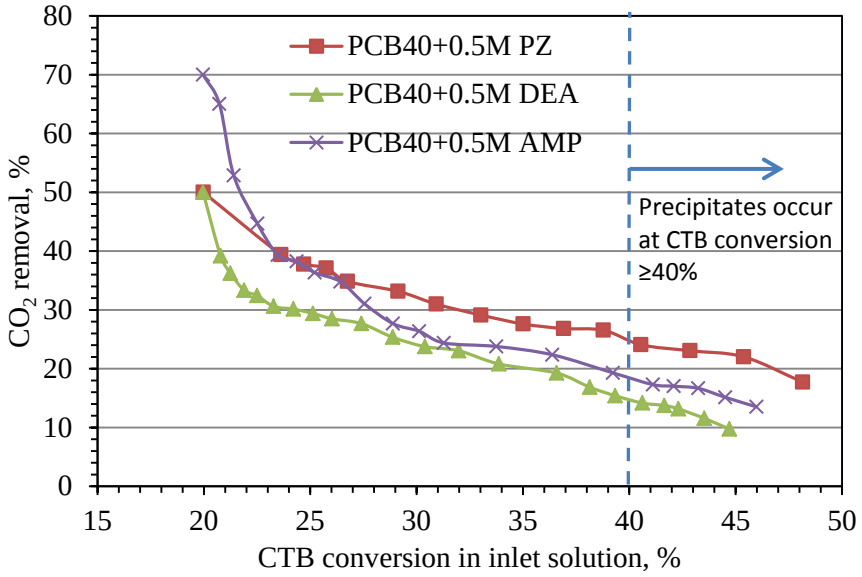

Figure 2B-13. CO_2 absorption performance in the promoted PCB40 solution without and with the occurrence of precipitation (CO_2 absorption at L/G = 4 L/m^3, an inlet CO_2 concentration of 14 vol%, and 70°C).

Comparison with the benchmark 5 M MEA solution. Figure 2B-14 compares the results of tests performed with un-promoted PCB40 and PCB40 promoted with PZ, DEA, or AMP at the baseline dosage of 0.5 M, and a 5 M MEA solution for their effectiveness at CO_2 removal. The absorption temperature used was 70°C for the PCB without or with a promoter and 50°C for the MEA solution, which are typical of the Hot-CAP and MEA processes, respectively. The other variables were kept at the baseline conditions, i.e., an L/G ratio of 4 L/m^3, a CO_2 inlet concentration of 14 vol%, and a liquid flow rate of 0.56 LPM. Since PCB and MEA absorb CO_2 through different chemical pathways, the reporting method for CO_2 loading is different. The Hot-CAP uses PCB40 solution with a lean CO_2 loading equivalent to 15 to 20% CTB conversion and a rich CO_2 loading equivalent to 40 to 45% CTB conversion. In comparison, the MEA process operates with 5 M MEA at a lean CO_2 loading of about 0.2 mol of CO_2/mol of MEA and a rich loading of about 0.4 to 0.45 mol/mol. Therefore, the CO_2 removal efficiencies at these corresponding lean and rich values were compared.

The comparison showed a significant increase in the CO_2 removal rate for each of the promoters used over the un-promoted PCB solution. At the lean CO_2 loading, CO_2 absorption was increased by 5-to-7 times with the promoters; and at the rich loading (e.g., a CTB conversion of 45%), the rate was promoted by 3-to-7 times. Both the promoted and un-promoted PCB solutions showed similar trends over the CTB conversion range tested; as the CO_2 loading increased, CO_2 absorption from the simulated flue gas declined. The promoters tested indeed increased the rate of CO_2 absorption into the concentrated PCB solution significantly, by about 5 times on average, over their un-promoted counterparts.

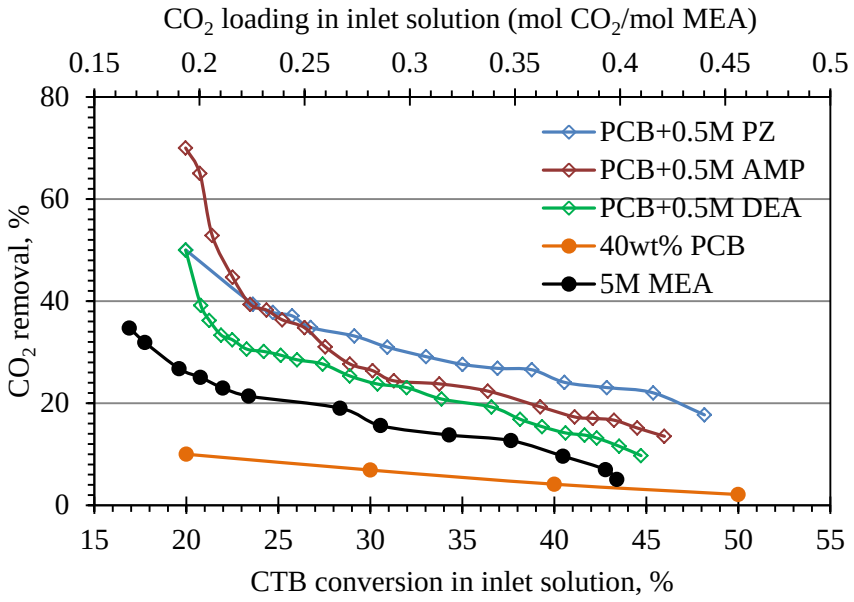

Figure 2B-14. Comparison of CO_2 removal efficiency in a 5 M MEA solution at 50°C and in PCB40 solutions with and without promoters at 70°C (CO_2 absorption at an inlet CO_2 concentration of 14 vol% and L/G = 4 L/m^3).

From these data, it was observed that the PCB40 solution promoted with AMP had the highest initial CO_2 removal efficiency. However, the efficiency declined quickly as the CTB conversion increased. By 25% CTB conversion in the inlet solution, the PCB40 solution promoted with PZ

had a higher removal efficiency. The PCB solution promoted with DEA began with the same removal as that promoted with PZ, but quickly declined as the CO_2 loading increased. Over the entire lean-to-rich loading range (20 to 45% CTB conversion), the addition of PZ gave the highest CO_2 removal.

The promoted PCB solutions outperformed 5 M MEA solution. At a lean loading of 0.2 mol of CO_2/mol of MEA, 5 M MEA had a removal efficiency of 25%; and at a rich loading of 0.4 mol/mol, only 5% of the CO_2 was removed. On the basis of the trends observed in these experiments, CO_2 removal rates into the promoted lean and rich PCB solutions at 70°C were considerably higher than their respective 5 M MEA counterparts at 50°C. At the lean loading, CO_2 removal rates in the promoted PCB were 1-to-3 times higher than with 5 M MEA; and at the rich loading, there was an even higher discrepancy with rates 3-to-5 times higher than 5 M MEA solution.

2B.4.4 CO_2 absorption into an SCB solution

An SCB solution can potentially be used as an alternative carbonate-based solvent to the PCB solution in the Hot-CAP. SCB has some advantages over PCB, including the fact that sodium bicarbonate ($NaHCO_3$) can more easily precipitate out via cooling to form a $NaHCO_3$ slurry for CO_2 stripping, because it has lower solubility than does $KHCO_3$. In addition, a $NaHCO_3$ slurry can produce a higher stripping pressure than can a $KHCO_3$ slurry, because the CO_2 equilibrium pressure over SCB is higher than that over PCB.

Similar absorption tests were performed with SCB solutions (Table 2B-4). Because the solubility of $NaHCO_3$ is much lower than that of $KHCO_3$, a SCB solution with a total concentration (Na_2CO_3-equivalent) of 15 wt% (SCB15) was used instead of the 40 wt% concentration for PCB. To meet the comparable goal of CO_2 removal with this lower concentration, a wider operating range of CTB conversion, e.g., from 15% (lean) to 55-to-60% (rich), might be required for the SCB15 if similar conditions are used for both the SCB15 and PCB40 solvents.

To establish a baseline to compare the promoted SCB15 solution, un-promoted SCB15 was first tested at L/G ratios of 4 and 12 L/m^3, which are equivalent to 0.55 and 1.65 times the minimum L/G, respectively, based on the VLE data in the literature.[11] Results for the CO_2 absorption at varying L/G ratios and CTB conversions are shown in Figure 2B-15.

The addition of 0.5 M PZ into the SCB solution significantly promoted the rate of CO_2 absorption. Figure 2B-15 also shows CO_2 removal by SCB15 solutions promoted by 0.5 M PZ at L/G ratios of 4, 8, and 12 L/m^3, which are equivalent to 0.55, 1.10, and 1.65 times the minimum L/G. For the SCB15 + 0.5 M PZ solution at the L/G ratio of 4 L/m^3, the solution with 15% initial CTB conversion removed 50% of the CO_2, whereas that with 60% initial CTB conversion removed 15% of the CO_2. When the L/G ratio was increased to 12 L/m^3, the removal efficiency increased significantly, but again a larger difference was seen at a lower CTB conversion. At a 15% initial CTB conversion, the higher L/G of 12 resulted in 90% removal of the CO_2, and at a 60% initial CTB conversion, it removed 20% of the CO_2. This showed an increase in removal efficiency of 80% in the lean SCB + PZ solution, but only 30% in the rich solution. As described

earlier, higher CO_2 removal efficiencies at higher L/G ratios can be attributed to better gas–liquid contact and longer gas residence times.

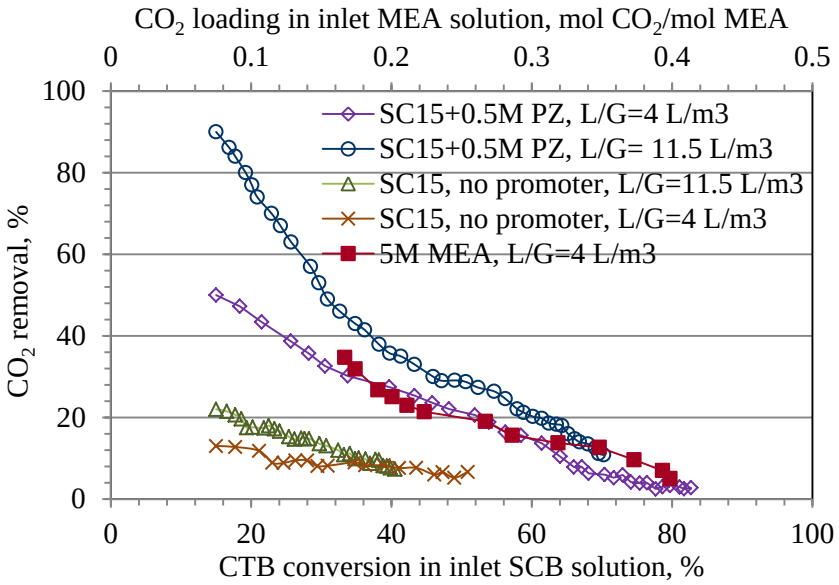

Figure 2B-15. CO_2 removal by the SCB15 solution promoted with 0.5 M PZ at varying L/G ratios (absorption at a CO_2 inlet concentration of 14 vol% and 70°C).

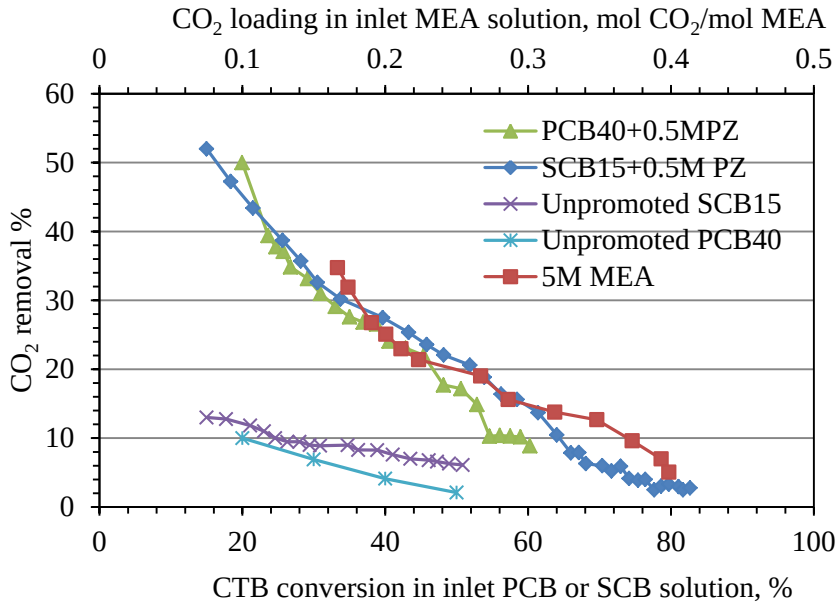

Figure 2B-16. Comparison of CO_2 removal rates in un-promoted and promoted SCB15, un-promoted and promoted PCB40, and 5 M MEA (absorption at an L/G ratio of 4 L/m^3, a CO_2 inlet concentration of 14 vol%, and 70°C for SCB or PCB and 50°C for MEA).

In Figure 2B-16, the results of the un-promoted SCB15 and the SCB15 promoted with 0.5 M PZ are compared with those of 5 M MEA, un-promoted PCB40, and PCB40 promoted with 0.5 M PZ. All these data are from tests conducted at the same conditions, with an L/G ratio of 4 L/m^3, a

CO_2 inlet concentration of 14 vol%, and a temperature of 70°C. The un-promoted SCB15 had a slightly higher removal rate than did the un-promoted PCB40. This was to be expected based on the previous discussion on the effect of PCB concentration on CO_2 removal, because SCB follows a similar trend of having a maximum removal efficiency at 10 to 20 wt%.[12]

The addition of 0.5 M PZ significantly promoted the rate of CO_2 absorption into the SCB15 solution: the removal was amplified by about 3.8 times for the lean solution (15% initial CTB conversion) and by 3.5 times for a rich solution (50% CTB conversion) over the respective un-promoted solutions. It is clear that the addition of PZ promoter into the SCB solution was as effective as its addition to the PCB solution to promote the absorption of CO_2.

As described before, the CO_2 loading in a typical MEA absorber changes from approximately 0.20 mol/mol (lean) to 0.45 mol/mol (rich) as the solution runs through the column. For the SCB absorber, the CTB conversion change from 15% at the top to 55 to 60% at the bottom is desired to achieve 90% CO_2 removal, based on the VLE behavior of SCB15. Figure 2B-16 also shows that at the same L/G ratio (4 L/m^3), the SCB15 + 0.5 M PZ had a CO_2 removal efficiency at 70°C that was higher than that of the 5 M MEA solution, with the corresponding CO_2 loading range at 50°C.

2B.4.5 CO_2 absorption into the PCB/SCB mixture

A mixture solution of PCB (25 wt%, K_2CO_3-equivalent) and SCB (10 wt%, Na_2CO_3-equivalent), symbolized as PCB25/SCB10, was also tested. The composition of the solution was selected based on the observation, from a preliminary crystallization test in a continuous stirred tank reactor, that by cooling the CO_2-rich PCB25/SCB10 with a CO_2 loading equivalent to 40% CTB conversion from 70 to 35°C, $NaHCO_3$ crystal (in the form of nahcolite) was a dominant phase. Since a mixture would be advantageous for the crystallization operation owing to its lower solubility compared with a plain PCB solution while still maintaining a high solvent concentration compared with a plain SCB solution, the absorption performance of the mixture solution was tested to investigate whether it was comparable with the promoted PCB40 and other solutions tested. In the test, an L/G ratio of 4 L/m^3 was chosen as the baseline for the SCB25/PCB10 solution for comparison purposes, because the VLE data for this solution was not available. A dose of 0.5 M PZ was used as a baseline promoter for the PCB/SCB solutions.

The effects of L/G ratio and CO_2 loading on CO_2 removal were investigated in the PCB/SCB solutions in the same manner as previously performed in plain PCB or SCB solutions (Figure 2B-17). Similar to the PCB and SCB solutions, at the same inlet CTB conversion, the rate of CO_2 absorption into the PCB/SCB solution increased with increasing L/G ratio. At L/G = 4 L/m^3 and an inlet CO_2 concentration of 14%, the PCB25/SCB10 solution with 20% initial CTB conversion removed about 60% of the CO_2, whereas the solution with 45% initial CTB conversion removed 17% of the CO_2. When the L/G ratio was increased to 8 and 12 L/m^3, the removal efficiency increased, but a larger difference was seen at lower levels of CTB conversion. When the L/G was increased from 4 to 8 L/m^3, the removal efficiency increased by 33% in the lean solution and 18% in the rich solution.

Tests were also conducted by varying the inlet CO_2 concentration from 14 to 8 vol%, with the other conditions held constant (L/G = 4 L/m^3). At a lower CO_2 inlet concentration, the CO_2 removal efficiency of the lean PCB25/SCB10 + 0.5 M PZ solution increased. However, the removal efficiency was almost identical to that under the rich solution conditions.

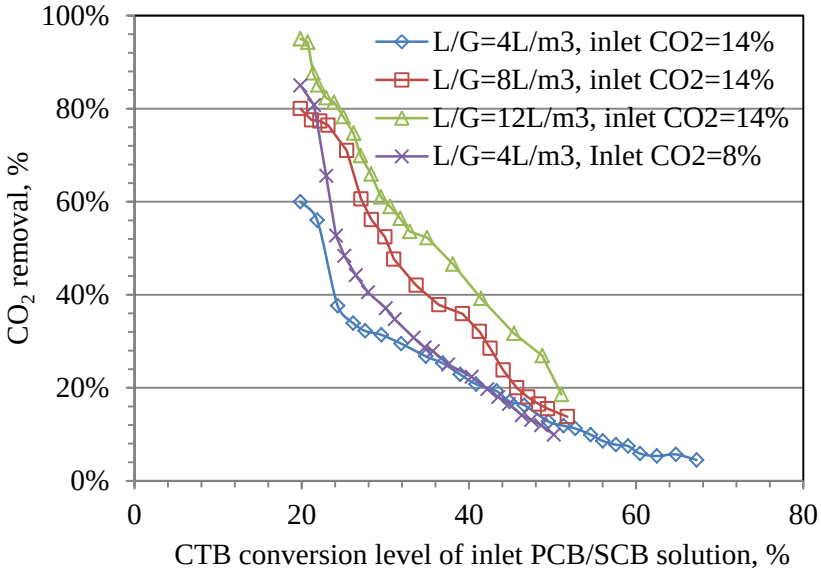

Figure 2B-17. CO_2 removal by the PCB25/SCB10 + 0.5 M PZ solution at 70°C at varying L/G ratios (4, 8, and 12 L/m^3) and CO_2 inlet concentrations (14 and 8 vol%).

As with the plain PCB or SCB, it was important to see how different promoters increased the CO_2 absorption rate into the PCB/SCB mixture solution. Other mixture solutions included PCB20/SCB15, which had a slightly higher total SCB concentration and a lower total PCB concentration, as well as PCB12.5/SCB5, which represented both a lower PCB and a lower SCB concentration. The PCB20/SCB15 and PCB25/SCB10 solutions promoted with 0.5 M PZ had a similar total concentration of PCB and SCB. As shown in Figure 2B-18, the removal efficiency was comparable at corresponding CTB conversion levels; they absorbed about 60% of the CO_2 at a 20% inlet CTB conversion and absorbed about 20% at a 40% inlet CTB conversion. The PCB25/SCB10 solution performed slightly better than the PCB20/SCB15 solution. The PCB12.5/SCB5 solution, which had the lowest total PCB and SCB concentration, had the highest removal efficiency among all of the solutions tested. This trend was previously reported for PCB and SCB. However, a low-concentration solution may not necessarily be a good option, because even with a higher removal efficiency, a larger flow rate of liquid is required to achieve the same amount of CO_2 removal; alternatively, a richer CO_2 loading level, corresponding to a lower mass transfer driving force and thus kinetics, is required to increase the CO_2 absorption capacity. It was also observed that bicarbonate precipitation was less likely to occur in the tested PCB/SCB mixture solutions than in the plain PCB solutions at similar CO_2 loadings.

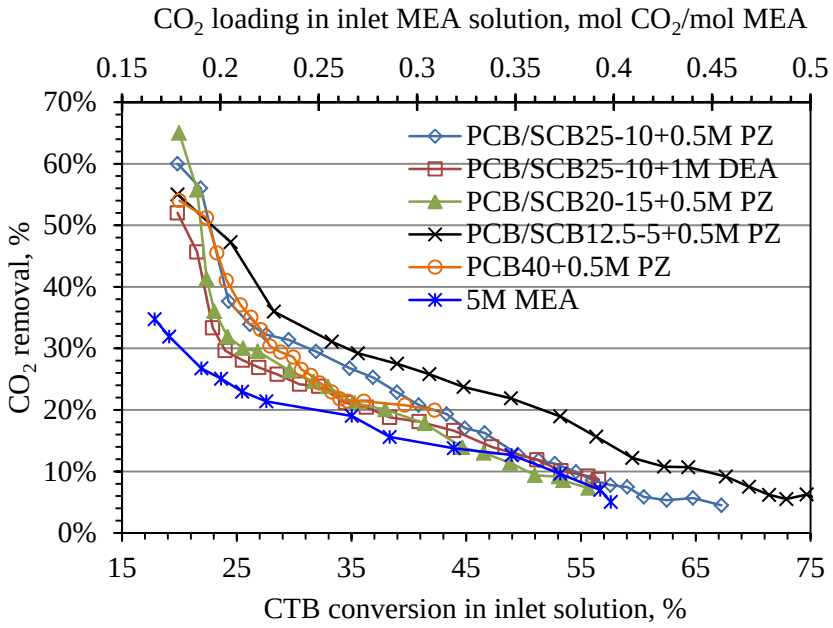

Figure 2B-18. CO_2 removal by 5 M MEA and PCB/SCB solutions (PCB25/SCB10, PCB20/SCB15, PCB12.5/SCB5, and PCB40) promoted with 0.5 M PZ or 1 M DEA. The PCB/SCB solutions were tested at 70°C, and the MEA was tested at 50°C at an inlet CO_2 of 14 vol% and an L/G ratio of 4 L/m^3.

CO_2 absorption into a PCB25/SCB10 mixture promoted with 0.5 M PZ was compared with the same mixture promoted with 1 M DEA, when all other conditions were the same (also shown in Figure 2B-18). At CTB conversion levels less than 50%, the PCB25/SCB10 solution promoted with 0.5 M PZ performed slightly better than the same solution promoted with 1 M DEA. As the CTB conversion increased to more than 50%, the CO_2 removal efficiencies of these solutions became comparable with each other. Throughout the entire CTB conversion range, the addition of 0.5 M PZ was more effective than the addition of 1 M DEA in promoting the rate of CO_2 absorption into the PCB/SCB solution.

The absorption results of the baseline PCB25/SCB10 + 0.5 M PZ mixture were compared with previous data gathered for 5 M MEA and PCB40 promoted with 0.5 M PZ. The results of the CO_2 removal efficiency as a function of CTB conversion are shown in Figure 2B-18.

The temperature used for the tests with the promoted PCB25/SCB10 and PCB40 solutions was 70°C and the tests with 5 M MEA solution were conducted at 50°C. All other conditions, such as the L/G ratio (4 L/m^3) and liquid flow rate (0.56 LPM), were again held the same for comparison purposes. At the same L/G ratio, both the PZ-promoted PCB25/SCB10 and PCB40 solutions outperformed 5 M MEA solution in terms of CO_2 removal efficiencies under either CO_2-lean or CO_2-rich conditions. The PCB25/SCB10 and PCB40 solutions with a 20% inlet CTB conversion removed 60% and 54%, respectively, whereas 5 M MEA with 0.20 mol/mol CO_2 loading absorbed 25% of the CO_2. This tendency continued as the CO_2 loading increased in each of the solutions.

2B.5 Summary

A bench-scale packed-bed column was designed to test the kinetic performance of CO_2 absorption into hot carbonate solutions. Gas and liquid phase mass transfer coefficients of the column were determined experimentally. The overall liquid phase coefficient was measured by the absorption of O_2 in air into water, assuming O_2 is a sparingly soluble gas. The overall gas phase coefficient was measured by the absorption of CO_2 into a 1 M NaOH solution. The measurement methods were validated by the good agreement between the measured mass transfer values and those reported in the literature for random Pall ring packing. Consequently, the mass transfer coefficients for the bench-scale column filled with the structured packing were obtained: $k_L a_e$ ranging from 0.0055 to 0.017 s^{-1} and $K_G a_e$ ranging from 0.34 to 0.61 s^{-1} for gas velocities ranging from 0.23 to 0.47 m/s and liquid velocities ranging from 0.0012 to 0.005 m/s. The results confirmed that the structured packing provided more efficient mass transfer than the random packing.

Parametric tests were conducted in the bench-scale packed-bed column to evaluate the CO_2 removal performance of the 40 wt% PCB solution without and with a promoter. Three promoters, AMP, DEA, and PZ, were selected in the tests. The process parameters investigated included dosage of the promoter, L/G ratio, inlet CO_2 concentration, and CO_2 loading in solution. Results confirmed that in all the PCB solutions tested, the CO_2 removal rate increased as the L/G ratio increased, as the promoter dosage increased, as the CO_2 loading decreased, or as the inlet CO_2 concentration decreased. It was observed that the precipitation of $KHCO_3$ occurred at a CTB conversion rate of 40 to 45%. However, the accumulation of precipitates in the PCB solution did not result in a pronounced decrease in CO_2 removal efficiency. Results also revealed that the use of rate promoters greatly increased the rate of CO_2 removal into the PCB solution. Among the promoters tested, the addition of PZ to the PCB solution was the most effective in accelerating the rate.

CO_2 absorption into the promoted 40 wt% PCB and 5 M MEA were compared over their typical operating ranges of CO_2 loading. The concentrated PCB40 solution promoted with 0.5 M PZ, DEA, or AMP tested at 70°C performed 1-to-3 times better than 5 M MEA at 50°C at the representative lean loading levels, and 3-to-5 times better at the rich CO_2 loading levels when all other conditions were the same.

If desired, an SCB or PCB/SCB solution can potentially be used as an alternative solvent to a PCB solution in the Hot-CAP. $NaHCO_3$ may be crystallized more easily than or preferentially over $KHCO_3$ from the CO_2-rich solution via cooling crystallization to form a $NaHCO_3$-based slurry that can be used for CO_2 stripping at a higher pressure than can a $KHCO_3$ slurry. A lower concentration of SCB (15 wt%) was tested and compared with PCB, because of its lower solubility. The SCB solution promoted with 0.5 M PZ exhibited a higher CO_2 removal efficiency at 70°C than 5 M MEA solution at 50°C within the corresponding CO_2 loading range. The promoted SCB solution is as effective as the PCB solution in promoting CO_2 absorption.

The performance of CO_2 absorption into PCB/SCB mixtures varied with the PCB and SCB concentration. Mixtures with similar total PCB and SCB concentrations revealed comparable CO_2 removal efficiencies, whereas at the same total concentration, the one with a higher PCB

concentration showed slightly higher CO_2 removal efficiency. All the tested PCB/SCB solutions promoted with 0.5 M PZ at 70°C outperformed 5 M MEA solution at 50°C at their representative lean and rich conditions. The PCB25/SCB10 solution promoted with 0.5 M PZ had a CO_2 removal efficiency at 70°C comparable with that of the promoted PCB40 and a removal efficiency significantly higher than 5 M MEA at 50°C.

References

1. Bird R.B., Stewart W.E., Lightfoot E.N. *Transport Phenomena,* revised 2nd edition. John Wiley & Sons Inc., New York, 2006.
2. Kim S., Deshusses M.A. Determination of mass transfer coefficients for packing materials used in biofilters and biotrickling filters for air pollution control. 1. Experimental results. *Chemical Engineering Science* 2008, *63*, 841–855.
3. Cents A.H.G., Brilman D.W.F, Versteeg G.F. CO_2 absorption in carbonate/bicarbonate solutions: the Danckwerts-criterion revisited. *Chemical Engineering Science* 2005, *60,* 5830–5835
4. Liao C., Li M. Kinetics of absorption of carbon dioxide into aqueous solutions of monoethanolamine + *N*-methyldiethanolamine. *Chemical Engineering Science* 2002, *57,* 4569–4582.
5. Onda, K., Takeuchi, H., Okumoto, Y., Mass transfer coefficients between gas and liquid phases in packed columns, *Journal of Chemical Engineering of Japan* 1968, *1*, 56–62.
6. Kelly R.M., Rousseau R.W., Ferrell J.K. Design of packed, adiabatic absorbers: physical absorption of acid gases in methanol. *Industrial & Engineering Chemistry Process Design and Development* 1984, 23, 102–109.
7. Sanyal D., Vasishtha N., Samf, D. Modeling of carbon dioxide absorber using hot carbonate process. *Industrial & Engineering Chemistry Research* 1988, *27*, 2149–2156.
8. Tontiwachwuthikul P., Meisen A., Lim C.J. CO_2 absorption by NaOH, monoethanolamine and 2-amino-2-methyl-1-propanal solutions in a packed column. *Chemical Engineering Science* 1992, *47*, 381–390.
9. Piche S., Grandjean B.P.A., Iliuta I., Larachi F. Interfacial mass transfer in randomly packed towers: a confident correlation for environmental applications. *Environmental Science and Technology* 2001, *35*, 4817–4822.
10. Hook, R.J. An Investigation of some sterically hindered amines as potential carbon dioxide scrubbing compounds, *Industrial & Engineering Chemistry Research* 1997, *36*(5), 1779–1790.
11. Knuutila, H., Juliussen, O., Svendsen, H.F. Kinetics of the reaction of carbon dioxide with aqueous sodium and potassium carbonate solutions. *Chemical Engineering Science* 2010, *65*(23), 6077–6088.
12. Comstock, C., Dodge, B. Rate of carbon dioxide absorption by carbonate solutions in a packed tower. *Industrial & Engineering Chemistry* 1937, *29*(5), 520–529.

Chapter 3. Studies of Bicarbonate Crystallization from Carbonate/Bicarbonate Solutions

Part 3A. Kinetic Behavior of $KHCO_3$ Crystallization

3A.1 Introduction

Crystallization of the bicarbonate salt is a critical step in Hot-CAP. Reliable data on the crystallization kinetics (nucleation and growth rates) are indispensable for optimizing the design and operation of the crystallizer. The performance of steady-state crystallization has been studied for a wide variety of inorganic and organic chemicals, such as potassium sulfate,[1] calcium oxalate,[2] and adipic acid,[3] by the widely adopted crystal population balance technique.[1,4,5] Previous research has indicated that the degree of supersaturation, residence time, magma density, and hydrodynamic conditions are the predominant factors affecting the crystal size and population density distribution.[1,4] For example, at a high magma density, crystal–crystal collisions become more important to nucleation than do crystal–agitator or crystal–wall collisions, because the former collisions result in a second-order dependence on the secondary nucleation rate that is "removal limited" on magma density.[4,6] In addition, secondary nucleation is expected to show a first-order dependence on magma density if crystal–agitator or crystal–wall collisions are important.[7] Hydrodynamics can also exert a profound effect on both the primary and secondary nucleation rates; thus, it plays an important role in the crystallization process.[4] It has been reported that for a crystallizer operating in the "removal limited" regime, the nucleation rate is proportional to the cubed speed of agitation.[7,8] However, even for similar systems, poor specification of hydrodynamic conditions and their lack of standardization have been the most probable causes for the observed deviations in kinetics measured among different studies.

In this study, the crystallization kinetics of potassium bicarbonate from PCB solutions under conditions typical of Hot-CAP was investigated using a laboratory mixed-suspension, mixed-product-removal (MSMPR) reactor. A series of experiments were carried out under various combinations of agitation speed, mean residence time, feed and crystallization temperatures, and feed solution compositions. Experimental results were used to obtain the rate constants of the crystallization process based on a size-dependent growth (SDG) model. Preliminary analysis of the crystallization process in Hot-CAP was conducted based on the experimental results.

3A.2 Materials and methods

3A.2.1 Experimental setup

A schematic diagram of the experimental setup is shown in Figure 3A-1. The feed solution was prepared in a glass flask placed in a thermostat water bath at a predetermined temperature. A 1-L continuous stirred tank reactor (Atlas Potassium, Syrris Inc.) was used as an MSMPR crystallizer. The reactor, a round-bottomed glass vessel, was double-jacketed, with the inner oil jacket for temperature control and the outer vacuum jacket for thermal insulation from the environment. A peristaltic pump (Masterflex) continuously withdrew the feed solution into the continuous stirred tank reactor at a constant flow rate. The tube (Masterflex Norprene) connecting the feed pump to the reactor was heated with heating tape controlled by a Variac power transformer to maintain the temperature at a preset value. Another peristaltic pump (Masterflex L/S) was used to

continuously extract the product suspension (slurry) from the reactor through an overflow tube, to maintain a constant liquid level inside the reactor. Operation of the system, including control of the reactor temperature and agitation speed, and data logging, was performed by a computer with Atlas software.

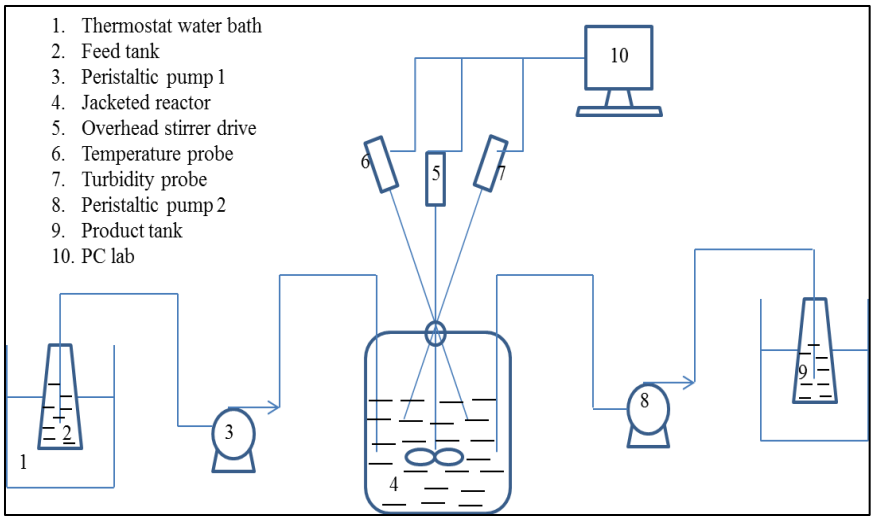

Figure 3A-1. Schematic and photograph of a continuous MSMPR reactor setup.

3A.2.2 Experimental conditions and procedure

The experiments were carried out at various agitation speeds (350, 525, and 700 rpm) and mean residence times (15, 30, and 45 min). The crystallization temperature in the MSMPR reactor varied at 55, 45, and 35°C, and the corresponding temperature of the feed solution was at least 10°C higher. All the feed solutions used in the experiments were freshly prepared and free of seed crystals. A 40 wt% PCB solution with 40% carbonate-to-bicarbonate (CTB) conversion (PCB40-40, and so forth hereafter) fed at 70°C was used to simulate the CO_2-rich solution

exiting the Hot-CAP absorber. PCB38-35 and PCB37-31 solutions were used to approximate the saturated mother solutions generated during cooling of the PCB40-40 solution from 70 to 55°C and from 70 to 45°C, respectively, based on solubility data.[9] In addition, PCB37.5-36.5 and PCB35-32.5 solutions, both of which contained the same weight percentage of K_2CO_3 as in the PCB40-40 solution, were used as feed solutions to investigate the effect of the supersaturation level of $KHCO_3$ on the crystallization kinetics.

Because piperazine (PZ) is a typical promoter for CO_2 absorption, the effect of the addition of PZ (0.05, 0.1, and 0.2 M) in PCB40-40 on the $KHCO_3$ crystallization was also studied under the selected conditions (e.g., feeding at 70°C, crystallization at 55°C, agitation speed of 350 rpm, and mean residence time of 15 min). An alternative set of experiments were conducted using a feed solution prepared by bubbling CO_2 into a mixture of PCB40-20 and PZ (0.2 or 0.5 M) until the overall CTB conversion reached 40%.

In a typical experiment, approximately 390 mL of deionized water was initially charged to the stirred reactor, heated to the preset crystallization temperature, and maintained at that temperature. The feed solution at the desired temperature was then continuously pumped into the reactor, where it was immediately cooled to the crystallization temperature by instantaneous heat exchange with an oil cooling medium circulating in the jacket. The solution or suspension was withdrawn to maintain a constant liquid level within the reactor. When the $KHCO_3$ concentration reached and exceeded its solubility limit, massive crystallization began to occur in the reactor. The $KHCO_3$ crystals then began to accumulate (a net effect of crystal generation and withdrawal), and the suspension in the reactor became denser over time before a steady state was finally approached. The steady state in a typical experiment was generally achieved after a period of 6-times the mean residence time of the suspension in the reactor.[5]

3A.2.3 Crystal characterization

After the crystallization system reached a steady state, 20 mL of suspension was collected from the reactor with a syringe. The sample was immediately vacuum-filtered through a 200-nm membrane (Whatman). Crystal solids collected on the membrane were oven-dried (Precision) at 60°C, and a standard gravimetric analysis was performed on the dried sample to estimate the solids concentration of the slurry or suspension in the reactor. The size and morphology of crystal particles were analyzed using a scanning electron microscope (SEM; JEOL 6060LV). The crystal size distribution (CSD) was analyzed with a laser-diffraction particle size analyzer (Horiba LA950). The CSD measurements were performed at least twice for each sample to verify reproducibility. The compositions of crystal samples were analyzed by X-ray diffraction (XRD; Siemens-Bruker D5000 XRD), using Cu Kα (λ = 0.15418 nm) radiation (40 kV, 30 mA). Diffraction peaks were measured by step-scanning from 5 to 60° at a speed of 0.5° per minute and a step width of 0.05°.

3A.3 Theory of crystallization kinetics

For a steady-state MSMPR crystallizer, the general population balance equation is as follows: [5]

$$\frac{d[G(L)n(L)]}{dL} + \frac{n(L)}{\tau} = 0 \qquad \text{(3A-1)}$$

where $G(L)$ is the crystal growth rate (m/s), L is the characteristic dimension of crystal particles (diameter for spherical particles, m), $n(L)$ is the population density (m^{-4}), and τ is the mean residence time (s). Nonlinearity of the logarithmic $n(L)$ is evident for many systems mainly owing to the feature of size-dependent growth or growth rate dispersion.[10] Growth rate dispersion has been modeled by two possible mechanisms: the random fluctuation model,[11] according to which the growth of crystals fluctuates during the course of crystallization as a result of both flow and velocity fluctuations; and the constant crystal growth model, according to which crystals have an inherent growth rate but the rate varies from crystal to crystal.[12] SDG can be described by an empirical correlation based on the three-parameter, exponential model of size-dependent crystal growth proposed by Mydlarz and Jones:[13]

$$G(L) = G_m\{1 - \exp[-a(L+c)]\} \tag{3A-2}$$

where G_m is the limiting or effective size-independent growth rate for large crystal particles (m/s), and both a and c are empirical constants. Because $G(L)$ approximates the constant G_m at large L, it is also called the linear growth rate, because it remains the same after reaching some critical size. By integration of Eq. (3A-2) over an entire range of particle sizes, the average crystal growth rate (G_{av}, m/s) can be obtained as follows:

$$G_{av} = G_m\left\{1 + \frac{1}{aL_m}\left[e^{-a(L_m+c)} - e^{-ac}\right]\right\} \tag{3A-3}$$

where L_m is the maximum crystal size actually obtained (m). The minimum crystal size is assumed to be 0. Because, on average, the crystals in the MSMPR reactor are replaced within a mean residence time, G_{av} can be estimated from the measured slurry density and CSD according to the following equation:

$$G_{av} = \frac{M_T}{3\rho_s \tau k_v \int_0^\infty n(L)L^2 dL} \tag{3A-4}$$

where M_T is the solids concentration of the suspension(kg m^{-3}), ρ_s is the density of $KHCO_3$ solids (2,170 kg m^{-3}), and k_v is the volumetric shape factor ($\pi/6$ for spherical particles).

By solving Eqs. (3A-1) and (3A-2) simultaneously, the following logarithmic population density equation can be obtained:

$$\log n(L) = \log n_0 + aL - \left(1 + \frac{1}{a\tau G_m}\right)\log\left(\frac{e^{aL} - e^{-ac}}{1 - e^{-ac}}\right) \tag{3A-5}$$

where n_0 is the "zero size" (nuclei) population density (m^{-4}). The population density $n(L)$ can be determined from the measured CSD and slurry density by the following equation:

$$n(L) = \frac{M_T q_i}{k_v \rho_s L^3 \Delta L} \tag{3A-6}$$

where q_i is the mass or volumetric fraction of the ith size fraction from the measured CSD and ΔL is the crystal size range between two neighboring size fractions. The resultant $n(L)$ was least-squares-fitted to Eq. (3A-5) to retrieve the parameters G_m, a, and c using a Python program (Python version 2.7).

The fitted G_m can be further correlated to the supersaturation level, i.e., the driving force for crystallization, by the following power-law relationship:

$$G_m = k_g \sigma^g \tag{3A-7}$$

where σ is the relative supersaturation level, k_g is the overall growth rate coefficient (m/s), and g is an empirical constant. For simplicity, as shown in Eq. (3A-8), σ is estimated based on the weight concentration as a reasonable approximation of the activity:

$$\sigma = \frac{w - w_{eq}}{w_{eq}} \tag{3A-8}$$

where w is the prevailing concentration of $KHCO_3$ (kg m^{-3}) and w_{eq} is the solubility of $KHCO_3$ (kg m^{-3}). It should be noted that the coexistence of K_2CO_3, which is highly soluble, is assumed to have no effect on the solubility of $KHCO_3$. The variable k_g represents the two stages of the crystal growth process following the formation of stable nuclei: bulk diffusion to the crystal surface and surface reaction or integration.[14] The value of k_g is a function of temperature following an Arrhenius relationship:[15]

$$k_g = \alpha e^{\frac{-E_g}{RT}} \tag{3A-9}$$

where α is a constant (m s^{-1}), E_g is the activation energy for crystal growth, including both the diffusion and reaction (kJ mol^{-1}), R is the universal gas constant (8.314 J mol^{-1} K^{-1}), and T is the absolute temperature (K).

The total nucleation rate (B_{TOT}, s^{-1} m^{-3}), the sum of primary and secondary nucleation, is the number of new crystal particles formed per unit of suspension volume per unit of time. The formation of nuclei relies on the relative supersaturation level, the solids concentration of the suspension, and hydrodynamic factors. B_{TOT} can be expressed in a semiempirical power-law form:

$$B_{TOT} = k_n G_{av}{}^h N^i M_T{}^j \tag{3A-10}$$

where h, i, and j are the empirical exponents to be determined by data fitting, N is the agitation speed (rpm), and k_n is the nucleation rate coefficient, which is a function of temperature, hydrodynamics, and impurity concentration [1] and can be expressed as follows:

$$k_n = \beta e^{\frac{-E_n}{RT}} \tag{3A-11}$$

where β is a fitting constant and E_n is the apparent activation energy of nucleation, which could be negative.[1,16] The values of B_{TOT} were determined from the experimental data based on Eq. (3A-12), and the results were used to obtain the exponents and constants in Eqs. (3A-10) and (3A-11) by data fitting:

$$B_{TOT} = \frac{\int_0^\infty n(L)dL}{\tau} \tag{3A-12}$$

It should be noted that rather than considering an infinite range of crystal particle sizes, the above equation was integrated over a size range from the minimum to maximum sizes detected by the particle size analyzer.

To predict the crystal size under various crystallization conditions, the mass median size (L_M) was estimated by using Eq. (3A-13):[17]

$$L_M = 3.67 G_{av} \tau \quad \text{(3A-13)}$$

where L_M represents the mass median size. The value of L_M is correlated to the mass mean size ($\bar{L}$). Assuming a log-normal particle size distribution, L_M can be estimated according to

$$L_M = \bar{L} \exp[-0.5(\ln \sigma_g)^2] \quad \text{(3A-14)}$$

where σ_g is the geometric standard deviation. The value of $\bar{L}$ was determined by the measured CSD data according to Eq. (3A-15):

$$\bar{L} = \frac{\int_0^\infty n(L) L^4 dL}{\int_0^\infty n(L) L^3 dL} \quad \text{(3A-15)}$$

3A.4 Results and discussion

3A.4.1 Composition and morphology of crystal particles

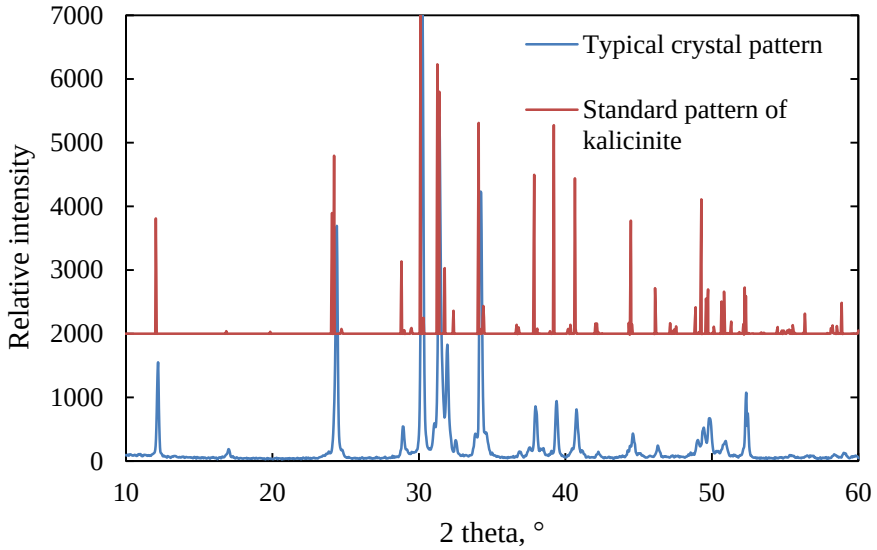

Figure 3A-2. Typical XRD patterns of crystal particles (obtained from crystallization at 55°C, an agitation speed of 350 rpm, and a mean residence time 1,732 s with a feed solution of 70°C PCB40-40).

The XRD analysis revealed that kalicinite ($KHCO_3$) was the only crystal phase formed in all the tests conducted, regardless of whether PZ was added to the feed solution. As an example, Figure

3A-2 displays typical XRD patterns of crystal particles formed at 55°C, an agitation speed of 350 rpm, and a residence time of 1,732 s with a 70°C PCB40-40 feed solution.

Kalicinite crystals produced under various test conditions generally showed similar morphology. Figure 3A-3 displays a typical SEM image of crystal particles obtained under the same conditions as those used in Figure 3A-2. Note that most crystals have a hexagonal prism shape.

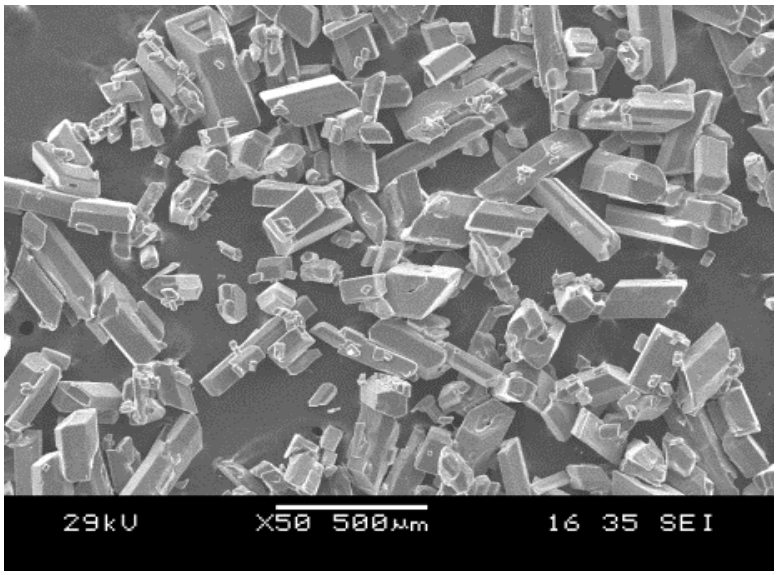

Figure 3A-3. A typical SEM image of kalicinite particles (obtained from crystallization at 55°C, an agitation speed of 350 rpm, and a mean residence time of 1,732 s with a feed solution of 70°C PCB40-40).

3A.4.2 Parametric effects on crystallization kinetics

Several operating variables, including mean residence time, agitation speed, and relative supersaturation level, are critical to the crystallization process. Parametric experiments were conducted to investigate their effects on the crystallization kinetics. The results and corresponding experimental conditions are summarized in Table 3A-1.

Table 3A-1. Experimental conditions and results of crystallization kinetics

Test	Feed solution	Feed temperature (°C)	Density of feed solution (g L^{-1})	Agitation speed (rpm)	Crystallization temperature (°C)	Relative super-saturation σ	Mean residence time (s)	Solids concentration (g L^{-1})	Mean crystal size (μm)	Mean growth rate × 10^{8} (m s^{-1})	Total nucleation rate × 10^{-8} (s^{-1} m^{-3})
1	PCB40-40	70	1,340	350	55	0.271	926	63.0	232	3.84	3.87
2	PCB40-40	70	1,330	350	55	0.288	1,732	65.7	263	2.39	3.21
3	PCB40-40	70	1,370	350	55	0.245	2,706	59.4	440	2.02	2.44
4	PCB40-40	70	1,340	525	55	0.266	1,804	62.1	202	2.32	3.68
5	PCB40-40	70	1,330	700	55	0.259	1,775	60.3	141	1.76	4.31
6	PCB38-35	55	1,330	350	45	0.238	893	47.0	324	5.39	6.28
7	PCB38-35	55	1,310	350	45	0.220	1,772	43.5	387	4.12	0.40
8	PCB38-35	55	1,330	350	45	0.235	2,716	46.5	430	3.25	0.30
9	PCB38-35	55	1,330	525	45	0.178	1,765	37.0	366	3.60	1.14
10	PCB38-35	55	1,330	700	45	0.184	1,786	38.0	129	1.59	6.30
11	PCB37-31	45	1,330	350	35	0.372	911	57.5	415	9.98	0.92
12	PCB37-31	45	1,330	350	35	0.350	1,746	55.0	464	4.90	0.75
13	PCB37-31	45	1,340	350	35	0.321	2,666	52.0	486	3.60	0.66
14	PCB37-31	45	1,320	525	35	0.320	1,797	51.0	431	4.06	2.51
15	PCB37-31	45	1,320	700	35	0.307	1,768	49.5	381	3.40	2.64
16	PCB40-40	70	1,320	700	35	1.084	1,799	151.5	478	6.21	1.23
17	PCB40-40	70	1,350	700	45	0.498	1,823	99.0	393	3.93	2.10
18	PCB38-35	55	1,330	700	35	0.577	1,788	89.5	407	4.74	1.79
19	PCB37.5-36.5	70	1,310	700	35	0.804	1,787	111.0	381	4.34	1.52
20	PCB35-32.5	70	1,300	700	35	0.204	1,824	35.0	343	3.47	1.93
21	PCB40-40 + 0.05 M PZ	70	1,330	350	55	0.290	937	66.0	298	6.12	2.07
22	PCB40-40 + 0.1 M PZ	70	1,330	350	55	0.307	874	69.0	358	7.75	1.74
23	PCB40-40 + 0.2 M PZ	70	1,330	350	55	0.331	889	73.0	426	9.34	0.49
24	PCB40-40 + 0.2 M PZ-CO_2	70	1,330	350	55	0.313	865	70.0	391	10.07	0.39
25	PCB40-40 + 0.5 M PZ-CO_2	70	1,330	350	55	0.319	924	71.0	397	7.46	1.81

3A.4.2.1 Mean residence time

As shown in Figure 3A-4, increasing the residence time increased the mean crystal size, but decreased the total nucleation rate and crystal growth rate. At a longer residence time, more crystal fragments were formed because of attrition between crystal particles by mechanical agitation. The resultant fragments could have acted as secondary nuclei, inhibiting crystal growth. In addition, a longer residence time could have led to a lower level of local supersaturation, as reported in other studies,[5,18] which would have slowed crystal growth. It was observed that the measured solids concentration of the suspension was independent of the mean residence time for a feed solution with given feed and crystallization temperatures. This result indicates that the crystallization of $KHCO_3$ was kinetically fast, and equilibrium was closely approached even within the shortest mean residence time examined.

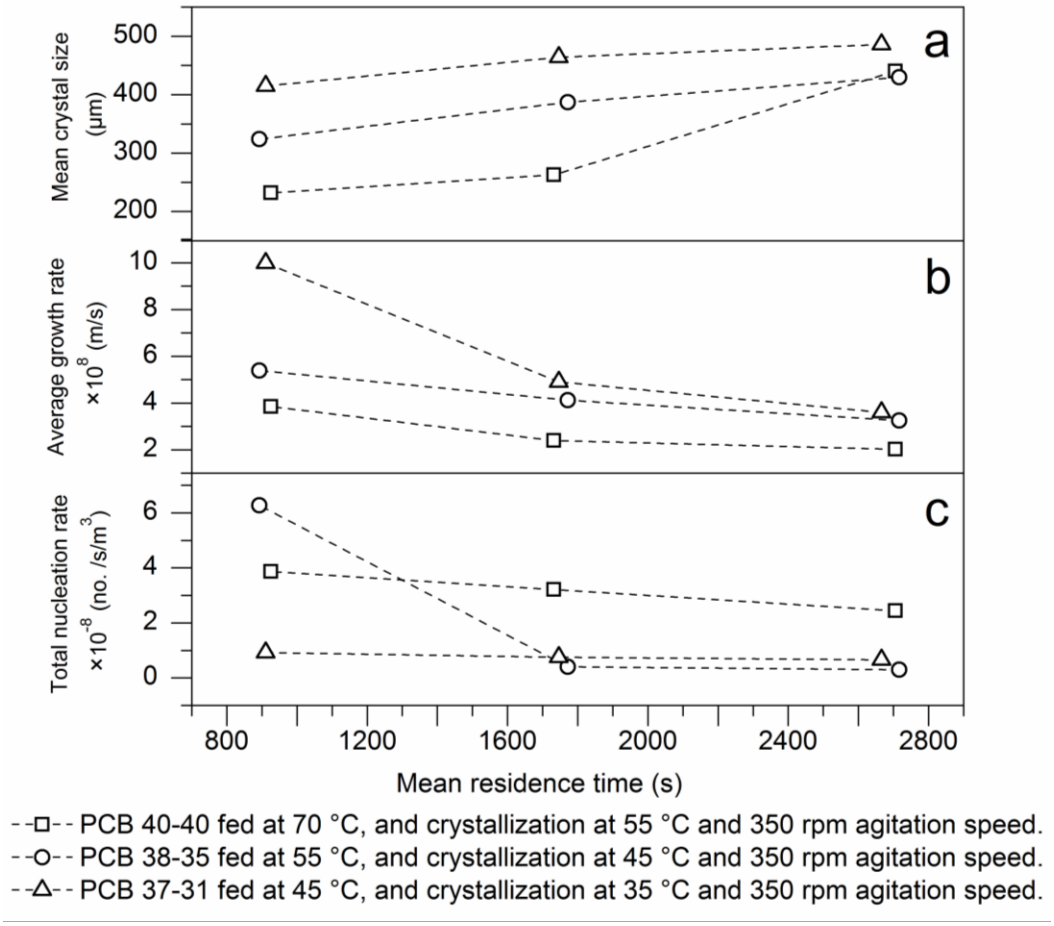

Figure 3A-4. Effect of mean residence time on (a) mean crystal size, (b) average crystal growth rate, and (c) total nucleation rate.

3A.4.2.2 Agitation speed

The agitation speeds were selected to ensure a well-mixed suspension while avoiding the formation of vortexes and air entrainment. As shown in Figure 3A-5, increasing the agitation speed reduced the mean crystal size and crystal growth rate while enhancing the nucleation rate.

This observation is supported by work in the literature.[19,20,21] Nucleation can be significantly improved in an agitated system because stronger agitation favors the formation of smaller crystal fragments resulting from larger shear forces and the exertion of a more significant attrition effect.[5] Moreover, the air bubbles generated with strong agitation could potentially facilitate the onset of nucleation because they could act as dark spots and provide surfaces for crystallization. The results also show that the crystal growth rate varied with agitation speed, indicating that the growth process was bulk diffusion controlled.

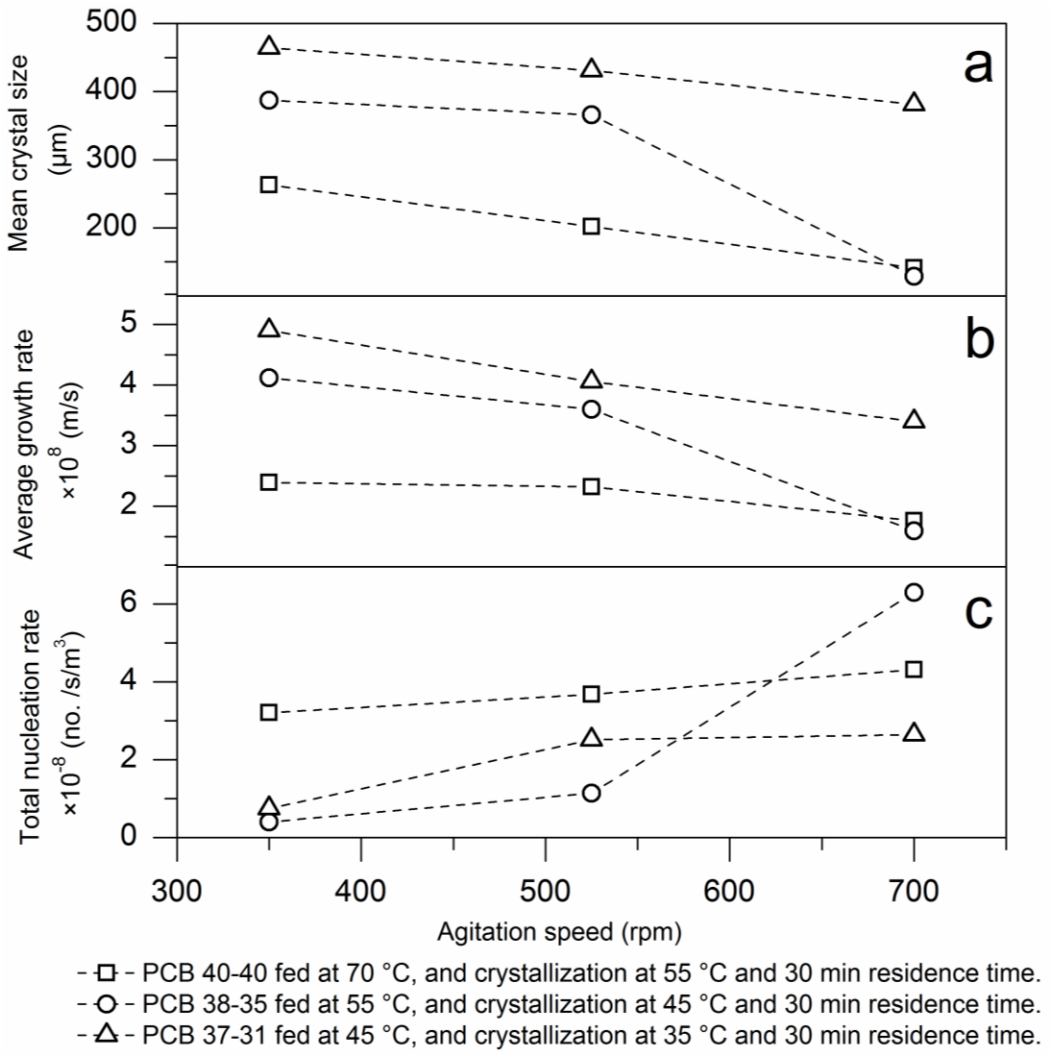

Figure 3A-5. Effect of agitation speed on (a) mean crystal size, (b) average crystal growth rate, and (c) total nucleation rate.

3A.4.2.3 Relative supersaturation level

The relative supersaturation level was adjusted by varying either the crystallization temperature (with a lower temperature implying higher supersaturation for the same feed solution), or the feed solution composition. Figure 3A-6 presents the experimental results for three solutions (PCB40-40, PCB37.5-36.5, and PCB35-32.5) fed at 70°C and crystallized at 35°C under the same mean residence time (about 30 min) and agitation speed (700 rpm). These feed solutions

contained the same content of K_2CO_3 but different contents of $KHCO_3$ so that their respective supersaturation levels (σ) were different from each other (1.084, 0.804, and 0.204). As shown in Figure 3A-6, both the crystal growth rate and mean crystal size increased with increasing supersaturation level, and this was consistent with the report by Tanrikulu et al.[22] However, the nucleation rate decreased slightly with the relative supersaturation level. In general, the primary nucleation rates were enhanced with increasing supersaturation, so the observed trend might reflect the effect of the secondary nucleation. Secondary nucleation could be incurred by the catalytic effect of parent crystals in a supersaturated solution. When the supersaturation level was high, primary (spontaneous) nucleation prevailed and secondary nucleation could have been inhibited. However, in a solution with a low supersaturation level, the catalytic effect of the parent crystals might not have been inhibited and secondary nucleation could have dominated. Overall, the total nucleation rate could be higher at a lower supersaturation level.

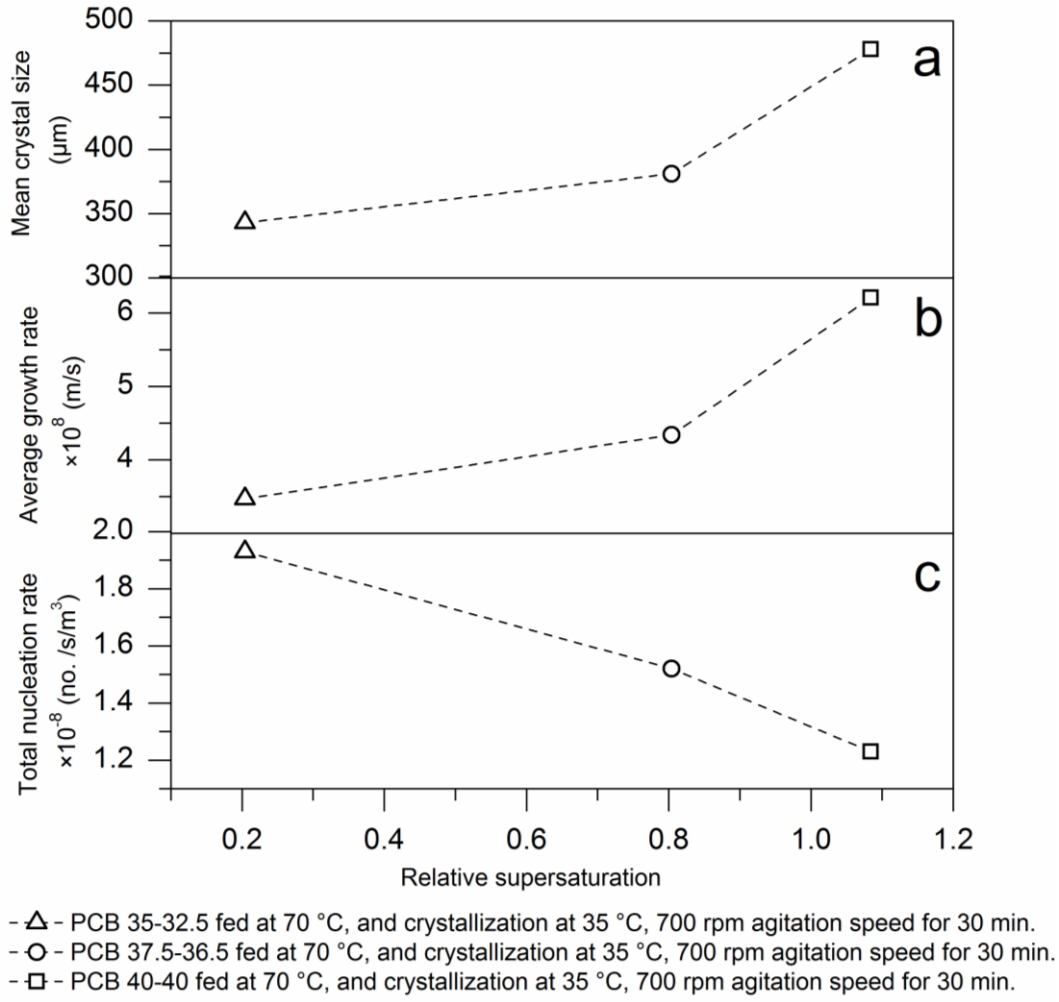

Figure 3A-6. Effect of relative supersaturation level on (a) mean crystal size, (b) average crystal growth rate, and (c) total nucleation rate. All the experiments were performed at the same crystallization temperature (35°C).

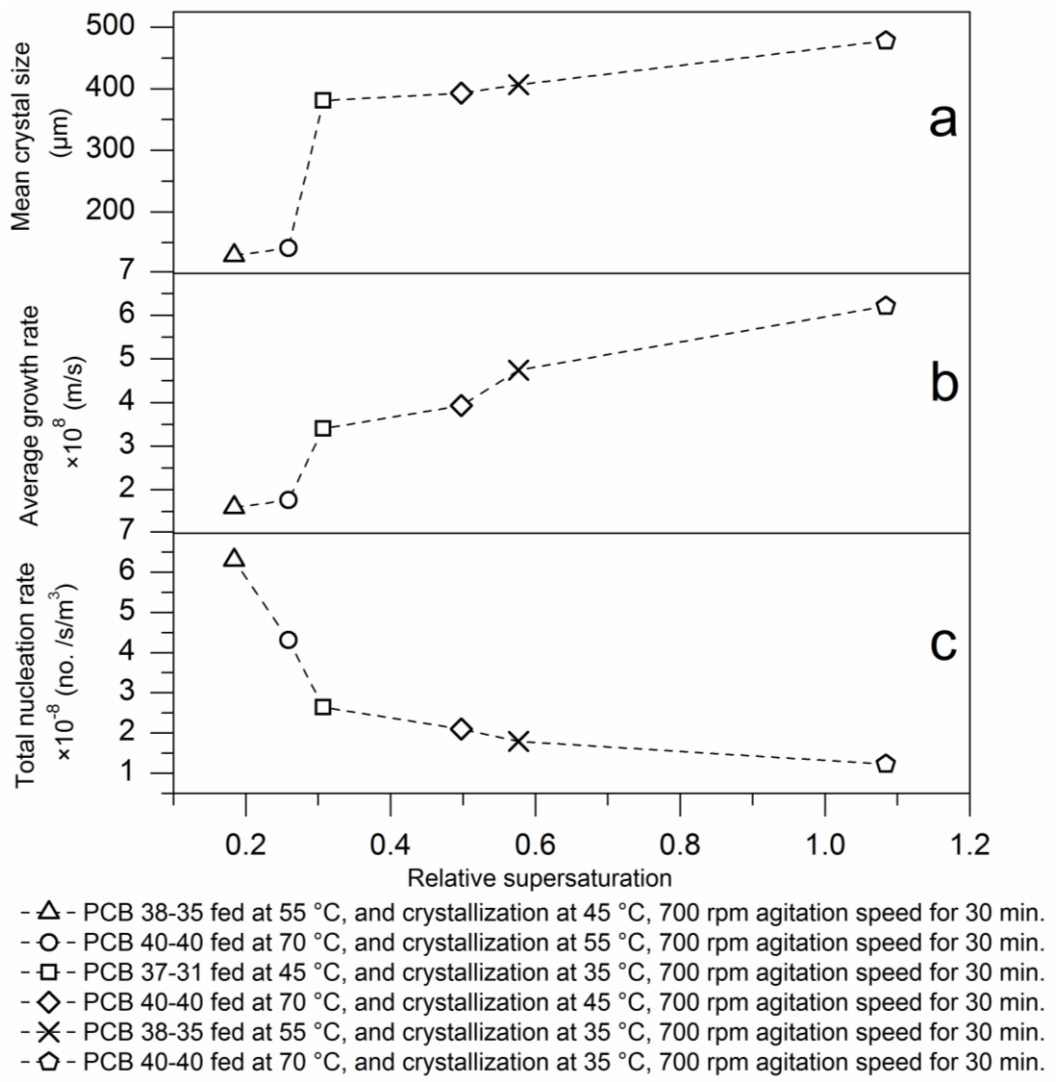

Figure 3A-7. Combined effect of relative supersaturation level and crystallization temperature on the crystallization kinetic performance. Effect on (a) mean crystal size, (b) average growth rate, and (c) total nucleation rate. The crystallization experiments were performed at different temperatures (35, 45, or 55°C).

Figure 3A-7 presents the crystallization kinetic performance obtained at different supersaturation levels. Six feed solutions were used: PCB40-40, fed at 70°C and tested for crystallization at 55°C (σ = 0.259), 45°C (σ = 0.498), and 35°C (σ = 1.084); PCB38-35, fed at 55°C and tested at 45°C (σ = 0.184) and 35°C (σ = 0.577); and PCB37-31, fed at 45°C and tested at 35°C (σ = 0.307). All these tests were carried out at an agitation speed of 700 rpm and a mean residence time of 30 min. Note that, in these tests, the relative supersaturation level depended not only on the composition of the feed solution, but also on the cooling temperature. The kinetic performance of the bicarbonate crystallization shown in Figure 3A-7 was similar to that in Figure 3A-6; the nucleation rate shown in Figure 3A-7 appeared to be more sensitive to the supersaturation level than that shown in Figure 3A-6. It should be noted that in addition to the effect of secondary nucleation described above, the effect of crystallization temperature on the nucleation rate was not separate from the effect of the supersaturation level. For a given feed solution, a higher

crystallization temperature corresponded to a lower level of supersaturation. Nucleation proceeded faster at a higher crystallization temperature according to the Arrhenius relationship. Several studies [23,24] have indicated that at a low temperature (high supersaturation level), nucleation is inhibited by retarded molecular diffusion. The combined effect of crystallization temperature and supersaturation level on the nucleation rate would thus result in a low nucleation rate at a higher supersaturation level, induced by a lower temperature.

3A.4.2.4 Presence of PZ

As shown in Table 3A-1, compared with the neat PCB40-40 feed, the solids concentration of $KHCO_3$ slurry in the presence of PZ was higher, probably because the solubility of $KHCO_3$ was affected. When 0.2 M PZ was added to PCB40-40, the solids concentration of the slurry increased by approximately 20%. Results also indicated that the kinetics of $KHCO_3$ crystallization was significantly boosted in the presence of PZ. As shown in Figure 3A-8, with the addition of 0.2 M PZ in the PCB40-40 feed, the particle size of $KHCO_3$ solids almost doubled and the average growth rate was more than two-fold higher. However, nucleation was considerably inhibited in the presence of PZ (only 1/6 of that in the absence of PZ). Such results are favorable for the Hot-CAP, because PZ is used as the promoter for absorption and is contained in the CO_2-rich PCB solution entering the crystallization tanks.

The alternative set of experiments (No. 24–25 in Table 3A-1) mimicked the CO_2-rich PCB solution obtained from CO_2 absorption. In these experiments, a portion of PZ was present in the forms of both molecular PZ and its carbamate species, because the PCB and PZ mixture was prepared with CO_2 bubbling to reach the required total CO_2 loading. Similar to the prior set of experiments, the presence of PZ also accelerated the crystallization of $KHCO_3$. It appeared that in the presence of either 0.2 or 0.5 M PZ, the HCO_3^- concentration would not significantly change because of the small doses of PZ compared with HCO_3^-, which might explain the similarity between their solids concentrations measured in slurry (70 and 71 kg/m^3). However, the average growth and total nucleation rates between the two PZ doses were significantly different: the addition of 0.2 M PZ resulted in higher growth yet lower nucleation rates than did the addition of 0.5 M PZ, which, as a net effect, could result in similar mean crystal sizes (391 and 397 μm). Such a trend was quite different from the results shown in Figure 3A-8, where PZ was generally present in its molecular form. The results indicated PZ molecules and their ionic derivatives could have distinct solubilization behaviors.

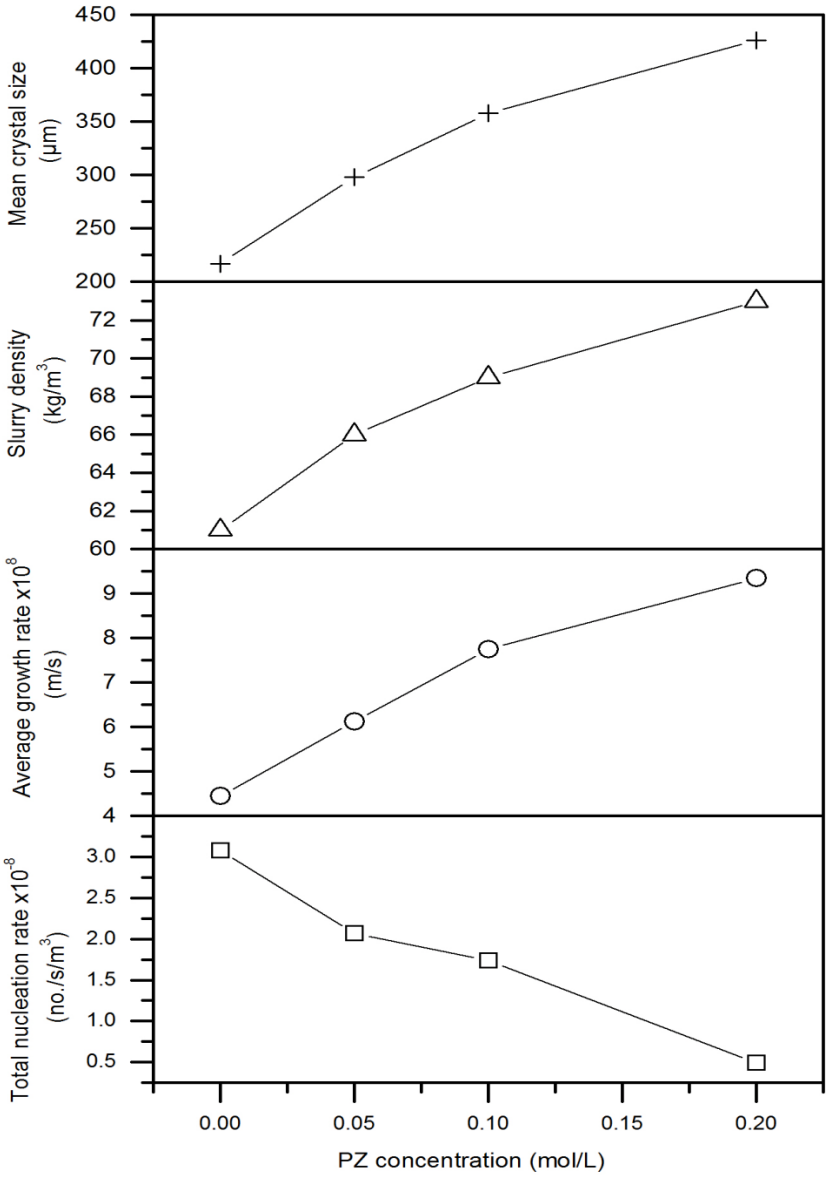

Figure 3A-8. Effect of the presence of PZ in PCB40-40 on (a) mean crystal size, (b) slurry concentration, (c) average crystal growth rate, and (d) total nucleation rate. Solutions were fed at 70°C, and crystallization was operated at 55°C, an agitation speed of 350 rpm, and a residence time of 15 min).

3A4.2.5 Presence of sulfate

The effect of the presence of 0.05 M K_2SO_4 in the PC40-40 solution on the kinetic performance of bicarbonate crystallization was investigated at a mean residence time of approximately 17 min and a crystallization temperature of 45°C. Results were compared with those obtained under the same conditions but without the addition of K_2SO_4. As shown in Figure 3A-9, the presence of K_2SO_4 did not significantly change the properties of PCB and resulted only in a slightly lower mean crystal size and average growth rate compared with those without the presence of K_2SO_4.

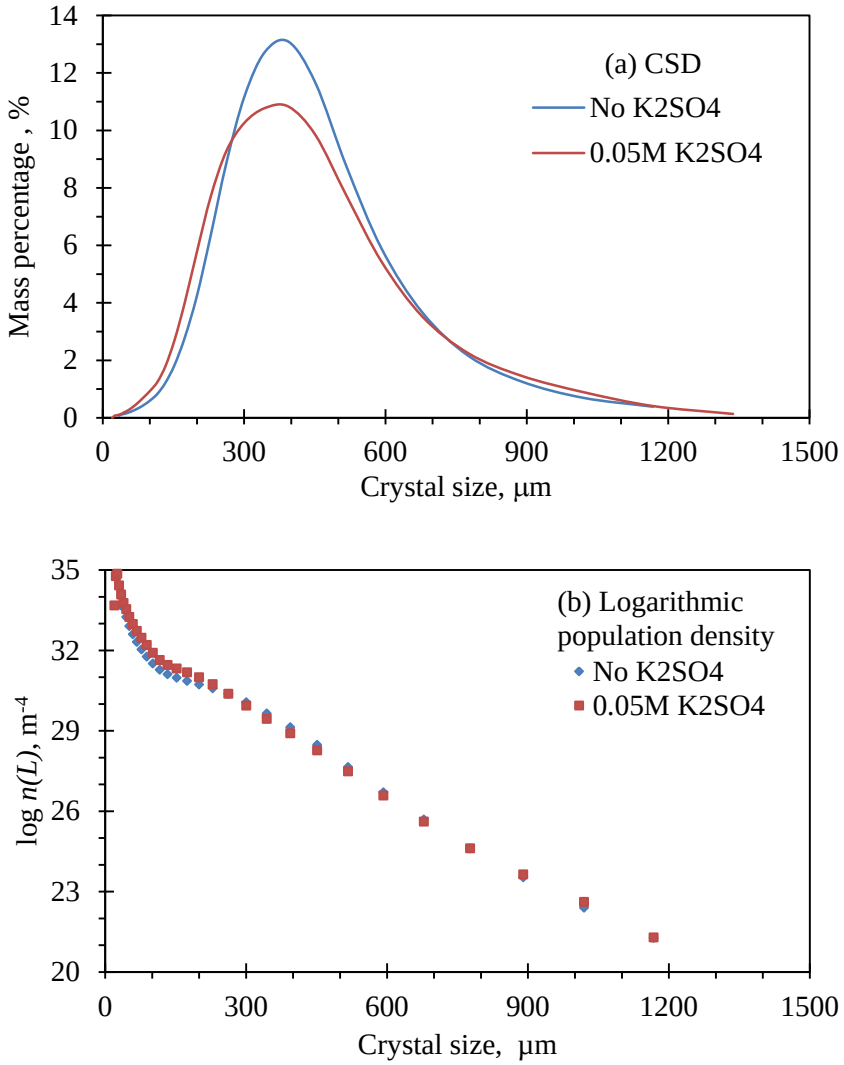

Figure 3A-9. Comparison of (a) CSD and (b) logarithmic population density $n(L)$ of particles crystallized from PCB40-40 with and without the presence of K_2SO_4 (PCB fed at 70°C, crystallization at 45°C and mean residence time of ~17 min).

3A.4.3 Modeling of crystallization kinetics

On the basis of the measured CSD and solids concentration of the suspension under various experimental conditions, the logarithmic population density distribution curves were plotted according to Eq. (3A-5) to regress the model parameters (a, c, and G_m). As an example, Figure 3A-10 illustrates the logarithmic population density distribution curve for the PCB38-35 solution fed at 55°C and tested for crystallization at 45°C, a mean residence time of 30 min, and an agitation speed of 350 rpm. Note that the logarithmic population density was not linear with the crystal size until the size was larger than 600 μm. As indicated by the coefficients of determination (R^2) listed in Table 3A-2, the models determined by nonlinear data fitting agreed well with the experimental data.

Table 3A-2. Parameters of the SDG model determined from experimental data fitting

No.	Test condition	$\ln(n_0)$	G_m	a	c	R^2 (%)
1	PCB40-40, 70–55 °C, 350 rpm, 15 min[a]	39.13	1.21e-07	3,305.6	2.56e-05	99.5
2	PCB40-40, 70–55 °C, 350 rpm, 30 min	59.18	4.85e-08	7,312.1	4.59e-09	99.2
3	PCB40-40, 70–55 °C, 350 rpm, 45 min	69.15	6.50e-08	2,984.2	2.91e-10	99.2
4	PCB40-40, 70–55 °C, 525 rpm, 30 min	63.49	3.69e-08	11,469.2	1.86e-10	99.3
5	PCB40-40, 70–55 °C, 700 rpm, 30 min	57.38	2.08e-08	28,624.1	5.57e-10	98.6
6	PCB38-35, 55–45 °C, 350 rpm, 15 min	66.61	1.27e-07	5,234.1	2.83e-10	99.7
7	PCB38-35, 55–45 °C, 350 rpm, 30 min	60.27	6.85e-08	6,158.6	5.03e-10	99.9
8	PCB38-35, 55–45 °C, 350 rpm, 45 min	61.32	4.78e-08	5,981.3	2.14e-10	99.1
9	PCB38-35, 55–45 °C, 525 rpm, 30 min	62.19	5.84e-08	6,810.3	3.66e-10	99.1
10	PCB38-35, 55–45 °C, 700 rpm, 30 min	63.41	2.09e-08	22,829.1	1.01e-10	99.2
11	PCB37-31, 45–35 °C, 350 rpm, 15 min	61.49	1.41e-07	6,107.6	1.96e-10	98.4
12	PCB37-31, 45–35 °C, 350 rpm, 30 min	64.67	8.92e-08	4,153.6	2.31e-10	98.3
13	PCB37-31, 45–35 °C, 350 rpm, 45 min	64.26	6.09e-08	4,212.7	1.53e-10	98.3
14	PCB37-31, 45–35 °C, 525 rpm, 30 min	67.05	8.72e-08	3,788.3	1.88e-10	98.5
15	PCB37-31, 45–35 °C, 700 rpm, 30 min	65.38	7.37e-08	4,693.5	3.16e-10	99.1
16	PCB40-40, 70–35 °C, 700 rpm, 30 min	61.45	7.98e-08	5,929.3	1.40e-10	98.4
17	PCB40-40, 70–45 °C, 700 rpm, 30 min	60.99	6.58e-08	6,232.2	5.21e-10	99.5
18	PCB38-35, 55–35 °C, 700 rpm, 30 min	64.08	7.39e-08	5,486.0	1.45e-10	98.2
19	PCB37.5-36.5, 70–35 °C, 700 rpm, 30 min	60.86	7.19e-08	5,699.7	6.09e-10	99.0
20	PCB35-32.5, 70–35 °C, 700 rpm, 30 min	65.62	5.67e-08	6,441.1	1.30e-10	98.9
21	PCB40-40, 70–55 °C, 350 rpm, 15 min, 0.05 M PZ	41.49	1.07e-07	7,440.9	2.16e-06	99.6
22	PCB40-40, 70–55 °C, 350 rpm, 15 min, 0.1 M PZ	39.96	1.68e-07	4,275.8	5.17e-06	99.3
23	PCB40-40, 70–55 °C, 350 rpm, 15 min, 0.2 M PZ	36.54	1.52e-07	4,417.9	2.57e-05	99.8
24	PCB40-40, 70–55 °C, 350 rpm, 15 min, 0.2 M PZ-CO_2	49.06	1.24e-07	10,389.2	1.14e-08	99.7
25	PCB40-40, 70–55 °C, 350 rpm, 15 min, 0.5 M PZ-CO_2	40.29	1.48e-07	4,792.2	4.39e-06	99.8

[a]Feed solution of PCB40-40 fed at 70°C and tested for crystallization at 55°C, an agitation speed of 350 rpm, and a mean residence time of 15 min. Likewise for other feed solutions in the table.

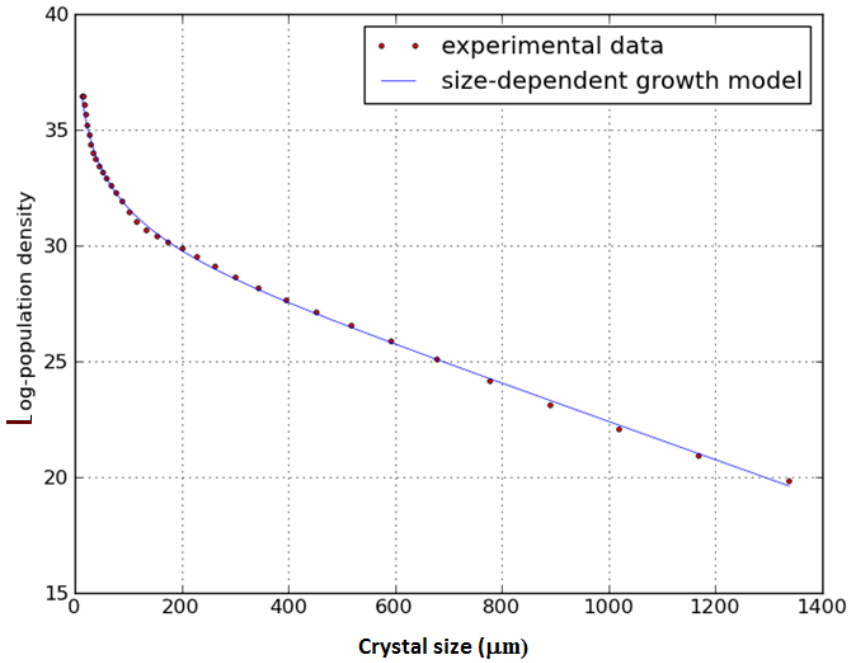

Figure 3A-10. Logarithmic population density distribution of kalicinite crystal particles obtained from the PCB38-35 solution fed at 55°C and crystalized at 45°C, a mean residence time of 30 min, and an agitation speed of 350 rpm.

When PZ is absent from the PCB solution, the effective crystal growth rate, G_m, determined above could be further correlated with the relative supersaturation level according to Eqs. (3A-7) and (3A-9) (R^2 = 0.96):

$$G_m = 0.46e^{-\frac{39906}{RT}}\sigma_0^{0.56} \qquad \text{(3A-16)}$$

The constants a and c described above varied with the experimental conditions (Table 3A-2). The average values of a and c were estimated to be 7,673, with a relative standard deviation of 84.7%, and 2.88 × 10^{-10}, with a relative standard deviation of 3.9%, respectively. According to the parameters determined above, the SDG model can be expressed as follows:

$$G(L) = 0.46e^{-\frac{39906}{RT}}\sigma_0^{0.56}\left[1-e^{-7673(L+2.88\times10^{-10})}\right] \qquad \text{(3A-17)}$$

For illustrative purposes, Figure 3A-11 shows the rate and differential rate change of crystal growth as a function of crystal size predicted by Eq. (3A-17) for the PCB38-35 solution fed at 55°C and tested for crystallization at 45°C, a mean residence time of 30 min, and an agitation speed of 350 rpm. The predicted trends were in good agreement with those reported in the literature.[5,21] The rate of crystal growth initially increased with increasing particle size and was then independent of size when the crystal particles reached approximately 600 μm. This critical size was consistent with that observed experimentally (i.e., in Figure 3A-10). Accordingly, the differential rate change of crystal growth decreased with increasing particle size and leveled off [dG/dL = 0, $G(L) = G_m$] at a crystal size of approximately 600 μm.

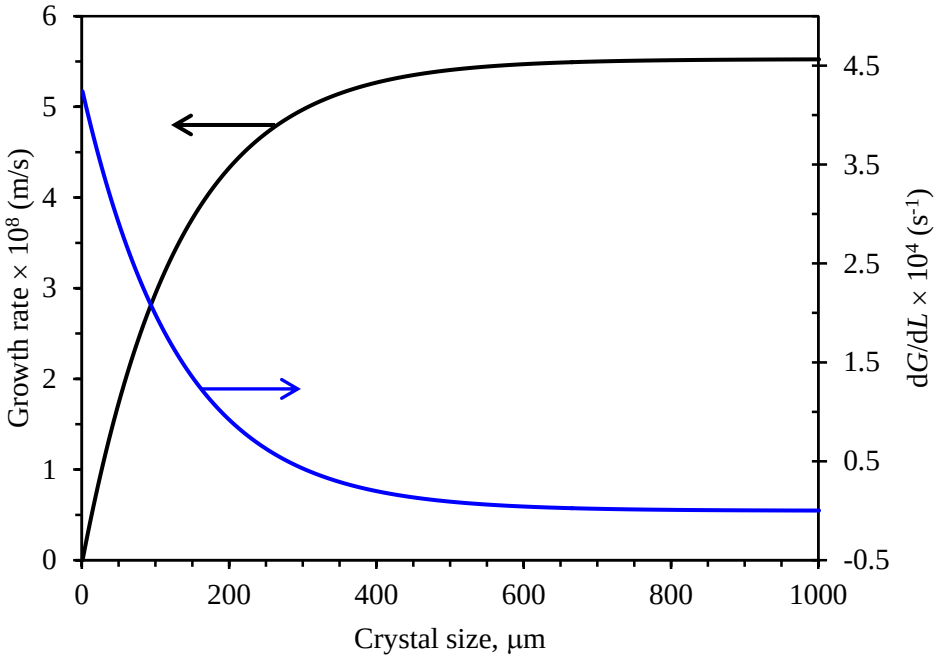

Figure 3A-11. The rate and differential rate change of crystal growth as a function of crystal size for the PCB38-35 solution fed at 55°C and crystalized at 45°C, a mean residence time of 30 min, and an agitation speed of 350 rpm.

A least-squares regression of experimental data was also performed, based on Eqs. (3A-10) and (3A-11), to determine the nucleation model parameters. The resultant power-law equation can be applied to predict the total nucleation rate:

$$B_{TOT} = 9.40 \times 10^{14} \exp\left(-\frac{52{,}463}{RT}\right) G_{av}^{\ 0.20} N^{1.46} M_{T0}^{\ -0.26} \qquad \text{(3A-18)}$$

The value of R^2 for the above regression was estimated to be 0.39. Note that the exponents of both G_{av} and M_{T0} approached 0, indicating a weak correlation of the total nucleation rate with either the average crystal growth rate or the solids concentration of the suspension. In comparison, the rate of total nucleation was strongly affected by the agitation speed (N), as indicated by its exponent of greater than 1. Unlike the agitation speed, the parameters G_{av}, M_{T0}, and T were coupled with each other; therefore, it was not surprising to see that M_{T0} was applied with a negative exponent. It should be noted that the empirical model obtained was specific to the investigated test conditions representative of Hot-CAP.

The presence of PZ resulted in an increase in relative supersaturation. When the data obtained for the PCB and PZ mixture systems were included, G_m could be regressed according to Eqs. (3A-7) and (3A-9) (R^2 = 0.996):

$$G_m = 3 \times 10^{-4} e^{-\frac{20142}{RT}} \sigma'^{0.54} \qquad \text{(3A-19)}$$

The average values of a and c were estimated to be 7,391, with a relative standard deviation of 80.0%, and 1.16×10^{-9}, with a relative standard deviation of 16.4%, respectively. Thus, the SDG model including the effect of PZ can be expressed as follows:

$$G(L) = 3\times10^{-4} e^{-\frac{20142}{RT}} \sigma'^{0.54} \left[1 - e^{-7391(L+1.16\times10^{-9})}\right] \quad \text{(3A-20)}$$

Similar to the derivation of Eq. (3A-18), a power-law equation for the total nucleation rate was obtained based on experimental data, including those of the PCB and PZ mixture systems:

$$B_{TOT} = 5.68\times10^{5} \exp\left(-\frac{25{,}736}{RT}\right) G_{av}^{\ -0.53} N^{1.05} M_T'^{-0.03} \quad \text{(3A-21)}$$

The value of R^2 for the above regression was estimated to be 0.37. The correlation of the total nucleation rate with either the average growth rate or the solids concentration was weaker than that with the agitation speed. Similar to the analysis above, the negative exponents were not strange because the parameters G_{av}, M_T', and T were intertwined.

3A.4.4 Design considerations for Hot-CAP crystallizers

As described in detail in Chapter 6, a configuration of multiple MSMPR crystallizers is proposed for Hot-CAP. Five consecutive MSMPR tanks can be used instead of a single crystallizer. Such a configuration would facilitate the heat recovery required in the process and could reduce the temperature difference between the inlet and outlet streams of each crystallizer. In comparison, a single-crystallizer design requires heat exchange when a large temperature difference exists between the inlet solution and the mother liquid, thus jeopardizing the heat recovery. A schematic diagram of the multi-crystallizer process is displayed in Figure 3A-12.

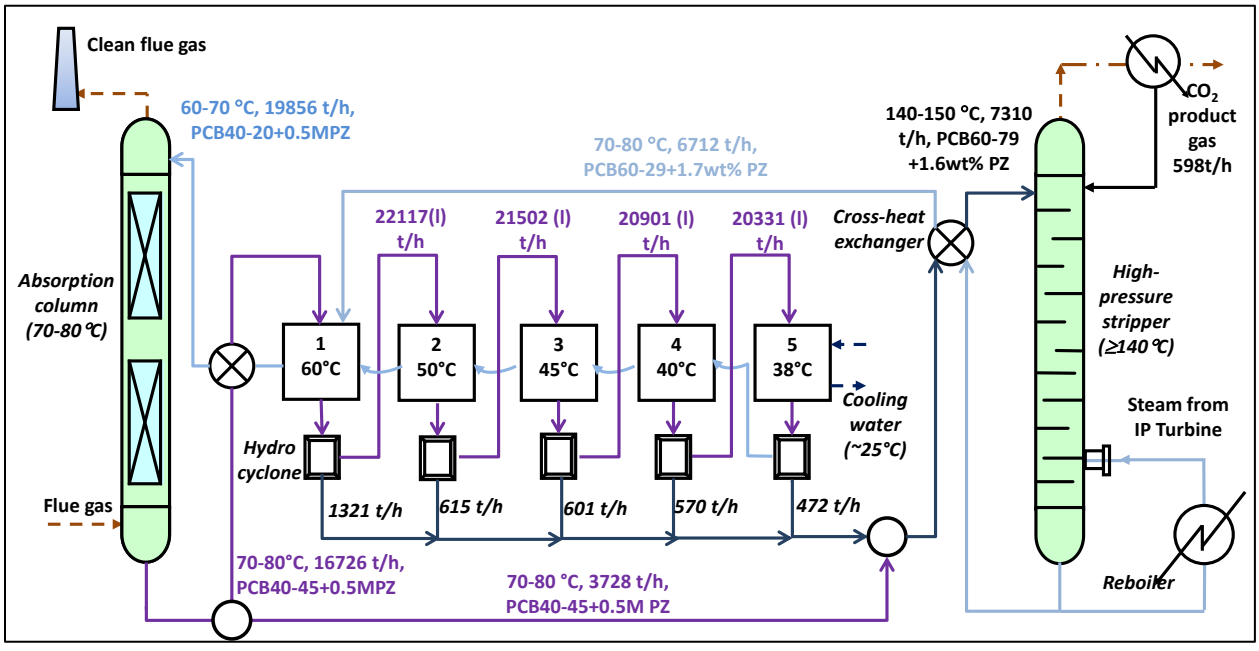

Figure 3A-12. Process flow diagram with multiple MSMPR crystallizers.

The residence time in the crystallizers (i.e., equipment size) and the size of crystal particles are the critical parameters in the design of crystallizers and crystal separators. The size of crystal particles depends on the nucleation and crystal growth performance. According to Eq. (3A-13), the mean crystal size is a function of the average growth rate and mean residence time.

Assuming a log-normal particle size distribution with a geometric standard deviation of 1.47 (an average over all the measured CSD data), L_M can be estimated by the following equation:

$$L_M = \bar{L}\exp(-0.5(\ln 1.47)^2) = 0.93\bar{L} \quad \text{(3A-22)}$$

As described, the addition of PZ in the PCB solution would incur changes in both the relative supersaturation ratio and solids concentration of the slurry. A simple regression formula is applied to account for such effects (R^2 = 0.88):

$$\frac{\sigma'}{\sigma_0} = 1.22[PZ]^{0.04} \quad \text{(3A-23)}$$

$$\frac{M_T'}{M_{T0}} = 1.16[PZ]^{0.03} \quad \text{(3A-24)}$$

where σ_0 and M_{T0} denote the relative supersaturation ratio and solids concentration of the suspension, respectively, in the absence of PZ in PCB; σ' and M_T' denote those in the presence of PZ; and [PZ] is the molar concentration of PZ (molecular PZ-equivalent). In addition, the solids concentration of the suspension can be determined according to:

$$M_T = \frac{F_1 \times \tau}{V} = \frac{F_1 \times \rho}{F} \quad \text{(3A-25)}$$

where V is the volume of the crystallizer (m^3), F_1 is the discharge rate of $KHCO_3$ solids in the outflow slurry (kg s^{-1}), ρ is the density of the suspension (kg m^{-3}), and F is the flow rate of the feed solution (kg s^{-1}).

For practical purposes, a hydrocyclone is considered a low-cost option for separating crystal solids from slurry. The grade efficiency of solid–liquid separation is a strong function of particle size. A mean crystal particle size of 80 μm was adopted as a design criterion for each crystallizer, assuming newly formed nuclei grow to a certain mean particle size and the other content of new solids are crystals grown on the surfaces of existing particles (i.e., seeds). Solids separation by a hydrocyclone for crystal particles with a mean diameter of 80 μm was assumed to be almost complete.[25,26] When necessary, a portion of solids were recycled to the crystallizer to maintain the required solids concentration (e.g., 10 wt%). It has been reported that the contribution of newly produced nuclei to crystallization is significant at a low seed concentration, whereas the contribution of crystal growth on seed particles becomes dominant at a higher seed concentration.[27,28] In our case, the seed concentration was so high that the latter mechanism was believed to be dominant. Thus, the size of newly produced crystal particles could be deduced based on the mass balance principle. The criterion mean size was used to obtain a preliminary estimate of the required residence time and volume of each crystallizer based on Eqs. (3A-13), (3A-22), and (3A-25).

On the basis of the experimental results and the model described above, a preliminary design calculation was performed to size the crystallizers for the Hot-CAP fully integrated with a 609-MWe (net output with CO_2 capture) coal-fired power plant. The CO_2 removal rate by the Hot-CAP was 598 tonne/hr, and the detailed mass and energy balances referred to in this sizing calculation are provided in Chapter 6. The primary process conditions used in the calculation are summarized in Table 3A-3.

Table 3A-3. Design parameters assumed for the crystallization process with five consecutive crystallizers

Unit no.	Feed solution				Crystallization					Solids separation in hydrocyclone	
										Mean size (μm)	
	Composition	Flow rate (t/h)	Temperature (°C)	Density (kg/m^3)	Temperature (°C)	Relative super-saturation σ	Flow rate of solids[a] (t/h)	Solids concentration M_T (kg/m^3)	Agitation speed N (rpm)	New crystals	All crystals
In the absence of PZ in the CO_2-rich PCB solution											
1	PCB45-36.6 + seeds	22,263 + 1,733	70-80	1,330	60	0.143	1,219	126.3	350	29.5	100
2	PCB44-33.6 + seeds	21,597 + 1,693	60	1,320	55	0.158	634	125.3	350	29.5	100
3	PCB43-30.4 + seeds	20963 + 1,658	55	1,310	50	0.177	604	124.4	350	29.5	100
4	PCB42-27.1 + seeds	20,359 + 1,622	50	1,300	45	0.203	576	123.5	350	29.5	100
5	PCB41-23.6 + seeds	19,784 + 1,587	45	1,290	38	0.240	550	122.5	350	29.5	100
In the presence of PZ (622 t/h) in the CO_2-rich PCB solution											
1	PCB45-36.6/PZ + seeds	22,885 + 1,689	70-80	1,330	60	0.169	1,321	126.3	350	29.5	100
2	PCB43.8-33.1/PZ + seeds	22,117 + 1,774	60	1,320	55	0.156	615	125.4	350	29.5	100
3	PCB42.9-30.0/PZ + seeds	21,502 + 1,721	55	1,310	50	0.180	601	124.4	350	29.5	100
4	PCB41.9-26.7/PZ + seeds	20,901 + 1,689	50	1,300	45	0.206	570	123.5	350	29.5	100
5	PCB40.9-23.2/PZ + seeds	20,331 + 1,734	45	1,290	40	0.206	472	122.5	350	29.5	100

[a]95 wt% $KHCO_3$, 1 wt% K_2CO_3, and 4 wt% of water were assumed.
[b]The outlet solution from the last crystallizer was estimated to be PCB40-20.

The results of the design analysis are summarized in Table 3A-4 and Figure 3A-12. When PZ was present in the PCB solution for crystallization, the total volume and residence time were predicted to be 3,226 m^3 and 10.9 min, respectively, smaller than those in the absence of the PZ promoter (3,473 m^3 and 12.1 min). Moreover, both the volume and residence time of each crystallizer were similar when PZ was used as the promoter, which is favorable for the crystallizer design. The total slurry flow was estimated at 3,581 tonne/hr (95% $KHCO_3$, 1% K_2CO_3, and 4% H_2O).

Table 3A-4. Predicted performance for the crystallization process with five consecutive crystallizers without and with the presence of PZ in the CO_2-rich PCB solution

Unit no.	Effective growth rate G_m (m/s[1])	Average growth rate G_{av} (m/s)[a]	Total nucleation rate B_{TOT} (1/s·m^3)	Residence time τ (s)	Crystallizer volume V (m^3)
1	8.57/7.97E-08	7.45/6.89E-08	3.09/1.33E+08	100/108	501/555
2	7.27/6.84E-08	6.32/5.92E-08	2.24/1.25E+08	118/126	578/633
3	6.18/6.59E-08	5.37/5.70E-08	1.62/1.10E+08	139/131	666/644
4	5.28/6.31E-08	4.59/5.46E-08	1.15/0.97E+08	162/137	763/660
5	4.09/5.58E-08	3.56/4.83E-08	0.69/0.89E+08	210/154	965/734

[a]The maximum crystal size L_m was assumed as 1,000 μm as a conservative estimate.

Note that the above estimation is relatively conservative. Because the solids concentration of the suspension could be elevated to more than 10 wt%, the effect of seed crystals in each crystallizer could be enhanced. It was expected that with an increasing solids concentration of the suspension, the crystal growth in each crystallizer could be accelerated and the required residence time (equipment size) of the crystallizers could be further reduced to some extent.

3A.5 Summary

A kinetic study of the crystallization of $KHCO_3$ from the PCB solution was performed using a continuous stirred tank reactor system under the MSMPR mode. Parametric experiments were conducted using the MSMPR reactor to investigate the CSD and the rates of crystal growth and nucleation of $KHCO_3$ crystallization under simulated process conditions.

Results revealed that the rate of crystal growth was size dependent, increasing with increasing particle size and then leveling off when a certain critical size was reached (~600 μm). The crystallization of $KHCO_3$ was kinetically fast and could be completed within a residence time of as little as 15 min. A longer residence time decreased the overall rates of both nucleation and crystal growth, but resulted in the formation of larger crystal particles. An increase in agitation speed enhanced the nucleation process but slowed crystal growth, which resulted in an overall reduction in crystal size. It was also observed that a higher level of supersaturation favored crystal growth and the formation of larger particles. The presence of PZ as a promoter in the CO_2-rich PCB solution accelerated crystallization owing to the increasing crystal growth rate and mean particle size. In addition, the presence of 0.05 M K_2SO_4 in the PCB solution did not significantly change the kinetic performance of bicarbonate crystallization.

A three-parameter, size-dependent crystal growth model was developed to describe the rates of crystal growth and nucleation and to predict the mean crystal size. The model was further applied

to perform a preliminary analysis of the crystallizer design for the CO_2 capture process equipped for a 609-MWe (net) power plant, and a total crystallizer volume of approximately 3,226 m^3 was found to be sufficient in a conservative process case.

References

1. Jones, A.G., Budz, J., Mullin, J.W. Crystallization kinetics of potassium sulfate in an MSMPR agitated vessel, *AIChE Journal* 1986, 32: 2002–2009.

2. Bretherton, T., Rodgers, A. Crystallization of calcium oxalate in minimally diluted urine, *Journal of Crystal Growth* 1998, 192: 448–455.

3. David, R., Villermaux, J., Marchal, P., Klein, J.P. Crystallization and precipitation engineering. IV. Kinetic model of adipic acid crystallization, *Chemical Engineering Science* 1991, 46: 1129–1136.

4. Garside, J., Shah, M.B. Crystallization kinetics from MSMPR crystallizers, *Industrial & Engineering Chemistry Process Design and Development* 1980, 19: 509–514.

5. Kougoulos, E., Jones, A.G., Wood-Kaczmar, M.W. Estimation of crystallization kinetics for an organic fine chemical using a modified continuous cooling mixed suspension mixed product removal (MSMPR) crystallizer, *Journal of Crystal Growth* 2005, 273: 520–528.

6. Evans, T.W., Margolis, G., Sarofim, A.F. Mechanisms of secondary nucleation in agitated crystallizers, *AIChE Journal* 1974, 20: 950–958.

7. Ottens, E.P.K., de Jong, E.J. Model for secondary nucleation in a stirred vessel cooling crystallizer, *Industrial & Engineering Chemistry Fundamentals* 1973, 12: 179–184.

8. Garside, J., Davey, R.J. Secondary contact nucleation: kinetics, growth, and scale-up, *Chemical Engineering Communications* 1980, 4: 393–424.

9. Kohl, A.L., Nielson, R.B. *Gas Purification*, 5th edition, Gulf Publishing, Houston, 1997.

10. Garside, J., Phillips, V.R., Shah, M.B. Size-dependent crystal growth, *Industrial & Engineering Chemistry Fundamentals* 1976, 15: 230–233.

11. Randolph, A.D., White, E.T. Modeling size dispersion in prediction of crystal size distribution, *Chemical Engineering Science* 1977, 32: 1067–1076.

12. Myerson A.S. (editor). *Handbook of Industrial Crystallization*, 2nd edition, Elsevier, Amsterdam, 2002.

13. Mydlarz, J., Jones, A.G. On the estimation of size-dependent crystal growth rate functions in MSMPR crystallizers, *The Chemical Engineering Journal and the Biochemical Engineering Journal* 1993, 53: 125–135.

14. Karpinski, P.H. Importance of the 2-step crystal growth model, *Chemical Engineering Science* 1985, 40: 641–646.

15. Garside, J., Brecevic, L., Mullin, J.W. The effect of temperature on the precipitation of calcium oxalate, *Journal of Crystal Growth* 1982, 57: 233–240.

16. Wey, J.S., Terwilliger, J.P. Effect of temperature on suspension crystallization processes, *Chemical Engineering Communications* 1980, 4: 297–305.

17. Mullin, J.W. *Crystallization*, 4th edition, Butterworth Heinemann, 2001, p. 447.

18. Zauner, R., Jones, A.G. Determination of nucleation, growth, agglomeration and disruption kinetics from experimental precipitation data: The calcium oxalate system, *Chemical Engineering Science* 2000, 55: 4219–4232.

19. Camblor, M.A., Mifsud, A., Perezpariente, J. Influence of the synthesis conditions on the crystallization of zeolite beta, *Zeolites* 1991, 11: 792–797.

20. Herrera, M.L., Hartel, R.W. Effect of processing conditions on crystallization kinetics of a milk fat model system, *Journal of the American Oil Chemists Society* 2000, 77: 1177–1187.

21. Sha, Z.L., Hatakka, H., LouhiKultanen, M., Palosaari, S. Crystallization kinetics of potassium sulfate in an MSMPR stirred crystallizer, *Journal of Crystal Growth* 1996, 166: 1105–1110.

22. Tanrikulu, S.U., Eroglu, I., Bulutcu, A.N., Ozkar, S. Crystallization kinetics of ammonium perchlorate in MSMPR crystallizer, *Journal of Crystal Growth* 2000, 208: 533–540.

23. McClements, D.J. Crystals and crystallization in oil-in-water emulsions: Implications for emulsion-based delivery systems, *Advances in Colloid and Interface Science* 2012, 174: 1–30.

24. Ooshima, H., Igarashi, K., Iwasa, H., Yamamoto, R. Structure of supersaturated solution and crystal nucleation induced by diffusion, *Journal of Crystal Growth* 2013, 373: 2–6.

25. Hsieh, K.T., Rajamani, R.K. Mathematical model of the hydrocyclone based on physics of fluid flow, *AIChE Journal* 1991, 37: 735–746.

26. Monredon, T.C., Hsieh, K.T., Rajamani, R.K. Fluid flow model of the hydrocyclone: an investigation of device dimensions, *International Journal of Mineral Processes* 1992, 35: 65–83.

27. Chivate, M.R., Palwe, B.C., Tavare, N.S. Effect of seed concentration in a batch dilution crystallizer, *Chemical Engineering Communications* 1979, 3: 127–133.

28. Kubota, N., Doki, N., Yokota, M., Sato, A. Seeding policy in batch cooling crystallization, *Power Technology* 2001, 121: 31–38.

Part 3B. Kinetic Behavior of $NaHCO_3$ Crystallization

3B.1 Introduction

In addition to a $K_2CO_3/KHCO_3$ (PCB) solution, a mixed solution of PCB and $Na_2CO_3/NaHCO_3$ (SCB) can potentially be used as an alternative solvent in the Hot-CAP. When a PCB/SCB mixture is used as a solvent, $NaHCO_3$ is preferentially crystallized out and used for CO_2 stripping, and the PCB-dominant mixture solution is used for CO_2 absorption. The major advantage of using a PCB/SCB mixture as the solvent lies in the fact that the stripping pressure of the $NaHCO_3$ slurry is much higher than that of $KHCO_3$, because the CO_2 equilibrium pressure over a SCB solution is several-fold higher than that for a PCB solution under the same conditions.

Two process concepts are proposed for using the PCB/SCB mixture as a solvent in the Hot-CAP. A schematic diagram is displayed in Figure 3B-1. Both are similar for absorption and stripping but differ in the crystallization of $NaHCO_3$, $KHCO_3$, or both. The first process option involves mixing the CO_2-rich solution from the absorber and the lean solution from the stripper and cooling them to precipitate $NaHCO_3$, $KHCO_3$, or both according to the following reaction (Figure 3B-1a):

$$KHCO_3\ (L) + NaHCO_3\ (L) = KHCO_3\ (s) + NaHCO_3\ (s) \qquad (3B\text{-}1)$$

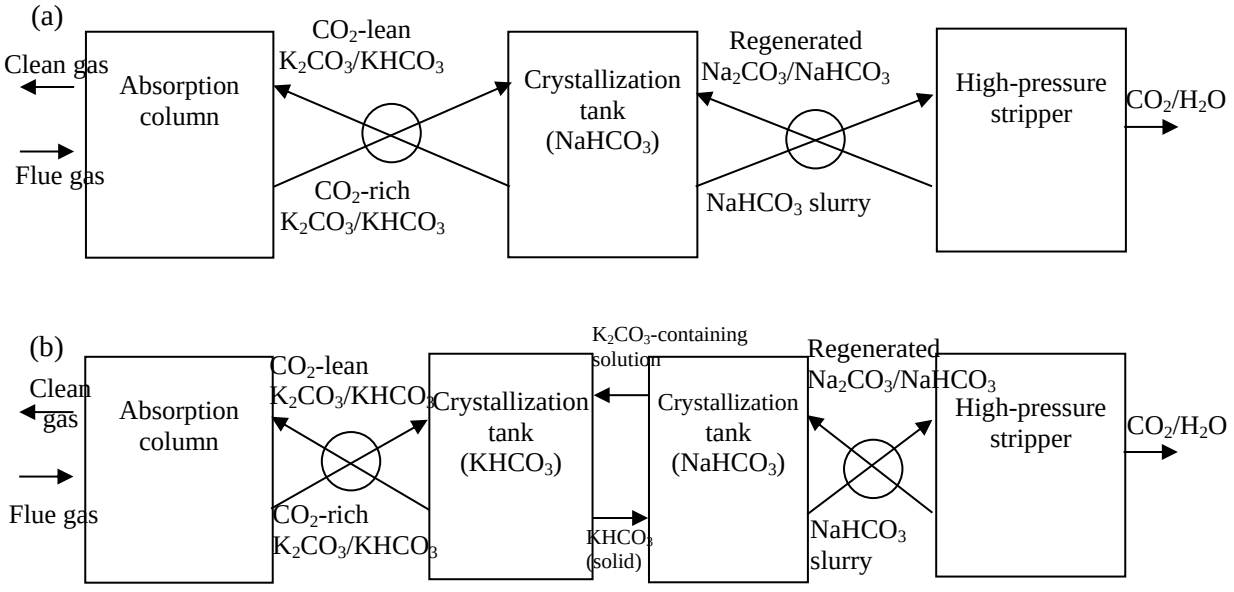

Figure 3B-1. Process concepts (a) and (b) of the Hot-CAP using a PCB/SCB mixture as the solvent for CO_2 absorption and stripping.

In the second process (Figure 3B-1b), $KHCO_3$ may be directly precipitated out by cooling the CO_2-rich PCB-dominant solution from the absorber. The recovered $KHCO_3$ solids are then added to the SCB solution regenerated from the stripper (after cooling and separating the resulting precipitates). Because the solubility of $NaHCO_3$ is much lower than that of $KHCO_3$, $NaHCO_3$ may precipitate by the following reaction:

$$KHCO_3\,(s) + Na^+ = NaHCO_3\,(s) + K^+ \qquad (3B\text{-}2)$$

The main objective of this task was to experimentally evaluate the feasibility of these two process concepts. Tests in both a batch mode and a continuous MSMPR mode were conducted to investigate the kinetics of the crystallization process and compositions of crystal products under various conditions.

3B.2 Crystallization of $NaHCO_3$ from the PCB/SCB mixture solution

3B.2.1 Experimental methods

Details of the MSMPR experimental system are described in Chapter 3A. A 1-L double-jacketed calorimetric reactor (Atlas Potassium, Syrris Inc.) was used as the MSMPR reactor. The solution was continually fed into the reactor at the desired feed temperature and flow rate. The suspension was continuously withdrawn from the reactor to maintain the liquid level in the reactor.

In a typical test, approximately 390 mL of a feed solution was initially charged to the reactor. The reactor was stirred at 350 rpm and maintained at a constant temperature (35°C). The suspension in the reactor was sampled using a syringe when the system reached steady state (after 3-to-5 times the mean residence time). The sample was immediately vacuum-filtered, and the filtered crystal particles were dried at 60°C in an oven overnight and weighed to estimate the solids concentration of the suspension. Crystal particles were analyzed using an X-ray diffractometer (Siemens-Bruker D5000 XRD). The crystal size distribution (CSD) of crystal particles was also measured using a laser-diffraction particle size analyzer (Horiba LA950) to determine the population density (n), mean crystal size ($\bar{L}$), and other kinetic parameters, such as the average crystal growth rate (G_{av}) and total nucleation rate (B_{TOT}), as described in Chapter 3A.

The PCB/SCB mixture is denoted as PCB(X_1)/SCB(X_2)-Y-Z, where X_1 is the total K_2CO_3-equivalent PCB concentration, X_2 is the total Na_2CO_3-equivalent SCB concentration, Y is the total carbonate-to-bicarbonate (CTB) conversion, and Z is the mass ratio of carbonate to bicarbonate salts. Three PCB/SCB mixtures - PCB25/SCB10-40-1.02, PCB20/SCB12-40-1.02, and PCB30/SCB5-40-1.02 - were tested in the study. Table 3B-1 is a summary of the experimental conditions used.

Table 3B-1. Matrix for testing $NaHCO_3$ crystallization from the PCB/SCB mixtures

Solution composition	PCB25/SCB10-40-1.02 (1.30 kg/L)		PCB20/SCB12-40-1.02 (1.33 kg/L)	PCB30/SCB5-40-1.02 (1.32 kg/L)
Mean residence time (τ, min)	15	30	30	30
Flow rate (g/min)	33.8	16.9	17.39	17.06
Feed temperature (°C)	70	70	70	70
Crystallization T (°C)	35	35	35	35

3B.2.2 Results and discussion

3B.2.2.1 Composition of the crystal particles

Results of the XRD analysis of crystal particles obtained by cooling the three tested PCB/SCB solutions in the MSMPR reactor at a mean residence time of approximately 30 min are shown in Figure 3B-2. Multiple crystal phases could be formed, depending on the composition of the mixture solution. Table 3B-2 lists the semi-quantitative XRD results for the crystal particles from these tests. It can be seen that the higher the total concentration of SCB in the feed solution relative to PCB, the higher the content of nahcolite ($NaHCO_3$) present in the crystal particles. Likewise, the higher the total PCB concentration in the feed solution, the more kalicinite ($KHCO_3$) was formed during the crystallization. For example, when the SCB concentration in the mixture was ≥10 wt%, little kalicinite crystallite phase ($KHCO_3$) was detected and nahcolite was dominant in the samples.

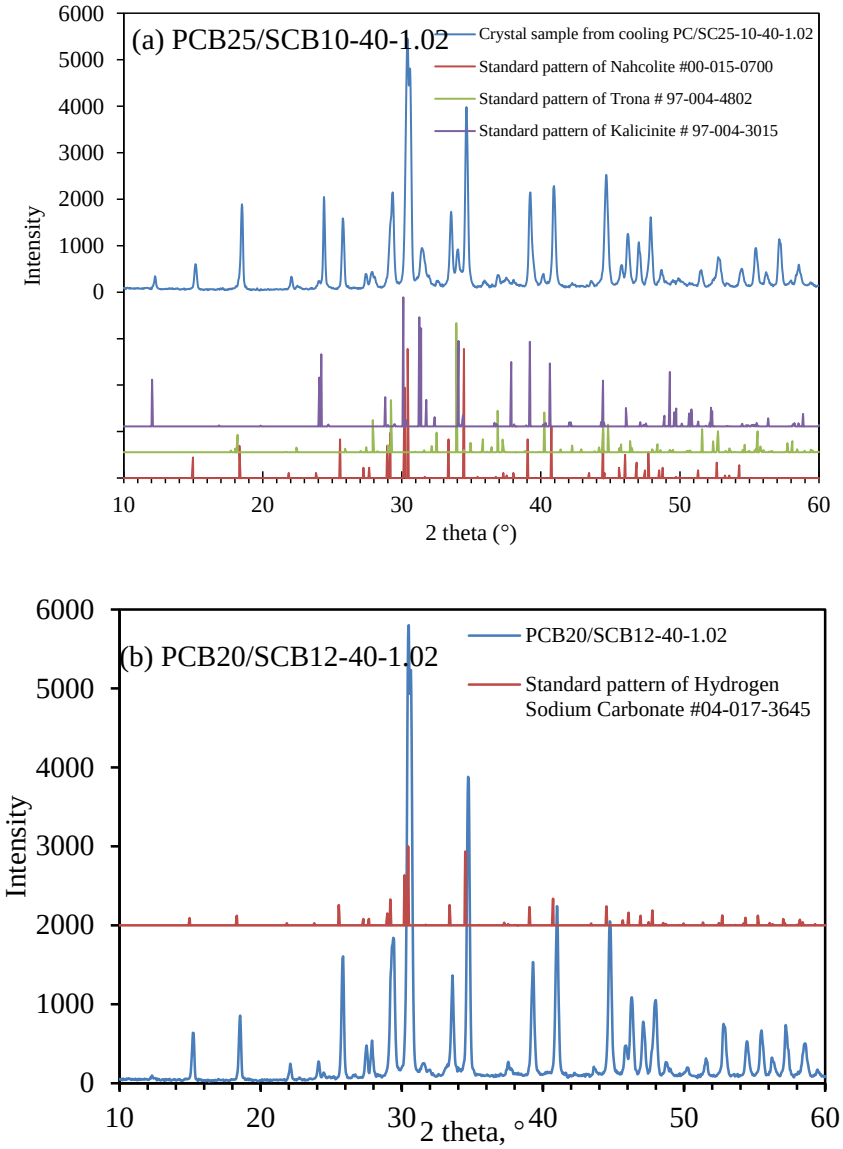

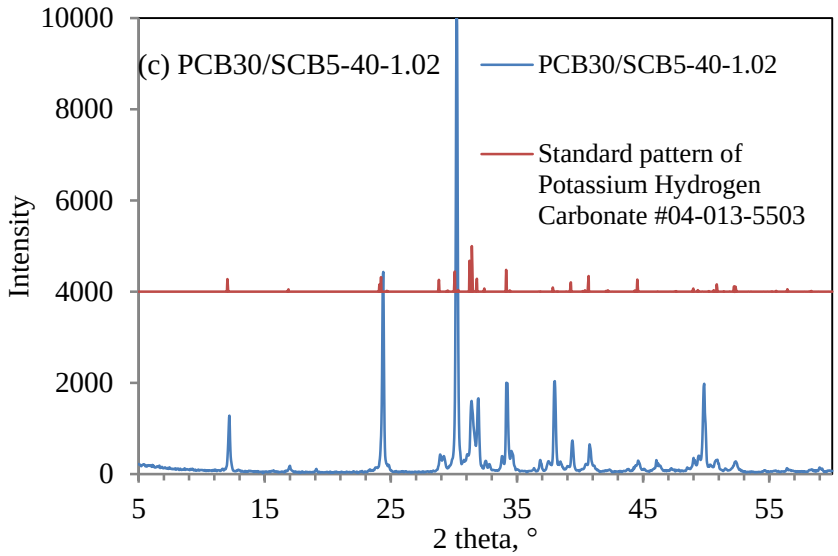

Figure 3B-2. XRD patterns of crystal particles obtained via cooling (a) PCB25/SCB10-40-1.02, (b) PCB20/SCB12-40-1.02, and (c) PCB30/SCB5-40-1.02.

Table 3B-2. Compositions of crystal samples obtained with three different PCB/SCB mixtures[a]

Feed solution	PCB20/SCB12-40-1.02	PCB25/SCB10-40-1.02			PCB30/SCB5-40-1.02
Crystal phase	Nahcolite	Nahcolite	Trona	Kalicinite	Kalicinite
Composition	100%	85.7%	7.4%	6.9%	100%

[a]Nahcolite ($NaHCO_3$), trona [$Na_3H(CO_3)_2 \cdot 2H_2O$], kalicnite ($KHCO_3$).

The morphology of crystal particles obtained with the PCB25/SC10-40-1.02 solution was characterized by scanning electron microscopy (SEM). Figure 3B-3a,b present the SEM images of crystal particles obtained at a mean residence time of 15 min, and Figure 3B-3c,d present those at a mean residence time of 30 min. $NaHCO_3$ crystals were rodlike, long, and thin, although other crystalized phases in different shapes (e.g., spherical, rectangular, etc.) were also observed. As shown in the figure, increasing the mean residence time resulted in expanding the particle size in all dimensions. Results also suggest that the mean residence time, type of species, and their relative concentrations in the mother solution played important roles in creating the morphology of the crystal particles formed.

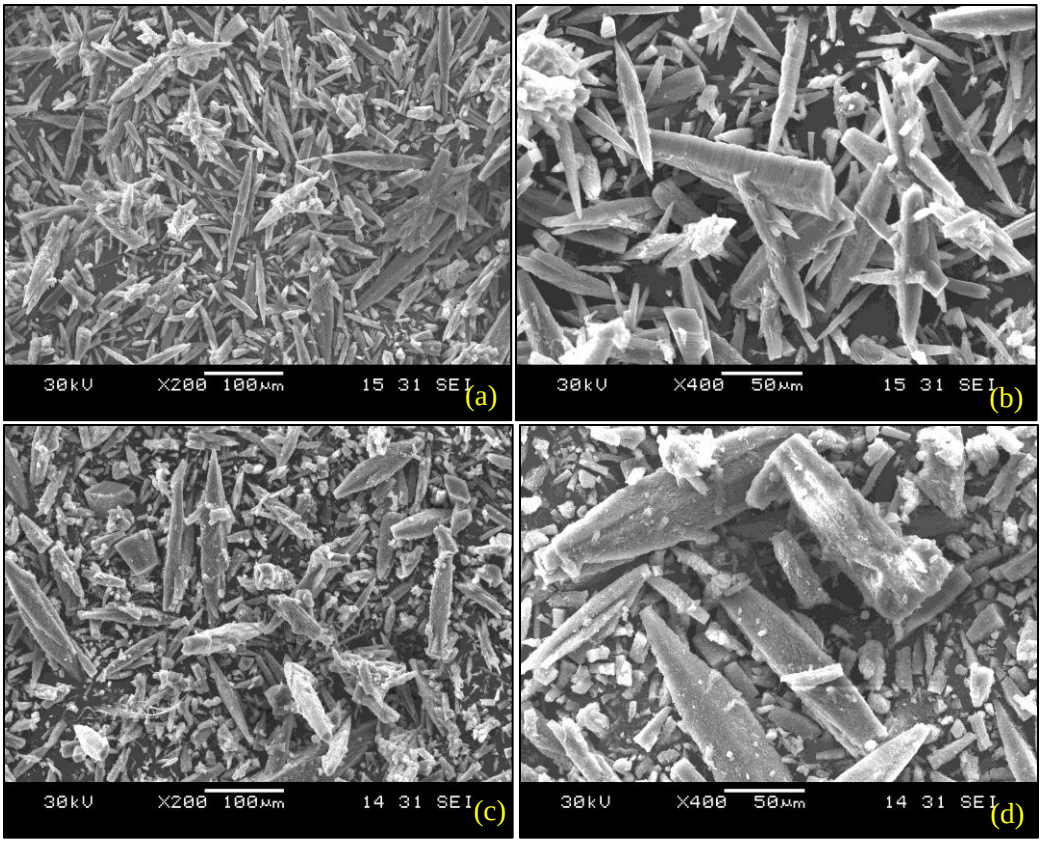

Figure 3B-3. SEM images of crystal particles obtained with PCB25/SCB10-40-1.02 in the MSMPR reactor at (a, b) a mean residence time of 15 min and (c, d) a mean residence time of 30 min.

3B.2.2 Crystallization kinetics

As described above, different crystallite phases [$NaHCO_3$, $KHCO_3$, $Na_3H(CO_3)_2 \cdot 2H_2O$] could be present in the crystal products obtained with different compositions of PCB/SCB mixtures. The CSD and population density curves of crystal particles obtained with different PCB/SCB mixture feed solutions are displayed in Figure 3B-4. All tests were conducted at a crystallization temperature of 35°C, a mean residence time of 15 or 30 min, and an agitation speed of 350 rpm.

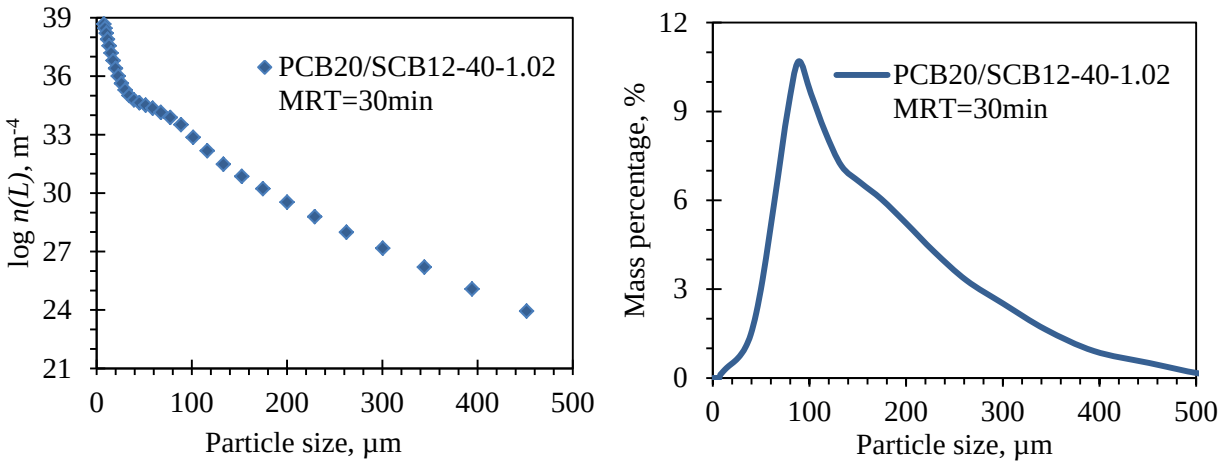

(a) Feed solution of PCB20/SCB12-40-1.02

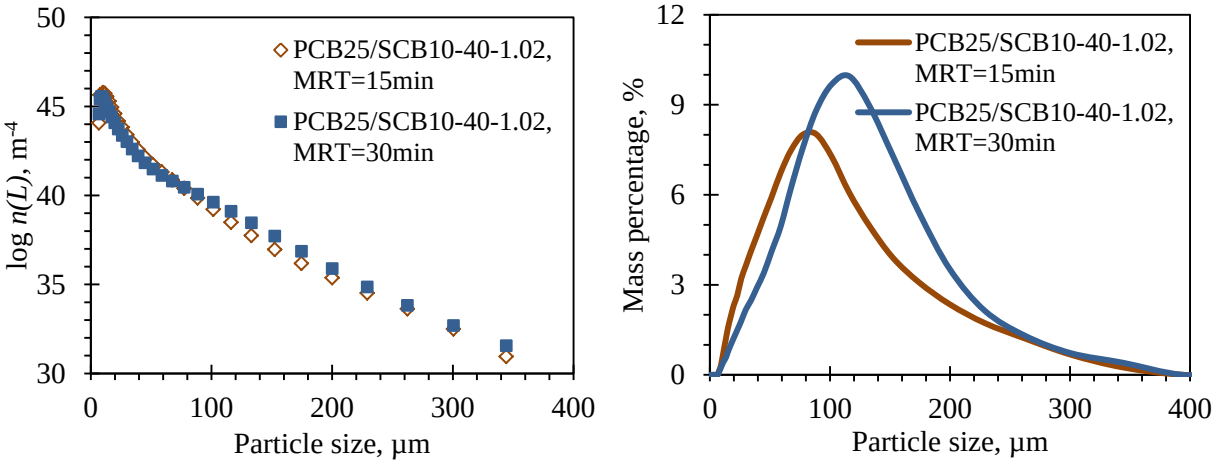

(b) Feed solution of PCB25/SCB10-40-1.02

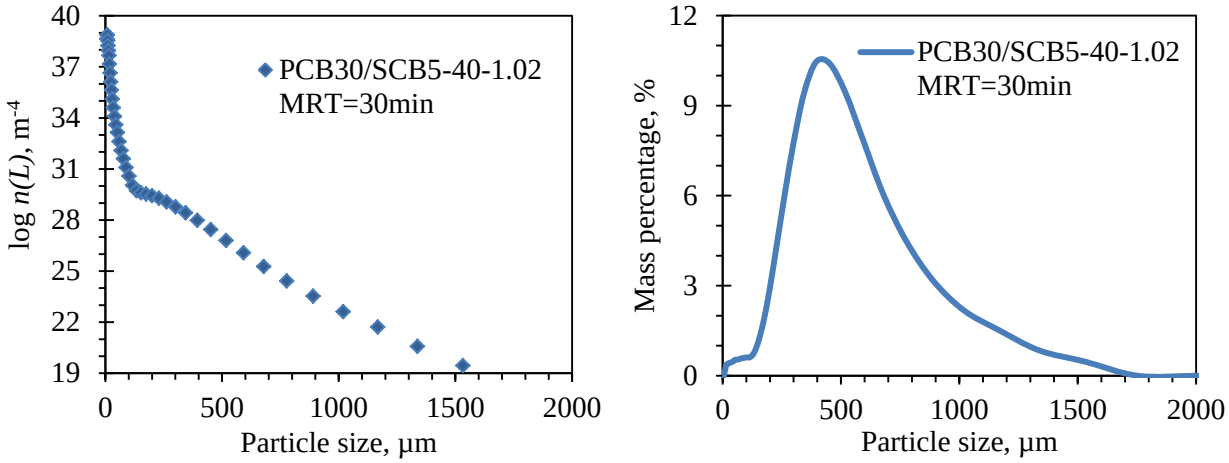

(c) Feed solution of PCB30/SCB5-40-1.02

Figure 3B-4. CSD (right) and logarithmic population density $n(L)$ (left) of particles crystallized from different PCB/SCB mixture solutions fed at 70°C, crystallized at 35°C, and with an agitation speed of 350 rpm.

Properties of the suspensions and kinetic parameters determined from the CSD measurements of crystal particles were summarized in Table 3B-3. Results indicated that the composition of the feed mixture solution had a significant effect on the crystallization kinetics. The degree of supersaturation at the crystallization temperature (35°C) varied with different feed solutions, resulting in different yields of $NaHCO_3$ crystals and solids concentrations of the suspensions. The solids concentration of the suspension was generally independent of the mean residence time used. Increasing the mean residence time of crystallization from 15 to 30 min increased the mean crystal size, but generally slowed the crystal growth rate and the secondary nucleation rate. Such results are consistent with observations reported in the literature.[1,2]

Table 3B-3. Properties of suspension and rate parameters for bicarbonate crystallization under different conditions

Property	Test 1	Test 2	Test 3	Test 4
Solution fed at 70°C	PCB20/SCB12-40-1.02	PCB25/SCB10-40-1.02	PCB25/SCB10-40-1.02	PCB30/SCB5-40-1.02
Crystallization temperature, °C	35	35	35	35
Mean residence time, min	30	15	30	30
Solids concentration in suspension (M_T), kg/m^3	30	23	26	47.5
Mean crystal size, μm	126	82	101	444
Average crystal growth rate (G_{av}), m/s	1.52×10^{-8}	1.77×10^{-8}	1.19×10^{-8}	3.47×10^{-8}
Total nucleation rate (B_{TOT}), 1/m^3·s	2.19×10^{8}	9.59×10^{11}	3.36×10^{11}	2.96×10^{8}

The logarithmic population density curves indicated that the crystallization process followed a pattern of size-dependent crystal growth for all the PCB/SCB mixture solutions tested. This means that the crystal growth rate did not change after the crystal particles grew to a critical size (i.e., the log-population density curves became linear). The breakpoint in the crystal growth rate corresponding to the critical size (after which crystal growth was size-independent) occurred at 40 to 60 μm for PCB20/SCB12-40-1.02, at approximately 40 μm for PCB25/SCB10-40-1.0, and at approximately 120 μm for PCB30/SCB5-40-1.02. The size-independent crystal growth rate after the critical size was reached was determined from the slope of the linear part of each logarithmic population density curve ($G_{linear} = -1$/slope/mean residence time). It should be noted that the mean crystal size of the $KHCO_3$ crystals (>400 μm) was significantly larger than that of the $NaHCO_3$ or $NaHCO_3$-dominant crystals (~100 μm).

3B.3 Crystallization of $NaHCO_3$ from an SCB solution with addition of solid $KHCO_3$

3B.3.1 Experimental methods

Two SCB solutions, 15 wt% SCB with 21% CTB conversion (SCB15-21) and 12 wt% SCB with 30% CTB conversion (SCB12-30), were used in the MSMPR tests to study the reactive crystallization by mixing solid $KHCO_3$ in the SCB solution as applied in process option (b).

MSMPR tests were conducted in the Syrris reactor described above. The reactor was initially charged with approximately 390 mL of an SCB solution and was maintained at 35°C during each test. Two mean residence times, 15 and 30 min, were selected in the present study (see the test matrix in Table 3B-4). The SCB feed solution was pumped continuously from a feed tank at 35°C into the reactor at a flow rate corresponding to the desired mean residence time. The suspension was pumped out continuously to maintain a constant liquid level in the reactor. Solid $KHCO_3$ (in the form of a powder) was fed into the reactor continuously (manually at 1-min intervals) at a rate stoichiometric to the inflow rate of Na^+ in the SCB feed solution according to Reaction (3B-2). A stirring speed of 350 rpm was used in all the tests.

Table 3B-4. MSMPR test conditions for $NaHCO_3$ crystallization from SCB solutions with the addition of solid $KHCO_3$

	SCB15-21 (density of 1.14 kg/L)		SCB12-30 (density of 1.11 kg/L)	
Initial solution composition	Test 1	Test 2	Test 3	Test 4
Mean residence time (τ, min)	15	30	15	30
Flow rate (g/min)	28.6	14.2	27.84	13.6
$KHCO_3$ (s) feeding rate (g/min)	6.31	3.13	4.35	2.12
Crystallization temperature (°C)	35	35	35	35

During each test, the $NaHCO_3$-containing suspension in the reactor became denser over time. After about 3 times the mean residence time, when the system almost reached steady state, 20 mL of the suspension was extracted using a syringe. The samples were immediately vacuum-filtered, dried at 60°C, and weighed to estimate the solids concentration of the suspension. CSD and XRD analyses were then performed for the crystal samples collected.

3B.3.2 Results and discussion

Figures 3B-5 shows XRD patterns of the crystal sample obtained by adding solid $KHCO_3$ to the SCB15-21 solution in the MSMPR test at a mean residence time of 15 min. XRD patterns for other crystal samples are not shown because they appear similar. All the samples contained three crystallite phases: nahcolite, kalicinite, and trona. Semi-quantitative XRD analysis revealed that nahcolite was dominant and kalicinite was minimal in all the crystal samples. Table 3B-5 summarizes the weight percentage of each phase present in the crystal samples.

Table 3B-5. Crystallite compositions of crystal samples under different conditions

	SCB15-21 (%)		SCB12-30 (%)	
Initial solution	Test 1	Test 2	Test 3	Test 4
Nahcolite	88.8	81.4	84.3	84.7
Kalicinite	2.2	3.9	4.7	3.1
Trona	9.0	14.7	11.0	12.2

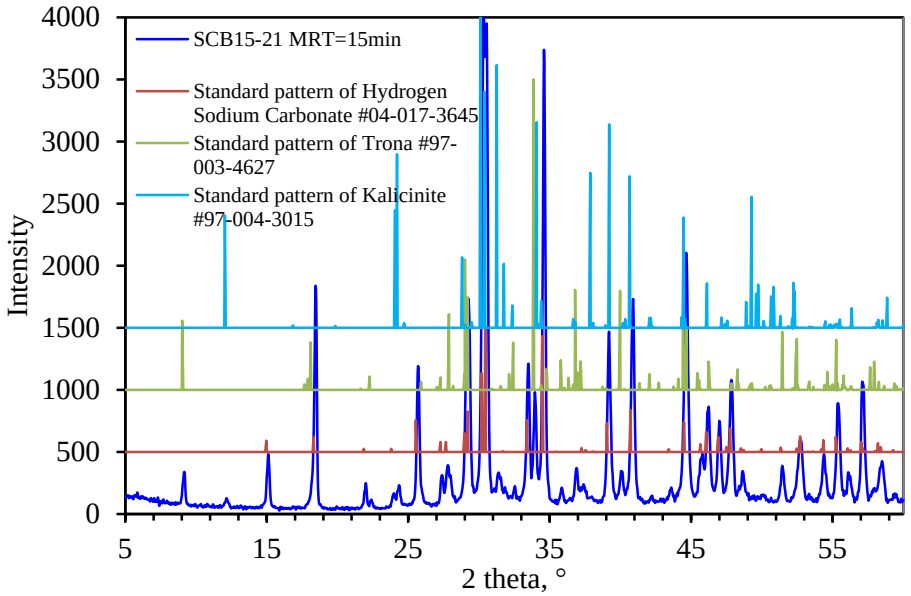

Figure 3B-5. XRD patterns of a crystal sample obtained by adding solid $KHCO_3$ into an SCB15-21 solution under MSMPR at a mean residence time of 15 min (Test 1).

It should be noted that no cooling effect was involved in the crystallization process because the crystallization temperature was the same as the feed temperature (35°C). The formation of nahcolite crystal phase was solely due to the instantaneous reaction between $KHCO_3$ and Na^+ in the $Na_2CO_3/NaHCO_3$ solution, as shown in Reaction (3B-2).

The yield of $NaHCO_3$ in the crystal product was estimated for each test. Both the SCB15-21 and SCB12-30 solutions were near saturation at 35°C. Assuming $NaHCO_3$ crystal particles were produced solely from the reaction between Na_2CO_3 in the SCB solution and solid $KHCO_3$, 155.2 kg/m^3 of $NaHCO_3$ would be crystalized out from the SCB15-21 and 83.2 kg/m^3 of $NaHCO_3$ would be crystalized out from the SCB12-30. In comparison, the measured crystal solids concentration of the SCB15-21 suspension was 151.9 kg/m^3 (~89 wt% of which was $NaHCO_3$) and that of the SCB12-30 suspension was 79.9 kg/m^3 (~84 wt% of which was $NaHCO_3$). Thus, the predicted yield of solid $NaHCO_3$ in the suspensions was generally comparable with those actually measured, indicating that $NaHCO_3$ crystals were mainly produced by the crystallization reaction between Na_2CO_3 and $KHCO_3$ rather than by physical causes, such as changes in solubility or ionic strength, when solid $KHCO_3$ was mixed into the SCB solution.

CSD analyses were performed for the crystal particles obtained from each test, and their mass mean particle sizes ($\overline{L}$) are shown in Table 3B-6. It can be seen that the mean particle size increased with an increase in the mean residence time for each solution tested. This result is consistent with those for the reactive precipitation systems reported in the literature.[3]

Table 3B-6. Mass mean particle sizes of crystal samples obtained by adding solid $KHCO_3$ to SCB solutions in the MSMPR tests

	SCB15-21		SCB12-30	
Initial solution	Test 1	Test 2	Test 3	Test 4
Mean residence time (τ, min)	15	30	15	30
Mass mean particle size (μm)	71.6	105.0	92.9	124.8

As described above, the Na_2CO_3 in the SCB solution was mostly consumed by the reaction with solid $KHCO_3$ to generate $NaHCO_3$ crystals. A comparison of crystal particle size between these tests indicates that the greater the initial concentration of $NaHCO_3$ in the SCB solution (SCB12-30 in this case), the larger the crystal size that could be obtained under the same mean residence time. This could be because the degree of supersaturation of $NaHCO_3$ attained in the SCB12-30 solution was higher than that in the SCB15-21 solution. Such a result was also consistent with results reported in the literature.[3]

3B.4 Summary

A PCB/SCB mixture solution can potentially be used as an alternative solvent to PCB in the Hot-CAP. When the PCB/SCB mixture is used, $NaHCO_3$ is preferentially crystallized out and used for CO_2 stripping, whereas a PCB-dominant PCB/SCB mixture is used for CO_2 absorption. A higher stripping pressure with the $NaHCO_3$ slurry is expected compared with the pressure with $KHCO_3$. Two process concepts were proposed for this purpose.

The feasibility of the first process option, which involved mixing the PCB-dominant solution exiting the absorber with the SCB solution regenerated from the stripper for the cooling crystallization of $NaHCO_3$, was investigated using a continuous MSMPR reactor. XRD analyses of the crystal particles indicated that the crystal composition depended on the composition of the PCB/SCB solution: the higher the total SCB concentration in the feed PCB/SCB solution, the higher the content of nahcolite ($NaHCO_3$) in the crystal solids. Crystal growth and nucleation rates were determined for the crystallization of $NaHCO_3$ from various PCB/SCB solutions. The crystallization of $NaHCO_3$ followed a pattern of size-dependent crystal growth. The mass mean size of $NaHCO_3$ crystal particles (80 to 130 μm) was generally several times smaller than that of $KHCO_3$ particles (~400 μm).

MSMPR tests were also performed to investigate the feasibility of an alternative process concept involving the reactive crystallization of $NHCO_3$ in the regenerated SCB solution with the addition of $KHCO_3$ solids (formed from the cooling crystallization of the PCB-dominant solution exiting the absorber). Crystal particles obtained during the reactive crystallization process contained three crystallite phases: nahcolite, kalicinite, and trona. Semi-quantitative XRD analyses revealed that nahcolite was dominant (>81 wt%) and kalicinite was minor (<5 wt%) in all the crystal products, indicating that it is feasible to crystalize $NaHCO_3$ through the reaction between solid $KHCO_3$ and aqueous Na_2CO_3 under the test conditions. CSD analyses of the crystal particles showed that the mass mean particle size was larger at a longer mean residence time and in the SCB solution with a greater initial concentration of $NaHCO_3$.

References

1. Wierzbowska B., Piotrowski K., Koralewska J., Hutnik N., Matynia A. Kinetics of nucleation and growth of *L*-sorbose crystals in a continuous MSMPR crystallizer with draft tube: Size-independent growth model approach, *Korean Journal of Chemical Engineering* 2009, 26(1): 175–181.

7. Kougoulos E., Jones A.G., Wood-Kaczmar M.W. Estimation of crystallization kinetics for an organic fine chemical using a modified continuous cooling mixed suspension mixed product removal (MSMPR) crystallizer, *Journal of Crystal Growth* 2005, 273(3–4): 520–528.

3. Chen J.F., Wang Y.H., Guo F., Wang X.M., Zheng C. Synthesis of nanoparticles with novel technology: High-gravity reactive precipitation, *Industrial & Engineering Chemistry Research* 2000, 39(4): 948–954.

Part 3C. Measurement of Bicarbonate Solubility

3C.1 Introduction

Knowledge of the solubility of potassium and sodium bicarbonate salt in potassium carbonate/bicarbonate (PCB), sodium carbonate/bicarbonate (SCB), and PCB/SCB mixture solutions is necessary to help identify suitable solvent compositions and operating conditions for the Hot-CAP. The solubilities of PCB solutions at high temperatures have been reported in the literature.[1] However, data for PCB with varying CTB conversion levels at lower temperatures [≤80°F (26.67°C)], which are required to investigate the performance of bicarbonate crystallization over a wider temperature range, are not available. In addition, as mentioned, an SCB or a PCB/SCB mixture solution could potentially be used as an alternative solvent to PCB. The solubilities of SCB solutions have been reported in the literature, but the data are not representative of the Hot-CAP. For a PCB/SCB system, no such data are available in the literature because of its inherent complexity as a ternary system.

The objectives of this study were to (1) obtain the required solubility data necessary for process development, and (2) to develop a simple method of measuring the solubility data of PCB, SCB, and PCB/SCB systems without a detailed phase diagram study.

3C.2 Measurement method and conditions

3C.2.1 Measurement method

A 1-L calorimetric reactor (Atlas Potassium, Syrris Inc.) with a precise temperature control and thermal insulation, as previously described in detail, was used in the measurements. A thermocouple and a turbidity probe were attached to the reactor to continuously monitor the temperature and turbidity. The operation and data logging were controlled by Atlas software installed on a computer.

In a typical measurement, the turbidity probe was calibrated for the detection of 0% and 100% turbidity following the standard procedure specified by the manufacturer: 0% turbidity corresponds to the turbidity of the reactor containing deionized water without agitation, and 100% turbidity corresponds to that in a box with the light beam path in front of the mirror cell of the probe obstructed by a small piece of matte black rubber. About 500 g of slurry with a desired composition was charged to the reactor under 200 rpm of agitation. The initial temperature of the reactor was set at a low value to ensure the presence of enough solids and thus allow for sufficiently high (>99%) turbidity. The temperature was then increased at a slow rate (0.5 to 1 °C/hr) as programed by the software. During the heating process, the dissolution temperature corresponding to complete dissolution of the slurry (i.e., when the turbidity suddenly drops to almost 0%) was identified. The dissolution temperature and the preset solution composition were used to determine the solubility under this specific condition.

3C.2.1 Measurement conditions

The dissolution temperatures of various PCB systems with varying concentrations (20 to 40 wt%) and temperatures (10 to 100°C) were measured. The test matrix is shown in Table 3C-1. The measurement method was validated by comparing the measured solubility data of the selected PCB with values reported in the literature.[1]

Table 3C-1. Matrix for measuring the solubilities of PCB aqueous systems

PCB concentration (K_2CO_3-equivalent), wt%	20	25	30	35	40
CTB conversion level, %	65, 70, 75, 80, 90, 100	40, 45, 50	25, 30	15, 20	10
Temperature, °C	10–100				

The test matrix of the solubility measurements for SCB aqueous systems is shown in Table 3C-2. The total Na_2CO_3-equivalent SCB concentration ranged between 8 and 12%, and the CTB conversion ranged between 20 and 100%. Because $NaHCO_3$ decomposes and releases CO_2 at approximately 70°C (in an open system), the temperatures investigated in this study were controlled within 20 to 70°C.

Table 3C-2. Matrix for measuring the solubilities of SCB aqueous systems

SCB concentration (Na_2CO_3-equivalent), wt%	8	9	10	11	12
CTB conversion level, %	60–100	40–100	30–90	20–80	20–70
Temperature, °C	20–70				

A PCB/SCB system was denoted as PCB(X_1)/SCB(X_2)-Y-Z, where X_1 is the total PCB concentration (K_2CO_3-equivalent, wt%), X_2 is the total SCB concentration (Na_2CO_3-equivalent, wt%), Y is the CTB conversion level, and Z is the mass ratio of carbonates (i.e., K_2CO_3 and Na_2CO_3) to bicarbonates (i.e., $KHCO_3$ and $NaHCO_3$). The solubility measurement conditions for the PCB/SCB systems are listed in Table 3C-3. The temperatures ranged between 25 and 70°C, typical of CO_2 absorption and bicarbonate crystallization in the Hot-CAP.

Table 3C-3. Matrix for measuring the solubilities of PCB/SCB aqueous mixture systems

Variable	Test 1	Test 2	Test 3	Test 4	Test 5	Test 6	Test 7	Test 8	Test 9	Test 10	Test 11	Test 12	Test 13	Test 14	Test 15	Test 16
X_1	25	20	15	10	5	25	25	20	15	25	25	25	25	25	25	25
X_2	10	10	10	10	10	8	6	8	8	10	10	10	10	10	10	10
Y	40	40	40	40	40	40	40	40	40	40	40	40	35	30	25	20
Z	1.02	1.02	1.02	1.02	1.02	1.02	1.02	1.02	1.02	1.05	1.08	1.14	1.14	1.45	1.9	2.5

3C.3 Results and discussion

3C.3.1 Validation of the measurement method

To validate the measurement method, the measured dissolution temperatures for two PCB systems, denoted as PCB40-20 for 40 wt% PCB with 20% CTB conversion (and so forth hereafter) and PCB30-80, and two SCB systems, denoted as SCB8-100 and SCB9-100, were

compared with the values available in the literature. As an example, the profiles of the recorded temperature and turbidity for the two PCB measurements are displayed in Figure 3C-1. As the temperature increased slowly, the turbidity did not change until the dissolution temperature was reached, at which point the turbidity sharply decreased to approximately 0% and then leveled off. Note that such temperature and turbidity profiles are representative of all the solubility measurements.

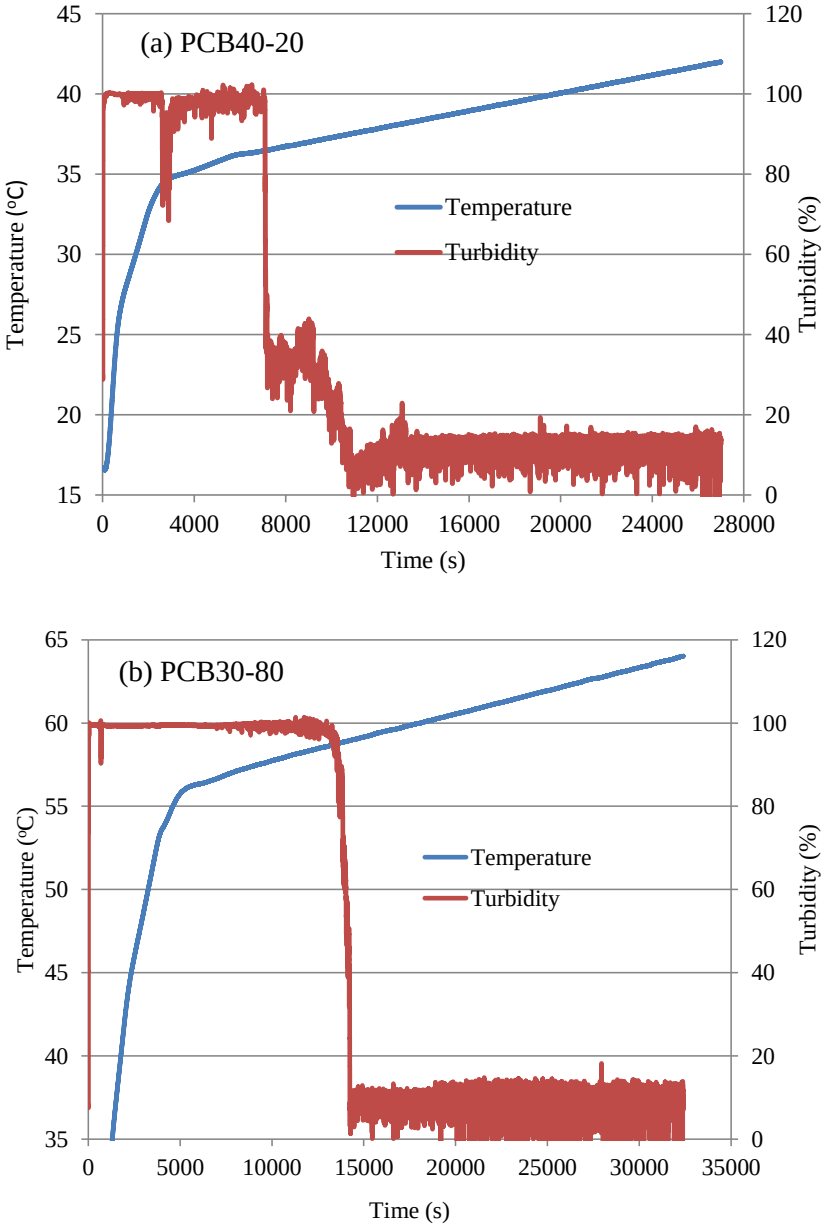

Figure 3C-1. Temperature and turbidity profiles during measurements of solubility for (a) PCB40-20 and (b) PCB30-80.

The measured dissolution temperatures for the PCB40-20 and PCB30-80 systems were 37.5°C (99.5°F) and 59°C (138.2°F), which are close to those reported in the literature, approximately

37.8°C (100°F) and approximately 60°C (140°F).[1] The measured value was 46.8°C for SCB8-100 and 60.0°C for SCB9-100, consistent with the data reported in the literature (47.8 and 59.3°C, respectively). The measurement method was thus validated by the good agreement between the measured data and literature values.

3C.3.2 Solubility of the PCB systems

A summary of the measured dissolution temperatures and the data available in the literature are shown in Table 3C-4. Following the format in the literature,[1] the solubility data for each PCB system of a certain PCB concentration was depicted as a relationship between the CTB conversion of PCB and the dissolution temperature, as shown in Figure 3C-2.

Table 3C-4. Dissolution temperatures of PCB solutions measured in this study (noted as M) and reported in the literature (noted as L)

	20 wt% PCB			25 wt% PCB			30 wt% PCB			35 wt% PCB			40 wt% PCB	
	T (°C)	CTB,%		T (°C)	CTB,%		T (°C)	CTB,%		T (°C)	CTB,%		T (°C)	CTB,%
M	26.2	100	L	48.2	100	L	68.3	100	L	89.9	100	L	116.9	100
	25.1	90		44.0	90		64.2	90		85	90		108.6	90
	20.3	80		39.9	80		60	80		79.4	80		101	80
	18.6	75		35	70		53.8	70		72.5	70		91.9	70
	16.5	70		28.1	60		46.1	60		64.2	60		83.6	60
	14.6	65	M	22.4	50		38.9	50		54.4	50		73.2	50
				19	45		28.8	40		44.7	40		62.8	40
				13.9	40	M	20.4	30		35	30		51.7	30
							16.9	25	M	24.3	20		37.8	20
										15.2	15	M	19.4	10

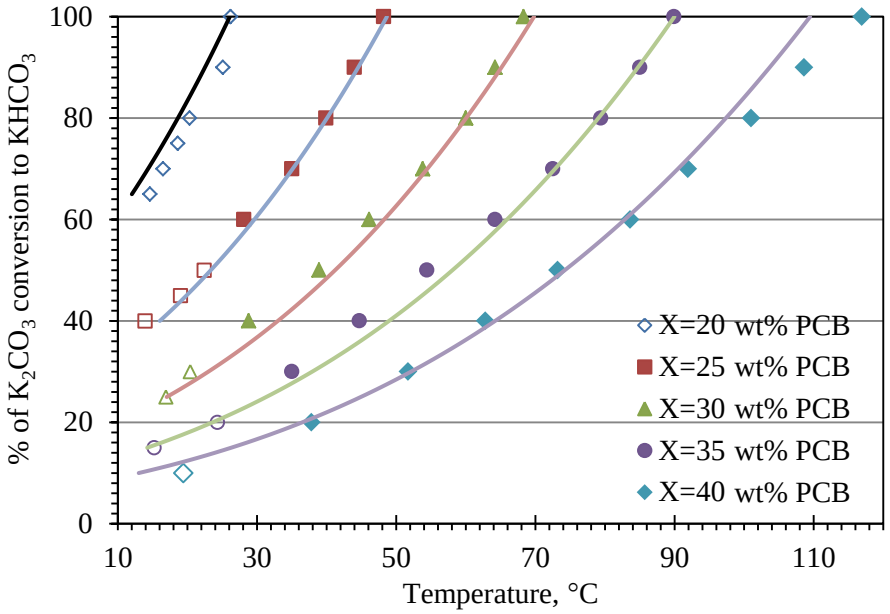

Figure 3C-2. Solubilities of K_2CO_3/$KHCO_3$ systems at various temperatures and CTB conversion levels. Open symbols indicate the measured data, and filled symbols indicate the literature data. Lines represent the solubility limits predicted by the empirical formula developed in this study.

An empirical formula was developed to describe the relationship between the dissolution temperature and the total PCB concentration and CTB conversion in the PCB solution:

$$^1/_T = 0.0083 - 0.0011\,ln(X) - 0.00038\,ln(Y) \qquad \text{(3C-1)}$$

where T is the dissolution temperature (°K), X is the PCB concentration (wt%), and Y is the CTB conversion (wt%). The lines representing the solubility limits predicted by Eq. (3C-1) are also displayed in Figure 3C-2. Note that the predicted values are in good agreement with the measured data and literature values.

3C.3.3 Solubility of the SCB systems

Solubility isotherms of Na_2CO_3-$NaHCO_3$-H_2O systems have been reported in the literature at temperatures of 25 to 50°C.[2] Unlike PCB, an SCB aqueous system is rather complicated because multiple crystal phases can be formed depending on the SCB composition. Figure 3C-3 shows the phase diagram of a ternary SCB system at 50°C. The area above the AKCD curve represents an unsaturated SCB solution; the triangles, such as AK-$NaHCO_3$, KCT, and CD-$Na_2CO_3{\cdot}H_2O$, are saturated SCB solutions in the presence of the $NaHCO_3$, trona, and $Na_2CO_3{\cdot}H_2O$ solid phases, respectively; and the dotted lines represent the saturated solid phases. The solubilities of bicarbonate and trona in an SCB system are relatively small. For practical purposes, only the regions near the AK line are applicable to the Hot-CAP. Therefore, this solubility study focused on SCB systems with relatively low total concentrations of Na_2CO_3 and $NaHCO_3$, which would not incur the formation of multiple solid phases other than bicarbonate, trona, or both.

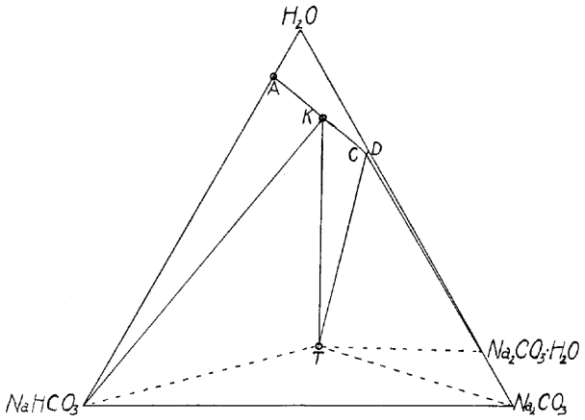

Figure 3C-3. Phase diagram of a Na_2CO_3-$NaHCO_3$-H_2O system at 50°C. A: solubility of pure $NaHCO_3$; AK: saturated SCB solution in equilibrium with solid phase $NaHCO_3$; KC: saturated SCB solution in equilibrium with solid phase trona [$Na_3(CO_3)(HCO_3){\cdot}2H_2O$]; CD: saturated SCB solution in equilibrium with a solid phase monohydrate; D: solubility of pure Na_2CO_3.[2]

Results of the measured dissolution temperatures for various SCB systems are shown in Figure 3C-4. Similar to the PCB solubility measurement, an empirical model was established to predict the temperature–solubility relationship:

$$1/T = 0.0064 - 0.00077\ln(X') - 0.00036\ln(Y') \quad \text{(3C-2)}$$

where T is the dissolution temperature (°K), X'(wt%) is the total SCB concentration (Na_2CO_3-equivalent), and Y' is the CTB conversion (%). The value of R^2 for the regression equation was estimated at 96.5%, indicating good agreement between the prediction and the measurement.

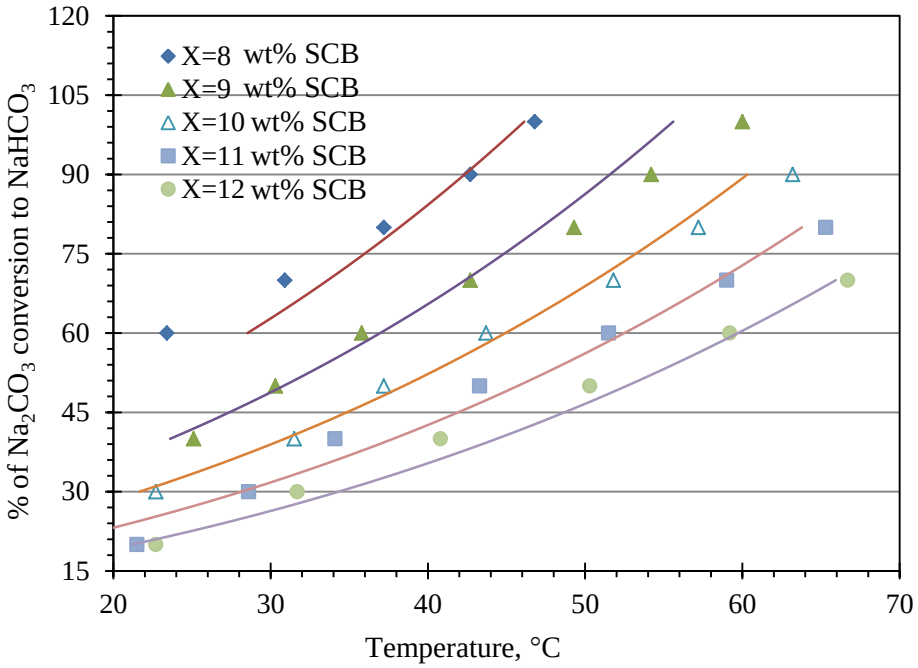

Figure 3C-4. Solubility of Na_2CO_3/$NaHCO_3$ aqueous systems at various temperatures and CTB conversions. The curves represent the solubility limits predicted by Eq. (3C-2), and the symbols represent the experimental results.

3C.3.4 Solubility of the PCB/SCB systems

The measured dissolution temperatures under various conditions are plotted as a function of the PCB/SCB mixture composition in Figure 3C-5.

Figure 3C-5a shows an almost linear correlation between the dissolution temperature and the total concentration of K_2CO_3/$KHCO_3$ (X_1) of the mixture system while the other conditions remained constant. A similar trend was also observed (Figure 3C-5b) for that between the dissolution temperature and the total concentration of Na_2CO_3/$NaHCO_3$ (X_2). When the mass ratio of CTB salts (Z) changed from 1.02, 1.05, and 1.08 to 1.14, the dissolution temperature (70.7 ± 0.6°C) did not vary significantly, as shown in Figure 3C-5c. Note that the value of Z did not change substantially (0.90 to 1.19) for the PCB25/SCB10-40-Z mixtures tested.

Because the dissolution temperature was not sensitive to the value of Z, the effect of the CTB conversion level was examined using the data for the PCB/SCB mixtures with fixed total PCB (X_1 = 25) and total SCB concentrations (X_2 = 10), but with varying Z within the range of potential Hot-CAP conditions. The results in Figure 3C-5d indicate that the greater the CTB conversion in the PCB/SCB mixture, the higher the dissolution temperature, which is consistent

with the fact that the bicarbonate salts have lower solubility than do carbonate salts at a given temperature.

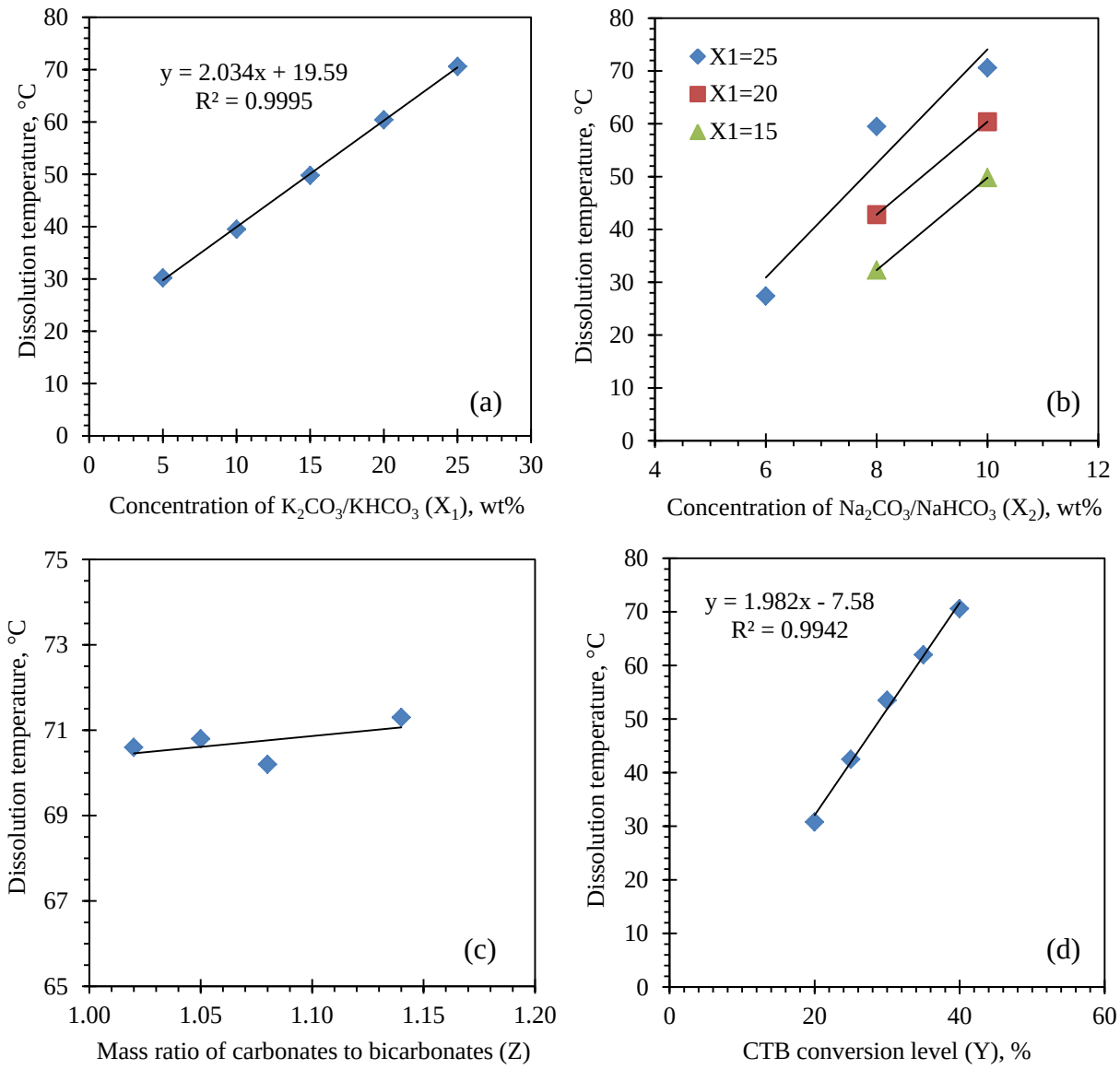

Figure 3C-5. Effect of the PCB/SCB composition on the solubility of bicarbonates: (a) effect of the total PCB concentration (X_2 = 10, Y = 40, Z = 1.02); (b) effect of the total SCB concentration (Y = 40, Z = 1.02); (c) effect of the CTB mass ratio (X_1 = 25, X_2 = 10, Y = 40); and (d) effect of the CTB conversion level (X_1 = 25, X_2 = 10).

On the basis of the measurement results, a multivariable linear regression model (R^2 = 0.9767) was developed to predict the solubility temperature of the PCB/SCB mixture:

$$T = 2.089\,X_1 + 9.815\,X_2 + 1.617\,Y - 5.666\,Z - 137.64 \qquad \text{(3C-3)}$$

where T is the dissolution temperature (°C), X_1 is the K_2CO_3-equivalent total PCB concentration (wt%), X_2 is the total Na_2CO_3-equivalent SCB concentration (wt%), Y is the CTB conversion (%), and Z is the mass ratio of carbonate salts-to-bicarbonate salts.

3C.4 Summary

Solubilities of the PCB, SCB, and PCB/SCB mixture solutions at various concentrations, CO_2 loading levels in solution, and temperatures were measured using a turbidity-based approach. Such data are required for identifying the design and operating conditions suitable for potential application in the Hot-CAP.

Dissolution temperatures of 20 to 40 wt% PCB aqueous systems at low temperatures [≤80°F (≤26.67°C)] were measured to complement the data unavailable in the literature. Lines representing the solubility limits were established to describe the effect of temperature, PCB concentration, and CTB conversion on the solubilities of PCB systems. An empirical correlation was developed based on the measured data and literature values to predict the solubilities of PCB at a wide range of temperatures (down to 10°C).

Unlike PCB, an SCB aqueous system is complex and may involve multiple crystal phases. Isotherms of the SCB systems at temperatures >50°C are not available in the literature. Solubilities were obtained for 8 to 12 wt% SCB systems at 20 to 70°C. On the basis of the measured results, an empirical model was developed that could predict solubility limits for the SCB systems.

Solubility data were measured for bicarbonates in various PCB/SCB systems at 30 to 70°C. These data included PCB/SCB systems with total PCB concentrations ranging between 5 and 25 wt%, total SCB concentrations between 6 and 10 wt%, CTB concentrations between 20 and 40%, and mass ratios of carbonate salts-to-bicarbonate salts between 1.02 and 1.14. An empirical model to predict dissolution temperatures of the PCB/SCB mixtures was also developed based on the experimental results.

References

1. Kohl A.L., Nielson R. *Gas Purification*, 5th edition, Gulf Publishing, Houston, 1997.

2. Hill A.E., Bacon L.R. Ternary systems. VI. Sodium carbonate, sodium bicarbonate and water, *Journal of the American Chemical Society* 1927, 49(10): 2487–2495.

Chapter 4. Phase Equilibrium and Kinetic Performance of High Pressure CO_2 Stripping

Part 4A. Vapor-Liquid-Equilibrium (VLE) Measurements of Concentrated CO_2-H_2O-K_2CO_3/$KHCO_3$ Systems

4A.1 Introduction

Knowledge of the phase equilibria of CO_2-H_2O-K_2CO_3/$KHCO_3$ systems at elevated pressures and temperatures is essential for the design, scale-up, and evaluation of the high-pressure stripping process, which is a technical innovation of the Hot-CAP. VLE data are of practical interest for the total concentrations of K_2CO_3/$KHCO_3$ (PCB) aqueous systems between 40 and 70 wt% (K_2CO_3-equivalent), at temperatures between 140 and 200°C, and pressures ranging from 1 to 40 bar (0.99 to 39.48 atm).

However, VLE data under such practical conditions typical of the Hot-CAP process are not available in the literature except for solutions of 40 wt% PC at 140°C reported by Tosh and colleagues (Benson, 1956; Tosh et al., 1959). Therefore, we measured the VLE data under these conditions. In this study, we measured the VLE data for 40 to 60 wt% aqueous PCB solutions or slurries with CTB conversions ranging from approximately 20 to 85%. To investigate the effect of K_2SO_4 impurities on the VLE behavior, data was also measured under a representative condition—a 50 wt% PCB solution with approximately 67% CTB conversion in the presence of 2 and 4 wt% K_2SO_4 at 140 to 200°C.

4A.2 Experimental section

4A.2.1 Experimental setup and apparatus

A schematic diagram of the experimental setup for measuring the VLE of the CO_2, water vapor, and K_2CO_3/$KHCO_3$ slurry system is shown in Figure 4A-1. It consists of a high-pressure stirred cell reactor (Parr Instrument Company, model 4531), a gas supply/control unit, data acquisition instrumentation, and a gas chromatograph (GC) for measuring the gas composition.

The high-pressure Parr reactor is a cylinder of 1-liter capacity with an inner diameter of 4.0 in. (10.2 cm) and a depth of 5.4 in. (13.7 cm). It is furnished with a self-sealing FFKM (perfluoroelastomer) O-ring closure to bear working temperatures up to 275°C and pressures up to 1,900 psia (129.3 atm). The reactor is equipped with a DC variable-speed magnetic stirrer with maximum torque of 16 in.-lb (1.8 N-m) supplied with and controlled through a Parr Series 4840 controller to provide stirring speeds for both the gas and liquid phases from 0 to 600 rpm. Multiple valves and gauges, including a gas inlet valve, gas release valve, liquid sampling valve, pressure gauge, and safety rupture disc for emergency ventilation, are built into the reactor. An external furnace is used to heat the reactor, and the temperature is controlled through a separate Parr Series 4840 Temperature Controller. A continuous flow of cold water with adjustable flow rates through a coil in a serpentine configuration optionally installed inside the reactor can be used to control the temperature, particularly when the desired operating temperatures are below 150°C.

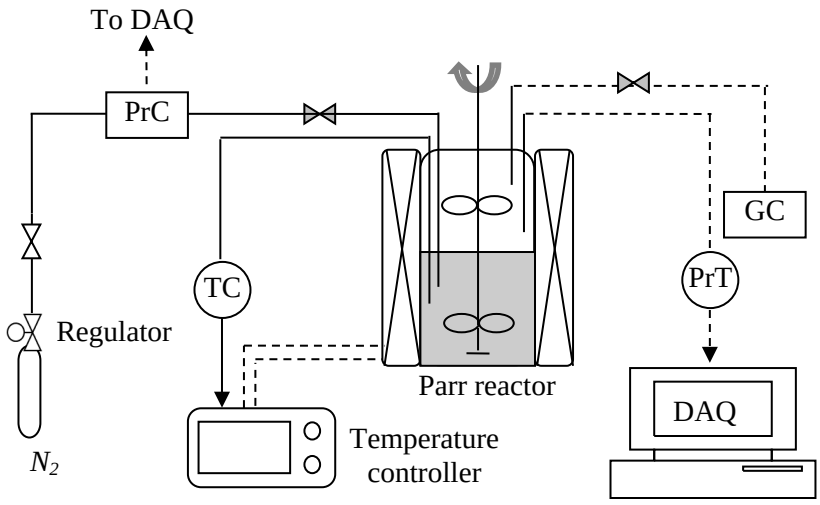

Figure 4A-1. Schematic diagram of the experimental setup for measuring the VLE of the CO_2-H_2O-K_2CO_3/$KHCO_3$ system (PrT: pressure transducer; PrC: pressure controller; TC: thermal couple; GC: gas chromatograph; DAQ: data acquisition).

Photographs of the experimental setup with the Parr reactor are displayed in Figure 4A-2. The Parr reactor is mounted on a movable cart. A vacuum pump (Dekker, RVL002H-01) is used to remove the residual air, inert gas, or other undesirable gases, if any, from the experimental system. The pressure of the reactor is measured by a pressure transducer (Omega, PX409-1.0KAUSB) and monitored or recorded by a computer. A GC (Shimadzu GC-2014) is used to measure gas composition. Gas samples are obtained using a 100-ml syringe (cat. #20162, Restek Corporation) through a 10-mm septum fit into a ¼-in. (6.35 mm) tee tubing gas sampling port.

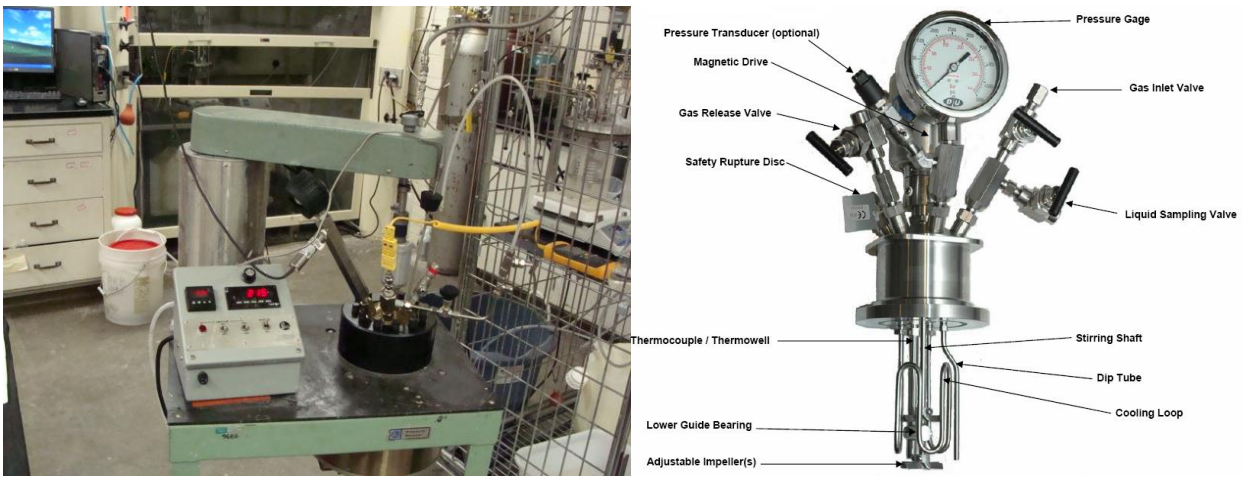

Figure 4A-2. Photograph of the Parr reactor and the system for measuring the CO_2 and water vapor pressures over the PCB aqueous solutions.

4A.2.2 Experimental method

The measurement is based on a desorption method, with PCB aqueous solutions of certain compositions exposed under a desorption process at the desired conditions. It was operated in batch mode with respect to both the gas and liquid phases. In a typical experiment, 1,000 g of

PCB slurry with a desired composition was fed to the Parr reactor. After careful assembly and leakage checking, the system was vacuumed to the desired level at room temperature. The stirrers for both the gas and liquid phases were then turned on (both at 250 rpm) while the furnace heater was started to heat the reactor to a desired set point temperature. In about 2 hr, when the system reached an equilibrium state, as evidenced by no substantial change in pressure over approximately one-half hour, a pure N_2 gas stream was introduced into the reactor to a predetermined pressure value. After stabilization, the N_2 gas partial pressure (P_{N2}) in the reactor was determined by the difference between the total pressures prior to and after the N_2 gas injection. The gas samples for GC analysis were extracted from the gas stream released from the reactor through a needle valve using a syringe. The CO_2 partial pressure (P_{CO2}) was determined from the gas composition analyzed by the GC and the known N_2 gas partial pressure in the reactor.

The parameters and conditions for GC operation are listed in Table 4A-1. Three standard N_2/CO_2 mixture gases with specified compositions of 98%/2%, 90%/10%, and 50%/50% (in volume) were routinely used to calibrate the GC. Representative chromatographs of the standard gas mixtures for GC calibration are shown in Figure 4A-3. The first peak corresponds to the N_2 gas component, and the second corresponds to the CO_2. The ratio of the peak areas of N_2 to CO_2 was calibrated using the composition of the standard CO_2/N_2 mixture gases. The GC analysis used for determining the CO_2 partial pressure in the Parr reactor demonstrated an accuracy equivalent to ±0.01 psi (68.9 Pa) of pressure.

Table 4A-1. Parameters and conditions for GC operation

GC make/model	Shimadzu GC-2014
Column	RT®-Q-Bond fused-silica porous layer open tubular), 0.53 × 30 mm, with 20 mm film thickness
Carrier	Helium 5 ml/min @ 60°C, constant flow mode
Oven	60°C constant
Injection	125°C, 100-ml syringe injection, direct mode
Detector	Thermal conductivity detector, preheated at 150°C

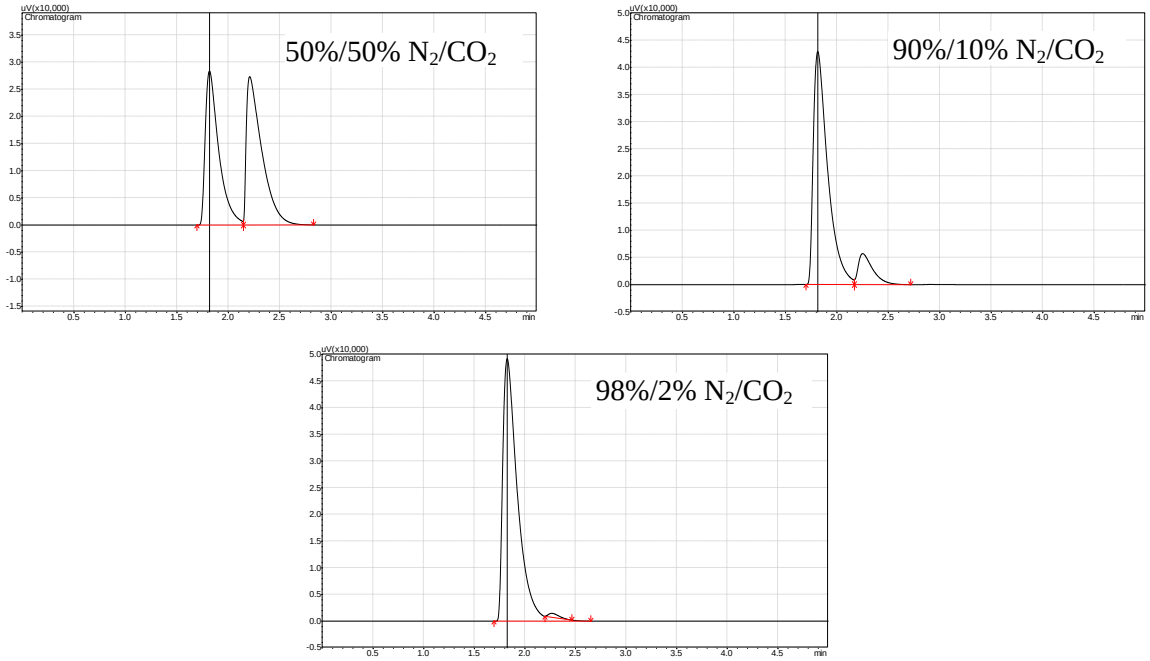

Figure 4A-3. Representative chromatographs of the standard gas mixtures for GC calibration.

The partial pressure of water vapor in the gas phase was consequently obtained by

$$P_{\mathrm{H_2O}} = P_t - P_{\mathrm{CO_2}} - P_{\mathrm{N_2}} \qquad \text{(4A-1)}$$

where P_t was the total pressure recorded by the pressure transducer.

The liquid composition at equilibrium was obtained from the predetermined composition of the initial PCB slurry and the mass balance for CO_2 in the system. Because a much larger amount of solution was used and the volume of the gas phase was small, the change in liquid composition was usually negligible and, if necessary, might be compensated for by CO_2 desorption.

4A.3 Results and Discussion

VLE data are presented by the equilibrium partial pressures of CO_2 or water vapor plotted as a function of the CTB conversion of the PCB solution. Because the CO_2 partial pressure approaches zero over a solution with zero CTB conversion and becomes very large with a CTB conversion of more than 90%, the VLE curves are usually reverse S-shaped. The measurements were focused on CTB conversions ranging between approximately 20 and 85% to encompass the composition range of the PCB solution or slurry in the stripping column designated in the Hot-CAP. Note that the PCB containing a high concentration of $KHCO_3$ is a slurry at room temperature, but becomes soluble at high temperatures (140 to 200°C).

4A.3.1 VLE data for 40 to 60 wt% PC at 140 to 200℃

Figure 4A-4 compares the VLE data measured for the 40 wt% PCB solution at 140°C in this work and in the work by Tosh *et al*. (1959). At CTB conversion levels below 50%, the data measured in this study closely match those reported by Tosh *et al.*; however, at CTB conversion

levels above 50%, both the P_{CO2} and the total pressures (the sum of P_{CO2} and P_{H2O}) measured in this study were lower, whereas the P_{H2O} values were higher than those reported by Tosh *et al*. Considering the fact that the measurements of the total pressure in the experiments are straightforward and were performed by using a reliable and calibrated pressure transducer and that the temperature was measured near the interface between the gas and liquid phases by a reliable and calibrated thermal couple, the source of variability is unknown.

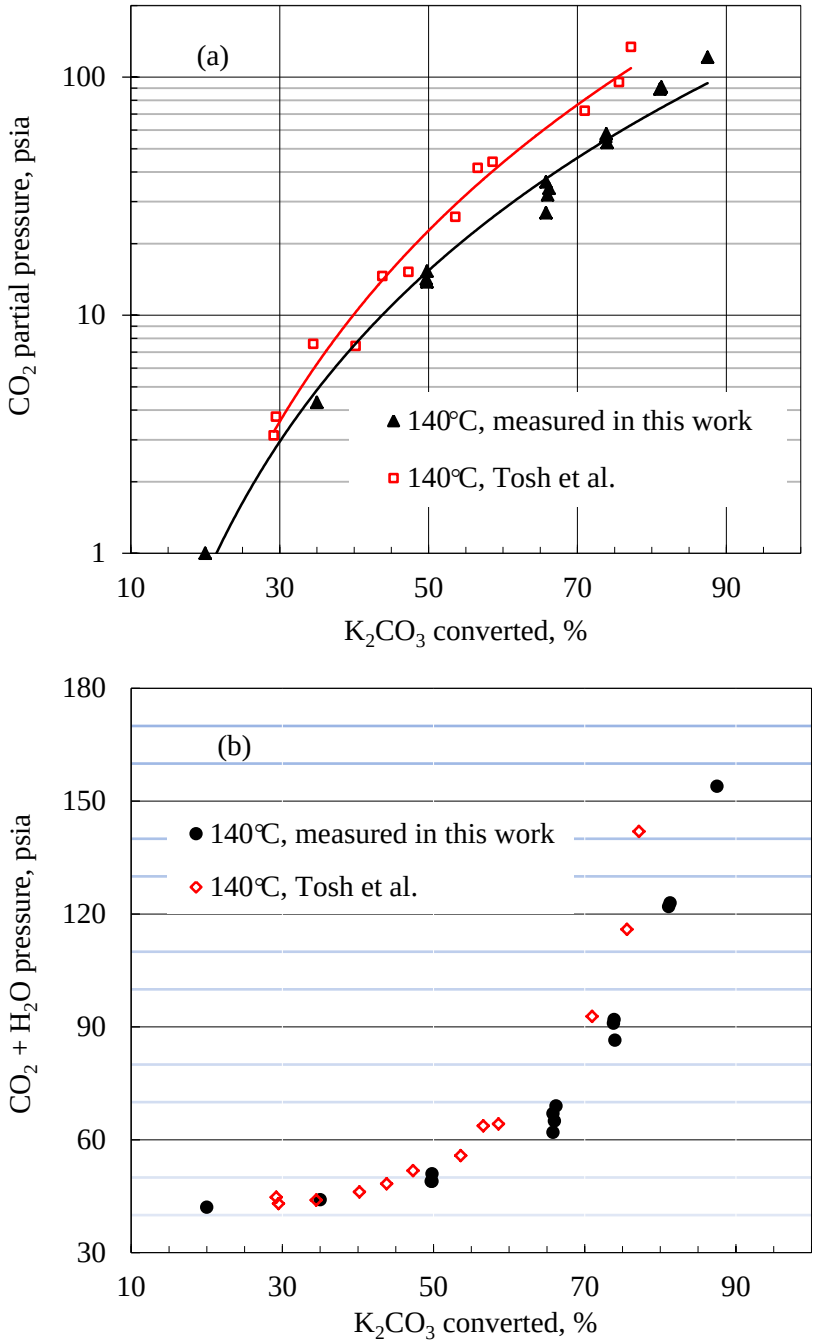

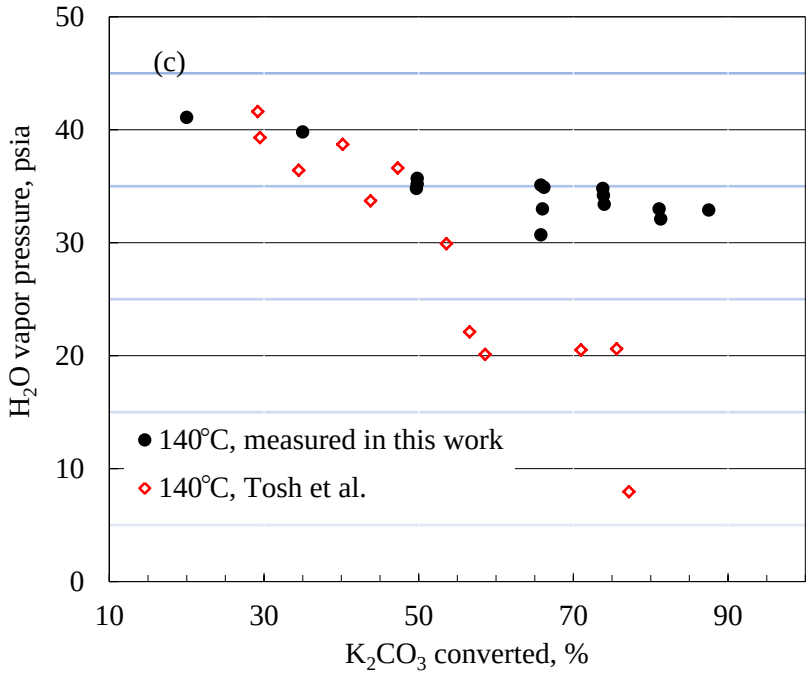

Figure 4A-4. VLE data for the 40 wt% PCB solution at 140°C measured in this work and reported in the literature: (a) CO_2 partial pressure, (b) total pressure of CO_2 and water vapor pressure, and (c) water vapor pressure.

Tosh *et al*. (1959) measured the VLE data by using a rocking autoclave consisting of a 3-in. (7.6 cm) schedule 40 stainless steel pipe (Type 304) about 3 ft (0.91 m) long, jacketed by a 4-in. (10.2 cm) schedule 40 pipe. The desired temperatures were obtained by boiling water at the appropriate pressures in the jacket, and heat was applied on the outside of the jacket through an electric winding. The rocking motion was conveyed to the autoclave by an assembly rocked through an arc of approximately 30° at a rate of 24 cycles per minute. Gas samples were drawn into a gas-sampling apparatus through a length of glass tubing. To prevent the water from condensing, the gas sampling assembly was heated by an electrical tape heater to a temperature at, or slightly above, the equilibrium temperature. Therefore, it is of concern that the rocking might not be sufficient to ensure thorough mixing for a uniform temperature and composition distribution in both the gas and liquid phases. In addition, water condensation might occur because of insufficient or discontinuous heating of the gas sampling assembly, which would result in a lower water vapor pressure and higher CO_2 pressure value.

To further confirm the measurement of the total pressure of the system, the saturation pressures of water vapor over pure water ($P_{W,S}$) at 140 to 200°C were measured. The $P_{W,S}$ data obtained are in good agreement with those in the literature (data not shown). Thus, the measurement of the total pressure in this work was trustworthy.

Figures 4A-5 to 4A-7 show the VLE data for the 40, 50, and 60 wt% PCB solutions at different CTB conversion levels at 140 to 200°C. For each PCB solution, the curves of isotherms for the P_{CO2} versus the CTB conversion at different temperatures were almost parallel to one another. As expected, both the P_{CO2} and P_{H2O} increased with increasing temperature. At the same temperature,

P_{CO2} increased substantially, whereas P_{H2O} decreased as the CTB conversion of the solution increased.

A high stripping pressure and a lower ratio of water vapor-to-CO_2 partial pressure can result in a significant reduction in the energy use associated with the CO_2 stripping heat and compression work. The VLE measurement results above indicate that a higher operating temperature and a PCB with a higher CTB conversion level were favored to obtain a relatively higher total pressure and a lower water vapor pressure. For example, at 200°C, the total pressure and the ratio of water vapor-to-CO_2 partial pressure over the 50 wt% PCB solution of 83% CTB conversion were 453 psia (30.8 atm) and 0.16:1. In comparison, at 160°C, those over the 50 wt% PC solution of 73% CTB conversion were 138 psia (9.4 atm) and 0.35:1, respectively. These results verify the advantage of the Hot-CAP: the energy use associated with the stripping heat and compression work can be reduced by using the PCB slurry for CO_2 stripping.

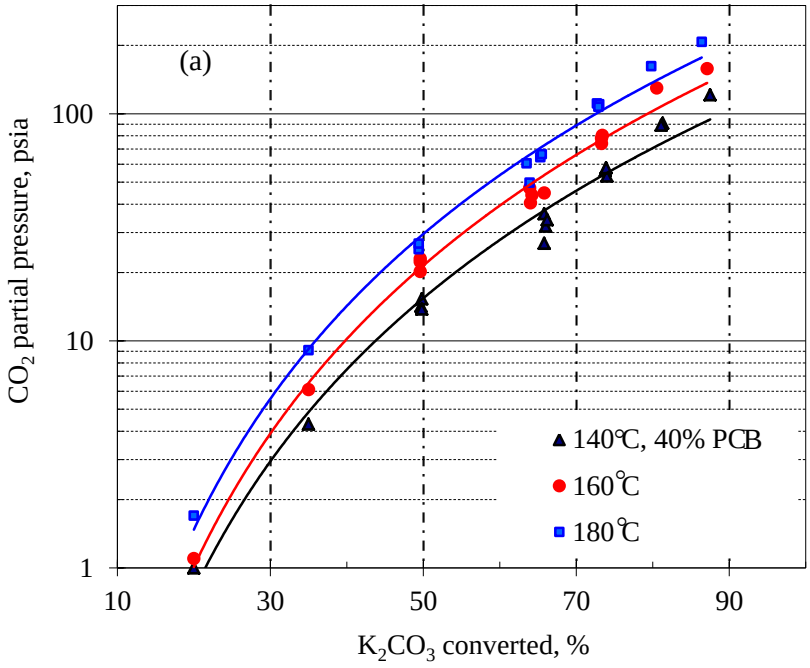

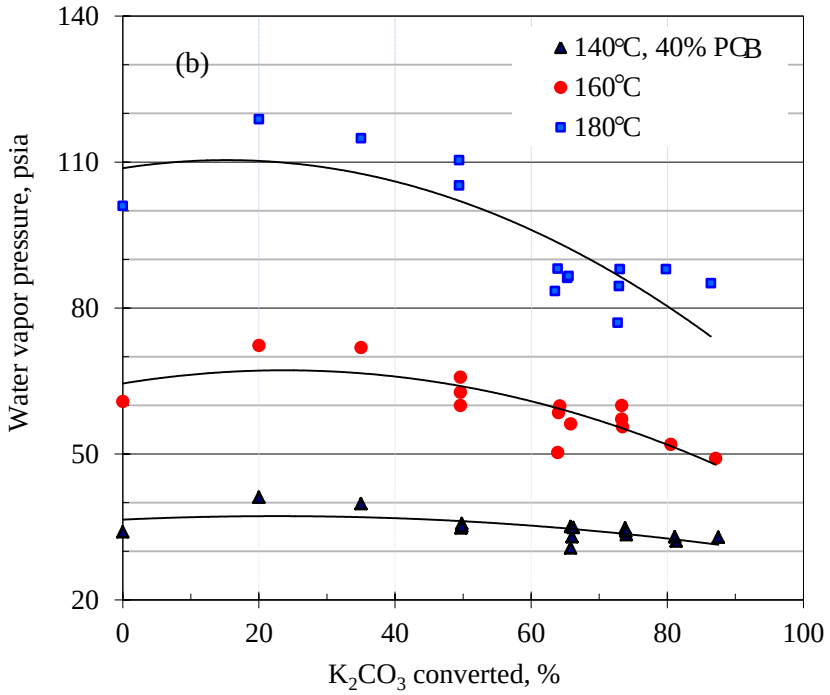

Figure 4A-5. VLE data for the 40 wt% PCB solution at 140, 160, and 180°C: (a) CO_2 partial pressure and (b) water vapor partial pressure.

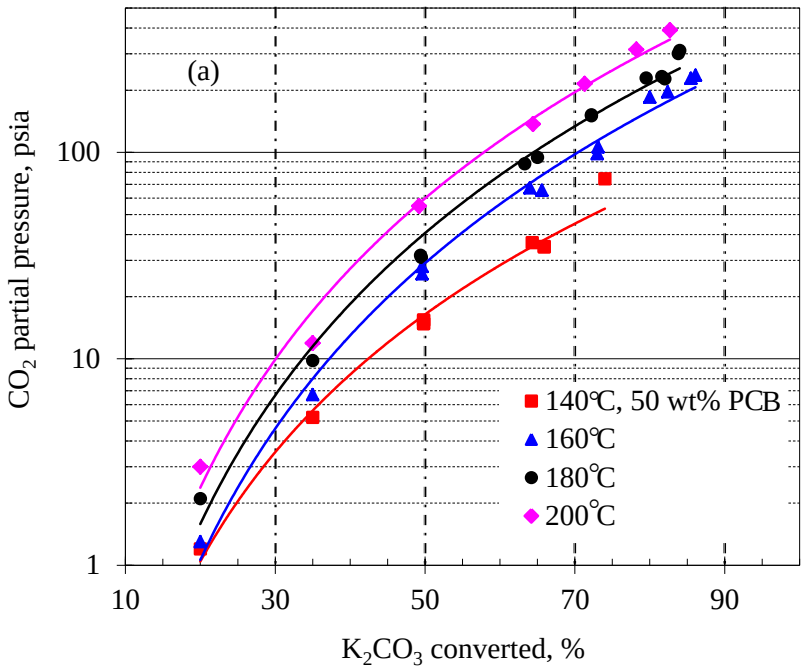

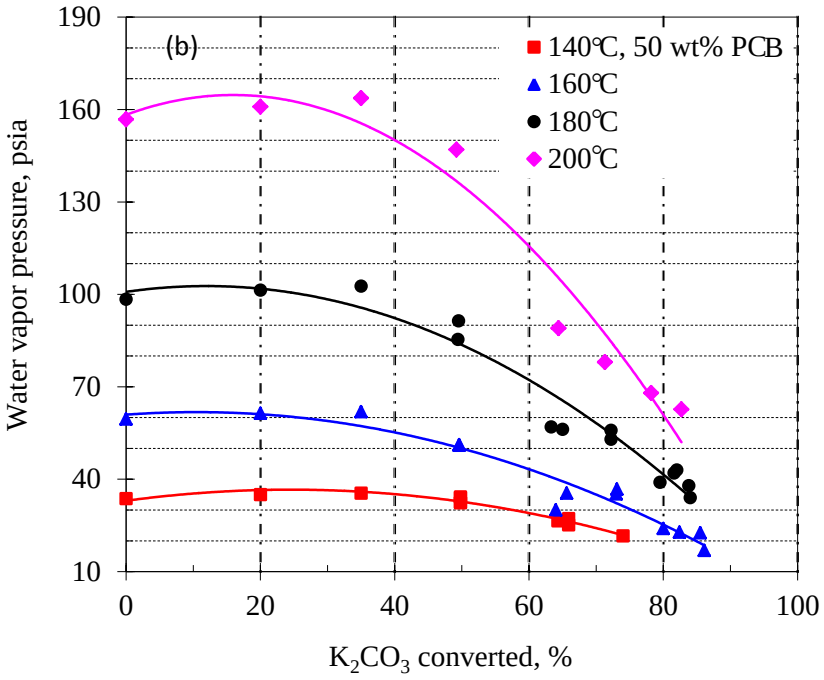

Figure 4A-6. VLE data for the 50 wt% PCB solution at 140, 160, 180, and 200°C: (a) CO_2 partial pressure and (b) water vapor pressure.

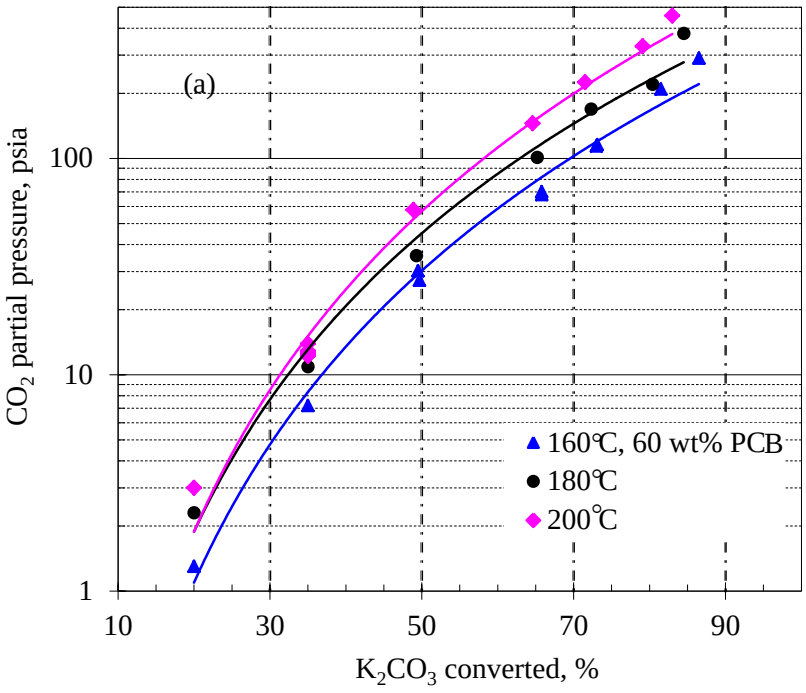

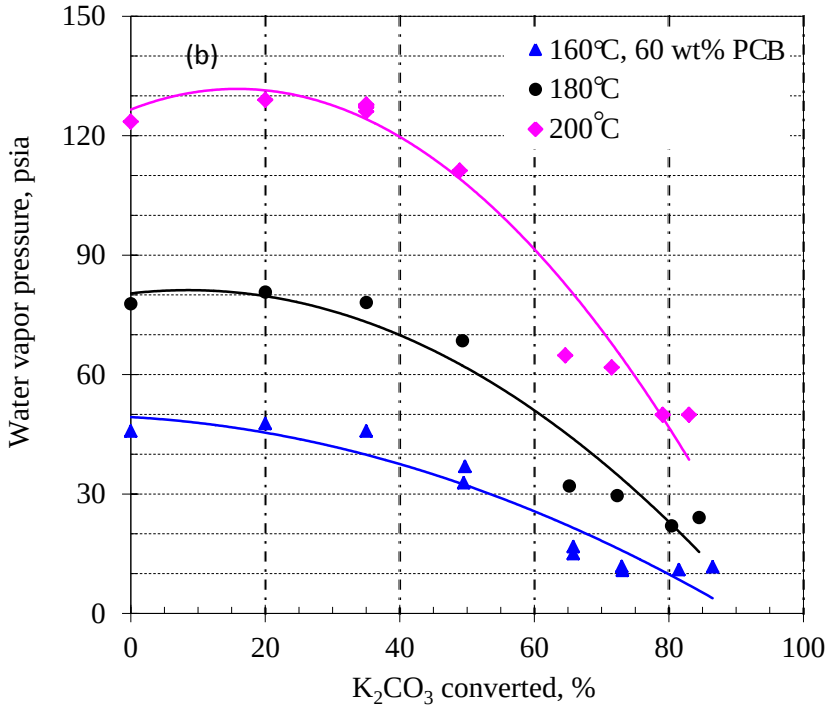

Figure 4A- 7. VLE data obtained for the 60 wt% PCB solution at 160, 180, and 200°C: (a) CO_2 partial pressure and (b) water vapor pressure.

4A.3.2 Comparison of VLE data for different PCB solutions

The equilibrium values of P_{CO2} and P_{H2O} measured for different PCB solutions (40, 50, and 60 wt%) at 140 to 200°C are compared in Figures 4A-8 and 4A-9, respectively. It can be seen that at the same temperature and CTB conversion level, P_{CO2} increased with PCB concentration. However, the increase was not as substantial as with the CTB conversion in the PCB solution, especially when the PCB concentration reached 50 wt% or above.

As expected, the value of P_{H2O} noticeably decreased as the PCB concentration increased from 40 to 60 wt%. Such results suggest that the stripping heat associated with water vaporization should be decreased (lower H_2O/CO_2 pressure ratio) by using a more concentrated $K_2CO_3/KHCO_3$ for CO_2 stripping. For example, over the 60 wt% PCB of 83% CTB conversion at 200°C, the total pressure and the ratio of H_2O/CO_2 partial pressure were 507 psia (34.5 atm) and 0.11:1, respectively. In comparison, at the same temperature and CTB conversion, the total pressure was 453 psia (30.8 atm) and the H_2O/CO_2 pressure ratio was 0.16 over the 50 wt% PCB.

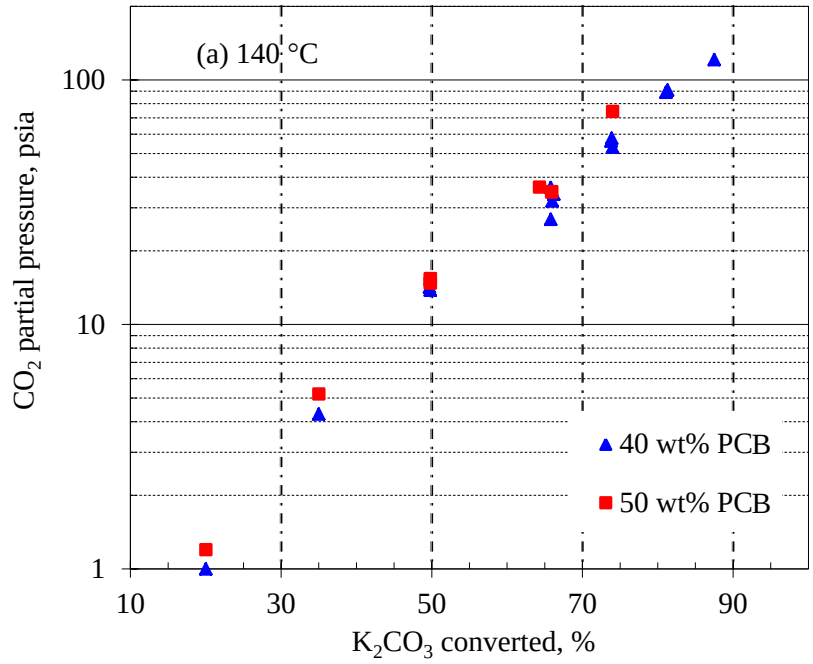
(a) 140 °C
100
10
1
CO2 partial pressure, psia
10
30
50
70
90
K2CO3 converted, %
40 wt% PCB
50 wt% PCB

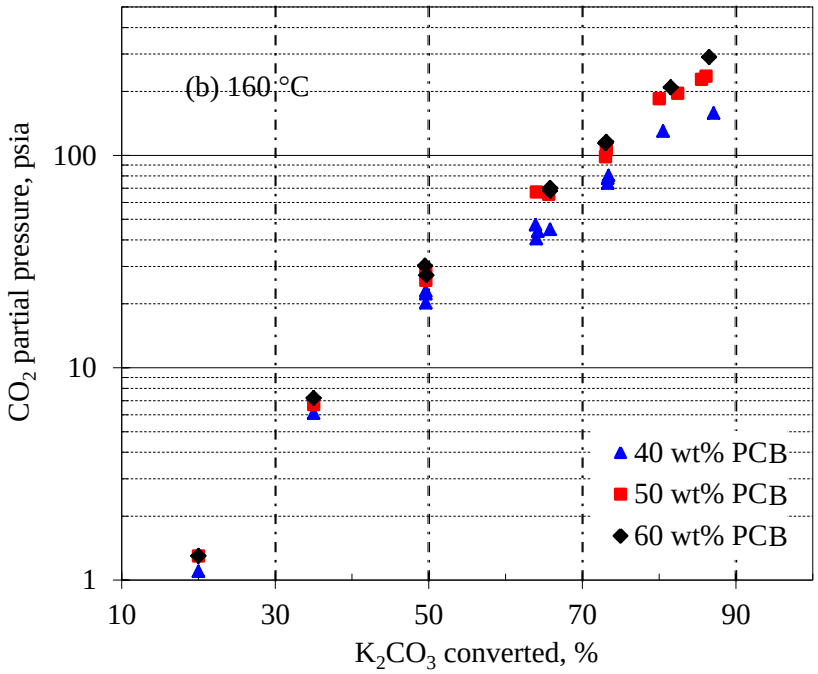
(b) 160 °C
100
10
1
CO2 partial pressure, psia
10
30
50
70
90
K2CO3 converted, %
40 wt% PCB
50 wt% PCB
60 wt% PCB

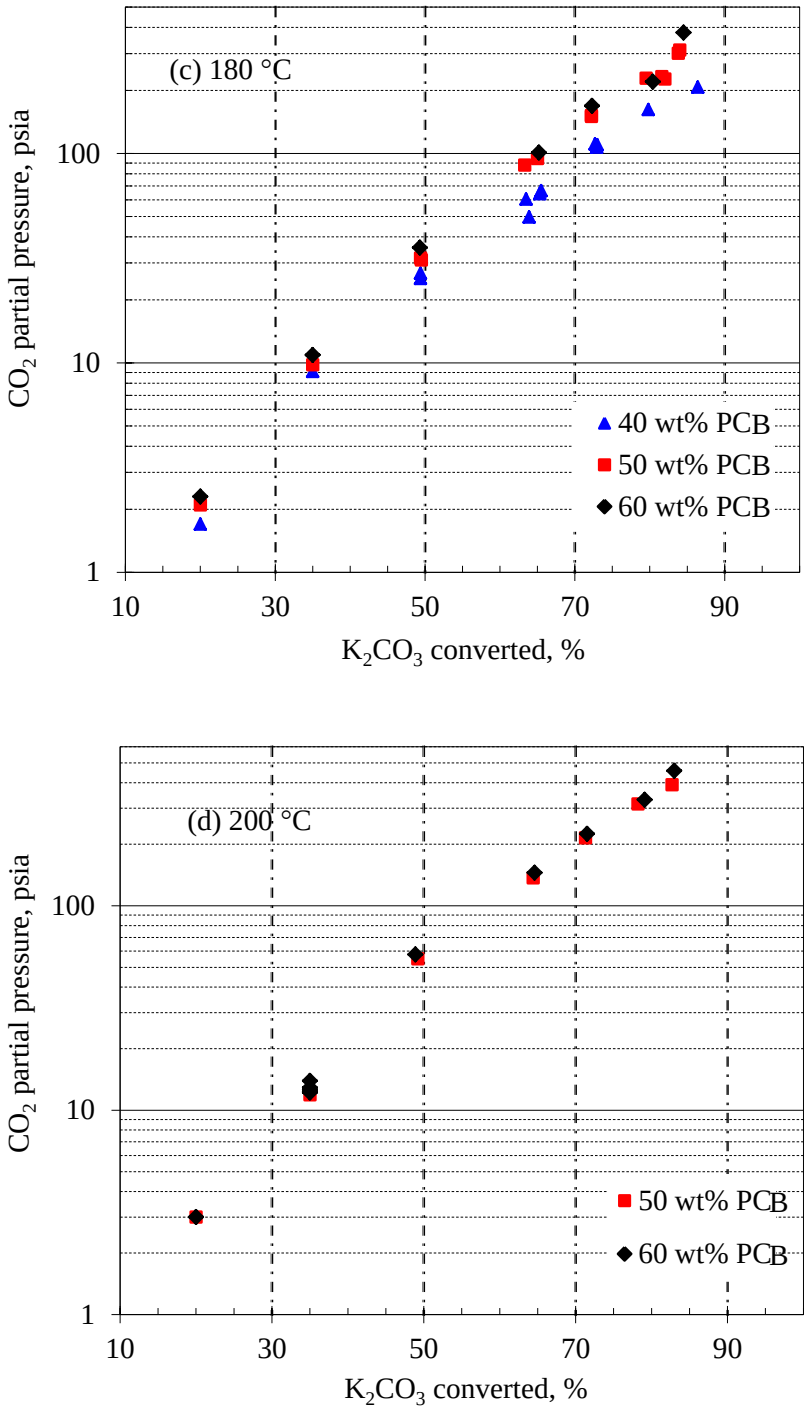

Figure 4A-8. Comparison of P_{CO2} for the 40, 50, and 60 wt% PCB solutions at (a) 140°C, (b) 160°C, (d) 180°C, and (d) 200°C.

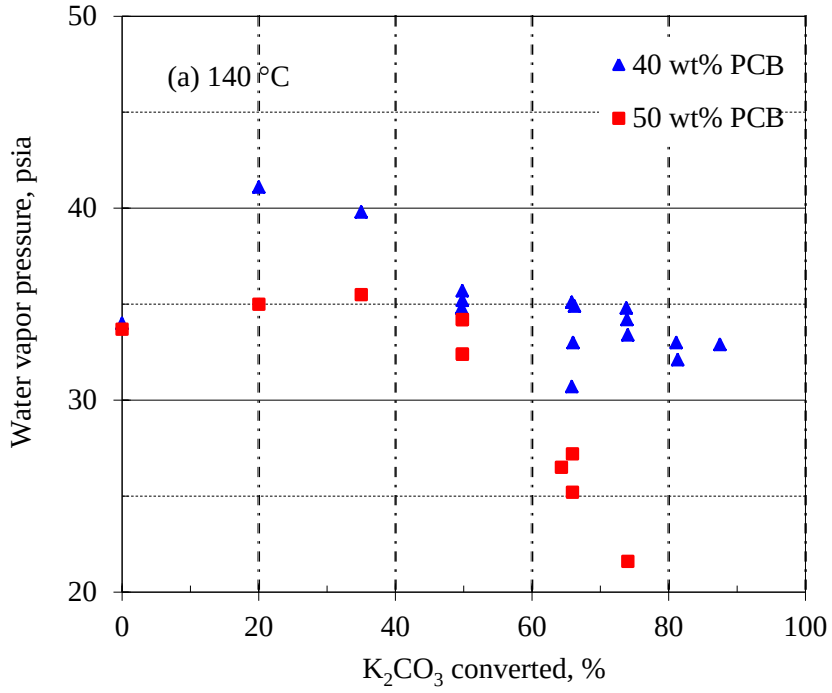
(a) 140 °C
40 wt% PCB
50 wt% PCB
Water vapor pressure, psia
50
40
30
20
0
20
40
60
80
100
K2CO3 converted, %

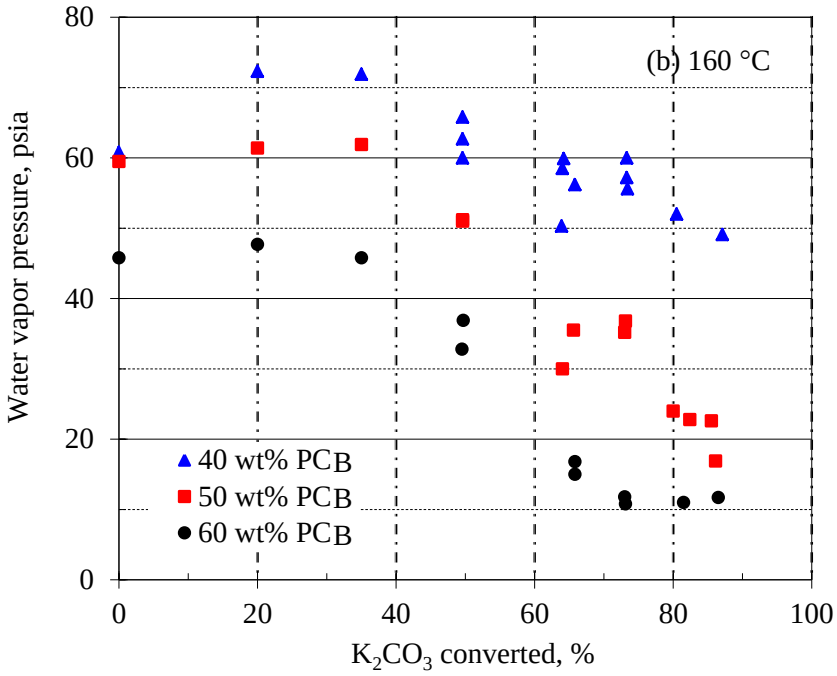
(b) 160 °C
40 wt% PCB
50 wt% PCB
60 wt% PCB
Water vapor pressure, psia
80
60
40
20
0
0
20
40
60
80
100
K2CO3 converted, %

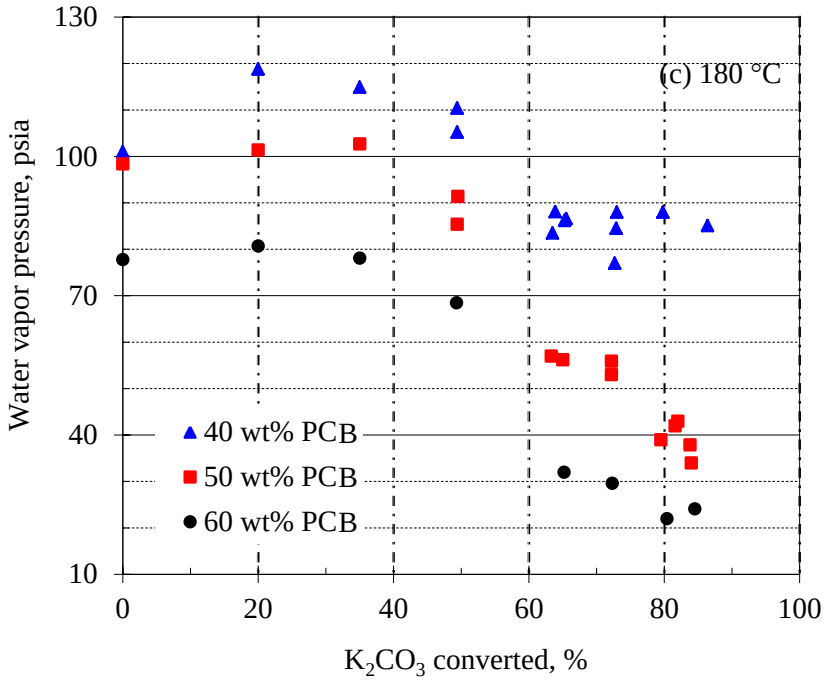

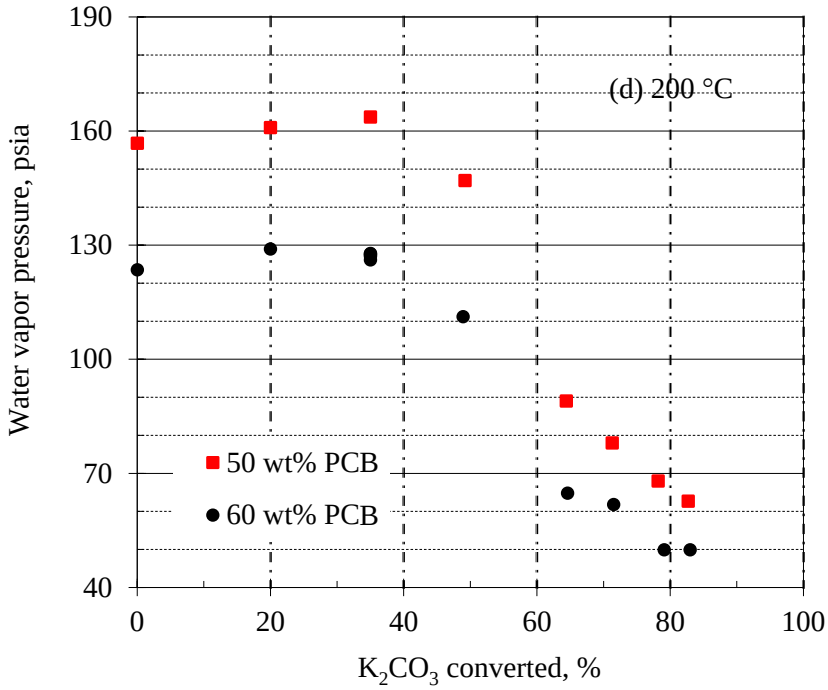

Figure 4A-9. Comparison of P_{H2O} for the 40, 50, and 60 wt% PCB solutions at (a) 140°C, (b) 160°C, (d) 180°C, and (d) 200°C.

4A.3.3 Impact of the presence of 2 to 4 wt% K_2SO_4

K_2SO_4 is produced when SO_2 in the flue gas is absorbed into the PCB solution during CO_2 absorption. To investigate the effect of K_2SO_4 on CO_2 stripping, the VLE data were measured at a selected condition for 50 wt% PCB solution with approximately 65% CTB conversion in the

presence of 2 and 4 wt% K_2SO_4 at temperatures of 140 to 200°C. Figure 4A-10 shows the VLE measurement results. The presence of 2 and 4 wt% K_2SO_4 did not noticeably affect P_{CO2}. Only the P_{H2O} values were slightly reduced.

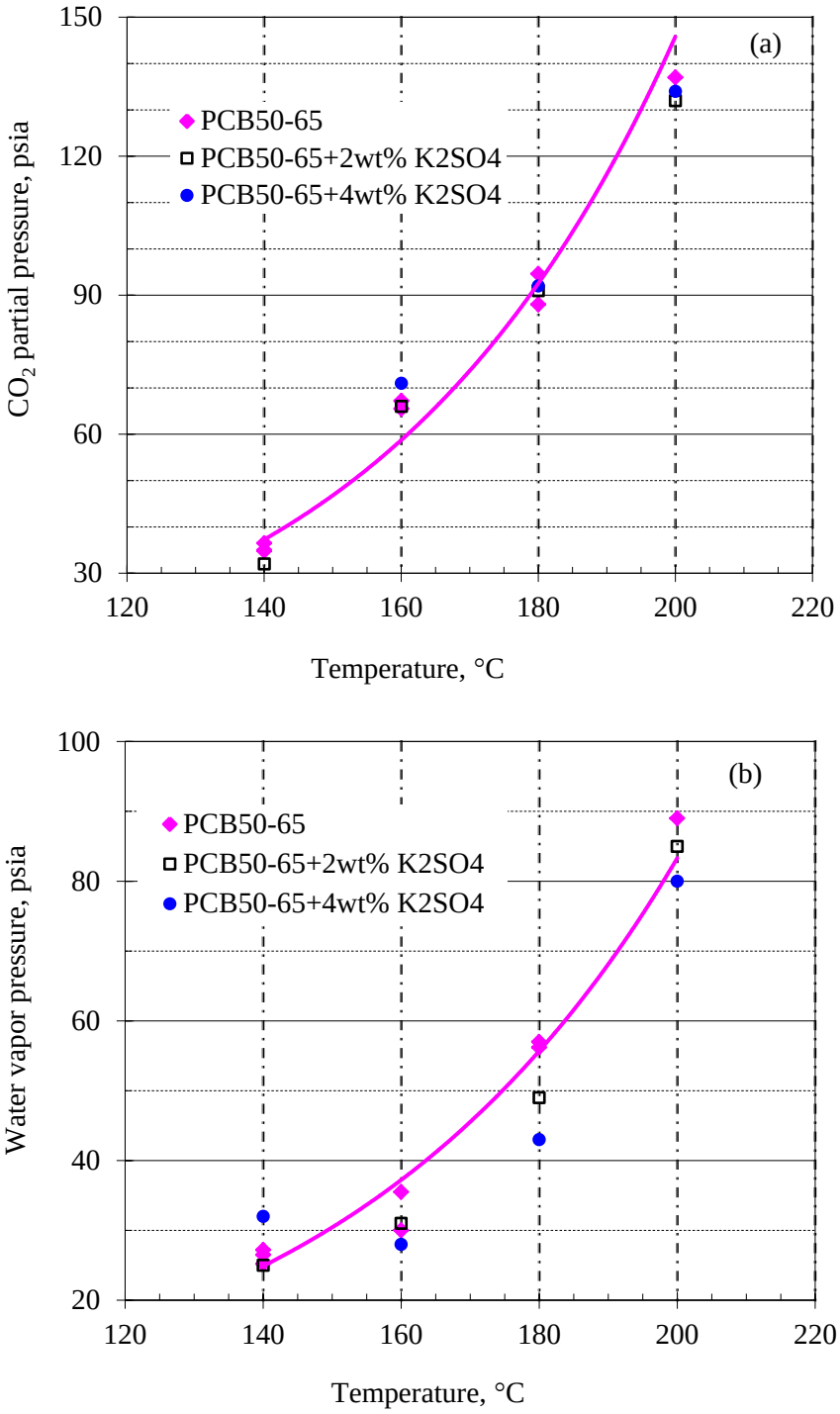

Figure 4A-10. Effect of the presence of 2 and 4 wt% K_2SO_4 on the VLE behavior of the 50 wt% PCB solution with approximately 65% CTB conversion (PCB50-65) at temperatures of 140 to 200°C: (a) P_{CO2} and (b) P_{H2O}.

4A.4 Summary

The VLE data were measured for the 40, 50, and 60 wt% PCB solutions with CTB conversion levels ranging from approximately 20 to 85% at 140 to 200°C. These data cover a full range of operating conditions for CO_2 stripping in the Hot-CAP.

The measured partial pressures of CO_2 and the total pressures over the 40 wt% $K_2CO_3/KHCO_3$ solutions with CTB conversion levels below 50% at 140°C were comparable with those reported by Tosh *et al.* (1959), whereas those with CTB conversion levels above 50% were generally lower.

The VLE data showed that the partial pressure of CO_2 increased substantially with increasing temperature and CTB conversion of the PCB solution, whereas the partial pressure of water vapor increased moderately with increasing temperature, but decreased slightly with increasing CTB conversion. The concentration of the PCB solution over the investigated range (40 to 60 wt%) did not substantially affect the partial pressure of CO_2, but remarkably reduced the partial pressure of water vapor.

A high stripping pressure and a lower ratio of water vapor-to-CO_2 partial pressure can result in a significant reduction in the energy use associated with water vaporization during CO_2 stripping and with CO_2 compression work. A higher operating temperature, high PCB concentration, and higher CTB conversion level in solution are favored to obtain a higher total pressure and lower H_2O/CO_2 partial pressure ratio. For example, over the 60 wt% PCB with 83% CTB conversion at 200°C, the total pressure and the ratio of H_2O/CO_2 partial pressure were 507 psia (34.5 atm) and 0.11:1, respectively. The results verify the energy use advantage of the Hot-CAP by using a concentrated PCB slurry for CO_2 stripping.

The presence of 2 and 4 wt% K_2SO_4 did not noticeably affect the partial pressures of CO_2, but did slightly reduce the partial pressures of water vapor, based on the measurements at selected conditions for the 50 wt% PC solution with approximately 65% CTB conversion.

References

1. Tosh J.S., Field J.H., Benson H.E., Haynes W.P. Equilibrium study of the system potassium carbonate, potassium bicarbonate, carbon dioxide, and water. *Bur. Mines Rep. Invest.* **1959,** *5484*, 23.

2. Benson H.E., Field J.H., Haynes W.P. Improved process for carbon dioxide absorption uses hot carbonate solutions. *Chem. Eng. Progr*. **1956,** *52*, 433–438.

Part 4B. Performance of CO_2 Stripping in a Bench-Scale Stripping Column

4B.1 Introduction

Given the proven thermodynamic feasibility of high-pressure stripping in the Hot-CAP, testing of CO_2 stripping in a column setup is necessary to investigate the performance of solvent regeneration, the hydrodynamics of a packed-bed configuration under high pressure, and the energy use performance of the stripping process. In addition, operational issues associated with the use of concentrated $KHCO_3/K_2CO_3$ (PCB) solutions, such as fouling and plugging of column packing, and high pressure and temperature, need to be studied.

In this study, a custom-designed, bench-scale, packed-bed stripping column system that can operate at temperatures up to 200°C and pressures up to 500 psia (34.0 atm) was designed and fabricated to evaluate the performance of CO_2 stripping with hot PCB solutions. Parametric tests to evaluate process variables, such as pressure, temperature, concentration, and CTB conversion, were conducted. The effects of potential impurities, including additives or promoters, and the flue gas desulfurization product K_2SO_4, were also investigated. In addition, the heat duty of the CO_2 stripping process with PCB solutions was estimated and compared with the benchmark MEA process based on the experimental results.

4B.2 Experimental methodology

4B.2.1 CO_2 stripping column system

A bench-scale, packed-bed stripping column system with a temperature rating of 200°C and a pressure rating of 500 psia (34.0 atm) was designed by a local engineering company. As shown in Figure 4B-1, the stripping column system consists of a stripping column, a liquid/slurry supply tank, and instrumentation for measuring gas and liquid compositions.

The stripping column is a stainless steel tube with an inner diameter of 1 in. (2.5 cm) and a total height of 7 ft (2.1 m). The column was randomly packed with a 6-ft (1.8-m) height of stainless steel pall rings (Hai-Yan New Century Petrochemical Device Co., Ltd.) having a specific surface area of 500 m^2/m^3. Five thermocouples (Omega, Type K, Model KMQSS-125-G-6) with wireless connectors (Omega, Model MWTC-A-K-915) were evenly equipped to measure the temperature profile along the column. Two pressure gauges (Ashcroft, Type 1008) were mounted at the top and bottom positions to measure the pressure drop of the column. A safety rupture disc (McMaster Carr, brass pipe-fitting rupture disc style B) rated to 500 psia (34.0 atm) was mounted at the top of the column for emergency ventilation.

A reboiler made of stainless steel with an inner diameter of 6 in. (15.2 cm) and a height of 1.5 ft (0.46 m) is attached to the bottom of the column to supply heat for CO_2 stripping. The reboiler is heated via three 1.0-kW mica band heaters (Tutco, Model BH91911) with a temperature control system consisting of a thermocouple (Omega, Model MWTC-A-K-915), solid-state relay (Allen Branley, Model SSR101A), and solid-state relay digital controller (Honeywell, Model UDC-1200). A wireless multimeter (Fluke, CNX3000) is used to measure the current and voltage supplied to the heaters to record the real-time power or energy consumption in the reboiler. The

liquid level in the reboiler is monitored by a 12-in.-long (30.5-cm) magnetic level gauge (Davis Control Ltd., Klinger level gauges).

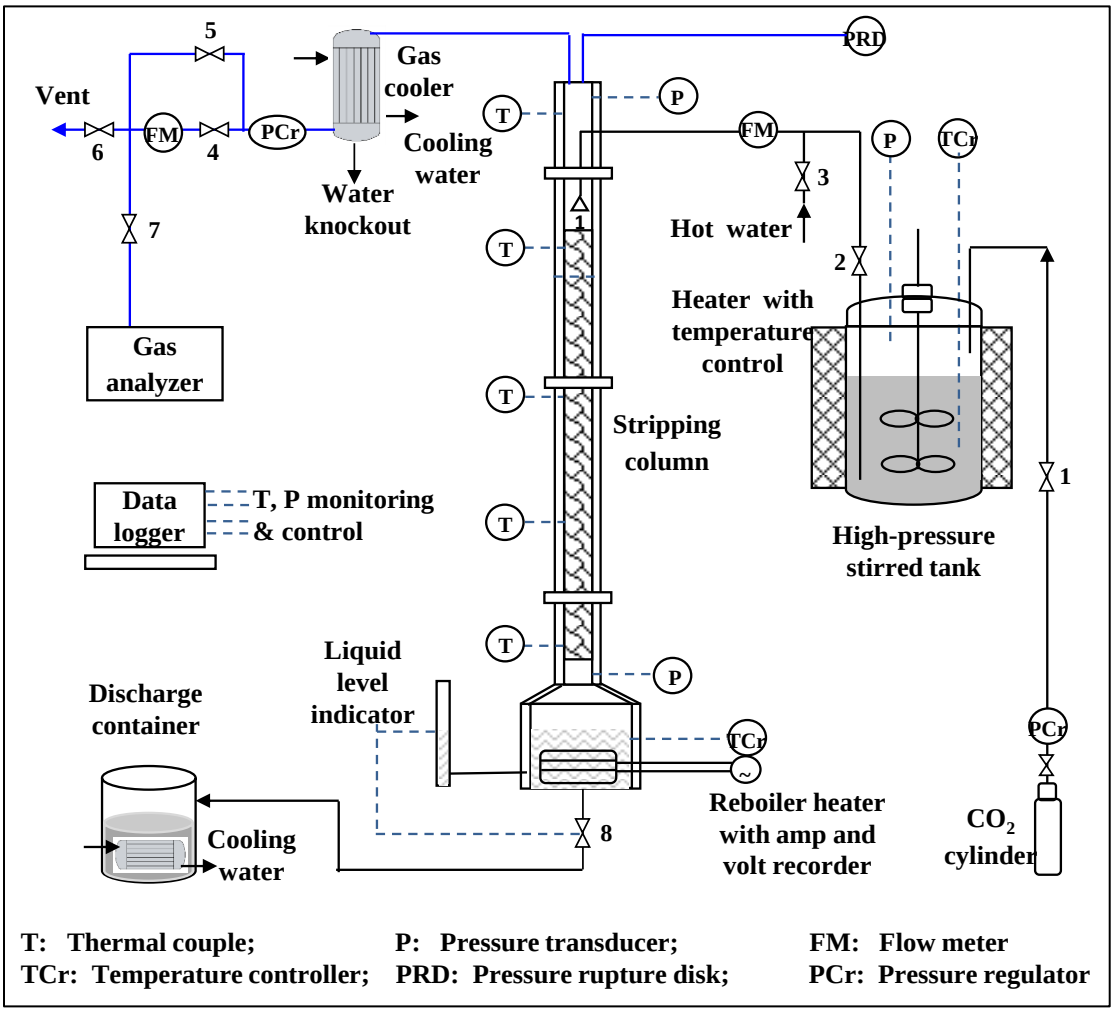

Figure 4B-1. Schematic of a bench-scale, high-pressure stripping column system.

The CO_2 product gas stream exiting the top of the column is cooled to condense water vapor by passing through a cooling coil made of stainless steel with a diameter of 0.5 in. (1.3 cm) and a length of 3.5 ft (1.1 m). The flow rate of the dry CO_2 gas is measured by a flow meter after the pressure is relieved by a back pressure controller. The regenerated PCB solution (CO_2-lean) is discharged to a 10-gal liquid container through a release valve at the bottom of the reboiler.

The PCB solution or slurry is continuously fed to the stripping column from a supply tank rated at 500 psia (34.0 atm) and 200 °C. The flow rate of the feed solution is controlled by adjusting the pressure difference between the tank (with the headspace balanced with N_2 gas from a cylinder at a controlled pressure) and the stripping column, and is read by a high-pressure liquid flow meter (Micro Motion, Inc., Model F025S319CRAAEZZZZ) equipped with a transmitter (Micro Motion, Inc. Model 1700C12ABAEZZZ). The tank is made of stainless steel with an inner diameter of 12 in. (0.3 m) and a height of 3 ft (0.91 m). Electrical mica band heaters (Tutco, Model BH91910) with a power output of 5.0 kW are used to heat the feed solution to the desired

temperatures. A temperature control system consisting of a thermocouple (Omega, Model MWTC-A-K-915), a solid-state relay (Allen Branley, Model SSR101A), and a solid-state relay digital controller (Honeywell, Model UDC-1200) is used to monitor and control the temperature of the solution in the tank. The tank is equipped with a variable-speed magnetic drive agitator (PDC Machines, Inc., 1699-0113) that can provide stirring speeds up to 500 rpm for the liquid phase. The power of the agitator is supplied with a torque up to 18 in.-lb (2.0 N-m) controlled through an inverter motor speed regulator (Teco Co., Ltd., Model JNEV-2P2~201-H3). A frequency converter is used to transport signals between the magnetic drive agitator and the inverter motor speed regulator. Two impellers with an external diameter of 4 in. (10.2 cm) are evenly equipped along a 36-in.-long (91.4 cm) shaft. The shaft is installed 2 in. (5.1 cm) above the bottom of the tank. A built-in 21-in. (53.3 cm) magnetic level gauge (Davis Control Ltd., Klinger level gauges) is used to monitor the liquid level in the tank.

Figure 4B-2. Photographs of the experimental setup for the CO_2 stripping system.

The stripping column, reboiler, supply tank, pipes, and liquid level gauges are insulated using rigid fiberglass pipe insulation (McMaster-Carr, K value of 0.23) with a thickness varying from 2 to 4 in. (10.2 cm). Photographs of the major parts of the experimental setup are shown in Figure 4B-2. Most of the electrical controllers and meters are installed on an electrical control panel, as shown in Figure 4B-3. The required data on temperatures, pressures, liquid levels, and flow rates are monitored or recorded by a computer data acquisition system.

Figure 4B-3. Photographs of the electrical control panel.

4B.2.2 Operating procedure

4B.2.2.1 CO_2 stripping from the hot PCB solutions

As presented in Table 4B-1, 30 to 60 wt% PCB solutions with CTB conversion levels ranging between 40 and 80% were used as feed solutions, and the stripping temperature was varied from 120 to 200°C. CO_2 stripping tests were performed in a continuous mode with respect to both the gas and liquid phases. The regenerated PCB solution was not recycled in each test. The CO_2 stripping performance from the PCB solution in the presence of K_2SO_4, piperazine (PZ), or methyldiethanolamine (MDEA) was also investigated. The concentration of K_2SO_4 (i.e., 1 wt%) was selected given the fact that only a small amount of SO_2, relative to CO_2, is present in a flue gas. For the Hot-CAP, 0.5 to 1.0 M PZ is typically used as a promoter for CO_2 absorption. However, only a small part of it may be introduced to a PCB slurry during the bicarbonate crystallization process and thereby enter the stripper. Thus, the addition of 0.2 M PZ in the PCB feed solution was selected. In addition, the impact of 0.5 M MDEA as a stripping additive was also investigated.

In a typical test, approximately 20 L of PCB slurry with the desired composition was added to the liquid supply tank. The slurry was preheated to the desired temperature, which was generally 5 to 10°C lower than the reboiler temperature but high enough to dissolve the solids in the tank. A magnetic drive agitator mounted on top of the tank was used to mix the solution. Meanwhile, approximately 1.5 L of a PCB solution (with a randomly low concentration) was initially charged to the reboiler and preheated to the desired temperature. Once the temperatures and pressures in both the supply tank and reboiler were stable, the hot PCB solution in the supply tank was fed to the top of the stripping column at a rate of 0.05 to 0.12 L/min by adjusting the pressure of a balancing N_2 gas from a cylinder connected to the tank. The liquid level of the reboiler was then held constant at approximately 1 to 1.5 L of liquid holdup. The water vapor in the gas stream exiting the column was condensed in the water cooler or condenser. The flow rate of dry CO_2 gas was measured using a flow meter after the pressure was released through a back pressure controller. The hot lean PCB solution exiting the reboiler was collected in a liquid

receiver. Each stripping test was run continuously for 40 to 60 min (>3 times the residence time of the liquid in the reboiler) after it reached steady state, as indicated by stable readings of the temperature, pressure, and CO_2 flow rate.

Table 4B-1. Matrix for the CO_2 stripping experiments in the bench-scale column

Test no.	Feed solution[a]	Temperature in the reboiler, °C
1	PCB30-60 + 0.5 M MDEA	120
2	PCB30-60 + 0.5 M MDEA	140
3	PCB30-60	120
4	PCB30-60	140
5	PCB30-60	160
6	PCB30-80	120
7	PCB30-80	140
8	PCB30-80	160
9	PCB40-40	120
10	PCB40-40	140
11	PCB40-40	160
12	PCB40-60	140
13	PCB40-60	160
14	PCB40-60 + 1 wt% K_2SO_4	140
15	PCB40-60 + 1 wt% K_2SO_4	160
16	PCB40-60 + 0.2 M PZ	140
17	PCB40-60 + 0.2 M PZ	160
18	PCB40-80	160
19	PCB50-40	160
20	PCB50-40	180
21	PCB50-60	160
22	PCB50-60	180
23	PCB50-80	160
24	PCB60-40	180
25	PCB60-40	200
26	MEA5-95	100

[a]MEA5-95: 5 M MEA with CO_2 loading of 0.475 mol/mol of MEA (95% conversion of MEA); PCB X-Y: X wt% PCB slurry with Y% CTB conversion; PCB X-Y + 1 wt% K_2SO_4: PCB X-Y slurry with the addition of 1 wt% K_2SO_4; PCB X-Y + 0.2 M PZ: PCB X-Y slurry with the addition of 0.2 M PZ; PCB X-Y + 0.5 M MDEA: PCB X-Y slurry with the addition of 0.5 M MDEA.

4B.2.2.2 CO_2 stripping from the CO_2-rich MEA solution

To validate the experimental methods as well as to provide a baseline for performance comparison, tests of CO_2 stripping with a CO_2-rich 5 M MEA solution typical of the conventional MEA process were performed. The test procedure with the benchmark 5 M MEA solution was relatively simple and did not involve slurry operation (e.g., a risk of precipitation when cooled down). In a typical test, the CO_2-rich MEA solution was stored in a 20-L tank at room temperature and pumped at a flow rate of approximately 0.1 L/min using a peristaltic pump. The solution was heated in stainless steel coils in a water bath to 80 to 90°C prior to entering the top of the stripping column. The liquid level in the reboiler was kept constant (~1.5-L liquid holdup) during the test. The regenerated MEA solution exiting the reboiler was discharged to a

liquid receiver, and samples were collected for analysis of CO_2 loading. The gas stream exiting the stripping column was dried in a cooler and water condensate was collected. The flow rate of the dried CO_2 gas was measured by a flow meter. The test was operated at atmospheric pressure and under continuous mode. The system reached steady state typically within 40 to 60 min (>3 times the liquid residence time in the reboiler), as indicated by constant readings of the temperature, pressure, and CO_2 flow rate.

In all the tests, the composition of regenerated lean solution was determined by the mass balance principle, assuming the measured amount of CO_2 gas was stripped from the PCB or MEA feed solution. In addition, the Chittick method described in Chapter 2 was used to measure CO_2 loading in the selected solutions. The measurement results were generally consistent with the theoretical calculations.

4B.3 Theoretical analysis

4B.3.1 Reboiler heat duty

Assuming that the solution does not flash upon injection to the stripper, the heat used for CO_2 stripping (reboiler heat duty) is a summation of the three heat elements:

$$Q_{total} = Q_{sensible} + Q_{reaction} + Q_{stripping} \qquad \text{(4B-1)}$$

where $Q_{sensible}$ is the sensible heat required to heat the inlet CO_2-rich solution to the reboiler temperature (kJ/kg), $Q_{reaction}$ is the heat required to desorb the CO_2 from the rich solution corresponding to the heat of absorption (kJ/kg), and $Q_{stripping}$ is the stripping heat for water evaporation (kJ/kg).

Phase equilibrium is usually not reached in the column. The three heat elements can be estimated based on the operating parameters measured, and the overall reboiler heat duty can thus be determined as follows:

$$Q_{total} = C_p \frac{(T_{reboiler} - T_{inlet})M_{solution}}{\Delta CTB \cdot x_{solv} M_{CO_2}} + \Delta H_{abs,CO_2} + \Delta H_{vap,H_2O} \frac{M_{H_2O}}{M_{CO_2}} \frac{P_{H_2O}}{P_{CO_2}} \qquad \text{(4B-2)}$$

where C_p is the specific heat capacity of the solution; $T_{reboiler}$ is the reboiler temperature and T_{inlet} is the temperature of the feed solution at the inlet of the stripper; ΔCTB is the difference in CTB conversion in the solution at the inlet (rich) and outlet (lean) of the stripper; x_{solv} is the molar fraction of PCB (K_2CO_3-equivalent) in the solution; $\Delta H_{abs,CO2}$ is the heat of absorption of the solution; $\Delta H_{vap,H2O}$ is the heat of water evaporation; P_{H2O} and P_{CO2} are the partial pressures of water vapor and CO_2 at the top of the stripper; and $M_{solution}$, M_{H2O}, and M_{CO2} are the molecular weights of the solution, water, and CO_2, respectively.

The amount of CO_2 released was measured by a flow meter to determine the total heat of absorption reaction. The measured CO_2/H_2O ratio on the top of the column, assuming water vaporization instantly reached equilibrium, was used to determine the stripping heat based on Eq. (4B-2). The sensible heat was determined based on the temperature difference between the influent and effluent solutions.

4B.3.2 CO_2-to-water vapor pressure ratio

To qualitatively analyze the trend in stripping pressure change with temperature and feed solution, a thermodynamic analysis can be conducted for the system in equilibrium. Assuming that the total pressure is a constant and that the gas phase behaves like an ideal gas, the H_2O and CO_2 partial pressures can be determined by the van't Hoff equation:

$$\frac{\mathrm{d}\ln P}{dT} = \frac{\Delta H}{RT^2} \tag{4B-3}$$

where R is the universal gas constant. Integrating the above equation from the reference temperature to the inlet temperature of the stripper gives

$$P_{CO_2} = P_{ref,CO_2} \exp[-\frac{\Delta H_{abs,CO_2}}{R}(\frac{1}{T_{inlet}} - \frac{1}{T_{ref}})] \tag{4B-4}$$

$$P_{H_2O} = P_{ref,H_2O} \exp[-\frac{\Delta H_{vap,H_2O}}{R}(\frac{1}{T_{inlet}} - \frac{1}{T_{ref}})] \tag{4B-5}$$

where T_{ref} is the reference temperature, and $P_{ref,CO2}$ and $P_{ref,H2O}$ are the partial pressures of CO_2 and water vapor over the feed solution at the reference temperature. The ratio of equilibrium partial pressure of water vapor and CO_2 can be described as follows:

$$\frac{P_{H_2O}}{P_{CO_2}} = \frac{P_{ref,H_2O}}{P_{ref,CO_2}} \exp[\frac{(\Delta H_{abs,CO_2} - \Delta H_{vap,H_2O})}{R}(\frac{1}{T_{inlet}} - \frac{1}{T_{ref}})] \tag{4B-6}$$

It should be noted that the pressure ratio of water vapor-to-CO_2 at the stripper inlet is a function of the heat of absorption of the solvent.

4B.4 Results and discussion

4B.4.1 Parametric testing of CO_2 stripping with hot PCB solutions

Table 4B-2 gives a summary of the data obtained from the experiments on CO_2 stripping with hot PCB solutions under different conditions (e.g., temperature, PCB concentration, inlet CTB conversion level, and presence of impurities). The total stripping pressure with the PCB60-40 feed reached as high as 180 psia (12.2 atm) at the reboiler temperature of 200°C. In general, the total stripping pressures obtained in these tests were slightly lower than those from our VLE measurements and those reported in the literature.[1] According to Eq. (4B-6), the CO_2-to-water vapor pressure ratio (P_{CO2}/P_{H2O}) is a function of the heat of absorption and the stripping temperature.

In the current study, the partial pressure of water vapor at the top of the stripper was determined using the VLE data measured in Chapter 4B, as reported in the literature, or both,[1] assuming that water evaporation equilibrated instantly. The P_{CO2}/P_{H2O} at the top of the stripper was estimated based on the equilibrium partial pressure of water vapor and the partial pressure of CO_2 derived using the measured total stripping pressure. The results of the parametric tests are described and discussed in the following sections.

Table 4B-2. Summary of the results of parametric testing of CO_2 stripping with hot PCB solutions

CO_2-rich solution	Total pressure, psia*	Temperature of the feed solution, °C	Equilibrium pressure of H_2O at the top of the stripper, psia	P_{CO2}/P_{H2O} at the top of the stripper	CO_2-lean solution
PCB30-60 + 0.5 M MDEA	31	115	18	0.72	PC30-52.7
PCB30-60 + 0.5 M MDEA	51	130	31.5	0.62	PC30-40.3
PCB30-60	27	115	18	0.50	PC30-59.4
PCB30-60	47	130	31.5	0.49	PC30-58
PCB30-60	83	150	56	0.48	PC30-55
PCB30-80	46	115	17	1.71	PC30-76
PCB30-80	77	132	29	1.66	PC30-74.5
PCB30-80	106	145	42	1.52	PC30-65.4
PCB40-40	22.4	118	18.6	0.20	PC40-38
PCB40-40	42.5	137	35	0.21	PC40-36
PCB40-40	79	158	63.3	0.25	PC40-30
PCB40-60	55	138	21.5	1.56	PC40-53.8
PCB40-60	97	158	42.2	1.30	PC40-47
PCB40-60 + 1 wt% K_2SO_4	56	135	21.5	1.60	PC40-54
PCB40-60 + 1 wt% K_2SO_4	95	154	42.2	1.25	PC40-45
PCB40-60 + 0.2 M PZ	56	136	21.5	1.60	PC40-53
PCB40-60 + 0.2 M PZ	92	156	42.2	1.18	PC40-45
PCB40-80	115	155	37	2.11	PC40-62
PCB50-40	86	155	56	0.54	PC50-31
PCB50-40	107	171	76	0.41	PC50-26.5
PCB50-60	100	155	41	1.44	PC50-47
PCB50-60	126	176	70	0.80	PC50-43
PCB50-80	121	155	25	3.84	PC50-56
PCB60-40	115	172	60	0.92	PC60-28
PCB60-40	180	185	96	0.88	PC60-26

* 1 psia = 6.893 kPa

4B.4.1.1 Effect of temperature

The levels of regeneration achieved with PCB30-80 at different stripping temperatures are displayed in Figure 4B-4. Results revealed that high temperatures drove off more CO_2 from the hot PCB solution, resulting in a leaner PCB solution exiting the stripper. For the PCB30-80 feed, the CTB conversion of the regenerated solution decreased from 76 to 65% when the stripping temperature was increased from 120 to 160°C. This could be attributed to the higher driving force for CO_2 stripping at a higher temperature. As shown in Figure 4B-5, the partial pressure of CO_2 at the top of the stripper increased from 29 to 64 psia (1.97 to 4.35 atm), and the total

pressure increased from 46 to 106 psia (3.13 to 7.21 atm) (as the stripping temperature was increased from 120 to 160°C. It should be noted that the CO_2 partial pressure was affected by both the composition of the regenerated lean solution and the stripping temperature. A higher temperature produced a higher CO_2 equilibrium pressure, as indicated in Eq. (4B-4), and it resulted in a leaner regenerated solution corresponding to a lower CO_2 pressure. Results indicated that the net effect of increased temperature favored an increase in CO_2 partial pressure.

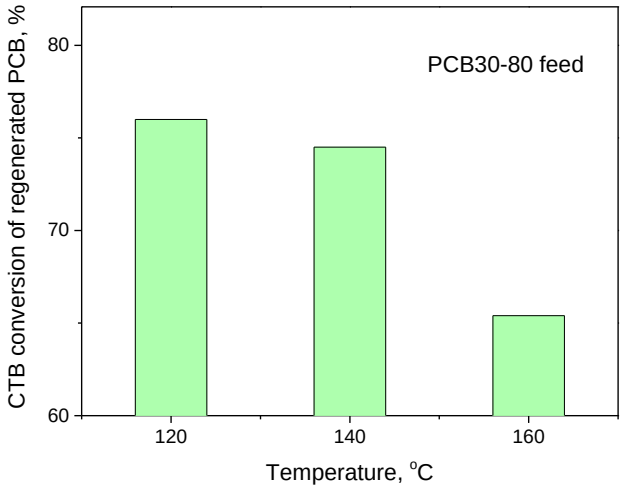

Figure 4B-4. Compositions of lean PCB solutions regenerated by CO_2 stripping at different temperatures with the PCB 30-80 feed solution.

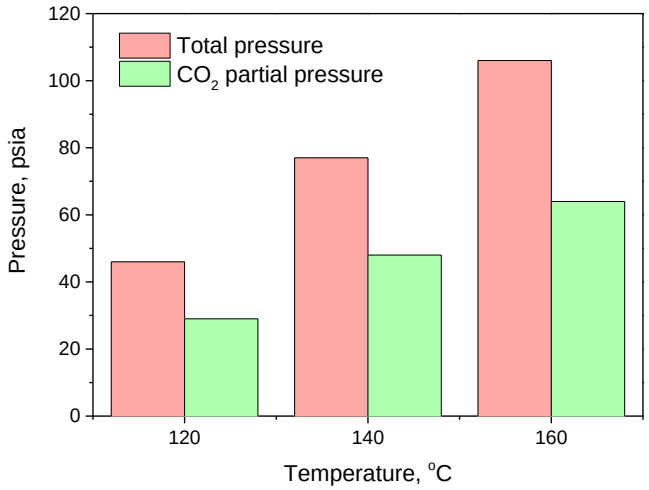

Figure 4B-5. Total pressures and partial pressures of CO_2 at the top of the stripper during CO_2 stripping at different temperatures with the PC30-80 feed solution.

As described previously, the P_{CO2}/P_{H2O} in the product gas stream will significantly influence the stripping heat associated with water evaporation, hence changing the energy consumption for CO_2 capture. Figure 4B-6 shows the P_{CO2}/P_{H2O} obtained at various stripping temperatures with the PC30-80 feed solution. As expected, the P_{CO2}/P_{H2O} in the gas stream exiting the stripping column slightly decreased from 1.71 to 1.52 under the tested conditions. Because the heat of

absorption in the PCB solution (~650 kJ/kg) is lower than the heat of water evaporation (~2,400 kJ/kg), the P_{CO2}/P_{H2O} will generally decrease with increasing temperature, as indicated by Eq. (4B-6).

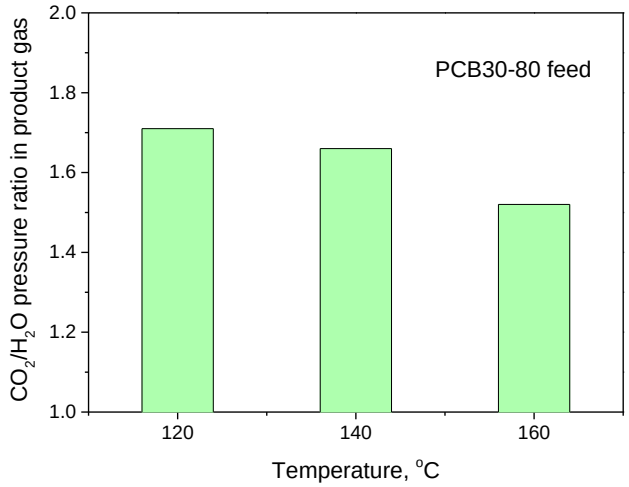

Figure 4B-6. CO_2/H_2O pressure ratios in product gas streams from CO_2 stripping at different temperatures with the PC30-80 feed solution.

4B.4.1.2 Effect of PCB concentration

Figure 4B-7 shows the lean CO_2 loading achieved in the 30 to 50 wt% PCB solutions, all with a rich CTB conversion level of 80%, after the stripping operation at 160°C. Results revealed that the higher the PCB feed solution concentration, the greater the amount of CO_2 desorbed, indicating that a more concentrated PCB feed solution favored a deeper level of $KHCO_3$ regeneration. The changes in CTB conversion for the 30 to 50 wt% PCB solutions varied from 14 to 24 percentage points, which is equivalent to an 18 to 30% regeneration efficiency of $KHCO_3$ contained in the feed solutions.

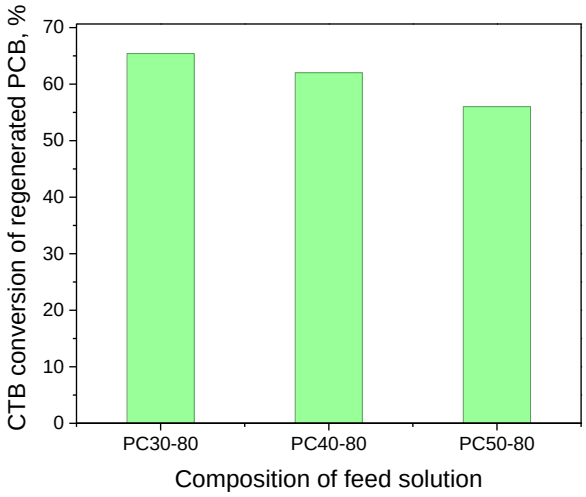

Figure 4B-7. Compositions of the lean PCB solutions regenerated by CO_2 stripping at 160°C with different PCB feed solutions.

Figure 4B-8 displays the total stripping pressures and the partial pressure of CO_2 at the top of the stripper attained under the different conditions examined. As expected, both a higher total pressure and a higher CO_2 partial pressure were attained with a more concentrated PCB feed solution, which is an advantage of the Hot-CAP using a high-concentration feed solution for CO_2 stripping. Increasing the total PCB concentration from 30 to 50 wt%, with the same 80% CTB conversion in the feed, increased the total stripping pressure from 106 to 121 psia (7.21 to 8.23 atm) and the CO_2 partial pressure from 64 to 96 psia (4.35 to 6.53 atm) at 160°C. As shown in Figure 4B-9, the CO_2/H_2O pressure ratio increased from 1.52 to 3.84 when the PCB concentration increased from 30 to 50 wt% at 160°C. This suggests that the concentrated PCB solution favored CO_2 stripping.

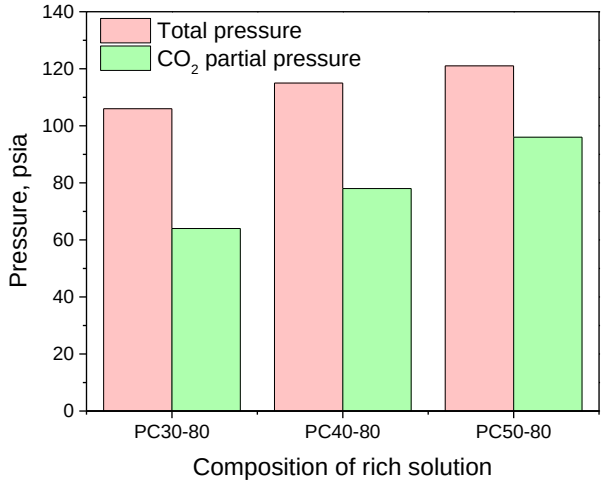

Figure 4B-8. Total pressures and partial pressures of CO_2 at the top of the stripper from CO_2 stripping at 160°C with different PCB feed solutions.

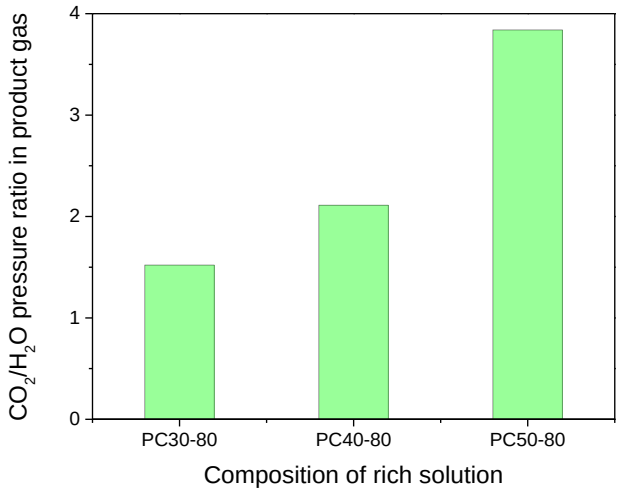

Figure 4B-9. CO_2/H_2O pressure ratios in product gas streams from CO_2 stripping at 160°C with different PCB feed solutions.

4B.4.1.3 Effect of CO_2 loading in the feed solution

Figure 4B-10 displays the change in CTB conversion during CO_2 stripping at 160°C with 40 wt% PCB feed solutions of varying CTB conversion levels (40 to 80%). As shown in Figure 4B-10, more $KHCO_3$ was regenerated from the PCB feed with a higher CTB conversion level. The change in CTB conversion throughout the stripper increased from 9.5 to 18% when the CTB conversion in the feed was increased from 40 to 80%.

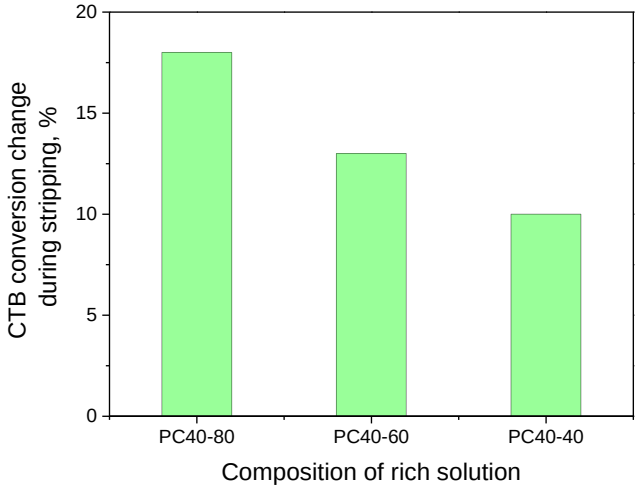

Figure 4B-10. Changes in CTB conversion in the 40 wt% PCB feed solutions during CO_2 stripping at 160°C.

Using the feed solution with a higher CTB conversion resulted in a higher total pressure and CO_2 partial pressure at the top of the stripper (Figure 4B-11). With an increase in the CTB conversion from 40 to 60% in the 40 wt% PCB feed solution, the total stripping pressure at 160°C increased from 79 to 115 psia (5.38 to 7.83 atm) and the CO_2 partial pressure increased from 16 to 79 psia (1.09 to 5.38 atm), whereas the P_{CO2}/P_{H2O} increased from 0.25 to 2.11 (Figure 4B-12). This is

also consistent with the VLE data measured in this project: at the same temperature, the CO_2 partial pressure increased while the water vapor partial pressure decreased with increasing CTB conversion in the feed solution, resulting in an increase in the P_{CO2}/P_{H2O} ratio.

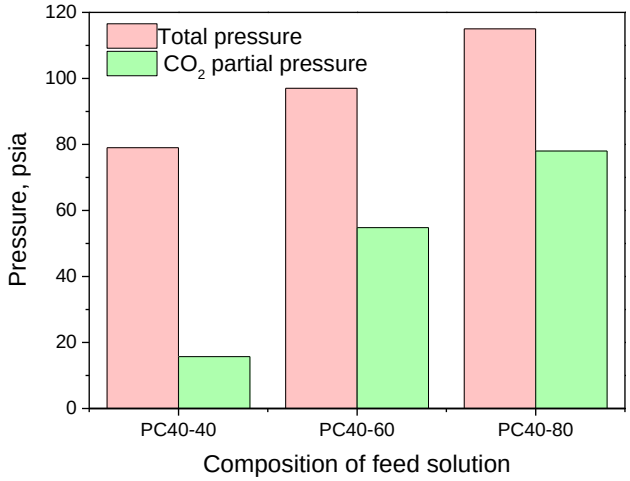

Figure 4B-11. Total pressures and partial pressures of CO_2 at the top of the stripper from CO_2 stripping at 160°C with the 40 wt% PCB feed solutions with different CTB conversion levels.

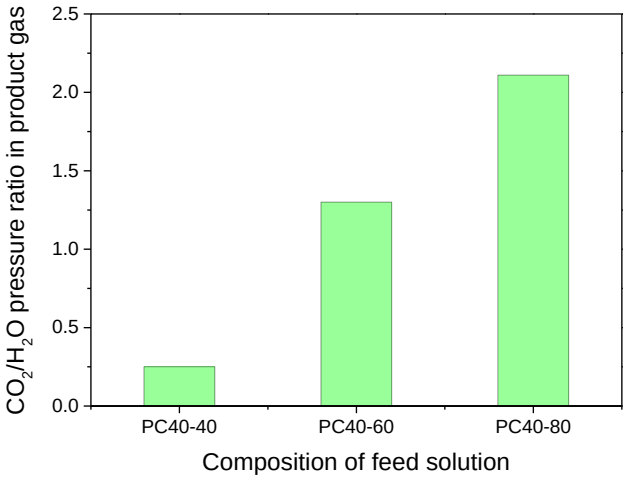

Figure 4B-12. CO_2/H_2O pressure ratios in product gas steams from CO_2 stripping at 160°C with the 40 wt% PCB feed solutions with different CTB conversion levels.

4B.4.2 Effect of the presence of an additive or promoter

4B.4.2.1 Effect of the presence of potassium sulfate

Because the flue gas still contains a small amount of SO_2 (up to 300 ppmv) after flue gas desulfurization (FGD), K_2SO_4 is formed as a by-product of the absorption of SO_2 in PCB, and some of it may be co-crystallized with $KHCO_3$ during the crystallization process. As a conservative consideration, 1 wt% K_2SO_4 was added into a PCB feed solution (PCB40-60) to evaluate its effect on the performance of CO_2 stripping. As shown in Figures 4B-13, 4B-14, and

4B-15, the total and CO_2 partial pressures, CO_2 loading of the regenerated PCB solution, and P_{CO2}/P_{H2O} did not change with the addition of the sulfate, indicating that the presence of K_2SO_4 did not affect the performance of CO_2 stripping with the PCB solution. In general, vapor pressures over a solution are suppressed by the presence of nonvolatile substances (i.e., salts), and the suppression tends to be more significant with increasing salt dosage.[2] Because the 40 wt% PCB was used in the stripping test, the addition of 1 wt% K_2SO_4 led to an increase in total salt concentration by only 2.5%. Thus, the equilibrium pressures of both water vapor and CO_2 would not change significantly at a small dosage of K_2SO_4. As a result, the driving force for CO_2 stripping was almost the same, and the composition of the regenerated lean solution was not affected in the presence of 1 wt% K_2SO_4.

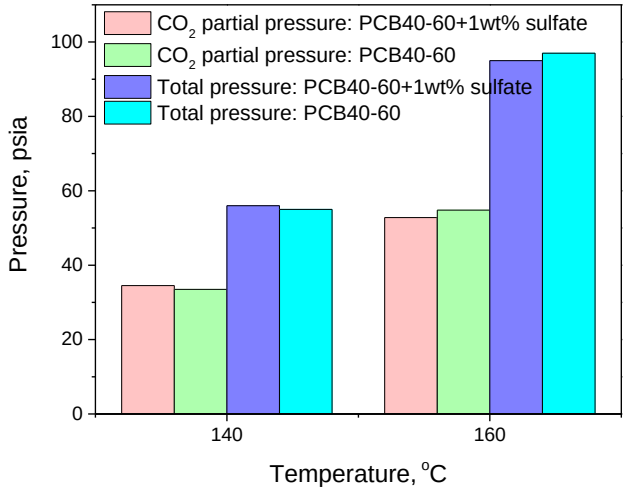

Figure 4B-13. Total pressures and partial pressures of CO_2 at the top of the stripper from CO_2 stripping with the PCB40-60 feed solution in the presence of 1 wt% K_2SO_4.

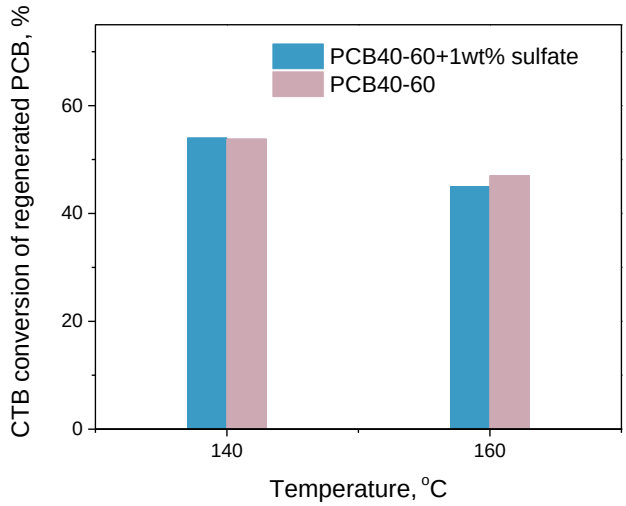

Figure 4B-14. CO_2 loading of regenerated PCB solutions in the presence of 1 wt% K_2SO_4.

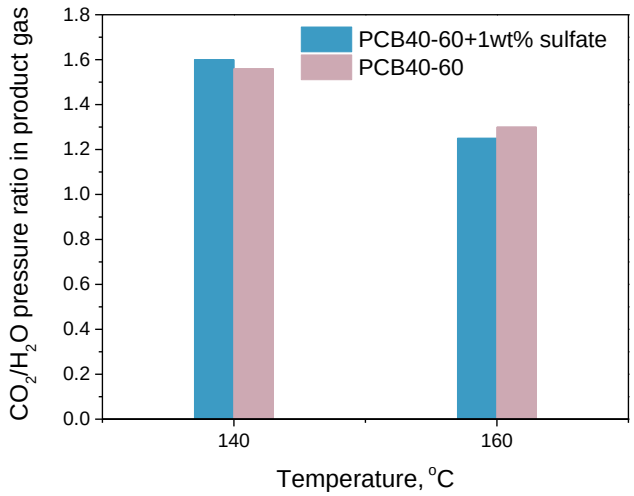

Figure 4B-15. CO_2/H_2O pressure ratios in product gas streams from CO_2 stripping in the presence of 1 wt% K_2SO_4.

4B.4.2.2 Effect of the presence of PZ

Because PZ is used as a promoter to enhance the rate of CO_2 absorption into PCB in the Hot-CAP absorber, it will be present in the CO_2-rich solution. In the $KHCO_3$ crystallization process, a small amount of PZ may be transferred with moisture content to the wet $KHCO_3$ crystal solids. As a conservative consideration, 0.2 M of PZ was added to a PCB feed solution (PCB40-60) to evaluate its effect on CO_2 stripping from the PCB solution. Because PZ has been found to be resistant to degradation up to 160°C,[3] the CO_2 stripping tests were operated at 140 and 160°C. Results indicated that the performance of CO_2 stripping was not affected by the addition of PZ compared with the performance without PZ (Figures 4B-16, 4B-17, and 4B-18). The heat of reaction between PZ and CO_2 is about twice that between PCB and CO_2. According to Eq. (4B-4), the partial pressure of CO_2 should increase in the presence of PZ. However, the dosage of 0.2 M PZ was only 1/20 of the PCB concentration. As a result, the partial pressure of CO_2 over such a PCB-dominant mixture would not noticeably change.

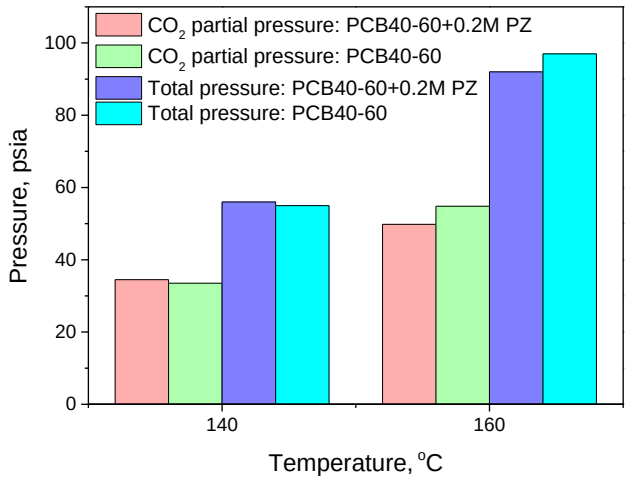

Figure 4B-16. Total pressures and partial pressures of CO_2 at the top of the stripper from CO_2 stripping with PCB solutions without and with the presence of 0.2 M PZ.

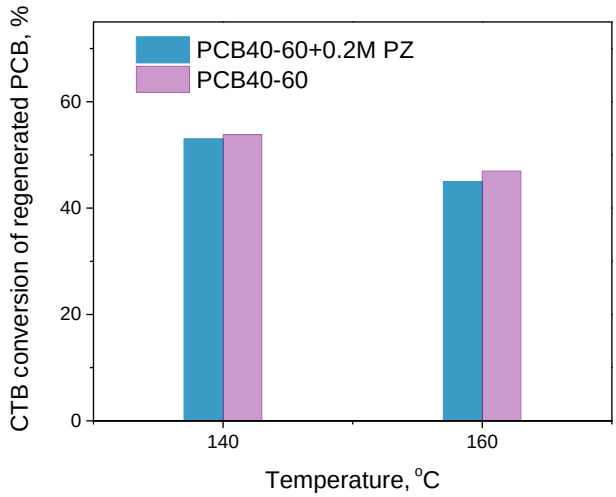

Figure 4B-17. CO_2 loading of regenerated lean PCB solutions without and with the presence of 0.2 M PZ.

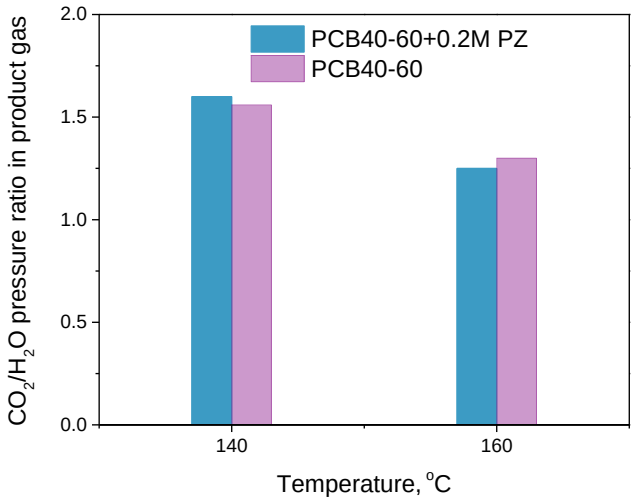

Figure 4B-18. CO_2/H_2O pressure ratios in product gas streams from CO_2 stripping with PCB solutions without and with the presence of 0.2 M PZ.

4B.4.2.3 Effect of the addition of MDEA

As demonstrated above, the use of concentrated PCB solutions for CO_2 stripping could result in high stripping pressures and thus reduce the stripping energy use. Some aqueous solutions of tertiary amines, ammonia bicarbonates, or amino acids that can react with CO_2 to form bicarbonate products have relatively high equilibrium partial pressures of CO_2 at typical stripping temperatures, even when they are loaded with a relatively small amount of CO_2. Therefore, it is hypothesized that the addition of such additives may help increase the CO_2 stripping pressure over the PCB solution. MDEA, a tertiary amine, has the advantage of a stable structure and high equilibrium partial pressure of CO_2 over its aqueous solution loaded with CO_2.[4-6] MDEA was thus selected as an additive for CO_2 stripping from the hot PCB solution. The PCB30-60 feed solution with the addition of 0.5 M MDEA was tested for CO_2 stripping at 120 and 140°C.

As shown in Figure 4B-19, compared with the PCB without MDEA, the regenerated PCB solution in the presence of 0.5 M MDEA had a leaner CO_2 loading, indicating that the addition of MDEA was beneficial for CO_2 stripping. The CTB conversion in the regenerated PCB solution with the addition of MDEA was 52.7% compared with 59.4% without MDEA. Meanwhile, increasing the temperature also favored CO_2 stripping from the PCB + MDEA solution. The CTB conversion in the regenerated solution decreased from 52.7 to 40.3% as the stripping temperature was increased from 120 to 140°C.

Figure 4B-20 displays the total pressure and the CO_2 partial pressures at the top of the stripper attained from CO_2 stripping with the PCB + MDEA feed solution. Compared with those without MDEA, the CO_2 partial pressure increased from 9 to 13 psia (0.61 to 0.88 atm) and the total pressure increased from 27 to 31 psia (1.84 to 2.11 atm) during CO_2 stripping at 120°C with the PCB30-60 + 0.5 M MDEA feed solution. It should be noted that the stripping pressure in the column generally depends on the composition of the regenerated solution. In general, the leaner the solution exiting the stripper, the lower the stripping pressure reached in the column at the

same temperature. Although a leaner PCB solution was obtained in the presence of MDEA after the regeneration, both a higher total pressure and a higher CO_2 partial pressure were still attained compared with the reference PCB. This suggests that the MDEA contributed favorably to stripping with the PCB solution.

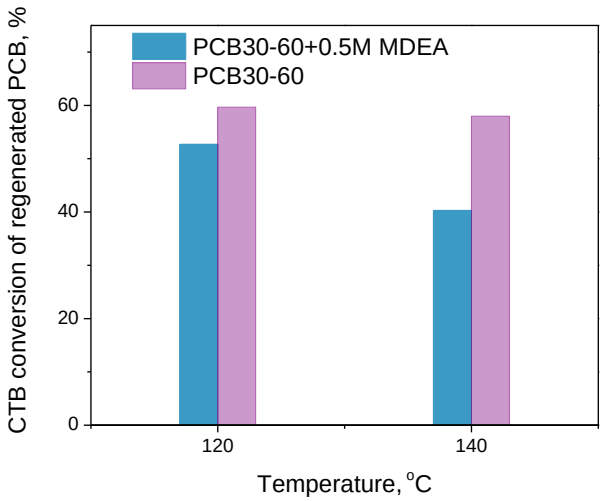

Figure 4B-19. CO_2 loading of regenerated lean PCB solutions without and with the presence of 0.5 M MDEA.

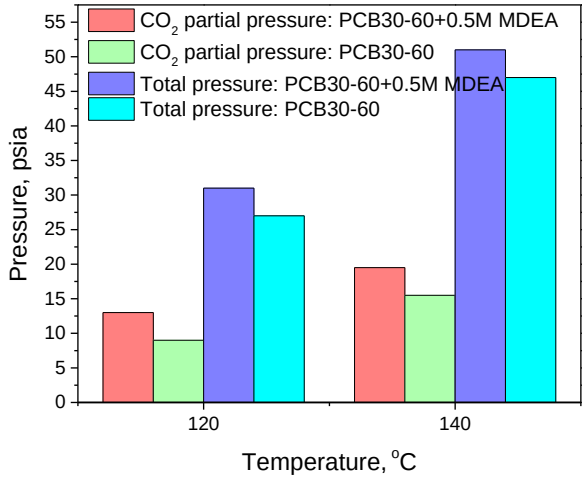

Figure 4B-20. Total pressures and partial pressures of CO_2 at the top of the stripper from CO_2 stripping at 120 and 140°C with PCB solutions without and with the presence of 0.5 M MDEA.

4B.4.3 Heat duty of CO_2 stripping in a bench-scale stripping column

4B.4.3.1 Heat duty of CO_2 stripping with 5 M MEA

In the stripping tests with MEA, the electrical power input of the band heaters to the reboiler was either 0.22 or 0.76 kW. The benchmark 5 M MEA solution loaded with 0.475 mol of CO_2/mol of MEA was used as a feed. As mentioned, the energy supplied was consumed by the three heat elements during stripping as well as by heat losses through the equipment walls.

As expected, a higher electrical power input to the reboiler favored CO_2 stripping (Figure 4B-21). The CO_2 loading of the regenerated solution exiting the column was 0.2 mol/mol MEA at 0.76 kW of power input, whereas it was 0.37 mol/mol at 0.22 kW of power input, indicating more CO_2 was desorbed from the MEA solution. With the consideration of heat losses through the equipment, the actual total heat use associated with CO_2 stripping increased from 4,300 to 6,200 kJ/kg of CO_2 when the lean CO_2 loading decreased from 0.37 to 0.2 mol/mol (Table 4B-3). The estimated heat use for CO_2 stripping with MEA is consistent with the values reported in the literature.[7,8] Results also showed that the leaner the CO_2 loading of the regenerated solution (i.e., the more heat use), the lower the CO_2/H_2O ratio in the product gas stream, indicating that more heat was used to vaporize water when a deeper level of MEA regeneration was required.

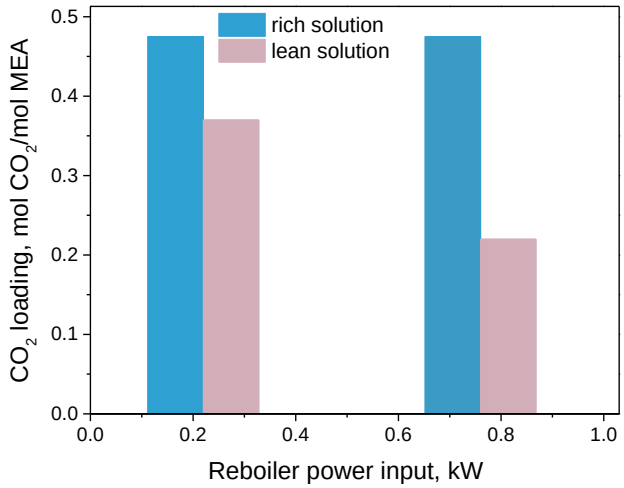

Figure 4B-21. Composition of the lean MEA solution with respect to the reboiler power input.

Table 4B-3. Estimated heat consumption for CO_2 stripping and the CO_2/H_2O ratio in the product gas stream

CO_2 loading of the regenerated solution (mol/mol of MEA)	Temperature at the top of the stripper (°C)	CO_2/H_2O pressure ratio in the product gas stream	Heat used for CO_2 stripping (kJ/kg of CO_2)
0.37	85	3:2	4,300
0.2	94	1:3	6,200

4B.4.3.2 Heat duty of CO_2 stripping with different PCB feed solutions

In the stripping tests with hot PCB solutions, the electrical power input of the band heaters to the reboiler was kept at 0.76 kW. The estimation of heat duty followed the same approach as for the MEA solution. As shown in Table 4B-2, the temperature changes between the stripper inlet and outlet varied under different testing conditions. The sensible heat associated with the temperature change accounted for a great portion of heat consumption. For comparison purposes, the variations in temperature difference at the top and bottom of the column under different test conditions were normalized to 5°C when comparing heat duties among the individual tests.

Figure 4B-22 shows the heat duty of CO_2 stripping with the PCB30-80 feed solution at different temperatures. It can be seen from the figure that the heat duty decreased with an increase in stripping temperature. According to Eq. (4B-2), the total heat duty is sensitive to the sensible heat and the stripping heat (associated with water vaporization), because the heat of reaction hardly changes under different operating conditions. A slight decrease in the CO_2/H_2O pressure ratio as a result of increasing the temperature from 120 to 160°C (Figure 4B-6) caused an increase in stripping heat. Meanwhile, the regenerated solution became leaner as the temperature was increased (Figure 4B-4), resulting in a decrease in the sensible heat according to Eq. (4B-2). Overall, as the stripping temperature changed, the sensible heat changed more significantly than did the stripping heat. Thus, the heat duty was lowered at a higher stripping temperature for the range of stripping temperatures examined.

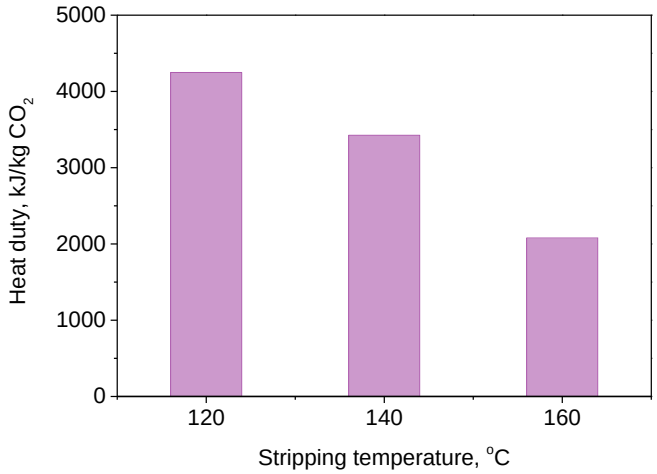

Figure 4B-22. Heat duty required for CO_2 stripping with the PCB30-80 feed solution at different temperatures.

As expected, using either a more concentrated PCB solution or a PCB feed solution with a higher CO_2 loading (i.e., higher CTB conversion) led to lower heat use for CO_2 stripping (Figure 4B-23 and 4B-24). For PCB feed solutions with the same CTB conversion (80%), the heat duty of CO_2 stripping decreased from 2,082 to 1,126 kJ/kg at 160°C when the PCB concentration increased from 30 to 50 wt% (Figure 4B-24). For the 40 wt% PCB solution, when the CTB conversion in the feed increased from 40 to 80%, the heat duty decreased from 5,113 to 1,522 kJ/kg at 160°C. Compared with the benchmark 5 M MEA solution, the heat duties required for stripping the 30 to 50 wt% PCB solutions with 80% CTB conversion in the feed were two-to-three times lower. Note that a leaner MEA solution was regenerated compared with the PCB solution in the tests.

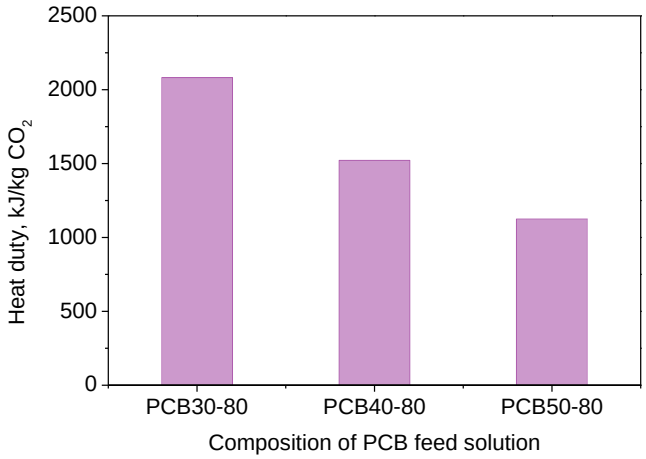

Figure 4B-23. Heat duty required for CO_2 stripping at 160°C for 30 to 50 wt% PCB solutions with 80% CTB conversion in the feed.

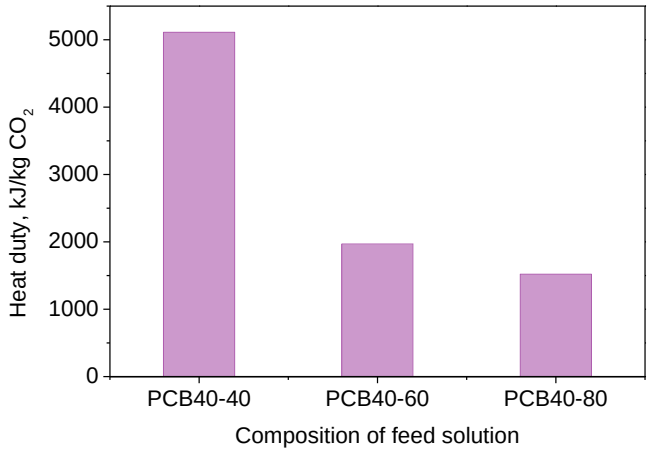

Figure 4B-24. Heat duty required for CO_2 stripping with 40 wt% PCB solutions of different CTB conversions at 160°C.

The effect of the three selected impurities or additives (i.e., K_2SO_4, PZ, and MDEA) on the heat duty for stripping CO_2 from hot PCB solutions was also investigated. As shown in Figure 4B-25, the presence of either K_2SO_4 or PZ exhibited no impact on the heat duty measured. When MDEA was used as an additive to PCB, the heat duty required for CO_2 stripping decreased dramatically (Figure 4B-26). For the PCB30-60 feed solution in the presence of 0.5 M MDEA, the heat duty for CO_2 stripping at 140°C was 2,735 kJ/kg, compared with 8,698 kJ/kg in the absence of MDEA. Thus, the preliminary results demonstrated the potential of MDEA as an additive in improving the performance of CO_2 stripping from the hot PCB solution. A further investigation of MDEA and other additives is deemed useful in the future.

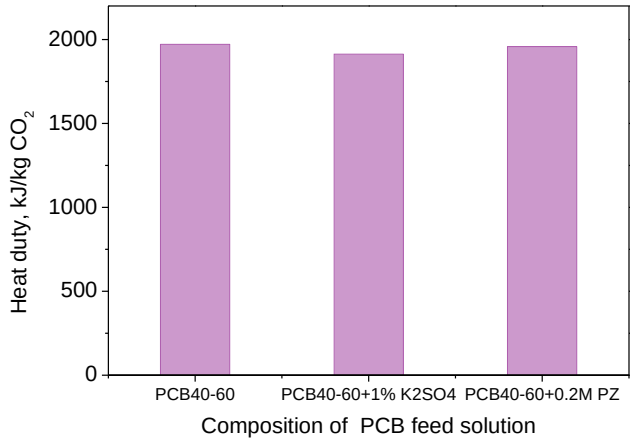

Figure 4B-25. Heat duty required for CO_2 stripping at 160°C with PCB40-60 feed solutions without and with the presence of K_2SO_4 or PZ.

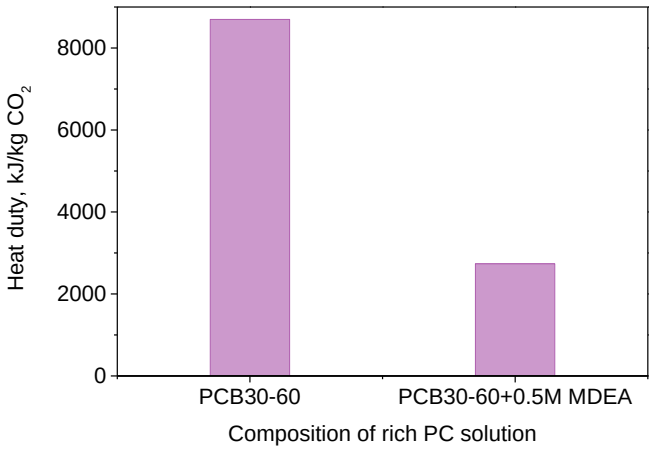

Figure 4B-26. Heat duty required for CO_2 stripping at 140°C with PCB30-60 feed solutions without and with the presence of 0.5 M MDEA.

4B.4 Summary

Parametric experiments of CO_2 stripping from hot concentrated PCB slurries or solutions were conducted in a bench-scale packed-bed stripping column. Results revealed that a higher stripping temperature favored a deeper level of $KHCO_3$ regeneration. Depending on the test conditions, the change in CTB conversion through the 7-ft-high (2.1-m-high) stripping column varied from 1 to 20 percentage points, equivalent to a 1 to 35% regeneration efficiency of the $KHCO_3$ contained in the feed solutions. As the stripping temperature was increased from 120 to 160°C, both the partial pressure of CO_2 in the product gas and the total stripping pressure increased, whereas the CO_2/H_2O pressure ratio in the product gas, an indicator of energy consumption for water vaporization, only slightly decreased.

Experimental results also indicated that increasing the CTB conversion or concentration of the PCB feed solution could significantly increase both the total stripping pressure and the CO_2/H_2O pressure ratio in the product gas, which is advantageous because the Hot-CAP uses a $KHCO_3$

slurry (i.e., high CTB conversion and high PCB concentration) for CO_2 stripping. When the high-concentration PCB solutions (e.g., PCB concentrations of 60 wt%) were used, the stripping pressure attained was 180 psia (12.2 atm) at a temperature of 200°C.

In addition, experiments demonstrated that the presence of K_2SO_4 (1 wt%) and PZ (0.2 M) in the PCB feed solution did not noticeably affect the performance of CO_2 stripping. In comparison, a deeper level of $KHCO_3$ regeneration from the PCB solution was achieved in the presence of 0.5 M MDEA. A leaner regenerated PCB solution was obtained in the presence of MDEA; however, both a higher total pressure and a higher CO_2 partial pressure were also attained. MDEA could be regarded as a favorable additive for CO_2 stripping from the hot PCB solution.

The heat duty values required for CO_2 stripping under different conditions were estimated based on heat supply to the reboiler, temperature measurements, and equipment heat losses. The performance of CO_2 stripping from a 5 M MEA feed solution loaded with 0.475 mol of CO_2/mol of MEA was tested for the comparison. The total heat use for CO_2 stripping varied from 4,300 to 6,200 kJ/kg of CO_2 when the obtained lean CO_2 loading varied from 0.37 to 0.2 mol/mol MEA. The heat use for CO_2 stripping with 5 M MEA was comparable with that reported in the literature.

Increasing either the concentration or CTB conversion of the PCB feed solution could significantly decrease the heat use for CO_2 stripping. Increasing the temperature was beneficial to reduce the total stripping heat use. The presence of impurities, such as $K_2SO_4$and PZ, had no impact on the heat use for CO_2 stripping. The addition of MDEA in the PCB feed solution could dramatically decrease the heat use for CO_2 stripping. For example, the heat use was reduced by 69% for the PCB30-60 feed solution when 0.5 M MDEA was present. Compared with the 5 M MEA solution, the heat duty for CO_2 stripping from the 30 to 50 wt% PCB feed solutions with 80% CTB conversion was two-to-three times lower.

References

1. Tosh J.S., Field J.H., Benson H.E., Haynes W.P. *Equilibrium Study of the System Potassium Carbonate, Potassium Bicarbonate, Carbon Dioxide and Water*, Bureau of Mines, Report of Investigations 5484, 1959.
2. Ohe S. Prediction of salt effect on vapor–liquid equilibria, *Fluid Phase Equilibria* 1998, 144: 119–129.
3. Freeman S.A., Davis J., Rochelle G.T. Degradation of aqueous piperazine in carbon dioxide capture, *International Journal of Greenhouse Gas Control* 2010, 4: 756–761.
4. Xu G., Zhang C., Qin S., Gao W., Liu H. Gas–liquid equilibrium in a CO_2-MDEA-H_2O system and the effect of piperazine on it, *Industrial & Engineering Chemistry Research* 1998, 37: 1473–1477.
5. Vrachnos A., Voutsas E., Magoulas K., Lygeros A. Thermodynamics of acid gas-MDEA-water systems, *Industrial & Engineering Chemistry Research* 2004, 43: 2798–2804.
6. Zhang Y., Chen C. Thermodynamic modeling for CO_2 absorption in aqueous MDEA solution with electrolyte NRTL model, *Industrial & Engineering Chemistry Research* 2011,

50: 163–175.

7. Sakwattanapong R., Aroonwilas A., Veawab A. Behavior of reboiler heat duty for CO_2 capture plants using regenerable single and blended alkanolamines, *Industrial & Engineering Chemistry Research* 2005, 44: 4465–4473.
8. Ciferno J., Dipietro P., Tarka T. *An Economic Scoping Study for CO_2 Capture Using Aqueous Ammonia*, DOE/NETL report, February 2005.

Chapter 5. Reclamation of Sulfate for Combining SO_2 Removal with CO_2 Capture

Part 5A. A Two-Step Process

5A.1 Introduction

One feature of the Hot-CAP is that SO_2 removal can potentially be integrated into the CO_2 capture process. This would downsize or even eliminate the need for a separate wet flue gas desulfurization (FGD) unit and/or polishing FGD unit. High SO_2 removal efficiency can be achieved in a system designed for 90% CO_2 capture, because SO_2 has stronger acidity and reacts more actively with a K_2CO_3 solvent than does CO_2 to form potassium sulfate (K_2SO_4). The overall reaction of SO_2 scrubbing is

$$SO_2 + ½O_2 + K_2CO_3 = K_2SO_4 + CO_2 \quad \text{(5A-R1)}$$

The solubility of K_2SO_4 in water ranges between 7.2 and 14.8 g/100 g of water at 30 to 80°C (Lange, 1961). K_2SO_4 exists in the dissociated form of sulfate (SO_4^{2-}) and potassium (K^+) ions in PCB aqueous solutions when the K_2SO_4 concentration is below solubility.

A process concept was preliminarily proposed for the combination of SO_2 removal and CO_2 capture in the Hot-CAP. The chemistry and principle of sulfate reclamation from the SO_2- and CO_2-rich solution have been described in detail in a technical report by the same group (Lu *et al*., 2012). The reclamation process consists of two steps. The first step (solution acidification) is to reduce the CO_3^{2-} concentration using a pressurized CO_2 gas stream according to the following reactions:

$$H_2O + CO_2 = HCO_3^- + H^+ \quad \text{(5A-R2)}$$

$$CO_3^{2-} + H^+ = HCO_3^- \quad \text{(5A-R3)}$$

The concentration of SO_4^{2-} in the PCB solution can be adjusted by controlling the portion of CO_2-rich solution withdrawn to reclaim the sulfate, which preferably ranges between 0.1 and 1 mol/L. The minimum attainable concentration of CO_3^{2-} depends on the operating conditions applied, such as the temperature, total PCB concentration, and pressure of CO_2.

The second step (K_2SO_4 reclamation) is to convert K_2SO_4 into $CaSO_4$ and $KHCO_3$ by adding hydrated lime to the solution under high-pressure CO_2. The overall reaction is

$$Ca(OH)_2 + K_2SO_4 + 2CO_2 = CaSO_4 + 2KHCO_3 \quad \text{(5A-R4)}$$

Both SO_4^{2-} and CO_3^{2-} ions in the solution react with Ca^{2+} to form $CaSO_4$ and $CaCO_3$ precipitates by the following reactions:

$$Ca(OH)_2 = Ca^{2+} + OH^- \quad \text{(5A-R5)}$$

$$Ca^{2+} + SO_4^{2-} = CaSO_4 \quad \text{(5A-R6)}$$

$$Ca^{2+} + CO_3^{2-} = CaCO_3 \quad \text{(5A-R7)}$$

The competitive precipitation between $CaSO_4$ and $CaCO_3$ depends on several factors, including the SO_4^{2-}/CO_3^{2-} ratio, reaction temperature, and residence time. When the concentrations of SO_4^{2-} and CO_3^{2-} are comparable, $CaCO_3$ rather than $CaSO_4$ will precipitate from the solution, because the solubility product of $CaCO_3$ is about four orders-of-magnitude lower than that of $CaSO_4$ (Mines, 2014). However, $CaSO_4$ may become the dominant precipitate phase when the CO_3^{2-} concentration is sufficiently smaller than SO_4^{2-}.

Figure 5A-1 shows a schematic diagram of the process concept. The desulfurization product, K_2SO_4, is formed in the Hot-CAP absorber during CO_2 absorption. A portion of the SO_2- and CO_2-rich solution is withdrawn for sulfate reclamation. A stream of pressurized CO_2 from a multistage compressor is used to reduce the CO_3^{2-} concentration to the minimal level. In the reclaimer, $CaSO_4$ is preferentially precipitated over $CaCO_3$ by reactions with the added hydrated lime. The $CaSO_4$ precipitates are recovered by filtration. The reclaimed solution passes through a flash process to recover CO_2 and then returns to the CO_2 dehydration and compression units. The flashed solution is mixed with the unreclaimed main SO_2- and CO_2-rich stream and enters the CO_2 crystallization tank.

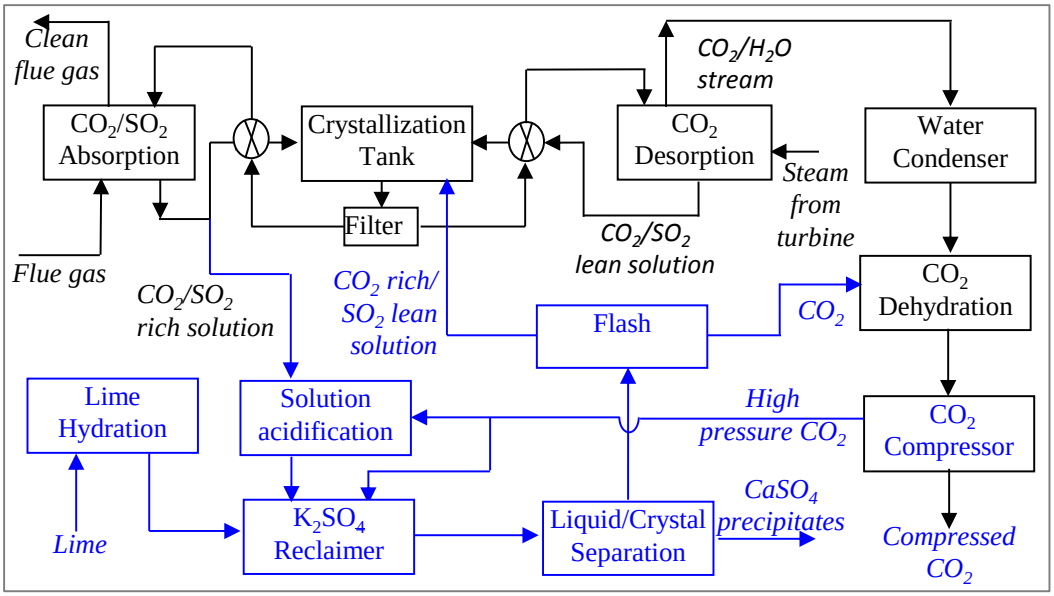

Figure 5A-1. Schematic diagram of the proposed process for combined SO_2 removal and CO_2 capture in Hot-CAP.

Our previous batch study identified that a high SO_4^{2-}/CO_3^{2-} ratio would favor the preferential precipitation of $CaSO_4$ over $CaCO_3$ (Lu *et al.*, 2012). Several operating parameters, including the total PCB concentration, reaction temperature, K_2SO_4 concentration, and residence time would substantially affect the competitive precipitation process. In this study, the team investigated the effects of more operating parameters on the preferential precipitation of $CaSO_4$ using both a batch and a semi-continuous operation. The objective of this study is to seek the optimal conditions to achieve a high yield of $CaSO_4$ precipitation.

5A.2 Experimental method

The experimental apparatus has been described in detail in a technical report (Lu *et al.*, 2012). It consists of a 1-L high-pressure Parr autoclave reactor, a gas supply and pressure control unit, a temperature control unit, and data acquisition instrumentation.

In a typical experiment, 500 mL of PCB solution with the desired composition of K_2CO_3, $KHCO_3$, and K_2SO_4 was charged into the reactor, and the stirrers for the gas and liquid phases (both at 350 rpm) were turned on. A pure CO_2 gas stream was introduced to the reactor, and the pressure of the reactor was maintained at 550 psia (37.4 atm) by adjusting a back-pressure regulator at the gas stream outlet of the reactor. When the conversion of CO_3^{2-} reached the equilibrium state, as indicated by no notable change in CO_2 pressure over time as the inlet and outlet CO_2 gas streams were closed, a certain amount of $CaCl_2$ or $Ca(OH)_2$ solution was added to the reactor for the precipitation reactions. In batch mode testing, the reactor outlet was closed and the CO_2 gas flowed in the reactor (without bubbling) only when the pressure decreased to below the 550 psia (37.4 atm) set point, whereas in semi-continuous mode testing, the CO_2 gas at approximately 0.5 slpm was continually purging (with bubbling) and leave the reactor at 550 psia (37.4 atm). After about a 1-hr reaction time (unless specified otherwise), 100 to 200 mL of the suspension sample was collected through a discharge valve and immediately filtered using a 0.2-μm Whatman nylon membrane filter. The solid retentate was collected, air-dried at 80°C (176°F) overnight, and analyzed for composition by powder X-ray diffraction (XRD).

5A.3 Results and discussion

5A.3.1 Batch testing: Effects of operating parameters on precipitate composition

Five groups of batch experiments were carried out to investigate the effect of solution and operating conditions on the competitive precipitation of $CaSO_4$ over $CaCO_3$. The test matrix is shown in Table 5A-1.

Group I experiments (high-concentration PCB solution) used a mixture of 40 wt% PCB solution with 100% initial CTB conversion (denoted as PCB40-100, and so forth) and 0.2 M K_2SO_4. Then, 0.2 M $CaCl_2$ or 0.2 M $Ca(OH)_2$ was added for the precipitation reaction for 1 hr at 70°C. Note that the mixture solution of PCB40-100 and 0.2 M K_2SO_4 with the addition of 0.2 M $Ca(OH)_2$ is denoted as PCB40-100-0.2 M K_2SO_4 + 0.2 M $Ca(OH)_2$ and so forth. XRD patterns of the precipitate sample obtained from this experiment show that the precipitates contained only calcite and vaterite (a less stable $CaCO_3$ phase than calcite); crystalline $CaSO_4$ was not observed (see Figure 5A-2).

Table 5A-1. Test matrix for the batch mode sulfate reclamation experiments

Group	Initial PCB solution			Ca^{2+}-containing reactant	Temp. (°C)	Reaction time (hr)
	Concentration [wt% or K_2CO_3-equiv. (M)]	Initial CTB conversion (%)	K_2SO_4 (M)			
I. High-concentration PCB	40 (1.8)	100	0.2	0.2 M $CaCl_2$	70	1
	40 (1.8)	100	0.2	0.2 M $Ca(OH)_2$	70	1
II. Low-concentration PCB	2.7 (0.2)	100	0.2	0.2 M $CaCl_2$	70	1
	2.7 (0.2)	100	0.2	0.2 M $Ca(OH)_2$	70	1
	2.7 (0.2)	100	0.4	0.2 M $Ca(OH)_2$	70	1
	2.7 (0.2)	100	0.4	0.2 M $CaCl_2$	70	1
III. Effect of temperature	2.7 (0.2)	100	0.4	0.2 M $CaCl_2$	50	1
	2.7 (0.2)	100	0.4	0.2 M $CaCl_2$	Room	1
IV. Effect of initial K_2SO_4 concentration	2.7 (0.2)	100	0.8	0.2 M $CaCl_2$	Room	1
V. Effect of reaction time	2.7 (0.2)	100	0.4	0.2 M $CaCl_2$	Room	6

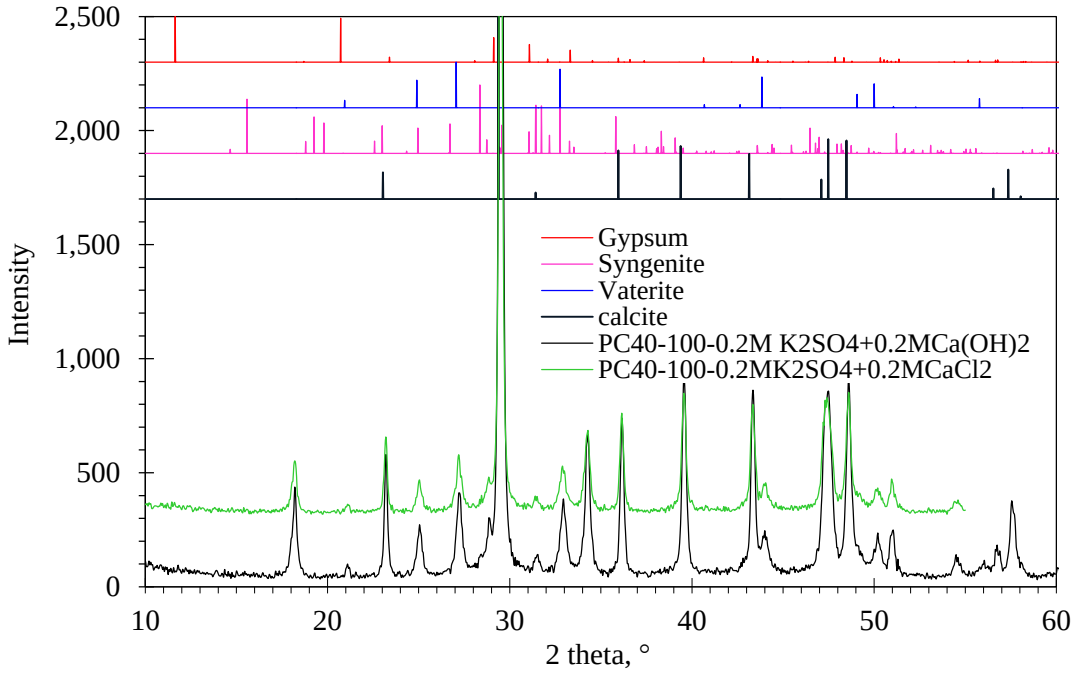

Figure 5A-2. XRD patterns of precipitate particles from the reactions in PCB40-100-0.2 M K_2SO_4 + 0.2 M $Ca(OH)_2$ or 0.2 M $CaCl_2$ at 70°C.

In Group II experiments, a mixture solution of PCB0.2M-100 and 0.2 or 0.4 M K_2SO_4 were used, whereas the other conditions were kept the same as for Group I. In these experiments, the concentration ratio of SO_4^{2-}/CO_3^{2-} in the mixture solution was increased by increasing the concentration of K_2SO_4 from 0.2 to 0.4 M. The 0.2 M $CaCl_2$ solution was added to the solution for the precipitation reactions at 70°C for 1 hr. XRD patterns of the precipitate samples revealed that $CaCO_3$ phases prevailed and no crystalline $CaSO_4$ phase was present (XRD data not shown). The precipitates produced for similar solutions at room temperature contained approximately 40% crystalline $CaSO_4$ in the form of syngenite [$K_2Ca(SO_4)_2{\cdot}H_2O$] and gypsum ($CaSO_4{\cdot}2H_2O$). This comparison indicated that the reaction temperature might be an important factor for the competitive precipitation between $CaSO_4$ and $CaCO_3$.

To investigate the effect of reaction temperature on the preferential precipitation, experiments (Group III) were performed at 70°C, 50°C, and room temperature by adding 0.2 M $CaCl_2$ to the mixture solution of PCB0.2M-100 and 0.4 M K_2SO_4. Figure 5A-3 shows XRD patterns of the obtained precipitate samples. In the precipitates obtained from the reactions at 70 and 50°C, a crystalline $CaSO_4$ phase was not observed, and the only crystal phase detected was for $CaCO_3$; for the precipitate sample obtained from the reaction at room temperature, the XRD patterns showed the presence of 42.3% syngenite [$K_2Ca(SO_4)_2{\cdot}H_2O$] and 1.5% gypsum ($CaSO_4{\cdot}2H_2O$) according to a semi-quantitative XRD analysis. This result indicated that the competitive precipitation of $CaSO_4$ over $CaCO_3$ was not favored by increasing the reaction temperature. The reason might be that increasing the reaction temperature reduced the CO_2 solubility in the PCB solution, resulting in a lower conversion rate of CO_3^{2-} to HCO_3^- (R5.2 and R5.3), although a higher temperature favors the precipitation kinetics.

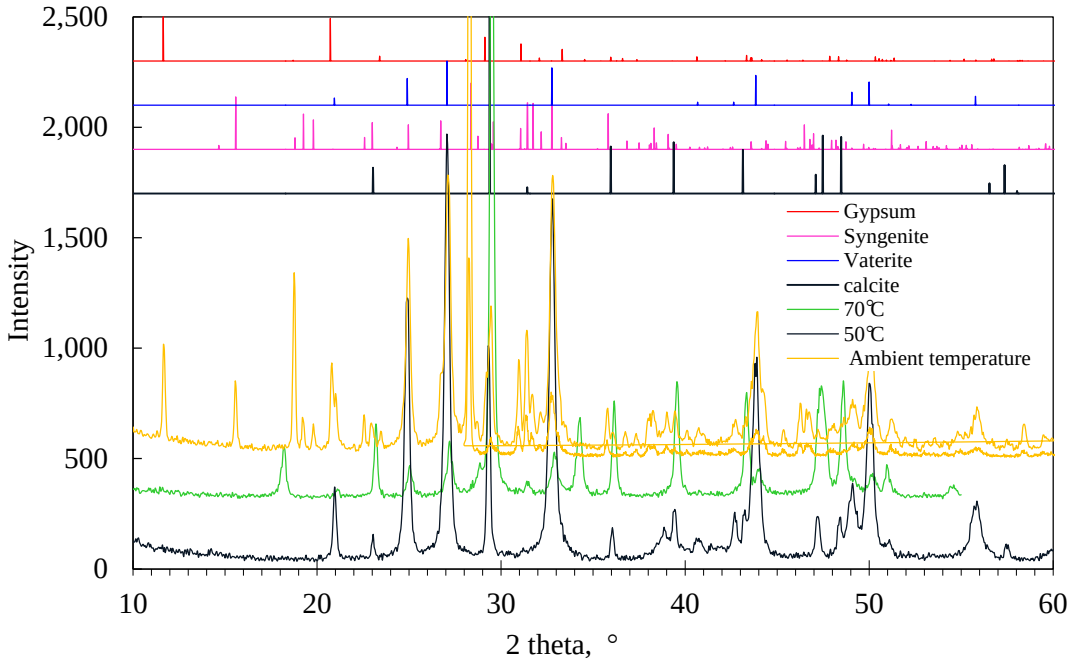

Figure 5A-3. XRD patterns of precipitate particles produced from the reactions in PCB40-100-0.4 M K_2SO_4 + 0.2 M $CaCl_2$ at 70°C, 50°C, or room temperature.

To explore the potential for achieving a high $CaSO_4$ yield, the initial K_2SO_4 concentration in the PCB0.2M-100 mixture solution was increased from 0.4 to 0.8 M in the Group IV experiments. The competitive precipitation reactions with the addition of 0.2 M $CaCl_2$ to the PCB0.2-100-0.8 M K_2SO_4 mixture solution were tested for 1 hr at room temperature. The semi-quantitative XRD analysis (see Figure 5A-4) revealed that the content of syngenite in the precipitates reached 96.8%.

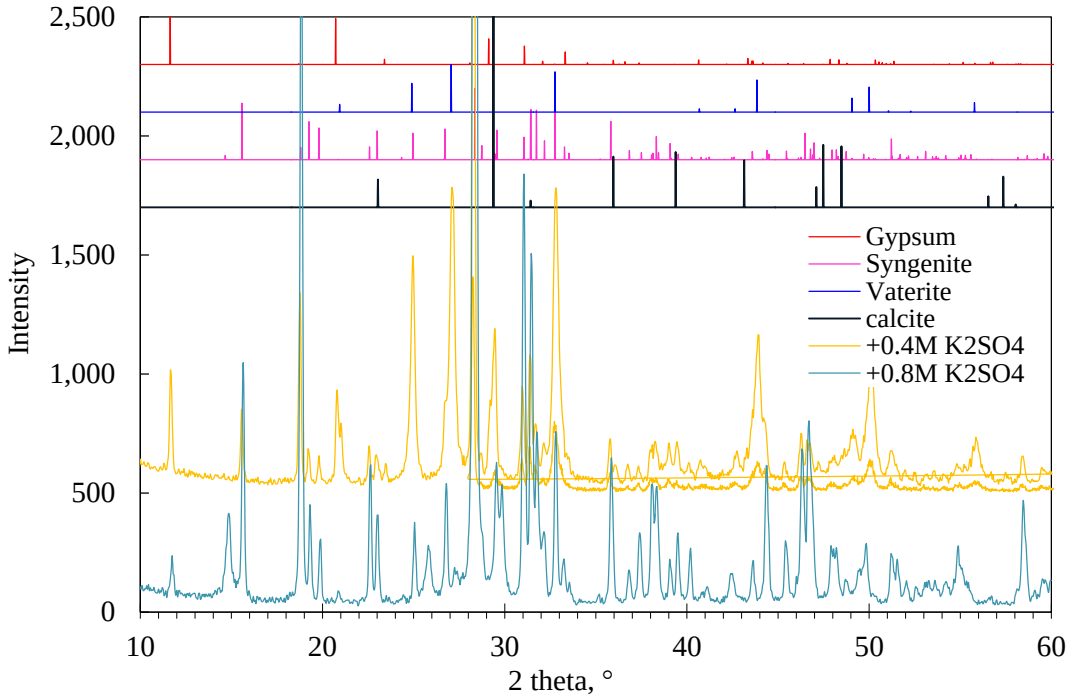

Figure 5A-4. XRD patterns of precipitate particles from the mixture solution of PCB0.2M-100 and 0.4 M or 0.8 M K_2SO_4 by adding 0.2 M $CaCl_2$ for reactions at room temperature.

To investigate the effect of residence time on $CaSO_4$ yield, the residence time of the reaction in the Group V experiment was increased from 1 to 6 hr while the other conditions were kept the same, i.e., the experiment was performed at room temperature for the mixture solution of PCB0.2M-100 and 0.4 M K_2SO_4 with the addition of 0.2 M $CaCl_2$. It was observed that 55.0% syngenite [$K_2Ca(SO_4)_2 \cdot H_2O$] and 38.9% gypsum ($CaSO_4 \cdot 2H_2O$) were present in the precipitate sample (Figure 5A-5).

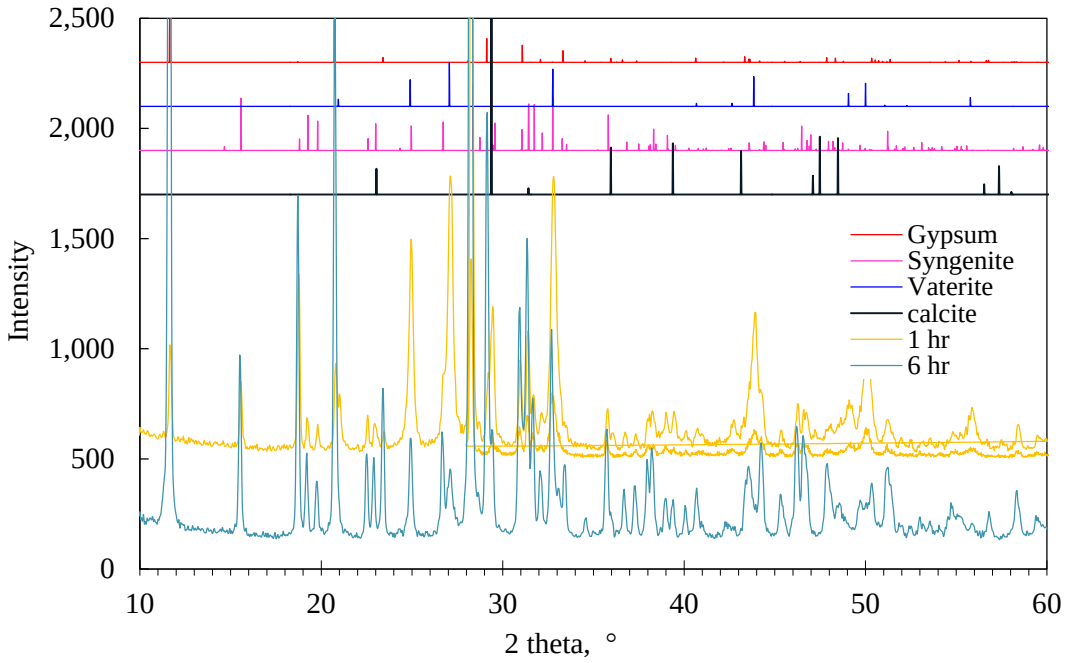

Figure 5A-5. XRD patterns of precipitate particles from the mixture of PCB0.2M-100 and 0.4 M K_2SO_4 by adding 0.2 M $CaCl_2$ for reactions at room temperature for 1 and 6 hr.

Table 5A-2. Compositions of precipitate samples obtained in different experiments

Group	Experiment	Temp. (°C)	Reaction time (hr)	Product composition
I. High-concentration PCB	PCB40-100-0.2 M K_2SO_4 + 0.2 M $CaCl_2$	70	1	100% calcite
	PCB40-100-0.2 M K_2SO_4 + 0.2 M $Ca(OH)_2$	70	1	100% calcite
II. Low-concentration PCB	PCB0.2M-100-0.2 M K_2SO_4 + 0.2 M $CaCl_2$	70	1	100% vaterite
	PCB0.2M-100-0.2 M K_2SO_4 + 0.2 M $Ca(OH)_2$	70	1	100% vaterite
	PCB0.2M-100-0.4 M K_2SO_4 + 0.2 M $Ca(OH)_2$	70	1	100% vaterite
	PCB0.2M-100-0.4 M K_2SO_4 + 0.2 M $CaCl_2$	70	1	100% vaterite
III. Effect of temperature	PCB0.2M-100-0.4 M K_2SO_4 + 0.2 M $CaCl_2$	50	1	100% vaterite
	PCB0.2M-100-0.4 M K_2SO_4 + 0.2 M $CaCl_2$	Room	1	42.3% syngenite + 1.5% gypsum
IV. Effect of initial K_2SO_4 concentration	PCB0.2M-100-0.8 M K_2SO_4 + 0.2 M $CaCl_2$	Room	1	96.8% syngenite
V. Effect of reaction time	PCB0.2M-100-0.4 M K_2SO_4 + 0.2 M $CaCl_2$	Room	6	55.0% syngenite + 38.9% gypsum

The composition of the precipitate samples obtained from the experiments under different conditions is summarized in Table 5A-2. It should be noted that PCB solutions of 100% initial CTB conversion were used in all of the experiments, and $CaCl_2$ rather than $Ca(OH)_2$ solutions were used in some experiments. The purpose of choosing these conditions was to facilitate the acidification reaction. Our previous results showed that the initial CTB conversion of the PCB solution and the type of Ca^{2+}-containing agent were not important factors for the competitive precipitation reactions (Lu *et al.*, 2012). The equilibrated CO_3^{2-} concentration would be attained in a high-pressure CO_2 gas stream regardless of the initial CTB conversion level. Using either $Ca(OH)_2$ or $CaCl_2$ as a source of calcium for the competitive precipitation would cause little difference in composition of the resulting precipitates. Thus, it can be anticipated that similar

results would be achieved by using a PCB solution with a lower initial CTB conversion, such as 40%, or reacting with $Ca(OH)_2$ rather than a $CaCl_2$ solution.

5A.3.2 Semi-continuous testing: effects of operating parameters on precipitate composition

In the batch mode operation, a longer residence time was found to substantially increase the content of $CaSO_4$ (in the forms of syngenite and gypsum) in the precipitates produced from the reactions between PCB0.2M-100-0.4 M K_2SO_4 and 0.2 M $CaCl_2$ at room temperature. The precipitates contained approximately 43% syngenite and 2% gypsum when the residence time was 1 hr; as the residence time was increased from 1 to 6 hr, the precipitates contained 55.0% syngenite and 38.9% gypsum. Such results suggested that the composition of precipitates was both thermodynamically- and kinetically-controlled.

The kinetics of preferential $CaSO_4$ precipitation were enhanced by continuously bubbling high-pressure CO_2 gas through the liquid phase to improve the gas–liquid mixing. The effect of total PCB concentration and residence time on the preferential $CaSO_4$ precipitation under CO_2-bubbling mode was investigated. The objective was to identify the optimal operating mode and process conditions to achieve a high yield of $CaSO_4$ precipitates.

Four groups of experiments were carried out to investigate the effect of several process variables on the competitive precipitation of $CaSO_4$ over $CaCO_3$ under the semi-continuous mode. The test matrix is shown in Table 5A-3. All the experiments were performed at room temperature, and the initial CTB conversion in the PCB solutions was 100%.

Table 5A-3. Matrix of semi-continuous experiments on sulfate reclamation at room temperature

Group	PCB concentration [wt% or K_2CO_3-equiv. (M)]	K_2SO_4 (M)	Ca^{2+}-containing reactant	Reaction time
I. Effect of CO_2 gas flow mode	2.7 (0.2)	0.4	0.2 M $CaCl_2$	1 hr
II. Effect of initial PCB concentration	15 (1.2)	0.4	0.4 M $CaCl_2$	1 hr
	5.4 (0.4)	0.4	0.4 M $CaCl_2$	1 hr
III. Effect of reaction time at 0.2 M PCB	2.7 (0.2)	0.4	0.2 M $CaCl_2$	40 min
	2.7 wt% (0.2)	0.4	0.2 M $CaCl_2$	20 min
V. Effect of reaction time at 0.4 M PCB	5.4 wt% (0.4)	0.4	0.4 M $CaCl_2$	6 hr

The Group I experiment was designed to investigate the effect of CO_2 gas flow mode on the precipitate composition. A 0.2 M PCB and 0.4 M K_2SO_4 mixture solution reacted with the added 0.2 M $CaCl_2$ at room temperature. This was different from the batch experiments, in which the reactor exit was closed, but the CO_2 gas stream could flow in when the pressure in the reactor was lower than at set point. In the semi-continuous experiments, a CO_2 gas stream was continuously bubbling through the liquid and exiting the system.

Figure 5A-6 compares XRD patterns of the precipitate samples obtained from the Group I experiment with continuous CO_2 gas bubbling (semi-continuous testing) and from the counterpart experiment without CO_2 gas bubbling (batch testing). A semi-quantitative XRD

analysis revealed 8.6% gypsum ($CaSO_4 \cdot 2H_2O$) and 91.4% syngenite [$K_2Ca(SO_4)_2 \cdot H_2O$] in the precipitate particles obtained in the semi-continuous test compared with only 1.5% gypsum and 42.3% syngenite in the batch test. This result indicated that the preferential precipitation of $CaSO_4$ over $CaCO_3$ was favored by the increased gas–liquid mixing via gas bubbling.

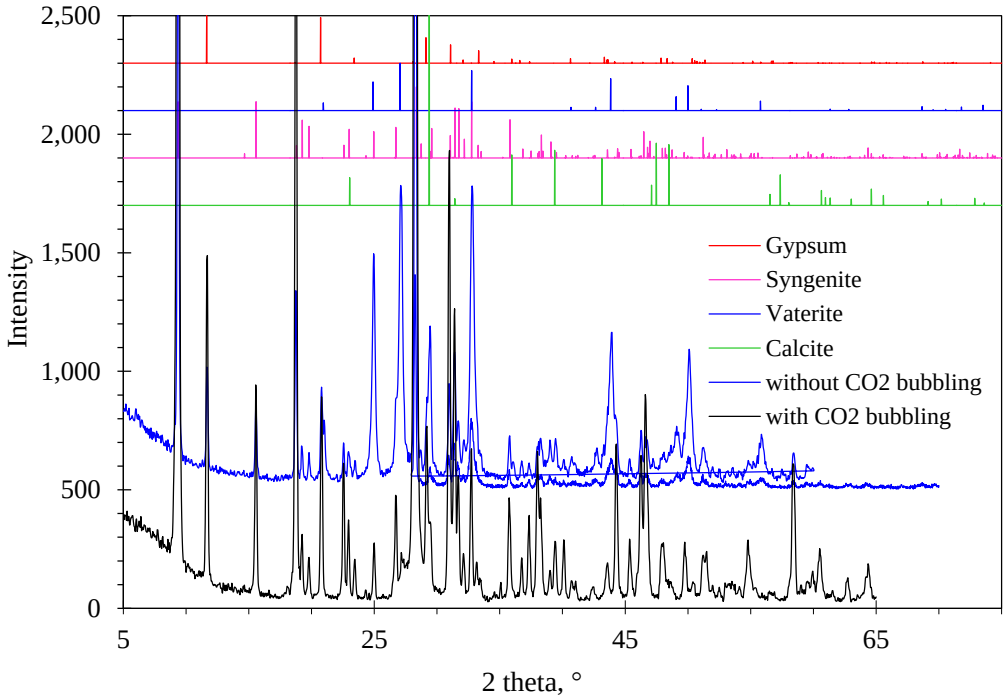

Figure 5A-6. XRD patterns of precipitate particles from PCB0.2M-100-0.4 M K_2SO_4 + 0.2 M $CaCl_2$ with (semicontinuous test) and without (batch test) CO_2 gas bubbling.

A two-step mechanism was thus suggested to explain the observed phenomena. First, $CaCO_3$ was precipitated by the reaction between CO_3^{2-} and the added Ca^{2+}:

$$Ca^{2+} + CO_3^{2-} \leftrightarrow CaCO_3 \qquad \text{(5A-R7)}$$

Second, the produced $CaCO_3$ precipitates reacted with the dissolved CO_2 to form $Ca(HCO_3)_2$:

$$CaCO_3 + CO_2 + H_2O \leftrightarrow Ca(HCO_3)_2 \qquad \text{(5A-R8)}$$

and

$$Ca(HCO_3)_2 \leftrightarrow Ca^{2+} + 2\,HCO_3^- \qquad \text{(5A-R9)}$$

$$Ca^{2+} + SO_4^{2-} \leftrightarrow CaSO_4 \qquad \text{(5A-R10)}$$

$Ca(HCO_3)_2$ has higher solubility in water than does $CaCO_3$. The dissolved $Ca(HCO_3)_2$ is disassociated into Ca^{2+} and HCO_3^-. Ca^{2+} ions further react with SO_4^{2-} to produce the $CaSO_4$ precipitates. The reaction (5A-R8) is kinetically slow, whereas the other reactions are fast. Thus, the overall reaction is dominated by the conversion of $CaCO_3$ into $Ca(HCO_3)_2$. CO_2 gas bubbling promoted the kinetics of the reaction (5A-R8) by increasing the gas–liquid interface and mixing strength, resulting in a higher $CaSO_4$ content in the precipitates within the same reaction time.

In the Group II experiments, the effect of PCB concentration was studied because if the PCB solution were withdrawn directly from the Hot-CAP for SO_2 removal, it would have an elevated concentration. The PCB concentration was initially increased from 0.2 to 1.2 M, whereas 0.4 M $CaCl_2$ solution was added to react with 0.4 M K_2SO_4 for precipitation. Figure 5A-7 shows XRD patterns of the obtained precipitate sample, which contained 100% calcite ($CaCO_3$). When the PCB concentration was adjusted from 1.2 M down to 0.4 M, the precipitate sample obtained contained 3.3% gypsum, 9.9% syngenite, 54.6% vaterite ($CaCO_3$), and 32.3% calcite ($CaCO_3$).

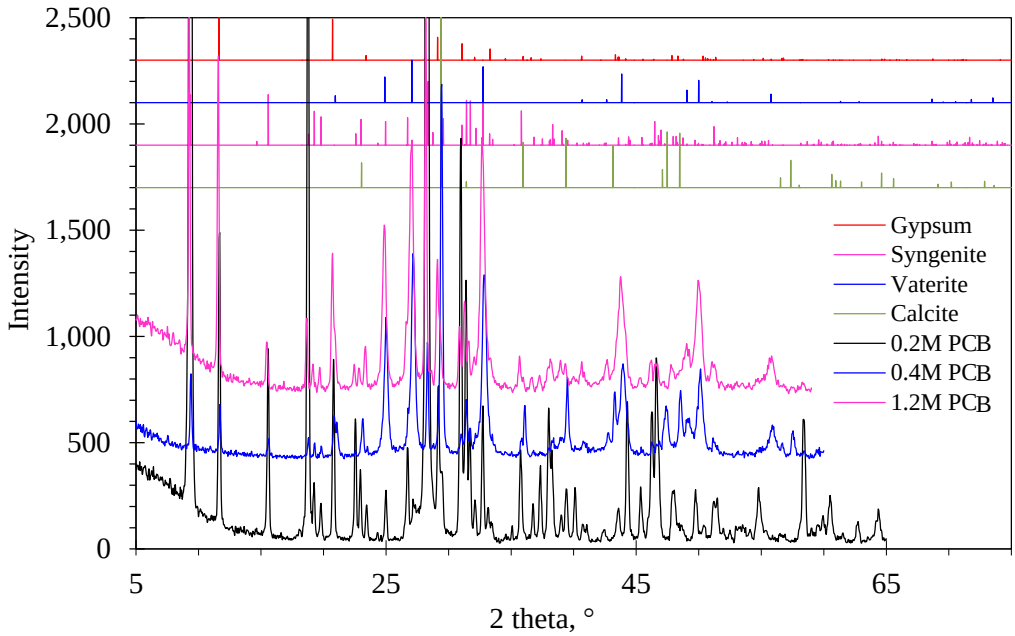

Figure 5A-7. XRD patterns of the precipitate particles obtained from the PCB 0.2 M-100-0.4 M K_2SO_4 + 0.2 M $CaCl_2$, PCB 0.4 M-100-0.4 M K_2SO_4 + 0.4 M $CaCl_2$, and PCB 1.2 M-100-0.4 M K_2SO_4 + 0.4 M $CaCl_2$ solutions.

In the Group III and IV experiments, the effect of reaction time on $CaSO_4$ yield was investigated for the 0.2 M and 0.4 M PCB solutions. For the 0.2 M PCB and 0.4 M K_2SO_4 mixture solution, the reaction time was varied from 20 to 40 min and 1 hr after 0.2 M $CaCl_2$ was added; for the 0.4 M PCB and 0.4 M K_2SO_4 mixture solution added with 0.4 M $CaCl_2$, the reaction time was varied from 1 to 6 hr.

XRD patterns of the precipitate samples obtained at different reaction times in the Group III and IV experiments are shown in Figure 5A-8. The compositions of the precipitate particles obtained from the reaction in PCB0.2M-100-0.4 M K_2SO_4 + 0.2 M $CaCl_2$ for 20 min, 40 min, and 1 hr were 14.7% gypsum + 28.6% syngenite + 56.7% vaterite, 58.0% gypsum + 10.9% syngenite + 31.2% vaterite, and 8.6% gypsum + 91.4% syngenite, respectively. The total $CaSO_4$ yield was markedly increased with increasing reaction time.

The compositions of the precipitate particles obtained in PCB0.4M-100-0.4 M K_2SO_4 + 0.4 M $CaCl_2$ after 1- and 6-hr reaction times were 3.3% gypsum + 9.9% syngenite + 54.6% vaterite + 32.3% calcite and 5.1% gypsum + 28.3% syngenite + 57.3% vaterite + 9.3% calcite. The total

$CaSO_4$ yield also increased with increasing reaction time, but less substantially than that observed for the 0.2 M PCB.

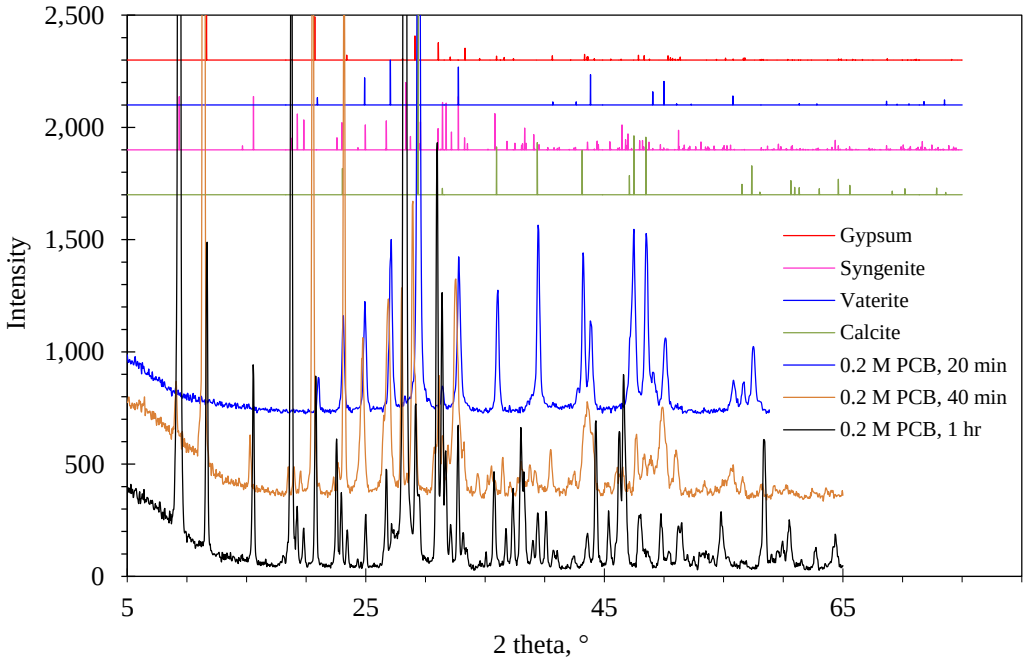

(a) PCB0.2M-100-0.4 M K_2SO_4 + 0.2 M $CaCl_2$ with 20-min, 40-min, and 1-hr reaction times.

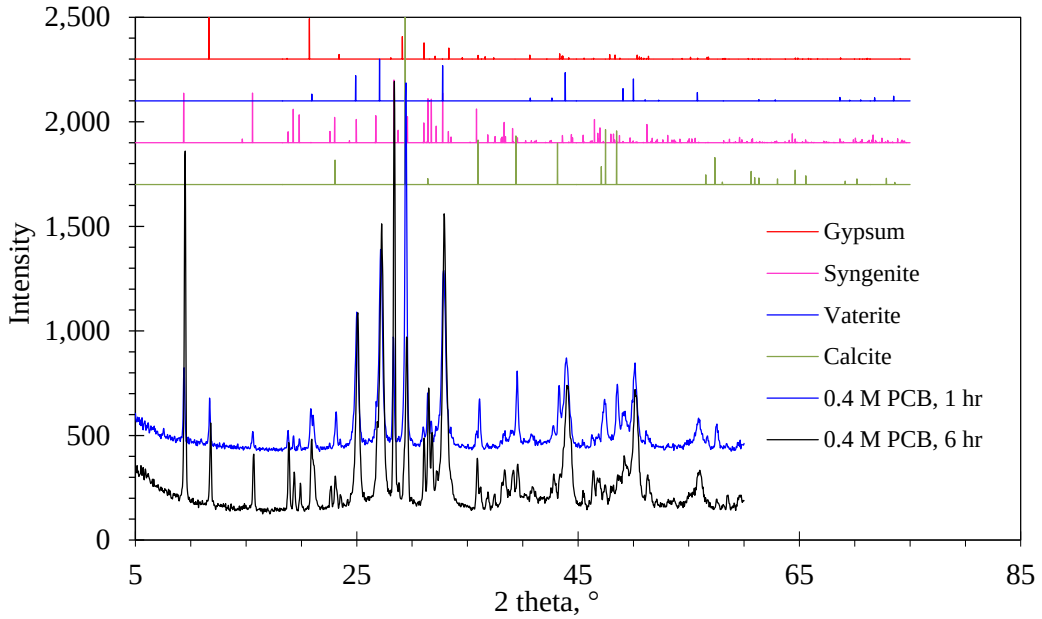

(b) PCB0.4M-100-0.4 MK_2SO_4 + 0.4 M $CaCl_2$ with 1- and 6-hr reaction times.

Figure 5A-8. XRD patterns of precipitate particles obtained from the reactions in the 0.2 and 0.4 M PCB mixture solutions within different reaction times.

This result can also be explained by the suggested two-step mechanism. When the PCB concentration was increased to 1.2 M, both the HCO_3^- and CO_3^{2-} concentrations were increased.

The equilibrated Ca^{2+} concentration specified by the reaction (5A-R9) would be small. When the PCB concentration was sufficiently small, the composition of precipitates was controlled by the kinetics of reaction (5A-R8); increasing the reaction time effectively increased the total content of gypsum and syngenite in the precipitates. The composition of precipitates obtained from the experiments under different conditions is summarized in Table 5A-4.

Table 5A-4. Compositions of precipitate samples obtained from different experiments

Group	Experiment	Temp. (°C)	Reaction time	Product composition
I. Effect of CO_2 gas flow mode	PCB0.2M-100-0.4 M K_2SO_4 + 0.2 M $CaCl_2$	Batch	1 hr	1.5% gypsum + 42.3% syngenite
	PCB0.2M-100-0.4 M K_2SO_4 + 0.2 M $CaCl_2$	Bubbling flow	1 hr	8.6% gypsum + 91.4% syngenite
II. Effect of initial PCB concentration	PCB1.2M-100-0.4 M K_2SO_4 + 0.4 M $CaCl_2$	Bubbling flow	1 hr	100% calcite
	PCB0.4M-100-0.4 M K_2SO_4 + 0.4 M $CaCl_2$	Bubbling flow	1 hr	3.3% gypsum + 9.9% syngenite + 54.6% vaterite + 32.3% calcite
III. Effect of reaction time at 0.2 M PCB	PCB0.2M-100-0.4 M K_2SO_4 + 0.2 M $CaCl_2$	Bubbling flow	40 min	58.0% gypsum + 10.9% syngenite + 31.2% vaterite
	PCB0.2M-100-0.4 M K_2SO_4 + 0.2 M $CaCl_2$	Bubbling flow	20 min	14.7% gypsum + 28.6% syngenite + 56.7% vaterite
IV. Effect of reaction time at 0.4 M PCB	PCB0.4M-100-0.4 M K_2SO_4 + 0.4 M $CaCl_2$	Bubbling flow	6 hr	5.1% gypsum +28.3% syngenite + 57.3% vaterite + 9.3% calcite

5A.3.3 Using catalysts to promote sulfate reclamation

The aforementioned absorption study identified that the use of an amine promoter, such as 0.5 M piperazine (PZ) or 0.5 M diethanolamine (DEA), effectively promoted the rate of CO_2 absorption into the PCB solutions. Therefore, it is necessary to investigate the impact of these promoters on the preferential $CaSO_4$ precipitation.

In this study, 0.5 M PZ or 0.5 M DEA (the typical dose used in Hot-CAP) was present in the mixture solution of 0.4 M PCB and 0.4 M K_2SO_4. Next, 0.4 M $CaCl_2$ was added as a Ca^{2+}-containing agent for the precipitation reactions. The experiments were performed at room temperature with a CO_2 gas stream continuously bubbling through the liquid under a pressure of approximately 550 psia (37.4 atm), controlled by a back-pressure regulator.

The XRD patterns and the compositions of the precipitates obtained from the experiments with the promoters were compared with those without any promoters. Figure 5A-9 shows XRD patterns of the precipitate samples obtained from 1- or 6-hr reactions in the mixture solution of 0.4 M PCB and 0.4 M K_2SO_4 with the added 0.4 M $CaCl_2$ with or without the addition of either a 0.5 M PZ or 0.5 M DEA promoter.

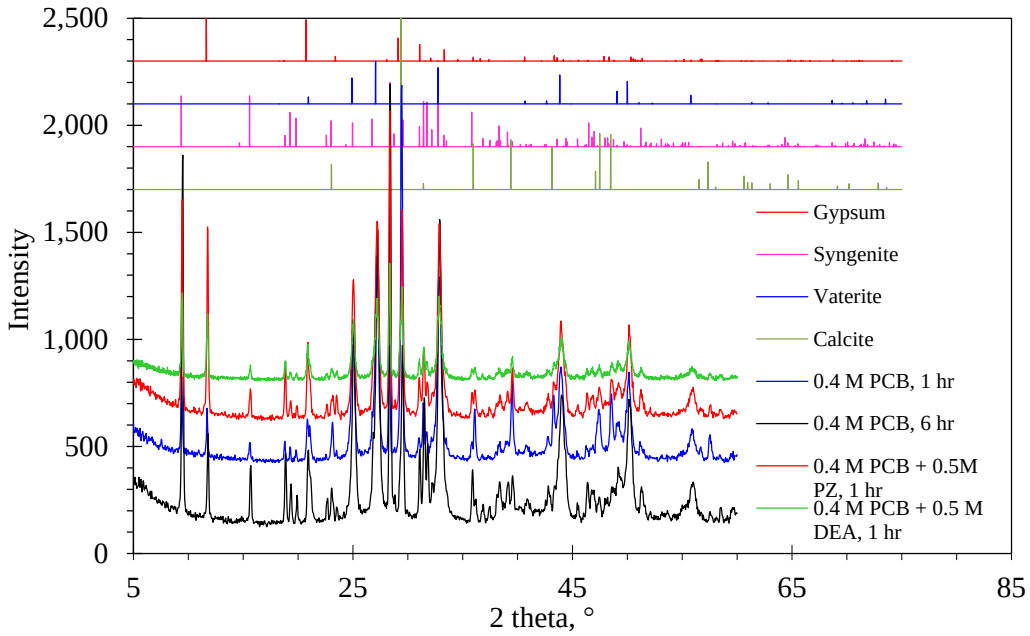

Figure 5A-9. XRD patterns of precipitate particles obtained from the reaction for 1 or 6 hr in 0.4 M PCB + 0.4 M K_2SO_4 + 0.4 M $CaCl_2$ with the addition of 0.5 M PZ or 0.5 M DEA promoter or without any promoters.

On the basis of a semi-quantitative XRD analysis, the compositions of the precipitate particles from these experiments are presented in Table 5A-5. The precipitate particles obtained for the 1-hr reaction in the presence of 0.5 M PZ and 0.5 M DEA contained 19.3% gypsum ($CaSO_4 \cdot 2H_2O$) + 49.1% syngenite [$K_2Ca(SO_4)_2 \cdot H_2O$] and 21.7% gypsum + 8.8% syngenite (the other parts are balanced by the calcite or vaterite phase, and so forth), respectively. In comparison, the precipitates obtained in their counterpart experiment without a promoter contained 3.3% gypsum + 9.9% syngenite for the same reaction time of 1 hr, and contained 5.1% gypsum + 28.3% syngenite for the 6-hr reaction time. Thus, the total $CaSO_4$ yield from the solution in the presence of either 0.5 M PZ or 0.5 M DEA with a 1-hr reaction time was greater than or comparable with that without a promoter, even for the 6-hr reaction time. The competitive precipitation of $CaSO_4$ over $CaCO_3$ was favored by the presence of PZ or DEA, because of the enhanced absorption of CO_2 into the PCB solutions. The presence of PZ enhanced the preferential precipitation slightly more effectively than did the DEA.

Table 5A-5. Compositions of precipitate samples obtained in different experiments

Experiment	Reaction time (hr)	Product composition
With 0.5 M PZ	1	19.3% gypsum + 49.1% syngenite
With 0.5 M DEA	1	21.7% gypsum + 8.8% syngenite
Without any promoter	1	3.3% gypsum + 9.9% syngenite
Without any promoter	6	5.1% gypsum + 28.3% syngenite

This result agrees well with that in our previous absorption study. It was found that the use of 0.5 M PZ more effectively promoted CO_2 absorption into the PCB solution than did the use of 0.5 M DEA, because PZ has a stronger affinity to CO_2 molecules by forming carbamate and dicarbamate species. The result also matches the suggested two-step mechanism. The presence of

a CO_2 absorption promoter also enhances the kinetics of $CaCO_3$ conversion into $Ca(HCO_3)_2$ and thus favored the formation of $CaSO_4$ precipitates.

5A.3.4 Reclamation of sulfates from sodium-containing solutions

As described in previous chapters, a sodium carbonate/bicarbonate (SCB) or SCB/PCB mixture solution can potentially be used as an alternative solvent to PCB in the Hot-CAP. In either case, the desulfurization product, i.e., Na_2SO_4 or K_2SO_4, must be reclaimed from the CO_2-rich solution. Thus, it is desirable to investigate the feasibility of reclaiming the sulfate salt, i.e., sodium or potassium sulfate (K_2SO_4), from the sodium-containing solvents.

For this purpose, we investigated the reclamation of Na_2SO_4 or K_2SO_4 from the SCB or PCB/SCB mixture solution in the two-step process for combined SO_2 removal and CO_2 capture by comparing the compositions of the precipitates obtained from different solutions under comparable operating conditions. The objective of this study was to examine how the sodium-containing solvents would affect the viability of the two-step process for combined SO_2 removal and CO_2 capture.

Two experiments were carried out to investigate the effect of the sodium-containing solvent on the competitive precipitation of $CaSO_4$ over $CaCO_3$. In Experiment I, the precipitation reactions proceeded for 1 hr at room temperature in a mixture solution of 0.2 M $NaHCO_3$ and 0.4 M Na_2SO_4 with the addition of 0.4 M $CaCl_2$. In Experiment II, a mixture solution of 0.1 M $NaHCO_3$ + 0.1 M $KHCO_3$ (instead of a 0.2 M $KHCO_3$ solution) containing 0.2 M K_2SO_4 and 0.2 M Na_2SO_4 was used for the precipitation reaction under the same conditions. During both experiments, a CO_2 gas stream was continuously bubbling in the liquid at a controlled pressure of approximately 550 psia/37.4 atm (semi-continuous testing).

Figure 5A-10 shows XRD patterns of the precipitate samples collected in Experiments I and II. For comparison purposes, XRD patterns of the precipitate sample obtained from the reaction in a 0.2 M $KHCO_3$ and 0.4 M K_2SO_4 mixture solution are also included. The precipitates were obtained from different carbonate solutions under comparable operating conditions.

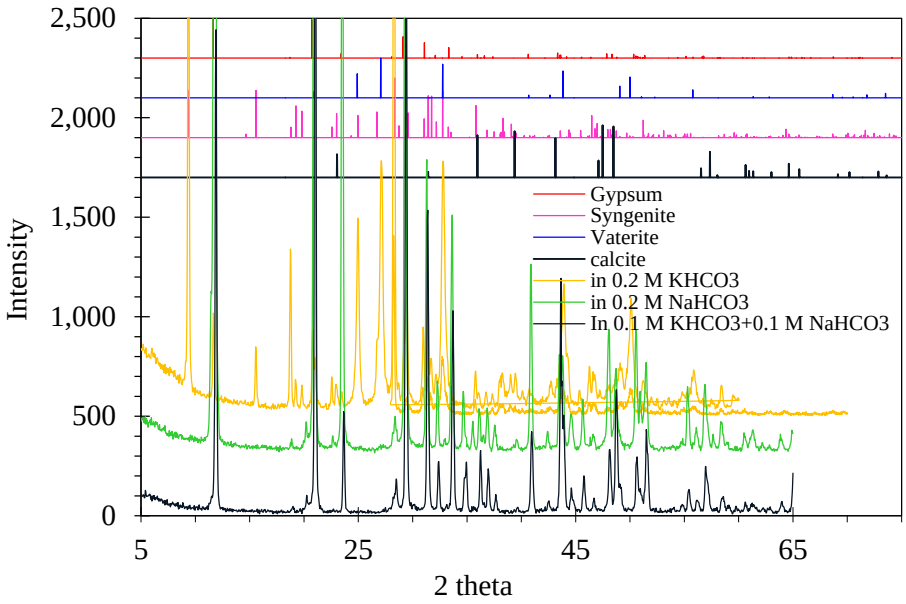

Figure 5A-10. XRD patterns of precipitate particles obtained from the precipitation reactions at room temperature in the 0.2 M $NaHCO_3$ + 0.4 M Na_2SO_4, 0.1 M $KaHCO_3$ + 0.1 M $NaHCO_3$ + 0.2 M Na_2SO_4 + 0.2 M K_2SO_4, and 0.2 M $KHCO_3$ + 0.4 M K_2SO_4 solutions with the addition 0.4 M $CaCl_2$.

The compositions of the collected precipitate samples determined by semi-quantitative XRD analysis are listed in Table 5A-6. The precipitate particles obtained from either the 0.2 M $NaHCO_3$ + 0.4 M Na_2SO_4 solution, or the 0.1 M $KaHCO_3$ + 0.1 M $NaHCO_3$ + 0.2 M Na_2SO_4 + 0.2 M K_2SO_4 solution contained 100% gypsum ($CaSO_4 \cdot 2H_2O$). In contrast, the precipitates obtained from the reaction in 0.2 M $KHCO_3$ + 0.4 M K_2SO_4 solution contained only 8.6 wt% gypsum and 91.4 wt% syngenite. These results indicate that the presence of sodium instead of potassium ions favored the competitive precipitation of $CaSO_4$ over $CaCO_3$ by prohibiting the formation of syngenite.

Table 5A-6. Compositions of precipitate samples obtained from different solvent solutions.

Initial solution	Composition of precipitates
0.2 M $NaHCO_3$ + 0.4 M Na_2SO_4	100 wt% gypsum
0.1 M $KHCO_3$ + 0.1 M $NaHCO_3$ + 0.2 M K_2SO_4 + 0.2 M Na_2SO_4	100 wt% gypsum
0.2 M $KHCO_3$ + 0.4 M K_2SO_4	8.6% gypsum + 91.4% syngenite

5A.4 Summary

A process concept was proposed for combining SO_2 removal with CO_2 capture in the Hot-CAP. The process involves two steps to reclaim the desulfurization product, K_2SO_4, from the PCB solution: the first step is to reduce the CO_3^{2-} concentration using a high-pressure CO_2 gas stream, and the second is to selectively precipitate $CaSO_4$ over $CaCO_3$ using lime. Batch and semi-continuous tests were performed to study the feasibility for K_2SO_4 reclamation.

Results of the batch tests indicated that the total PCB concentration, reaction temperature, and residence time were the critical factors affecting the preferential precipitation of $CaSO_4$ over $CaCO_3$. When the PCB concentration was above 0.2 M (2.7 wt%) or the reaction temperature was greater than 50°C, no $CaSO_4$ was formed but $CaCO_3$ crystallite phases were formed. For the 0.2 M PCB + 0.4 M K_2SO_4 mixture, the precipitates produced from the reactions with the added 0.2 M $CaCl_2$ for 1 hr at room temperature contained 43% syngenite and 2% gypsum; when the K_2SO_4 concentration was increased to 0.8 M, the content of syngenite reached 96.8%. As the reaction time was increased from 1 to 6 hr, the precipitates that formed at room temperature in the 0.2 M PCB + 0.4 M K_2SO_4 mixture with the addition of $CaCl_2$ contained 55.0% syngenite and 38.9% gypsum.

Results of the semi-continuous tests showed that improving the gas–liquid interface and mixing via CO_2 gas bubbling increased the $CaSO_4$ content from 1.5% gypsum + 42.3% syngenite to 8.6% gypsum + 91.4% syngenite in the precipitate particles obtained from the reactions of 0.2 M PCB + 0.4 M K_2SO_4 solution with 0.2 M $CaCl_2$ for 1 hr at room temperature.

On the basis of experimental observations, a two-step mechanism was suggested for the competitive precipitation of $CaSO_4$ over $CaCO_3$. $CaCO_3$ was firstly precipitated by the reaction between CO_3^{2-} and the added Ca^{2+}. The produced $CaCO_3$ precipitates then reacted with the dissolved CO_2 allowed by using high-pressure CO_2 to form $Ca(HCO_3)_2$. $Ca(HCO_3)_2$ has higher solubility and is dissociated into Ca^{2+} and HCO_3^-. Ca^{2+} ions further react with SO_4^{2-} to precipitate out $CaSO_4$. The composition of precipitates was controlled by the kinetics of $CaCO_3$ conversion into $Ca(HCO_3)_2$ and $Ca(HCO_3)_2$ dissociation.

High PCB concentrations resulted in less precipitation of the $CaSO_4$ phases. For example, the precipitates obtained from the reactions of 0.4 M $CaCl_2$ in the 0.4 M PCB + 0.4 M K_2SO_4 solution for 1 to 6 hr contained only 12 to 33% gypsum and syngenite (balanced with $CaCO_3$ crystal phases). When the PCB concentration ($\leq$0.2 M) was sufficiently small with respect to K_2SO_4, $Ca(HCO_3)_2$ dissociation as well as conversion of $CaCO_3$ to $Ca(HCO_3)_2$ were favored, resulting in a higher yield of $CaSO_4$ precipitation. Because the $CaSO_4$ yield was subjected to the kinetics of these two reactions, such measures as increasing the gas–liquid interface or mixing by CO_2 gas bubbling, increasing the reaction time, or using a CO_2 absorption promoter (e.g., PZ) could be favorable. For example, the use of a 0.5 M PZ or 0.5 M DEA promoter enhanced the competitive precipitation of $CaSO_4$ over $CaCO_3$. The total yield of $CaSO_4$ precipitates obtained from the reactions of 0.4 M $CaCl_2$ in the 0.4 M PCB + 0.4 M K_2SO_4 + 0.5 M PZ or 0.5 M DEA solution for 1 hr was greater than or comparable with that in the counterpart experiment without a promoter, even for the 6-hr reaction. This result also matches the previous observation that PZ and DEA were effective promoters in accelerating the rate of CO_2 absorption into PCB solutions.

The precipitate particles obtained from the reactions of 0.4 M $CaCl_2$ with either a 0.2 M $NaHCO_3$ + 0.4 M Na_2SO_4 or a 0.1 M $KaHCO_3$ + 0.1 M $NaHCO_3$ + 0.2 M Na_2SO_4 + 0.2 M K_2SO_4 solution contained almost 100% gypsum phase, whereas those with the 0.2 M $KHCO_3$ + 0.4 M K_2SO_4 solution contained 8.6% gypsum and 91.4% syngenite under comparable operating conditions. This result suggests that the presence of sodium instead of potassium ions favored the competitive precipitation of $CaSO_4$ over $CaCO_3$ by prohibiting the formation of syngenite.

References

Lange N.A. Tables of Solubilities of Inorganic Compounds in Water at Various Temperatures, *Handbook of Chemistry*, 10th ed., McGraw-Hill, New York, 1961.

Lu, Y. *et al*. *Development and Evaluation of a Novel Integrated Vacuum Carbonate Absorption Process*. Final Report, DOE Award No. DE-FC26-08NT00054, Illinois State Geological Survey, University of Illinois at Urbana-Champaign, July 27, 2012.

Mines R.O. *Environmental Engineering: Principles and Practice*, John Wiley & Sons, New York, 2014. http://www.csudh.edu/oliver/chemdata/data-ksp.htm (accessed Oct. 23, 2011).

Part 5B. A Modified Process

5B.1 Introduction

The process concept proposed previously, as shown in Figure 5A-1, was based on the experimental observation that only in a ≤0.2 M (2.7 wt%) PCB solution and at temperatures below 50°C can a high SO_4^{2-}/CO_3^{2-} ratio be achieved using a high-pressure CO_2 gas stream to reduce the CO_3^{2-} concentration and kinetically facilitate the competitive precipitation of $CaSO_4$ over $CaCO_3$. In the Hot-CAP, a 40 wt% PCB solution is a favorable solvent for CO_2 absorption, and the absorption process operates at approximately 70°C. Therefore, to use a portion of the CO_2-rich PCB solution from the Hot-CAP absorber, the process needs to be modified for compatibility between SO_2 removal and CO_2 capture.

A modified process, as shown in Figure 5B-1, was proposed for this purpose. A small portion of CO_2-rich PCB solution from the Hot-CAP absorber was used to absorb SO_2 to form K_2SO_3 in a separate scrubber according to the following overall reactions:

$$2K_2CO_3 + SO_2 + H_2O \rightarrow K_2SO_3 + H_2CO_3 \quad \text{(5B-R1)}$$

$$2KHCO_3 + SO_2 + H_2O \rightarrow K_2SO_3 + 2H_2CO_3 \quad \text{(5B-R2)}$$

K_2SO_3 was then air-oxidized to form K_2SO_4 in a forced-air oxidation unit:

$$K_2SO_3 + ½O_2 \rightarrow K_2SO_4\downarrow \quad \text{(5B-R3)}$$

Because the solubility of K_2SO_4 is much lower than those of K_2SO_3, $KHCO_3$, and K_2CO_3 in the mixture solution, the K_2SO_4 concentration is controlled at a level close to its solubility so that the K_2SO_4 produced by sulfite oxidation can be precipitated from the solution. After filtration of K_2SO_4 solids, the reclaimed solution returns to the main flow of the CO_2-rich PCB solution in the Hot-CAP (entering the crystallization unit). The K_2SO_4 solids obtained can be reclaimed by re-dissolving and then reacting them with lime to precipitate $CaSO_4$:

$$K_2SO_4 + Ca(OH)_2 + 2H_2O \rightarrow CaSO_4{\cdot}2\,H_2O\downarrow + 2KOH \quad \text{(5B-R4)}$$

The regenerated solution containing KOH is mixed with the CO_2-lean solution for CO_2 absorption in the Hot-CAP.

The modified process can integrate SO_2 removal with the CO_2 capture process. In addition, the SO_2 removal process involves a separate SO_2 scrubber, forced-air oxidation reactor, and solid–liquid separation unit (such as a conventional hydrocyclone and thickener), all of which are mature and available in flue gas desulfurization (FGD) applications. Therefore, the experience gained from wet FGD development can potentially be applied to the development of the combined SO_2 removal and CO_2 capture technology.

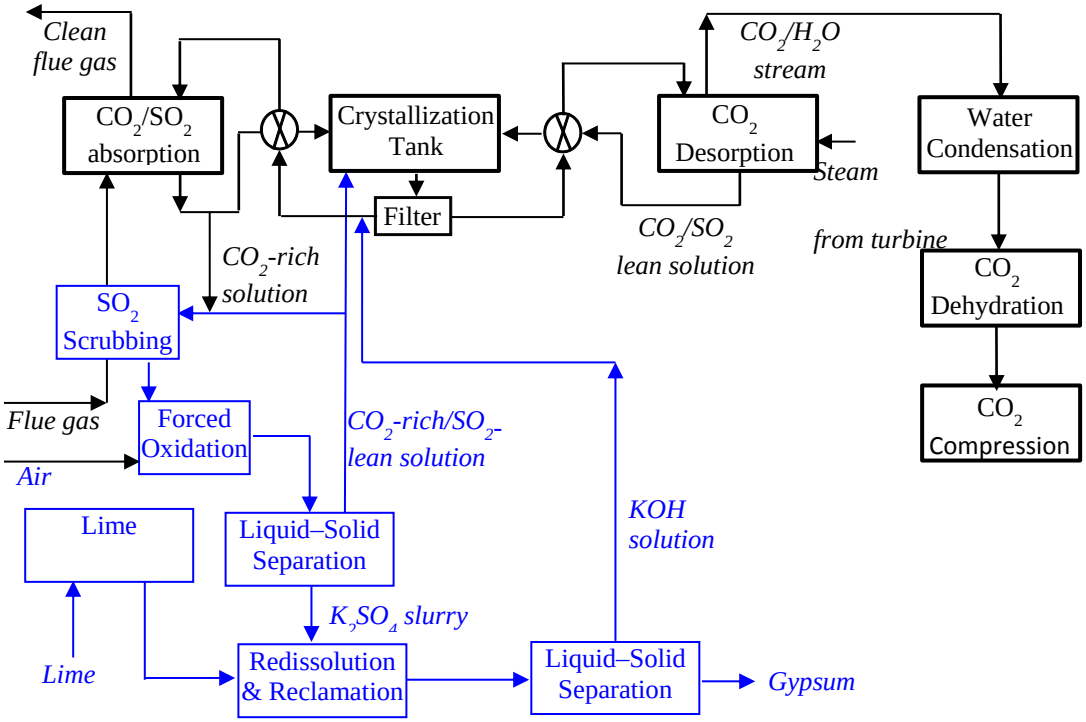

Figure 5B-1 A modified process for combined SO_2 removal and CO_2 capture in the Hot-CAP.

Solubility data for salts such as K_2SO_4 and K_2SO_3 in PCB mixture solutions are required for the process development, because they are either the intermediate or final products from SO_2 removal. Preliminary engineering data, including the equilibrium composition and rate of K_2SO_3 oxidation under typical operational conditions, are also necessary for evaluating the technical feasibility and economic performance of the modified process. Such technical information under typical process conditions (e.g., solution composition and temperature) was experimentally investigated in this study.

5B.2 Measurement of the solubility of K_2SO_4 and K_2SO_3 in a K_2CO_3/$KHCO_3$ solution

Solubility data for K_2SO_4 and K_2SO_3 in the PCB are useful for the design, scale-up, and operation of both SO_2 removal and CO_2 capture in the Hot-CAP. However, the literature data neither encompass the entire range of operating conditions nor cover multiple solutes in mixture solutions. The solubilities of K_2SO_4 and K_2SO_3 in 20 and 40 wt% PCB solutions at 50 to 80°C were measured following the test matrix shown in Table 5B.1.

Table 5B-1 Matrix for measuring the solubilities of K_2SO_4 and K_2SO_3 in the PCB20 and PCB40 solutions

Salt	PCB solution	Temperature (°C)
K_2SO_4 or K_2SO_3	20 wt% PCB with 30% CTB conversion rate (PCB20-30)	50, 60, 70
	20 wt% PCB with 40% CTB conversion rate (PCB20-40)	50, 60, 70
	20 wt% PCB with 50% CTB conversion rate (PCB20-50)	50, 60, 70
	40 wt% PCB with 30% CTB conversion rate (PCB40-30)	70, 80
	40 wt% PCB with 40% CTB conversion rate (PCB40-40)	70, 80

5B.2.1 Experimental methods

5B.2.1.1 Materials

K_2SO_4 (reagent plus®, ≥99.0%), K_2SO_3 (assay grade, 90%), K_2CO_3 (ACS reagent, ≥99.0%), $KHCO_3$ (ACS reagent, ≥99.7%), and iodine solution (volumetric, 0.5 M I_2), all purchased from Sigma-Aldrich, as well as N_2 gas (99.0% purity) supplied by S.J Smith were used as-received.

5B.2.1.2 *Experimental apparatus and operating procedure*

A schematic diagram of the experimental setup for measuring the solubility of a salt or a salt mixture is shown in Figure 5B-2. It consists of a solution cell, a temperature control and measurement unit, a magnetic stirrer, and a N_2 gas supply unit. The cell is a jacketed glass vessel of 340 cm^3 internal volume (6.0 cm inner diameter and 12.0 cm in height). The temperature of the solution was controlled by circulating water through the jacket using a thermostatic water bath (Neslab, Model RTE-110). A thermocouple (Omega, Type K, Model KMQSS-125-G-6) was used to measure the temperature of the solution. A magnetic stirrer equipped with a speed controller (Variomag Mobil 25, Thermo Scientific) and coupled with a 4-cm Teflon stirrer provided mixing for the solution at controllable speeds.

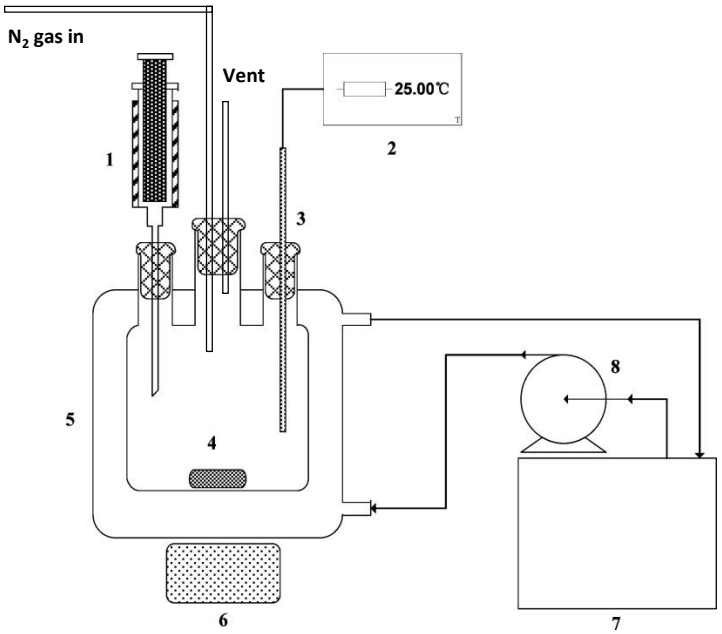

Figure 5B-2. A schematic of the apparatus for measuring salt solubility: (1) thermostated syringe; (2) digital temperature display; (3) thermocouple; (4) magnetic stirring bar; (5) jacketed glass cell; (6) magnetic stirrer; (7) temperature-controlled thermostatic water bath; (8) pump.

In a typical experiment, a small excess of a targeted salt was added to a solution of a certain composition of other salts in the cell. The magnetic stirrer was then turned on at 500 rpm to mix the liquid, and the thermostatic water bath, set at the desired temperature, was turned on to circulate water through the jacket to control the temperature of the solution. A N_2 gas stream at approximately 0.3 standard liters per minute (SLPM) was introduced into the headspace of the

cell for purging, if necessary, to prevent the oxidation of a salt. To avoid the formation of microcrystals and supersaturation, the solution was stirred for approximately 6 hr to ensure sufficient contact between the undissolved solid particles and the liquid phase. A certain amount of liquid sample (3 to 5 mL) was taken with a syringe equipped with a 0.45-μm filter and was transferred to a vial for composition analysis. Before sampling, the syringe and filter were thermostated to 5°C above the temperature of the solution.

5B.2.1.3 *Analysis of the liquid composition*

The concentration of HCO_3^- ions was determined by the titration method.[1] Approximately 4 to 5 g of liquid sample was added to a vessel containing an excess amount of KOH solution (0.1 M) so that the $KHCO_3$ was completely converted into K_2CO_3. An excess amount of $BaCl_2$ solution or solid (more than 5-times the required equivalent molar amount) was then added to the solution. After careful shaking or stirring to allow the precipitation of Ba_2CO_3 to complete, several drops of phenolphthalein were added to the solution. The titration was then performed using a standard hydrochloric acid (0.1 M) until the color changed sharply from fuchsia (red) to colorless. The volume of hydrochloric acid consumed was recorded to calculate the concentration of $KHCO_3$ in the solution. The relative error of the titration method was less than 2% according to an analysis using standard solutions with known $KHCO_3$ concentrations.

The concentration of K_2SO_3 in solution was titrated using a standard potassium iodide-iodate titrant. Free iodine, liberated by the iodide-iodate reagent, reacts with sulfite ions as shown below:

Liberation of iodine: $IO_3^- + 5I^- + 6H^+ \rightarrow 3H_2O + 3I_2$
Reduction of iodine by sulfite: $I_2 + SO_3^{2-} + H_2O \rightarrow SO_4^{2-} + 2I^- + 2H^+$

The titration endpoint was signaled by the blue color indicated by a starch agent from the reaction of an extra drop of iodine solution. In a typical titration measurement, approximately 10 g of liquid sample was added with a couple of drops of starch indicator. The sample solution was then titrated by the iodine solution until the blue color appeared sharply with an extra drop of iodine solution. The volume of the consumed potassium iodide-iodate was recorded to calculate the concentration of K_2SO_3 in the solution.

5B.2.2 Results and discussion

5B.2.2.1 Validation of the measurement method

The measurement method was validated by comparing the solubility of $KHCO_3$ in water at 25 to 60°C, as measured in this study, with the values reported in the literature. As shown in Figure 5B-3, the measured solubility values closely matched those reported in the literature.[2] The relative errors were less than 3%.

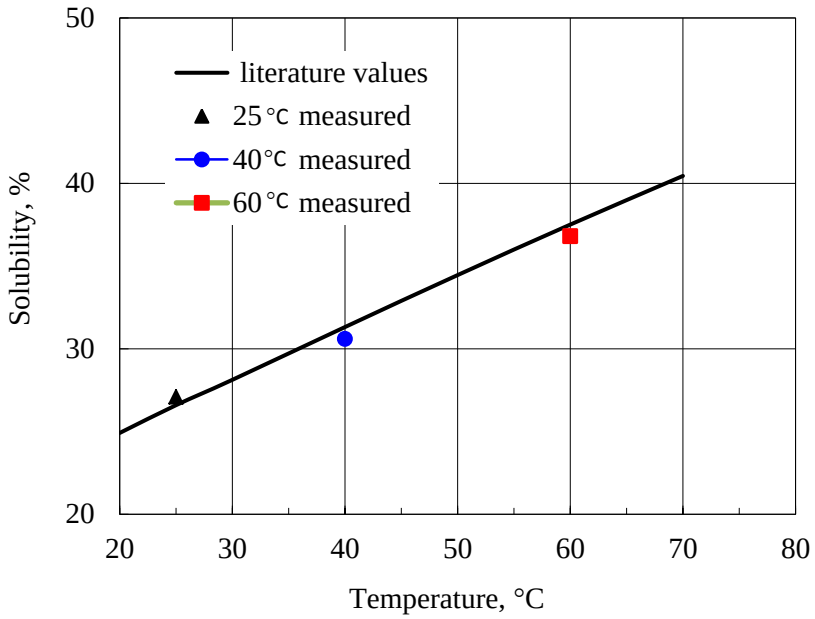

Figure 5B-3. Measured solubility of $KHCO_3$ compared with those in the literature at three different temperatures.

5B.2.2.2 Solubilities of K_2SO_4 and K_2SO_3 in $K_2CO_3/KHCO_3$ solutions

The measured solubility data for K_2SO_4 and K_2SO_3 in 20 and 40 wt% PCB solutions with different CTB conversion rates at 50 to 80°C are shown in Figure 5B-4. The total concentration of PCB solution substantially affected the solubility of K_2SO_4, whereas the CTB conversion level in the PCB solution did not. For example, the solubility of K_2SO_4 decreased from about 5.3 g/100 g of 20 wt% PCB solution to 0.8 g/100 g of 40 wt% PCB solution at 70°C. For the PCB solutions of the same concentration, the solubility of K_2SO_4 did not vary substantially with the CTB conversion in the PCB solution. As expected, the solubility of K_2SO_4 increased with increasing temperature in both the 20 and 40 wt% PCB solutions.

The solubility of K_2SO_3 varied appreciably with both PCB concentration and the CTB conversion in solution. For example, the solubility of K_2SO_3 decreased from about 13.6 g/100 g of PCB20-30 solution to 3.2 g/100 g of PCB40-30 solution at 70°C. The solubility of K_2SO_3 in 20 wt% PCB solutions at 70°C decreased from about 13.6 g to 12.5 and 11.8 g when the CTB conversion was increased from 30% to 40% and 50%. The solubility of K_2SO_3 did not substantially increase with increasing temperature, as indicated by the slight increase from 13.4 to 13.6 g in 100 g of PCB20-30 solution when the temperature was increased from 50 to 70°C.

The above results confirm that the solubility of K_2SO_4 was much less than that of K_2SO_3 in PCB mixture solution under similar conditions. For example, in the PCB 40-30 solution at 70°C, K_2SO_4 was >4 times more soluble than K_2SO_3. Meanwhile, the solubility of $KHCO_3$ in the 40 wt% PCB solution at 70°C amounted to 26 g/100 g of solution. Therefore, the solubility of K_2SO_4 was the lowest among the components in the mixture solution of potassium salts, and it was possible to precipitate out K_2SO_4 from such a solution.

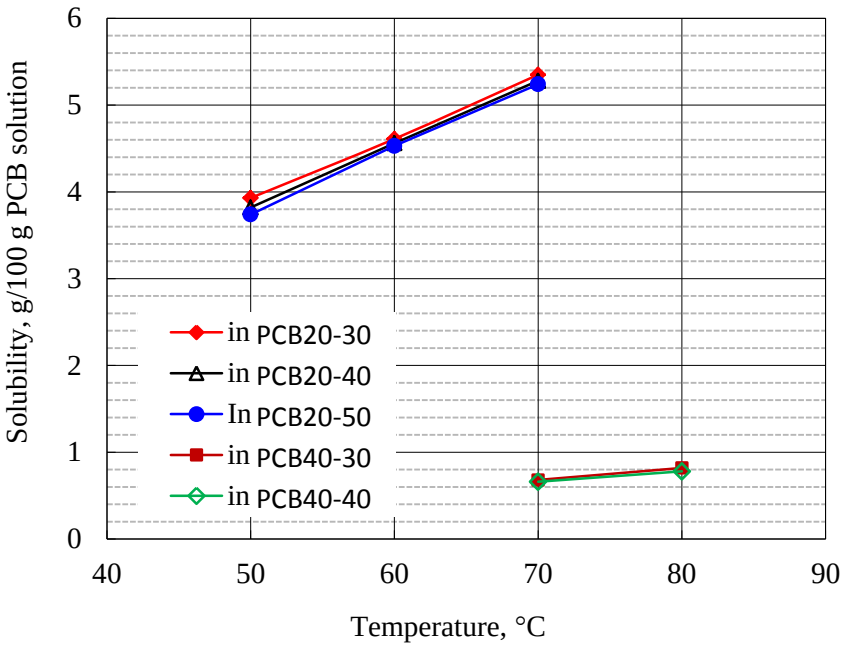

(a) Solubility of K_2SO_4

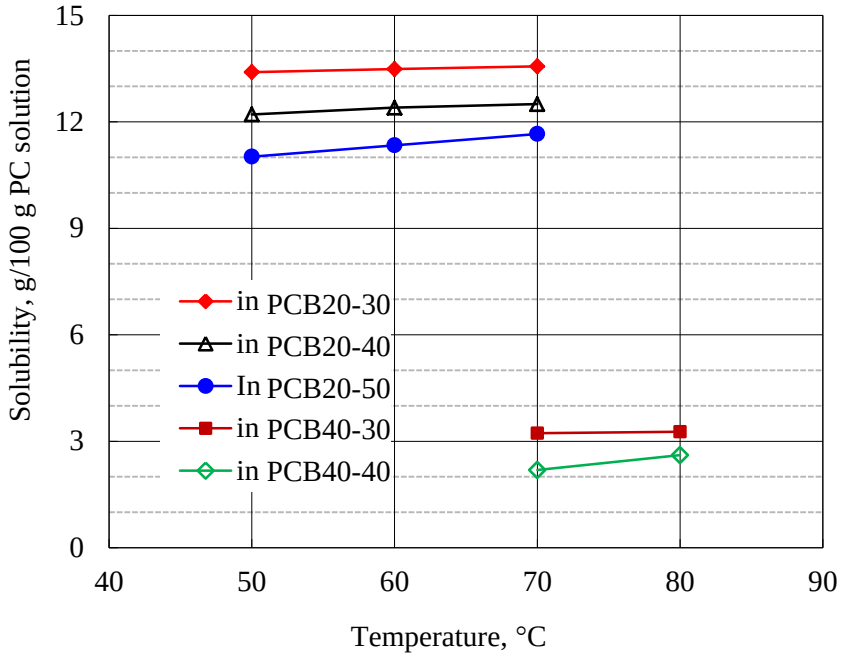

(b) Solubility of K_2SO_3

Figure 5B-4. The measured solubility of K_2SO_4 and K_2SO_3 in different PCB solutions at various temperatures.

5B.3 Oxidation of K_2SO_3 into K_2SO_4

The oxidation of K_2SO_3 into K_2SO_4 in a forced-air unit is an important step in the modified process. The equilibrium composition and the rate of sulfide oxidation under typical operating conditions were investigated to study the formation and precipitation of sulfate in this task.

5B.3.1 Experimental methods

A STR experimental system was used to measure the equilibrium composition and the rate of K_2SO_3 oxidation under the specified conditions. The experimental apparatus is the same as that used for the CO_2 absorption kinetic study, as described in Chapter 2.

The equilibrium composition of the oxidation reaction was investigated by performing the oxidation of 10 wt% K_2SO_3 in either the PCB20-40 or PCB40-40 solution at 70°C. In a typical measurement, 500 g of a mixture solution of PCB and K_2SO_3 was charged into the STR. Pure O_2 gas was continuously bubbling through the solution via a sparger at a flow rate of 250 standard cubic centimeters per minute (sccm). When the reaction was completed after a sufficiently long time, a suspension sample was collected and filtered in a chamber at approximately 75°C. After several rinses with deionized water and drying at 80°C overnight, the solid particles were collected for XRD analysis.

The rates of K_2SO_3 oxidation were measured for different K_2SO_3 concentrations [1 wt% (0.07 M) and 10 wt% (0.69 M)], PCB solutions (PCB20-40 and PCB40-40), temperatures (50 and 70°C), and O_2 pressures (~3, 6, and 13 psia/20.7, 41.4, and 89.6 kPa). A matrix for the experiments is shown in Table 5B.2.

Table 5B-2. Matrix for measuring the equilibrium composition and rate of sulfite oxidation

Experiment	Liquid condition	Gas condition	Temperature (°C)
Equilibrium composition of sulfide oxidation reaction	PCB 20-40 + 10 wt% K_2SO_3	250 sccm O_2 bubbling at 1 atm	70
	PCB 40-40 + 10 wt% K_2SO_3	250 sccm O_2 bubbling at 1 atm	70
Rates of oxidation reaction	PCB 20-40 + 10 wt% K_2SO_3	O_2 at ~3, 6, and 13 psia	50, 70
	PCB 20-40 + 1 wt% K_2SO_3	O_2 at ~3, 6, and 13 psi	50, 70
	PCB 40-40 + 1 wt% K_2SO_3	O_2 at ~3, 6, and 13 psi	70

The rate of sulfite oxidation was determined by measuring the rate of oxygen consumption, i.e., the absorption of O_2 into the liquid. The experiments were conducted in batch mode with respect to both the gas and liquid phases. In a typical experiment, 1,000 g of the desired sulfite–PCB solution was charged into the STR. The system was initially evacuated, and then a pure O_2 gas stream was introduced to the reactor to a predetermined pressure. Pure O_2 gas rather than air was used to minimize the effect of gas phase mass transfer resistance on O_2 absorption. A constant gas–liquid interfacial area was maintained by controlling the stirring speed to keep a flat

interfacial surface while providing efficient mixing in the liquid phase. The profile of the O_2 gas pressure change was measured to calculate the rate of sulfite oxidation.

5B.3.2 Results and discussion

5B.3.2.1 *Equilibrium composition of the sulfide oxidation reaction*

Figure 5B-5 shows XRD patterns of the precipitate samples obtained from a complete oxidation of 10 wt% K_2SO_3 in the PCB20-40 (for approximately 9 to 10 hr) and PCB40-40 solution (for approximately 14 hr) at 70°C. A semi-quantitative XRD analysis demonstrated that the precipitate product obtained from the PCB20-40 solution contained 100 wt% K_2SO_4, suggesting that the product of the complete sulfide oxidation reaction was desirable. However, the precipitate solids obtained from the PCB40-40 solution contained about 70 wt% K_2SO_4 and 30 wt% $KHCO_3$, indicating that co-precipitation of K_2SO_4 and $KHCO_3$ might occur. This result means that some solvent could be lost if a 40 wt% PCB with high CO_2 loading were used for the combined SO_2 and CO_2 removal. However, a PCB solution with a less rich CO_2 loading could be considered for SO_2 removal when necessary to minimize any loss of PCB.

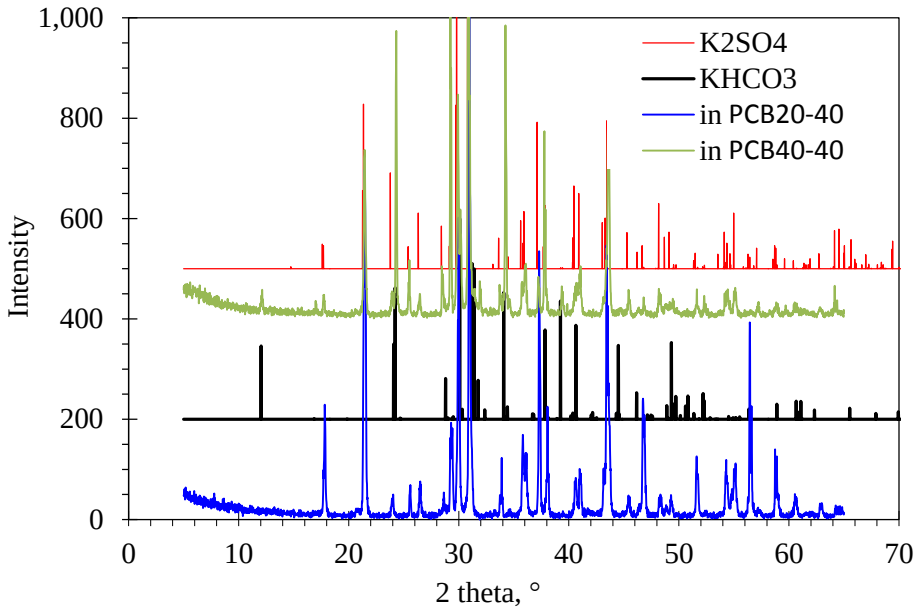

Figure 5B-5. XRD patterns of precipitate particles from the oxidation of 5 wt% K_2SO_3 in PCB20-40 and PCB40-40 solutions at 70°C.

5B.3.2.2 Rate of K_2SO_3 oxidation

The rate of sulfide oxidation was determined by measuring the rate of oxygen consumed at a specified liquid phase composition. The change in liquid composition could be negligible during the oxidation process because only a small volume of O_2 gas was consumed, and the amount of K_2SO_3 in the solution was relatively much greater. For the rate of oxidation in the STR, the following equation could be derived:

$$r = -\frac{V_G}{A \times R_{gas} T} \frac{dP_{O_2}}{dt} \qquad \text{(5B-1)}$$

where r is the rate of sulfite oxidation per unit of interfacial area (mol/m^2·s), V_G is the gas volume in the STR, A is the gas–liquid interfacial area, R_{gas} is the universal gas constant, T is the temperature, P_{O2} is the partial pressure of oxygen gas, and t is the time.

The effect of several process variables on the oxidation rate, including temperature, O_2 partial pressure, K_2SO_3 concentration, and PCB concentration in the mixture solution, were investigated. Figure 5B-6 shows the oxidation rates of 1 and 10 wt% K_2SO_3 in PCB20-40 at approximately 3 psia (20.7 kPa) of O_2 pressure (equivalent to the partial pressure of O_2 in air) at 50 and 70°C, respectively. The rates of oxidation of 1 and 10 wt% sulfite in PCB20-40 were comparable, indicating that the concentration of sulfite within the investigated range from 1 to 10 wt% was not critical to the sulfide oxidation reaction. As expected, increasing the temperature enhanced the kinetics of the oxidation reaction. When the temperature was increased from 50 to 70°C, the oxidation rate was increased from approximately 4.0×10^{-6} to 8.0×10^{-6} mol/m^{2}s for the solution containing either 1 or 10 wt% K_2SO_3.

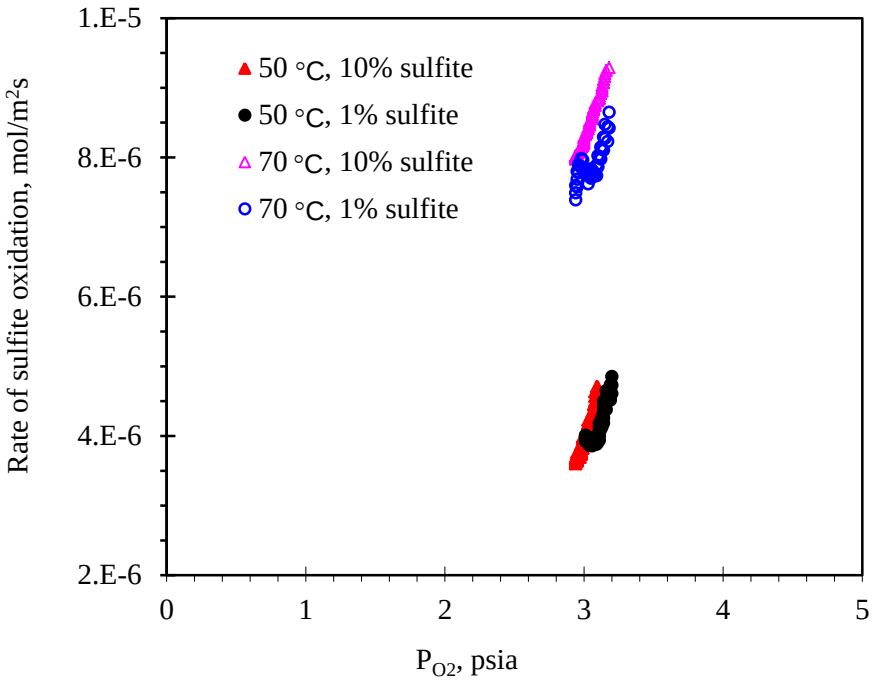

Figure 5B-6. Oxidation rates of 1 and 10 wt% K_2SO_3 in PCB20-40 under approximately 3 psia (20.7 kPa) of O_2 pressure at 50 and 70°C.

Figure 5B-7 displays the oxidation rates of 1 and 10 wt% K_2SO_3 in PCB20-40 under different O_2 pressures at 70°C. The oxidation rate was considerably dependent on O_2 pressure; when the O_2 pressure was increased from approximately 3 to 4 psia (20.7 to 27.6 kPa) and to 14 psia (96.5 kPa), the oxidation rate increased from approximately 1.0×10^{-5} to 2.0×10^{-5} and to 4.0×10^{-5} mol/m^2·s. This tendency was the same for either 1 or 10 wt% K_2SO_3 in the PCB20-40

solution. The results shown in Figure 5B-7 suggest that the sulfite oxidation should be almost zero-order with respect to the sulfite concentration and should be first-order to the O_2 pressure.

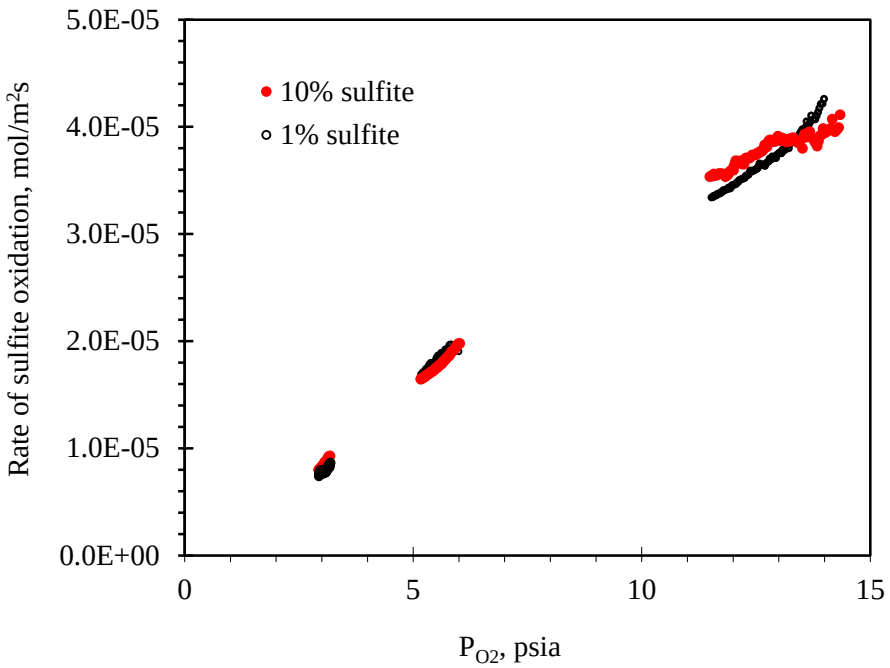

Figure 5B-7. Oxidation rates of 1 and 10 wt% K_2SO_3 in PCB20-40 at 70°C under different O_2 pressures.

The kinetics of the sulfite oxidation reaction has been extensively studied over the past several decades. However, the kinetic data reported in the literature are not consistent because the kinetics is complex and depends substantially on the specific conditions.[3] It has generally been accepted that the orders of the reaction vary with the levels of sulfite concentration and O_2 pressure.[4,5,6] Linek and Mayrhoferová[4] have reported that the orders of the reaction should be zero with sulfite and first-to-second with O_2 pressure over the range of sulfite concentration from 0.25 to 0.8 M, and the range in the partial pressure of O_2 should be from 2.8 to 14.7 psia (19.3 to 101.3 kPa) at pH 7.8 to 9.2 and at 15 to 35°C. Our results closely matched the values reported in the literature under comparable conditions,[4] although the orders of the reaction were not determined accurately.

Figure 5B-8 shows the oxidation rates of 1 wt% sulfite in the PCB20-40 and PCB40-40 solutions at 70°C under different O_2 pressures. The oxidation rates in PCB40-40 were 3-to-5 times lower than those in PCB20-40 when the other conditions were kept almost the same. This might be caused by the reduced concentration of dissolved oxygen in the more concentrated PCB solution (PCB40-40). A high PCB concentration "salts out" the dissolved oxygen, resulting in a greatly reduced concentration of dissolved oxygen, which is required for the oxidation reaction. In addition, the increased viscosity of the PCB40-40 solution might slow down mass transfer in the liquid phase.

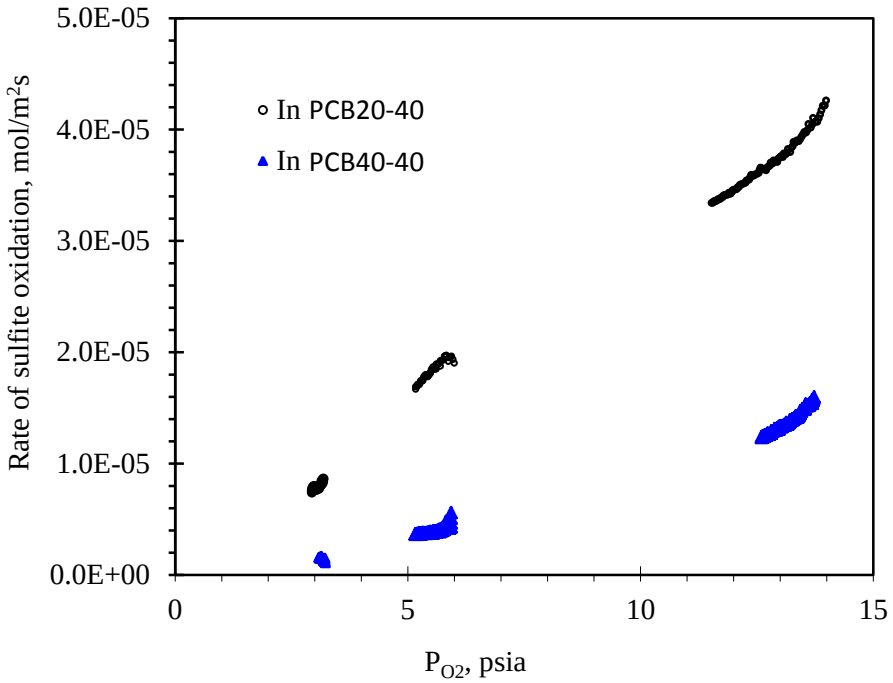

Figure 5B-8. Comparison of oxidation rates of 1 wt% K_2SO_3 in PCB20-40 and PCB40-40 solutions at 70°C under different O_2 pressures.

5B.3 Summary

A modified process was proposed to improve the compatibility of SO_2 removal with CO_2 capture in the Hot-CAP. The process consists of SO_2 scrubbing using the CO_2-rich PCB solution from the Hot-CAP absorber, the oxidation of K_2SO_3 into K_2SO_4 in a forced-air unit, and the precipitation and separation of K_2SO_4 from the solution. Preliminary engineering data, including the equilibrium composition and the rate of the K_2SO_3 oxidation reaction, were measured in an STR under typical operational conditions. These data provide guidance for the evaluation and design of the modified process.

Knowledge of the solubility of K_2SO_4 and K_2SO_3 in PCB solutions is necessary for process design and development. The solubility values of K_2SO_4 and K_2SO_3 in 20 and 40 wt% PCB solutions with different CTB conversions were measured at 50 to 80°C. Results showed that the total PCB concentration substantially affected the solubility of both K_2SO_4 and K_2SO_3. The solubility of K_2SO_4 increased with an increase in temperature more substantially than did that of K_2SO_3, whereas the solubility of K_2SO_3 varied with the CTB conversion of the PCB solution more appreciably than did that of K_2SO_4.

Precipitate solids containing 100% K_2SO_4 were obtained from the oxidation of 10 wt% K_2SO_3 in PCB20-40 at 70°C, which was desirable for the modified process. Precipitate solids obtained from PCB40-40 contained approximately 70 wt% K_2SO_4 and 30 wt% $KHCO_3$, indicating that solvent loss might occur if the CO_2 loading in the 40 wt% PCB for SO_2 removal were too high.

The rates of sulfite oxidation ranged from the order-of-magnitude of 10^{-6} to 10^{-5} mol/m^2·s under the investigated conditions: 1 to 10 wt% sulfite concentrations, at 50 to 70°C, and under O_2 pressures of 3 to 13 psia (20.7 to 89.6 kPa). The rate depended considerably on the temperature and oxygen pressure, but did not vary appreciably with sulfite concentration. The oxidation of sulfite was almost zero and was first-order with respect to the sulfite concentration and oxygen pressure, respectively, which closely matched those reported in the literature under comparable conditions. The rates of sulfite oxidation were 3-to-5 times lower in PCB40-40 than in PCB20-40, possibly owing to a lower concentration of dissolved oxygen and a less efficient mass transfer in a more concentrated PCB solution.

References

1. Shen K.P., Li M.H. Solubility of carbon dioxide in aqueous mixtures of monoethanolamine with methyldiethanolamine, *Journal of Chemical & Engineering Data* 1992, 37: 96–100.
2. Lide D.R. Section 5: Thermochemistry, electrochemistry, and kinetics—Aqueous solubility of inorganic compounds at various temperatures. In: Lide D.R. (Editor), *CRC Handbook of Chemistry and Physics*, 93rd edition, CRC Boca Raton, FL, 2013.
3. Sawicki J.E., Barron C.H. On the kinetics of sulfite oxidation in heterogeneous systems, *The Chemical Engineering Journal* 1973, 5: 153–159.
4. Linek V., Mayrhoferová J. The kinetics of oxidation of aqueous sodium sulphite solution, *Chemical Engineering Science* 1970, 25: 787–800.
5. Linek V., Mayrhoferová J. Chemical engineering use of catalyzed sulfite oxidation kinetics for the determination of mass transfer characteristics of gas–liquid contactors, *Chemical Engineering Science* 1981, 11: 1747–1768.
6. Sivaji K., Murty G.S.R.N. Kinetics of sulfite oxidation reaction, *Industrial & Engineering Chemistry Fundamentals* 1982, 21: 344–352.

Chapter 6. Techno-Economic Analysis

6.1 Introduction

Under the DOE's Capture Program, a technology and economic feasibility study is required as a deliverable in the Statement of Project Objectives (SOPO). This study analyzes a fully-integrated pulverized coal (PC) power plant equipped with the Hot-CAP technology for post-combustion CO_2 capture (PCC) and is carried out, to the maximum extent possible, in accordance with the methodology and data provided in Attachment 3—Basis for Technology Feasibility Study of DOE Funding Opportunity Number: DE-FOA-0000403.[1]

The DOE/NETL report titled *Cost and Performance Baseline for Fossil Energy Plants, Volume 1: Bituminous Coal and Natural Gas to Electricity* (Revision 2, November 2010), NETL Report No. DOE/NETL-2010/1397,[2] was used as the main reference source to be followed, as per the guidelines in Attachment 3 of DE-FOA-0000403. The design and economic evaluation basis from Case 10 of the DOE/NETL report was adopted in this study. This case corresponds to a nominal 550-MWe (net) subcritical PC power plant that utilizes a benchmark 30 wt% MEA-based absorption system for PCC.

For this techno-economic analysis (TEA), the Hot-CAP process replaces the MEA-based CO_2 absorption system in the original case. The objective of this study was to assess the performance of Hot-CAP when fully-integrated into a subcritical PC plant similar to Case 10 of the DOE/NETL report, such that it corresponds to a nominal 550-MWe subcritical PC plant with 90% CO_2 capture. This plant has the same boiler firing rate and generated steam pressure as the Case 10 PC plant in the DOE/NETL report. However, because of the difference in performance between the Hot-CAP and benchmark MEA-based CO_2 absorption technology, the net power output fluctuates.

6.2 Design Basis

6.2.1 Power plant design criteria

6.2.1.1 General

This study is based on the design of a 550-MWe (net) subcritical PC power plant with carbon capture, consistent with Case 10 in the DOE/NETL-2010/1397 report. The original gross output of the power plant is about 673 MWe. The steam generator for the subcritical PC plant is a drum-type, wall-fired, balanced-draft, natural-circulation, totally enclosed dry-bottomed furnace, with a superheater, reheater, economizer, and air heater. The steam turbine generator (STG) operates at throttle conditions of 16.5 MPa/566°C/566°C (2,400 psig/1,050°F/1,050°F).

The plant is designed for NO_x reduction by using a combination of low-NO_x burners and overfire air, as well as through the installation of a selective catalytic reduction (SCR) system. Particulate control is designed with a fabric filter or baghouse, which consists of two separate single-stage, in-line, multi-compartment units. The flue gas desulfurization (FGD) system is a wet limestone forced-oxidation, positive-pressure-absorber nonreheat unit, with wet stack and with gypsum

production for SO_2 removal. The combination of pollution control technologies used in the PC plant—SCR, fabric filters, and FGD—resulted in significant co-benefit capture of mercury. The mercury co-benefit capture is assumed to be 90% for this combination, sufficient to meet current mercury emissions limits; hence, no activated carbon injection is needed in this case.

The power plant is considered to operate as a base-loaded unit, but with consideration for daily or weekly cycling. The annual capacity factor is 85%, or 7,450 hr/year at full capacity.

6.2.1.2 Site-related conditions

The subcritical PC plant in this study is assumed to be located at a generic plant site in the midwestern United States, with site-related conditions as shown below:

- Location U.S. Midwest
- Elevation, ft above sea level 0
- Topography Level
- Size, acres 300
- Transportation Rail
- Ash/slag disposal Off-site
- Water Municipal (50%)/groundwater (50%)
- Access Landlocked, having access by train and highway
- CO_2 disposition Compressed to 152 bar (150 atm) at battery limit

6.2.1.3 Meteorological data

Maximum design ambient conditions for material balances, thermal efficiencies, system design, and equipment sizing are as follows:

- Atmospheric pressure, kPa 101
- Dry bulb temperature, °C 15
- Wet bulb temperature, °C 10.8
- Ambient relative humidity, % 60

6.2.1.4 Technical assumptions and data

Other technical data and assumptions include the following:

- Design coal feed to the power plant is Illinois No. 6. The coal properties are listed in Table 6-1 according to NETL's Coal Quality Guidelines.

Table 6-1. Illinois No. 6 coal properties

Rank	Bituminous
Seam	Illinois No. 6 (Herrin)
Source	Old Ben Mine
Ultimate analysis (as received), wt%	
Carbon	63.75
Hydrogen	4.5
Nitrogen	1.25
Chlorine	0.29
Sulfur	2.51
Oxygen	6.88
Ash	9.7
Moisture	11.12
Total	100
Proximate analysis (as received), wt%	
Volatile matter	34.99
Fixed carbon	44.19
Ash	9.7
Moisture	11.12
Total	100
HHV, kJ/kg	27,135

- Selected flows and operating conditions for the turbine are listed below:
  - Turbine gross power output, MW 673
  - Superheat (SH) high-pressure (HP) steam inlet flow, 1,000 kg/hr 2,364
  - HP turbine inlet pressure, MPa 16.65
  - HP turbine inlet temperature, °C 566
  - HP turbine outlet pressure, MPa 4.28
  - Intermediate-pressure (IP) turbine inlet pressure, MPa 3.90
  - IP turbine inlet temperature, °C 566
  - IP turbine outlet pressure, MPa 0.51
  - Low-pressure (LP) turbine inlet pressure, MPa 0.51
  - Surface condenser pressure, mm Hg 50.8

- To generate the 2,364,000 kg/hr of SH HP steam to the STG, the boiler will burn 278,956 kg/hr of as-received Illinois No. 6 coal. The boiler firing rate and the SH HP steam generation rate will be held constant for the PCC cases.

- Auxiliary loads for the overall plant can be separated into three categories: PCC-independent PC plant auxiliary loads, PCC-dependent plant auxiliary loads, and PCC loads. PCC-independent plant auxiliary loads total 31,170 kWe. The breakdown is listed in Table 6-2.

PCC-dependent PC plant auxiliary loads include cooling water circulation pump loads, cooling tower fan loads, and transformer loss. PC plant cooling water and cooling tower loads are proportional to the STG surface condenser duty, which varies with the PCC steam extraction requirement. Transformer loss is proportional to the STG gross power output, which also varies with the PCC steam extraction requirement.

PCC loads will vary depending on the PCC design and will include power consumed in the CO_2 capture and compression processes, as well as any new cooling water and cooling tower consumptions attributable to the PCC cooling loads.

Table 6-2. PCC-independent PC plant auxiliary load breakdowns

Auxiliary load breakdown	kWe
Coal handling and conveying	540
Pulverizers	4,180
Sorbent handling and reagent preparation	1,370
Ash handling	800
Primary air fans	1,960
Forced-draft fans	2,500
Induced-draft fans	12,080
SCR	70
Baghouse	100
Wet FGD	4,470
Miscellaneous balance of power plant	2,000
Steam turbine auxiliaries	400
Condensate pumps	700
Total	31,170

- It is assumed that the subcritical PC plant utilizes a mechanical-draft evaporative cooling tower, and all process-blowdown streams are treated and recycled to the cooling tower. The design ambient wet bulb temperature of 10.8°C is used to achieve a cooling water temperature of 15.6°C, using an approach of 4.7°C. The PC cooling water range is assumed to be 11.1°C. The cooling tower makeup rate was determined using the following conditions:
    - Evaporative losses of 0.8% of the circulating water flow rate per 5.6°C of range;
    - Drift losses of 0.001% of the circulating water flow rate;
    - Blowdown losses are calculated as follows:
      Blowdown losses = evaporative losses/(cycles of concentration – 1), where cycles of concentration are a measure of water quality, and a midrange value of 4 is chosen for this study.

- The raw water makeup is assumed to be provided at 50% by a publicly-owned treatment facility and 50% from groundwater.

6.2.1.5 Environmental or emissions requirements

Design emissions requirements and limits on the subcritical power plant with PCC in this study are listed in Table 6-3.

Table 6-3. Air emission targets

Controlled pollutant	kg/MWh
SO_2	0.008
NO_x	0.339
Particulate matter (filterable)	0.063
Hg	5.53E-6

The emission components NO_2 and SO_2 can potentially be further removed from the flue gas through nonreversible reactions with the Hot-CAP solvent. NO and Hg are assumed to pass through the PCC recovery unit and be released to the atmosphere with the treated flue gas. Particulate matter is assumed to be removed from the flue gas through water and absorption solvent scrubbing.

6.2.2 PCC design criteria

6.2.2.1 General

The PCC plant is designed as an integral part of the subcritical PC power plant to capture up to 90% of the CO_2 in the flue gas. It is assumed that all the fuel carbon is converted to CO_2 in the flue gas. CO_2 is also generated from limestone in the FGD system, and 90% of the total CO_2 exiting the FGD absorber is subsequently captured in the PCC.

The projected largest single train size of equipment will be used to maximize the economy-of-scale. Vessels exceeding transportation size limits (as specified in the Project Transportation Size Limitation section of this document) will be field-fabricated. The equipment is designed for a 30-year plant life.

Rotating equipment critical to continuous plant operation is spared. When sparing is not feasible, an alternate operation will be identified to maintain continuous power plant operation.

6.2.2.2 Flue gas feed specification

The PC plant boiler will be burning 278,956 kg/hr of as-received Illinois No. 6 coal to generate 2,364,000 kg/hr of SH HP steam to the STG based on the Case 10 subcritical PC plant in the DOE/NETL-2010/1397 report. Flue gas prior to the vent stack after it exits the wet FGD is the design feed for the PCC plant. The corresponding flue gas feed composition and flow rate are listed in Table 6-4.

Table 6-4. Flue gas composition and operating conditions for the CO_2 capture process

Parameter	Unit	Value
Flue gas inlet temperature	°C	58
Flue gas feed pressure	MPa	0.10
Flue gas flow rate	kg/hr	3,213,261
Flue gas composition		
N_2	vol%	67.94
O_2	vol%	2.38
CO_2	vol%	13.50
Ar	vol%	0.81
H_2O	vol%	15.37
Total		100

6.2.2.3 Design CO_2 product specifications

Recovered CO_2 is delivered at the battery limit with the following specifications:

- Inlet pressure, MPa 15.3
- Inlet temperature, °C 26
- CO_2 concentration (dehydrated), % >99.99
- N_2 + Ar concentration, ppmv <1,000 (revised for PCC processes)
- O_2 concentration, ppmv <100 (revised for PCC processes)
- H_2O, ppmv <50 (revised for molecular sieve drying)

6.2.2.4 Utility commodity specifications

- Intermediate low-pressure (ILP) steam
  ILP steam for PCC stripper reboiling can be extracted from the power plant to meet the following PCC boundary limit conditions:
  Minimum pressure — As required
  Temperature, °C — Saturation temperature + 10
  The ILP steam is assumed to be de-superheated to 10°C above the saturation temperature to allow positive control of the de-superheater condensate injection. The degree of ILP steam superheating can be varied to meet a minimum de-superheater design requirement.

- Return condensate
  The reboiler steam condensate will be pumped back to the power plant hot at:
  Minimum pressure, MPa — 1.2
  Temperature, °C — 75

- Cooling tower water

Cooling water from the plant cooling towers is available at the following conditions:
Maximum supply temperature, °C — 16
Maximum return temperature, °C — 38
Maximum supply pressure, MPa — 0.48

Maximum PCC pressure drop, MPa 0.21

6.2.2.5 Process water streams

The PCC plant is designed to minimize or eliminate the discharge of hydrocarbon solvent-containing wastewaters.

6.3 Simulations and Design of the Hot-CAP

6.3.1 Overview and description of the Hot-CAP

Figure 6-1 is a schematic diagram of the Hot-CAP. In this process, the flue gas from the baghouse or FGD of the power plant is introduced directly into the absorption column operating at 60 to 70°C and atmospheric pressure, where CO_2 and other acid gases are absorbed into a potassium carbonate (K_2CO_3) solution. The CO_2-rich carbonate solution exiting the absorption column is cooled through a cross-flow heat exchanger by the CO_2-lean carbonate solution returning from the crystallization tank. After passing the cross-flow heat exchanger, the CO_2-rich carbonate solution enters the crystallization tank, where potassium bicarbonate ($KHCO_3$) salt crystals are formed due to the low solubility of bicarbonate at low temperatures (30 to 40°C). The crystals are separated, and the resulting slurry is heated by the warmer-regenerated lean carbonate solution from the stripper through another cross-flow heat exchanger before entering a high-pressure stripper. The stripper operates at a high pressure (up to 10 atm) and high temperature (140 to 200°C). The CO_2 stream released in the stripper contains a relatively small amount of water vapor. The CO_2-rich gas stream exiting the stripper is further cooled, dehydrated, and compressed to a sequestration-ready pressure. The CO_2-lean solution exiting the bottom of the stripper enters the crystallization tank after exchanging heat with the feed slurry.

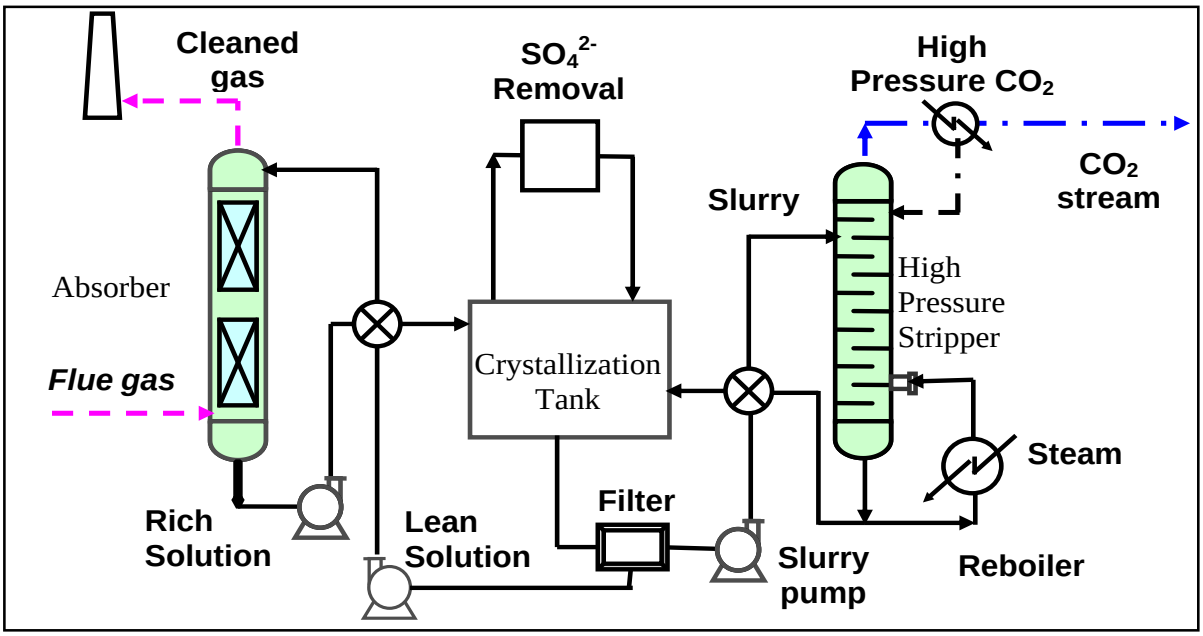

Figure 6-1. Schematic diagram of the proposed Hot-CAP.

The composition of the CO_2-rich stream from the absorption column is nominally 40 wt% (K_2CO_3-equivalent) solution with 40 to 50% CTB conversion. After $KHCO_3$ crystallization, the CTB conversion level of the lean stream is 20% or less and returns to the absorption column. The concentration of $KHCO_3$ in the absorption and crystallization process is subject to solubility under different conditions, as shown in Figure 6-2.

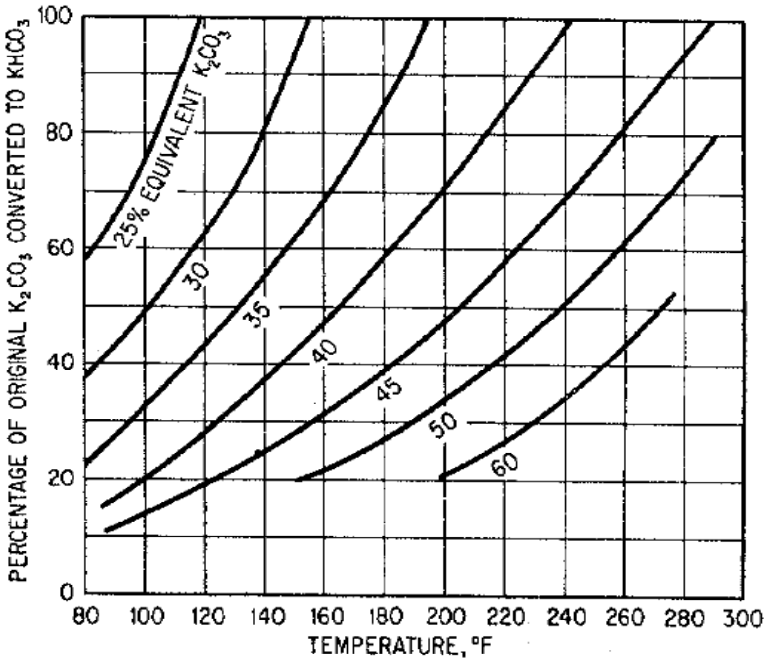

Figure 6-2. Effects of temperature and CTB conversion on the solubility of $KHCO_3$ in K_2CO_3/$KHCO_3$ solutions.

6.3.2 Risk analysis and mitigation strategy for the Hot-CAP

As part of the risk mitigation strategy analysis required by DOE/NETL, a technology-focused risk analysis was performed to identify critical technical risks and mitigate them through experiments, literature analysis, and discussion with equipment vendors. Five major technical risks were identified. The major technical risks are outlined in Figure 6-3.

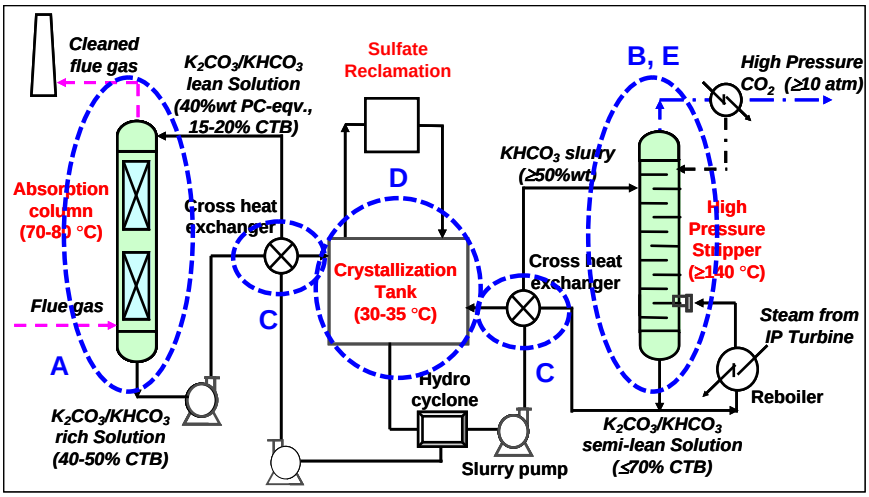

Figure 6-3. Five major technical risks identified for the Hot-CAP.

Risk A is related to the rate of CO_2 absorption at elevated temperatures (60 to 80°C) and the concentration of carbonate solution (about 40 wt%, K_2CO_3-equivalent). Risk B is related to the desired stripping pressure. The mitigation measures for these risks (A and B) were addressed through the experimental and process simulation studies. Risks C and D are related to the design of the heat exchanger and crystallizer, and Risk E is related to the design of the high-pressure stripping column and the related accessories. It was determined that Risks C, D, and E could be addressed through literature searches, consultations with equipment vendors and design companies, and equipment design analysis. Details of these risks and methods to mitigate them are shown in Table 6-5.

Table 6-5. Technical risks of Hot-CAP and mitigation strategies

Risk	Mitigation	Risk ID
Rate of CO_2 absorption at temperatures (60 to 80°C) and concentrations of K_2CO_3 solution (~40 wt%) insufficient to achieve process economics	Develop absorption promoters or catalysts, reconfigure the absorption column design, or both	A
Stripping pressure of potassium bicarbonate slurry is <10 atm, thereby unfavorably affecting the process economics	Develop a sodium bicarbonate-based slurry to obtain stripping pressures ≥10 atm.	B
Heat exchanger fouled by slurry streams	Literature search, vender consultation, and engineering analysis to identify means to alleviate fouling	C
Crystallizer must be quickly cooled to achieve process economics	Literature search, vender consultation, and engineering analysis to identify means to achieve fast cooling in large systems	D
Commercially-available strippers require modifications to handle slurry and operate at high pressure	Literature search, vender consultation, and engineering analysis to determine means to modify standard stripper design	E

6.3.2.1 Risk A mitigation strategy

Experimental and simulation studies were performed to address Risk A. The experimental study was conducted at the University of Illinois at Urbana-Champaign (UIUC) to screen promoters that could accelerate the rate of absorption. The promoters were evaluated by the measured CO_2 removal efficiency by the promoted 40 wt% K_2CO_3 solution in an absorption column. The selected experimental results are illustrated in Figure 6-4 (same as Figure 2B-14 for the convenience of discussion here).

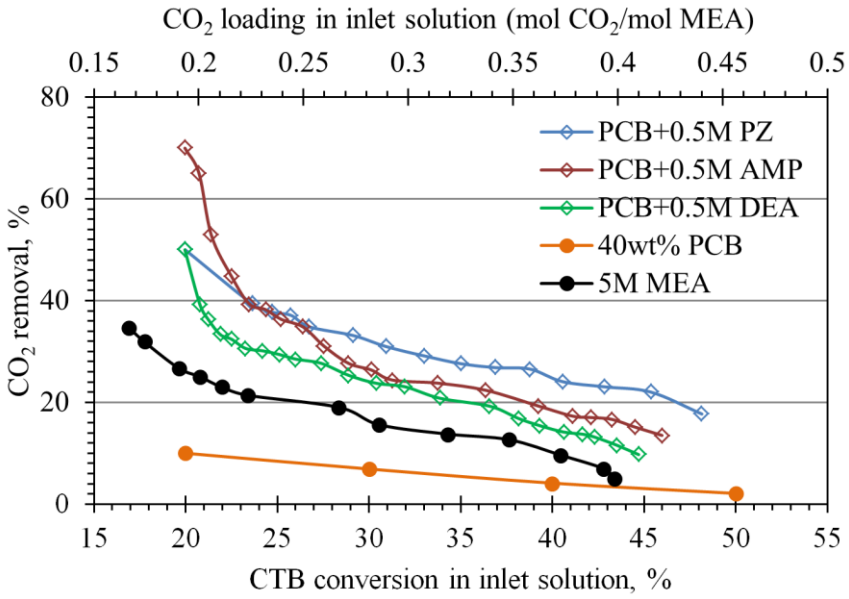

Figure 6-4. Experimental results of CO_2 absorption performance in the 40 wt% K_2CO_3 solution with the addition of various promoters at 70 °C and in the 5 M MEA solution at 50 °C.

Details of the experimental study were described in Chapter 2B. The key results from the experimental study include the following:

- CO_2 removal efficiency was low in the absence of a promoter; and
- CO_2 removal efficiency by the 40 wt% K_2CO_3 solution promoted with 0.5 M PZ, for either the CO_2 lean or rich solution, was higher than 5 M MEA under the similar operating conditions.

Simulations for the absorption process were performed to evaluate the performance of CO_2 absorption into carbonate solutions. Both thermodynamic and kinetic behaviors of the CO_2 absorption with or without a promoter were modeled. ChemCad software[3] was used for equilibrium-based process simulations, and ProTreat software[4] was used for rate-based simulations. Flue gas conditions were based on a 550-MWe subcritical PC plant, in reference to Case 10 of the DOE/NETL Cost and Performance Baseline, [2] as shown in Table 6-4.

Simulation results of CO_2 absorption into K_2CO_3 solutions at 70°C are summarized in Figures 6-5 to 6-8. The results demonstrate that the CO_2 removal efficiency was greatly increased by the

addition of a DEA or PZ promoter. The following conclusions were drawn from the simulation study:

- The absorption of CO_2 into the K_2CO_3 solution with 20% initial CTB conversion without a promoter cannot achieve the targeted 90% CO_2 removal within a reasonable range of L/G ratios. In addition, a high K_2CO_3 concentration is favorable for CO_2 removal.
- The kinetic analysis of CO_2 absorption into the K_2CO_3 solution without a promoter demonstrates that the CO_2 removal efficiency is much less than the equilibrium value within a feasible range of column heights. The cost of absorbing CO_2 is high when using the K_2CO_3 solution without a promoter.
- The kinetic analysis reveals that the CO_2 removal efficiency can be greatly increased by the use of either a DEA or PZ promoter. The CO_2 removal efficiency increases with increasing promoter concentration. The PZ promoter is more effective than the DEA promoter. In addition, 90% CO_2 removal efficiency can be achieved when using 40 wt% K_2CO_3 with a 20% initial CTB conversion promoted by 0.5 M PZ at 70°C.

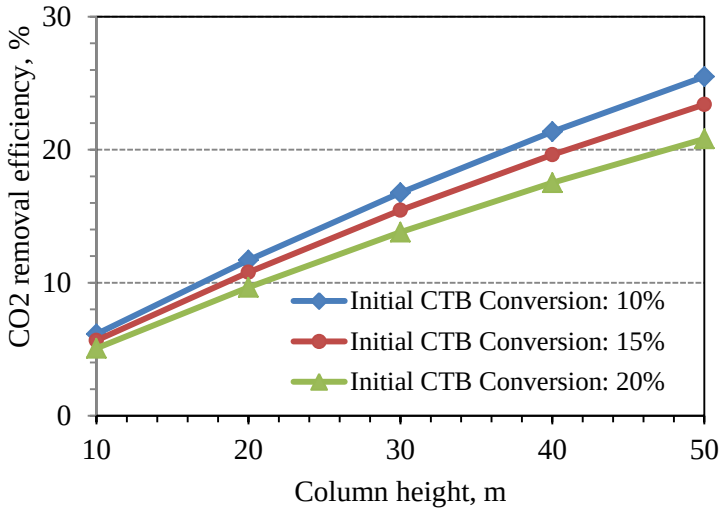

Figure 6-5. Simulation results of CO_2 absorption into a 40 wt% K_2CO_3 solution without a promoter (70 °C and L/G = 5.05 L/Nm^3).

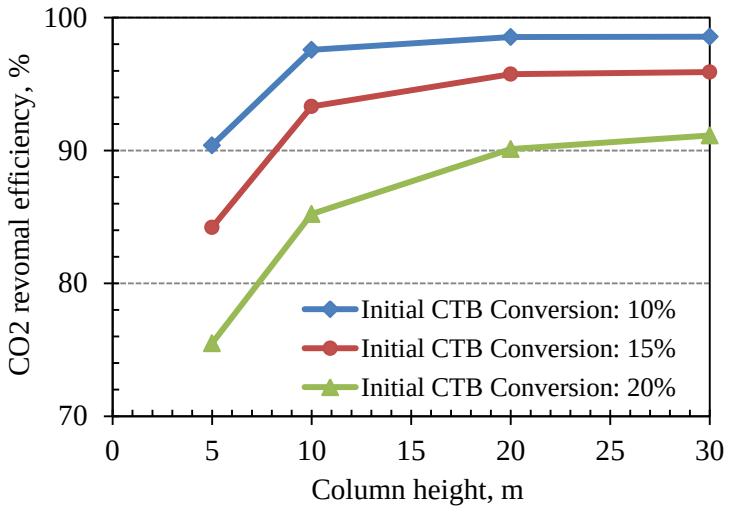

Figure 6-6. Simulation results of CO_2 absorption into 40 wt% K_2CO_3 with the addition of 0.5 M PZ as a promoter (70 °C and L/G = 5.05 L/Nm^3).

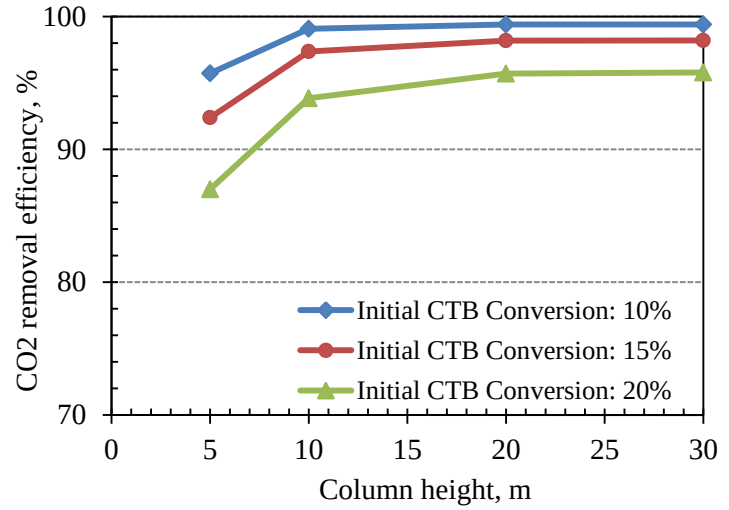

Figure 6-7. Simulation results of CO_2 absorption into 40 wt% K_2CO_3 with the addition of 1.0 M PZ as a promoter (70 °C and L/G = 5.05 L/Nm^3).

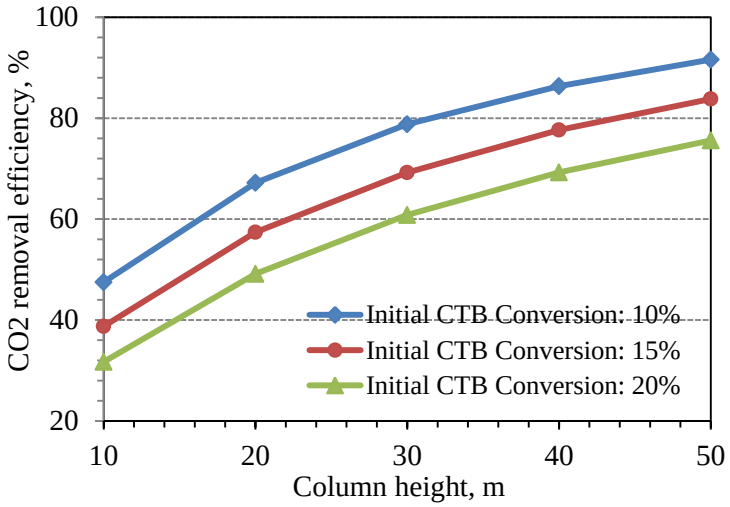

Figure 6-8. Simulation results of CO_2 absorption into 40 wt% K_2CO_3 with the addition of 1.0 M DEA as a promoter (70 °C and L/G = 5.05 L/Nm^3).

6.3.2.2 Risk B mitigation strategy

Risk B is addressed by the UIUC team based on the experimental results obtained from the phase equilibrium measurements and testing of CO_2 stripping in a high-pressure stripping column. The stripper design is critical, because a high stripping pressure and lower water vapor/CO_2 partial pressure ratio will significantly reduce the stripping heat (associated with water vaporization) during CO_2 stripping and the required compression work downstream. The measured VLE data confirmed the feasibility of high-pressure CO_2 stripping in the Hot-CAP process. A higher stripping temperature, a higher level of CTB conversion, and a higher K_2CO_3 concentration led to a higher stripping pressure and a lower water vapor/CO_2 ratio. However, an engineering analysis by the team revealed that CO_2 stripping under excessively high pressure has the following drawbacks that must be considered:

- The required excessively high-temperature steam reduces the net electric power generation; and
- Extra power is consumed in pumping the circulation solvent to higher pressures.

On the other hand, a low operating pressure results in a high stripping heat requirement. Therefore, the optimal stripping pressure is recommended to range between 5 and 10 bar (4.93 to 9.87 atm).

6.3.2.3 Risk C mitigation strategy

Risk C encompasses fouling caused by the need to manage slurry streams. Discussions with vendors indicated that fouling of the cross-flow heat exchangers and the cooler inside the crystallizer, owing to possible potassium bicarbonate scaling on equipment surfaces, can be solved. A variety of engineering solutions are available to reduce fouling, including the following:

- Reducing the temperature difference between the streams in the cross-flow heat exchangers;

- Pre-seeding the crystallization solution;
- Using plate-and-frame-type heat exchangers;
- Using a vacuum-cooling crystallizer or a surface-cooling crystallizer equipped with scrapers; and/or
- Adding extra heat exchangers.

6.3.2.4 Risk D mitigation strategy

In comparison, discussions with vendors in relation to Risk D indicated that the crystallizer design should be revised. The conventional crystallizer design requires a large temperature difference between the inlet solution (saturated or unsaturated carbonate solution entering the crystallizer) and the mother liquor (solution leaving the crystallizer). Therefore, the heat recovery from the incoming solution can be jeopardized if a single crystallizer configuration is used. Multiple continuous stirred tank reactor (CSTR)-type crystallizers are required. A schematic diagram of the revised design is shown in Figure 6-9. In this flowchart, five consecutive crystallization tanks are used instead of a single crystallizer (original design). The new configuration will reduce the temperature difference between the inlet and outlet streams in each crystallizer to about 5°C, thereby facilitating the heat recovery desired in the Hot-CAP. This design was developed after numerous discussions with vendors.

6.3.2.5 Risk E mitigation strategy

One of the major challenges in this project is the need to modify conventional strippers to handle slurry and operate at high pressure (Risk E). During detailed analysis of Risk E, it was determined that there is an interaction between Risks B and E [i.e., high-pressure stripping of the carbonate/bicarbonate slurry (Risk B), and recrystallization of the bicarbonate during cooling of the stripped lean solution (Risk E)]. In the Hot-CAP, the bicarbonate needs to be regenerated at a high pressure, which requires a combination of a high total concentration of bicarbonate slurry and a high CO_2 loading (high bicarbonate/carbonate ratio) for the regenerated lean solution. On the other hand, a higher CO_2 loading in the stripped lean solution will bring the risk of recrystallization (Risk E) in the cooling process. This indicates a potential interaction between Risks B and E. In the subsequent process simulation and design, a reasonably high stripping pressure of 6 bar (5.92 atm) can be achieved using power plant steam at a relatively high temperature (about 180°C) as the heat source for the stripper reboiler.

The results from the above risk analysis are considered in the subsequent TEA. These results are especially critical to the equipment capital cost. The use of a series of CSTRs in the crystallizer design will have a large impact on the overall capital cost of the Hot-CAP.

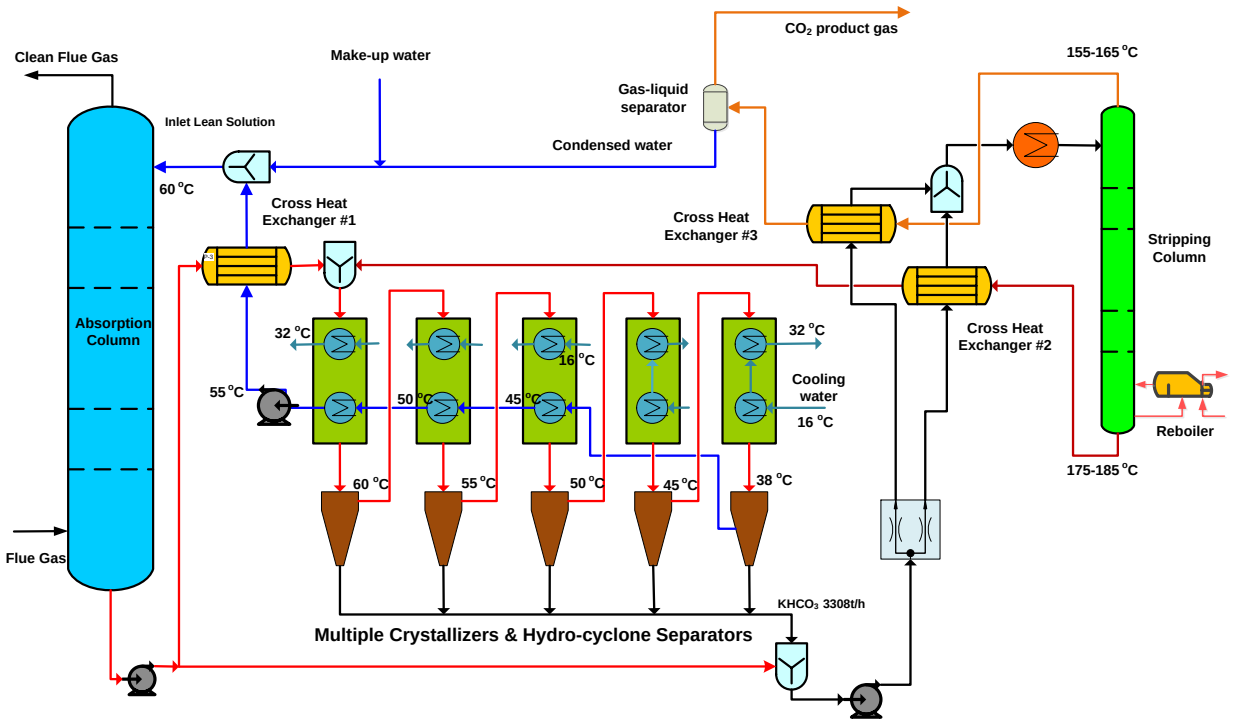

Figure 6-9. A multiple crystallizer unit design developed to address Risk D.

6.3.3 Design of the Hot-CAP

6.3.3.1 Design of the absorption column

In addition to the above risk analysis, process simulations using ProTreat® software for the absorption column have resulted in the following recommendations:

- A promoter, either DEA or PZ, is required to achieve 90% CO_2 removal. PZ is recommended because it can be used at a high temperature (160°C) without encountering significant degradation.
- A more concentrated K_2CO_3 solution is preferred for achieving a large CO_2 working capacity. However, the K_2CO_3 concentration will be limited by the solubility of $KHCO_3$ in the rich solvent. The carbonate concentration used in this study is 40 wt% K_2CO_3-equivalent.
- The initial level of CTB conversion (i.e., lean CO_2 loading) was selected by a trade-off between absorption and stripping performance, and 20% initial CTB conversion is applied in this study.
- The temperature of the inlet lean solvent has a great effect on the temperature of the effluent-rich solvent. A higher inlet temperature will result in a larger heat loss caused by evaporating water carried out in the purified flue gas, thus reducing the temperature of the rich solvent. Additionally, a reduced inlet temperature is beneficial for the PZ-promoted absorption reaction. Simulation results show that the addition of 1.0 M PZ is required to promote the absorption at 70°C to achieve 90% CO_2 recovery, whereas 0.5 M PZ is sufficient to achieve 90% CO_2 recovery at 60°C. On the other hand, a low inlet

solvent temperature will significantly reduce the solubility of $KHCO_3$ in the rich solvent, which, in turn, will reduce the working capacity of the solvent. Therefore, the inlet temperature of the lean solvent is 60°C.

In summary, the hot carbonate solvent is a 40 wt% (K_2CO_3-equivalent) solution with 20% initial CTB conversion containing 0.5 M PZ as a promoter. The design temperature of the inlet lean solvent is 60°C. Because absorption in the design solvent solution is sufficiently fast, the required flow rate of the solvent is limited by the $KHCO_3$ solubility in the rich solvent. Simulation results using ProTreat show that the outlet temperature of the rich solvent reaches 67°C, at which temperature the solubility of $KHCO_3$ corresponds to 45% CTB conversion in the solution. At a working capacity equivalent to a CTB conversion varying from 20 to 45%, the required solvent flow rate is estimated to be 19,300 tonne/hr. Under these design conditions, the absorption column dimensions required for 90% CO_2 recovery are determined: the absorber consists of two parallel absorption columns, each with effective packing 13 m in depth and 14.8 m in diameter.

6.3.3.2 Design of the stripping column

It was found that neither ChemCad nor ProTreat can provide sufficiently accurate performance predictions when the stripping temperature is higher than 140°C. However, the goal of this study is to achieve high-pressure stripping (usually accompanying a high temperature of >140°C) to reduce the stripping heat loss and the required CO_2 compression work. Therefore, the stripping column simulation is based on a self-developed, steady-state thermodynamic model using the VLE data measured in this project. The experimental VLE data for CO_2 and water vapor are shown in Figures 6-10 and 6-11.

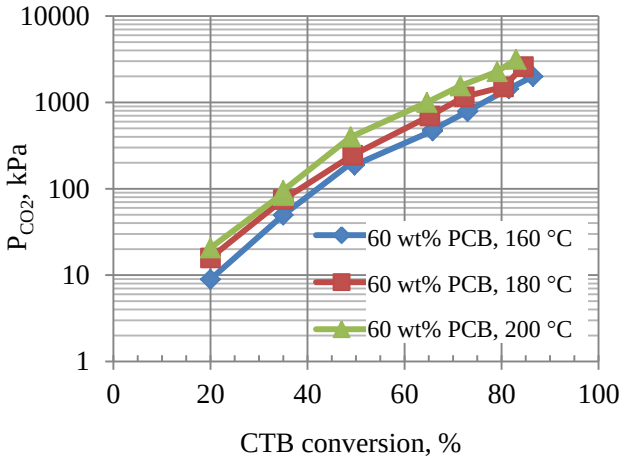

Figure 6-10. Experimental VLE data for CO_2 in a 60 wt% (K_2CO_3-equivalent) PCB solution.

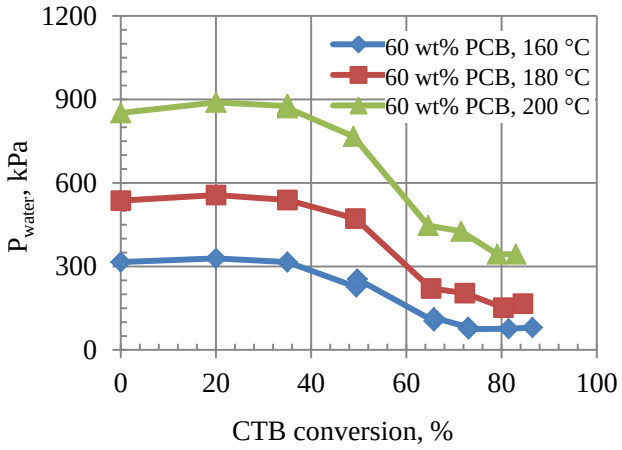

Figure 6-11. Experimental VLE data for water vapor in a 60 wt% (K_2CO_3-equivalent) PCB solution.

The following design assumptions were applied to the simulation:

- Each stage is under ideal conditions and the vapor phase is in equilibrium with the liquid phase.
- The vapor phase consists of only CO_2 and water vapor; any other components in the vapor phase are negligible.
- The rich solution entering the stripper is a 60 wt% (K_2CO_3-equivalent) solution, which is a blended slurry formed by potassium bicarbonate solids from the crystallization tanks and a portion of the CO_2-rich solution from the absorption column, as shown in Figure 6-9. The CTB conversion in the rich solution is 79%.
- To reduce the potential risk of $KHCO_3$ crystallization in the regenerated hot lean solution from the stripper when it is cooled during heat exchange (cross-flow heat exchanger #2 in Figure 6-9), the CTB conversion in the hot lean solution is kept at as low a level as possible.
- To reduce the use of stripping heat, the temperature of the inlet rich solution is kept at a relatively low level. On the basis of the simulation using ProTreat, the temperature difference between the top rich solution and the bottom lean solution is usually between 17 to 21°C.

Steady-state simulation results using the experimental VLE data indicated the CTB conversion in the hot lean solution can be reduced to 29% when the stripping pressure is maintained at 6 bar (5.92 atm). The corresponding temperature in the stripper reboiler is 181°C. The corresponding temperature of the inlet rich solution at the top of the stripper is 161°C. From the difference in CTB conversion between the lean and rich solutions, the flow rate of the 60 wt% rich solution can be estimated as 7,094 tonne/hr.

The size of the stripping column was estimated using ProTreat. Because the VLE database built in ProTreat is not available for temperatures above 140°C, the column sizing simulation was based on a 140°C stripping temperature at the bottom of the stripper with the reduced operating pressure of 2 bar (1.97 atm). With the same flow rate and composition of the inlet solution obtained from the above steady-state simulation, but with the inlet solution temperature reduced to 120°C, simulation results showed that the 29% CTB conversion in the hot regenerated lean

solution can be achieved when the stripper is a single column 10 m in height and 7.3 m in diameter. Because the CO_2 reaction kinetics usually increase with increasing temperature, the stripping column is conservatively-sized, using a single column with effective packing of 10 m in height and 7.3 m in diameter.

An important fact related to the stripper design is that all $KHCO_3$ solids in the inlet rich solution (79% CTB conversion and 161°C) entering the stripper are dissolved, according to an exploration of the solubility data shown in Figure 6-2. Therefore, the stripper design can alleviate Risk E.

6.3.3.3 Design of the crystallization tanks

Potassium bicarbonate crystallization is an important step in the Hot-CAP process. The risk analysis in Section 3.2.4 revealed that a configuration of five consecutive stages of CSTR crystallizers, as shown in Figure 3.9, can be used instead of a single crystallizer to facilitate the heat recovery required in the process and reduce the temperature difference between the inlet and outlet streams of each crystallizer.

It was concluded, based on an intensive literature review and discussions with vendors, that a simple concrete tanker type of crystallizer with submerged coils can achieve the desired crystallization requirement. In addition, such crystallizers are the least expensive. Figure 6-12 illustrates a schematic diagram of the crystallizer structure, which has a draft tube for internal circulation of magma and a downward-directed propeller agitator to provide controllable circulation within the crystallizer. One part of the spiral heat exchange works as the draft tube, and the rest is located in the top region of the crystallizer. Both the top and bottom of the crystallizer are in a conical shape so that the top region is able to provide a zone for fine crystal particles to settle. The clear mother solution leaves the crystallizer after overflowing to the next stage of the crystallizer or returning as a mother liquor. The product slurry is removed through an outlet at the conical bottom and is further separated by a hydrocyclone. The separated liquid merges with the clear mother solution and leaves for the next crystallizer, or it returns as mother liquor in the last crystallizer. The recovered crystal is used for preparing the inlet rich solution of the stripper.

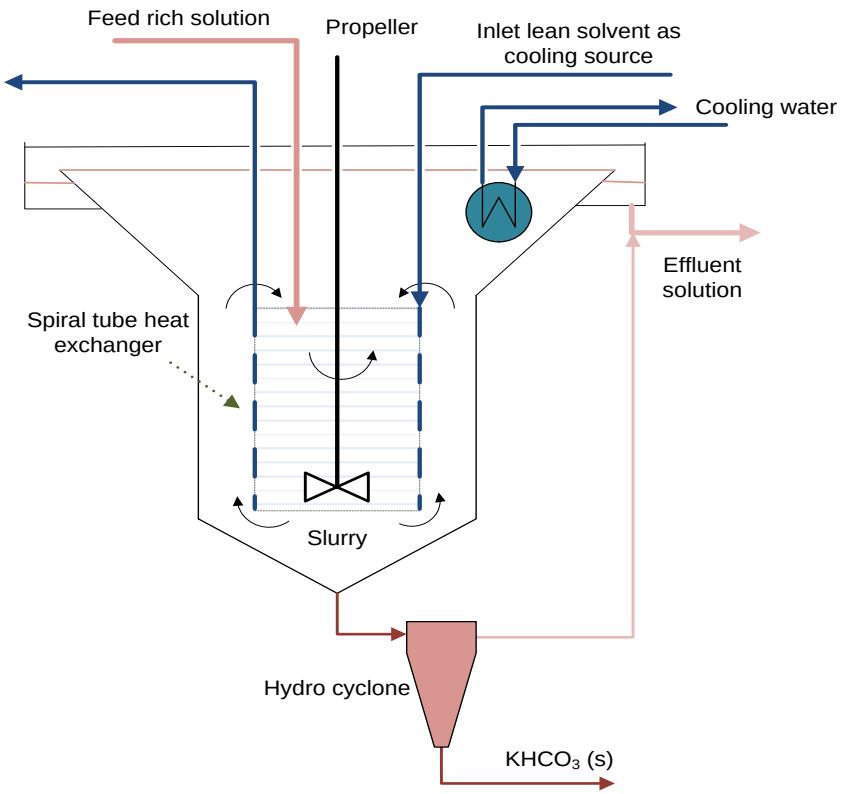

Figure 6-12. Schematic diagram of the crystallizer structure.

The residence time and size of crystal particles are the critical parameters for the design of crystallizers and crystal separators. The experimental results from the crystallization study conducted in this project showed that $KHCO_3$ crystallization is instantaneous, but it takes about 30 min for the crystal particles to grow to 80 μm and above. In the practical operation of a crystallizer, however, a large amount of crystal particles are circulated in the crystallizer, which can be more than those recovered. Therefore, the residence time of the feed solution can be substantially reduced. In the current design, the average crystal solids concentration in each stage of the crystallizer is assumed to be 10 wt%. The design volume of each crystallizer is estimated based on the crystallization kinetics obtained from the experimental results, as shown in Table 6-6.

On the other hand, a spiral tube heat exchanger soaked in a crystallizer to cool the inlet solution and remove the heat of $KHCO_3$ crystallization for each stage of crystallization also occupies a part of the crystallizer volume. The required volume of the heat exchanger is assumed to be at least one-third of the total volume of each crystallizer. Two types of cooling media are used in a crystallizer. One type is the returning lean solution (the mother liquor) for heat recovery, and the other is the external cooling water to remove the remaining cooling load to keep the crystallizer operating at the desired temperature. The approach to the crystallization temperature for cooling the lean solution is estimated using a logarithmic mean temperature approach. A temperature change in the cooling water from 17 to 32°C is adopted to determine the cooling water flow rate required for heat exchange in the crystallizer. As a result, the temperature approach for the external cooling water ranges from 17 to 38°C, depending on the temperature in the stage of the

crystallizer. The submerged coil heat exchanger is constructed with 5-cm-diameter stainless steel tubing. The average heat transfer coefficient of the tube is 1,300 $W/m^2 \cdot K$.

Table 6-6. Estimation of volumes for the five stages of crystallizers

Stage of crystallizer	1st	2nd	3rd	4th	5th	Total
Feed flow, tonne/hr	22,547	21,592	20,892	20,356	19,845	
Discharged crystal, tonne/hr	955	700	536	511	606	3308
Total cooling load, MW	88.6	143.9	127.7	123.6	159.3	643.1
Cooling by mother liquor, MW	74.5	73.4	101.7	0.0	0.0	249.6
Cooling by cooling water, MW	14.1	70.4	26.1	123.6	159.3	393.5
Crystallizer volume by cooling need, m^3	309	355	293	155	269	1,381
Design crystallizer volume, m^3	555	633	644	660	734	3,226
Actual residence time, s	152	176	181	186	206	901
Cooling water flow, tonne/hr	757	3,790	1,404	6,655	8,577	21,183

As shown in Figure 6-9, two sources of solutions are required to precipitate out the $KHCO_3$ salt: 81% of the rich solution from the absorber (16,142 tonne/hr of 40 wt% K_2CO_3 with 45% CTB conversion at 67°C), and all the lean solution regenerated from the stripper (6,406 tonne/hr of 60 wt% K_2CO_3 with 29% CTB conversion at 70°C). The density of the blended solution is estimated to be 1.71 kg/L at 68°C. The density of the returning mother liquor is 1.52 kg/L at 38°C.

The temperatures of the five consecutive crystallizers are controlled at 60, 55, 50, 45, and 38°C, respectively. The cooling load of each crystallizer is the sum of the sensible heat of the solution and the $KHCO_3$ crystallization heat. The rate of $KHCO_3$ crystallization in each crystallizer was estimated based on its solubility, as shown in Figure 6-2. The total $KHCO_3$ crystallization heat released was estimated based on the crystallization rate and the molar crystallization heat (26.2 kJ/mol of $KHCO_3$). The sensible heat was estimated using ProTreat. Table 6-6 summarizes the design parameters of the five crystallizers. It should be noted that some bicarbonate crystal particles are formed during heat exchange before the feed solutions enter the first crystallizer, especially for the lean solution from the stripping column that has a high carbonate equivalent concentration. This reduces the cooling load in the first crystallizer. The total volume of the five crystallizers is 3,226 m^3, which results in an actual total residence time of approximately 11 min. Thus, such a residence time is sufficient to meet both the heat exchange and crystal growth requirements. The total cooling water load is 393.5 MW, requiring a cooling water flow of 21,183 tonne/hr.

6.3.4 Mass and heat balances of the Hot-CAP

The mass and heat balances for the Hot-CAP are shown in Figure 6-13, based on the flue gas composition and flow rate specified in Case 10 of the DOE/NETL-2010/1397 report. The absolvent is a 40 wt% K_2CO_3 solution with 20% lean CTB conversion containing 0.5 M PZ at a total flow rate of 19,300 tonne/hr. The CO_2 loading of the solvent increases from 20% (lean) to about 45% (rich) CTB conversion. The rich K_2CO_3 solvent from the absorber is separated into two streams: 81% of the rich solvent goes through the heat exchange and crystallization process,

and the remaining part is mixed with $KHCO_3$ crystal solids recovered from the crystallization tanks to produce a 60 wt% (K_2CO_3-equivalent) carbonate slurry with 79% CTB conversion.

In the crystallization process, 3,308 tonnes of $KHCO_3$ solids are obtained from the blended solution made of 81% rich solvent from the absorber and all the regenerated lean solvent from the stripper. The mother liquor from the crystallization process is mixed with a small amount of make-up water to form a 40 wt% K_2CO_3 solution with 20% CTB conversion as the lean solution returning to the absorber. During crystallization, external cooling water is required to control the temperature of the different crystallizer units.

Although the crystallizers are designed to use covered tanks, water loss during the crystallization process is expected. The water loss rate is assumed to be 0.1 to 0.2% of the solvent circulation rate.

The heat recovered from the first to the third crystallizers is sufficient to heat the lean solvent to the desired absorber inlet temperature (60°C). In total, 598 tonne/hr of CO_2 is released from the regeneration of $KHCO_3$ during the stripping process. After heat recovery from the regenerated hot lean solvent and the CO_2 product gas, 395.7 MW of external low-pressure steam is required to meet the heat requirement, including 213.2 MW (thermal) in the reboiler and 182.5 MW (thermal) in the heat exchanger upstream of the stripping column. The total heat consumption in the Hot-CAP is estimated at 2,382 kJ/kg of CO_2.

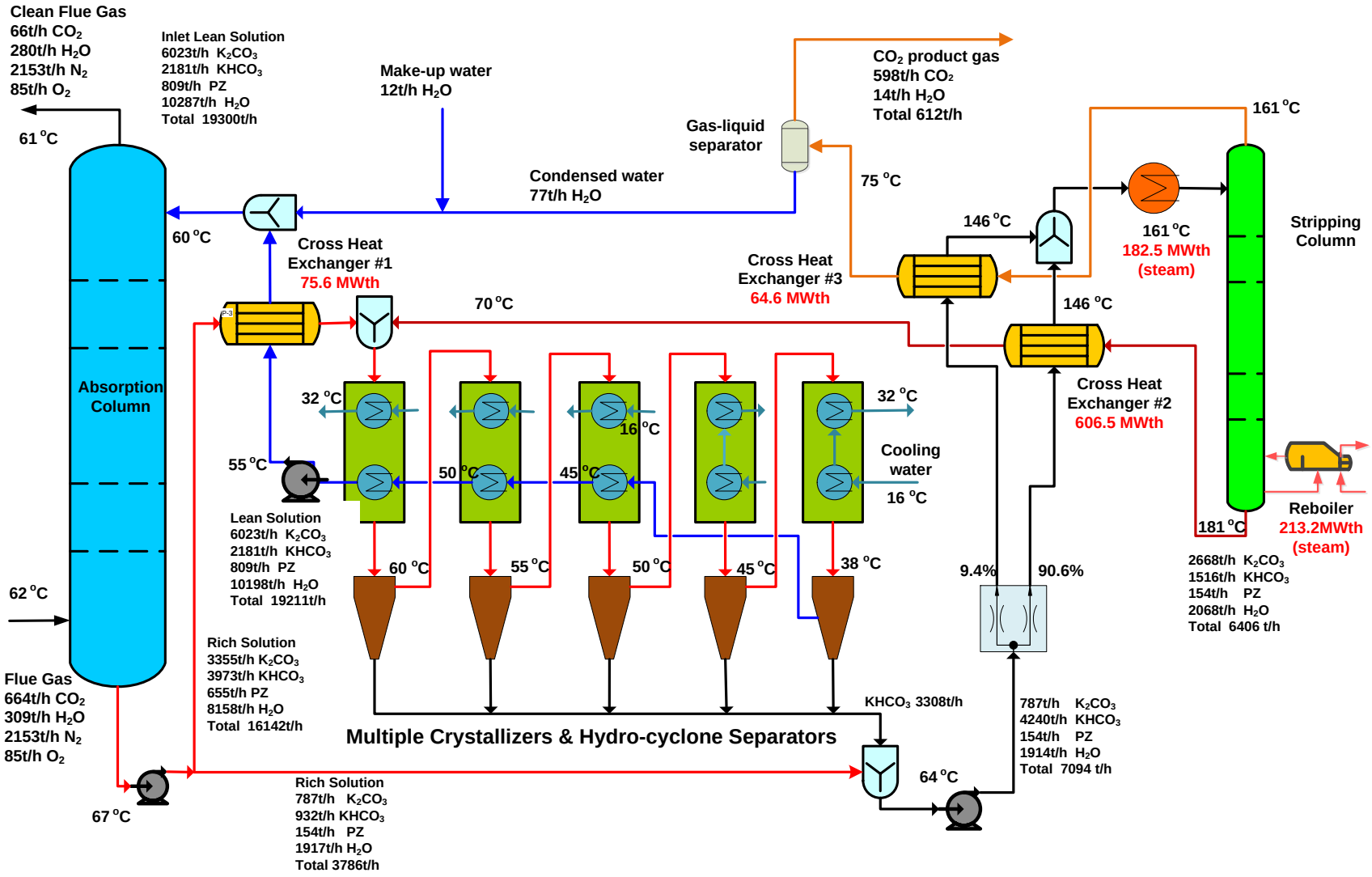

Figure 6-13. Schematic flowchart of the Hot-CAP with mass and heat balances.

6.4 Cost Estimation

6.4.1 Cost estimation methodology

The total plant cost (TPC) and operation & maintenance (O&M) costs for the subcritical PC power plant and the integrated CO_2 capture plant are estimated based on 2007 costs, using methodology introduced from Attachment 3 of DOE/NETL report DE-FOA-0000403[1].

6.4.1.1 Capital cost

Report DOE/NETL-2010/1397 provided a cost estimate for 14 major subsystems of the Case 10 subcritical PC plant with CO_2 capture. With this as the reference cost estimate, modifications to each subsystem were made either by capacity factoring, or by replacement with new estimates to obtain the overall cost estimate for the nominal 550-MWe subcritical PC plant with Hot-CAP-based PCC. For the subsystems in which capacity factoring was used to perform the cost estimates, a power factor of 0.7 was applied. The list of the Case 10 subcritical PC plant subsystems and bases for modifications are shown in Table 6-7.

Subcritical PC Plant

The capital cost estimates for the subcritical PC plant are developed based on the Case 10 costs provided in the DOE/NETL-2010/1397 report. The PCC section in this study differs from the CO_2 capture section provided in the report, resulting in a variation in the PC plant performance attributable to the differences in PCC design as well as solvent selection. As stated in Section 2.1.4, the revised PC plant with Hot-CAP-based PCC was estimated based on a different PCC LP steam extraction rate, hence resulting in a different power generation rate from the DOE/NETL Case 10 subcritical PC plant. For this reason, the PC plant equipment costs (primarily for the LP steam turbine, condenser, and cooling water/cooling tower sections) are re-estimated on a capacity-factor basis using the DOE/NETL reported costs as a baseline reference.

Materials, direct labor, engineering and construction management fees, home office costs, and contingencies consistent with those used in the DOE/NETL report Case 10 are added to arrive at the total subcritical PC plant cost estimate.

PCC Plant

The capital cost for Hot-CAP-based PCC is a major equipment (ME)-factored estimate for the DOE/NETL Case 10 subcritical plant, with a target accuracy of ±30%. Separate estimates are prepared for the CO_2 recovery facility and the CO_2 compression facility.

For the ME-factored estimate, ME material and labor costs were developed from equipment sizes, quantities, and design parameters defined by the PCC design discussed in the previous section. Bulk material and labor costs were factored from the ME costs. The sum of the ME and bulk material costs, including shipping costs, forms the total direct cost (TDC).

The construction indirect cost, factored from the total direct labor cost, is added to the TDC to arrive at the total field cost (TFC). The engineering and construction management fees, home office costs, and contingencies are added to the TFC to arrive at the TPC by using factors consistent with the DOE/NETL report for the Case 10 TPC.

Table 6-7. Cost estimate basis for the subcritical PC plant with CO_2 capture

Acct. No.	Item/description	Cost estimate basis	Capacity factor reference basis[a]
1	COAL & SORBENT HANDLING	Capacity factor	AR coal
2	COAL & SORBENT PREP & FEED	Capacity factor	AR coal
3	FEEDWATER & MISC. BOP SYSTEMS		
3.1	Feedwater system	Capacity factor	AR coal
3.2	Water makeup & pretreating	Capacity factor	CW makeup
3.3	Other feedwater subsystems	Capacity factor	AR coal
3.4	Service water systems	Capacity factor	AR coal
3.5	Other boiler plant systems	Capacity factor	AR coal
3.6	FO supply sys & nat gas	Capacity factor	AR coal
3.7	Waste treatment equipment	Capacity factor	AR coal
3.8	Misc. equipment (cranes, air comp, etc.)	Capacity factor	AR coal
4	PC BOILER	Capacity factor	AR coal
5	FLUE GAS CLEANUP	Capacity factor	AR coal
5B	CO_2 REMOVAL & COMPRESSION		
5B.1	CO_2 removal system	New estimate	N/A
5B.2	CO_2 compression & drying	New estimate	N/A
6	COMBUSTION TURBINE/ACCESSORIES	N/A	N/A
7	HRSG, DUCTING & STACK	Capacity factor	AR coal
8	STEAM TURBINE GENERATOR		
8.1	Steam TG & accessories	Capacity factor	STG output
8.2	Turbine plant auxiliaries	Capacity factor	STG output
8.3	Condenser & auxiliaries	Capacity factor	Cond. duty
8.4	Steam piping	Capacity factor	Gross power output
8.9	TG foundations	Capacity factor	Gross power output
8.10	Backpressure TG & accessories	Capacity factor	BPTG output
9	COOLING WATER SYSTEM		
9.1	Cooling tower	Capacity factor	CT load
9.2	Circulating CW pump	Capacity factor	CT load
9.3	Circulating CW syst aux	Capacity factor	CT load
9.4	Circulating CW piping	Capacity factor	CT load
9.5	Makeup water system	Capacity factor	CW makeup
9.6	Closed CW system	Capacity factor	CCW load
9.9	Circ CW syst foundations & structures	Capacity factor	CT load
10	ASH/SPENT SORBENT HANDLING SYS	Capacity factor	AR coal
11	ACCESSORY ELECTRIC PLANT	Capacity factor	Gross power output
12	INSTRUMENTATION & CONTROL	Capacity factor	AR coal
13	IMPROVEMENT TO SITE	Capacity factor	AR coal
14	BUILDING & STRUCTURES	Capacity factor	AR coal

[a]CW: cooling water; CT: cooling tower; AR: as-received; HRSG: heat recovery steam generator; BPTG: back pressure turbine generator; STG: steam turbine generator.

The absorption and stripping column dimensions were determined in the previous section. The dimensions of other major equipment used in the process are estimated based on the individual heat and material stream flows of the simulation.

Excluding the crystallization tanks, once the equipment was sized, the costs for the equipment and installation labor were estimated by scaling-up cost estimates for corresponding equipment in a TEA for "Post-Combustion Flue Gas CO_2 Capture Using Gas Pressurized Stripping Technology" performed by Nexant Inc. for CCS LLC. The costs of the crystallization tanks were estimated based on literature references and communication with vendors.

Costs for bulk materials, such as instrumentation, piping, structure steel, insulation, electrical equipment, painting, and concrete and site preparation associated with the major equipment were factored from ME costs based on historical data for similar services. Installation labor for each bulk commodity was factored from the historical data by type.

The construction indirect cost was factored from the total direct labor costs based on historical data. The construction indirect cost covers the cost for setup, maintenance, and removal of temporary facilities, warehousing, surveying and security services, maintenance of construction tools and equipment, consumables and utilities purchases, and field office payrolls.

The installation labor productivity and cost (wages, fringe benefit costs and payroll-based taxes, and insurance premiums) used to calculate the installation costs at 2007 price levels are based on the estimation from the Nexant TEA.

Engineering and Construction Management, Home Office Fees, & Contingencies

Engineering and construction management are estimated as a percentage of the TFC. These costs consist of all home office engineering and procurement services, as well as field construction management costs.

Both the project contingency and process contingency costs represent costs that are expected to be spent in the development and execution of the project that are not yet fully reflected in the design. Project contingency is added to the TFC to cover project uncertainty and the cost of any additional equipment that would result during detailed design. Likewise, process contingency is added to the TFC to cover the cost of any additional equipment that would be required as a result of continued technology development. For this study, the factors used for the above fees and contingencies are consistent with those used in the DOE/NETL study.

6.4.1.2 O&M costs

The O&M costs pertain to those charges associated with operating and maintaining the power plant over its expected life. These costs include

- Operating labor
- Maintenance—material and labor
- Administrative and support labor
- Consumables

- Fuel
- Waste disposal

There are two components of O&M costs: fixed O&M, which is independent of power generation, and variable O&M, which is proportional to power generation. The variable O&M costs are estimated based on an 85% capacity factor.

- Labor

The operating labor cost is determined based on the number of operators required to work in the plant. Other assumptions used in calculating the total labor cost include

2007 base hourly labor rate, $/hr	33
Length of work week, hr	40
Labor burden, %	30
Administrative/support labor, % of O&M labor	25
Maintenance material + labor, % of TPC	1.64
Maintenance labor only, % of maintenance material + labor	40

- Consumables and Waste Disposal

The cost of consumables, including fuel, is determined based on the individual rates of consumption, the unit cost of each specific consumable commodity, and the plant annual operating hours. Waste quantities and disposal costs are evaluated similarly to the consumables. The unit costs for major consumables and waste disposal are based on the values reported in the DOE/NETL report. These costs are escalated to 2010, the year when construction would be completed and production would start.

6.4.2 Financial modeling basis

The financial model used for this study follows the same methodology as the NETL/DOE-2010/1397 report. The figure-of-merit of the method is the levelized cost of electricity (LCOE) over a 20-year period. The parameters used to calculate the LCOE required by the model include the following:

Income tax rate, %	38
Percentage debt, %	45
Interest rate, %	11
Equity desired rate of return, %	12
Repayment term of debt, years	15
Depreciation	20 years, 150% declining balance
Working capital	None
Plant economic life, years	30
Tax holiday, years	0
Start-up costs (% of TPC less contingencies)	2
EPC escalation, % per year	0
Coal price nominal escalation, %	2.35

- O&M cost nominal escalation, % 1.87
- Duration of construction, years 3
- First year of construction 2007
- Construction cost distribution, %
  - Year 1 5
  - Year 2 65
  - Year 3 30

All costs are expressed in the "first-year-of-construction" year dollars, and the resulting LCOE is expressed in "first-year-of-construction" year dollars as well. The DOE/NETL report's net 550-MWe subcritical PC plant without CO_2 capture (Case 9) LCOE is to be used as the benchmark comparison for the subcritical PC plant with CO_2 capture. The Case 9 LCOE stated in the DOE/NETL report is 75.3 mills/kWh.

6.4.3 Performance summary of the Hot-CAP PCC

An overall utilities sheet can be developed based on the mass and heat balances described in Section 3.4, to summarize the total steam requirement and electrical consumption for the Hot-CAP PCC process. The process steam consumption is used to estimate the gross power generated by the steam turbines of the power plant.

The auxiliary loads for the overall plant are separated into three categories: PCC-independent PC plant auxiliary loads, PCC-dependent PC auxiliary loads, and PCC loads. The PCC-independent PC auxiliary loads are consistent with the values in the DOE/NETL report. The electrical load from the PCC utilities summary sheet is added directly to the total auxiliary loads as the PCC load. PCC-dependent PC auxiliary loads, such as cooling water circulation pump loads, cooling tower fan loads, and transformer losses, vary with the PCC steam extraction requirement. These are calculated based on the PCC utilities consumption from the summary sheet and added to the total auxiliary load as the PCC-dependent PC auxiliary loads. Tables 6-8 and 6-9 show the utility consumption of the Hot-CAP-based CO_2 capture section and CO_2 compression section, respectively, of the PCC plant.

Table 6-8. Hot-CAP-based PCC CO_2 capture section utilities

Item no.	Item name	Elec. power, kW	Steam, tonne/hr 0.8 MPa	Steam, tonne/hr 1.3 MPa	Water cond., tonne/hr	Cooling water Load, MW	Cooling water Circ. rate, tonne/hr	Regen. duty, MW
	Exchangers							
E-103	Stripping column inflow heater		247.3		(247.3)			182.5
E-104	Stripping column reboiler			274.8	(274.8)			213.2
E-105	Stage 1 crystallizer cooler					14.1	757	
E-106	Stage 2 crystallizer cooler					70.4	3,790	
E-107	Stage 3 crystallizer cooler					26.1	1,404	
E-108	Stage 4 crystallizer cooler					123.6	6,655	
E-109	Stage 5 crystallizer cooler					159.3	8,577	
	Pumps and drivers							
G-101	Absorber bottom rich pump	705						
G-102	60 wt% slurry pump	2,326						
G-103	Absorber ovhd wash water pump	338						
G-104	Stage 1 crystallizer outlet pump	826						
G-105	Stage 2 crystallizer outlet pump	786						
G-106	Stage 3 crystallizer outlet pump	566						
G-107	Stage 4 crystallizer outlet pump	731						
G-108	Stage 5 crystallizer lean pump	4,245						
G-109	Stage 1 crystallizer agitator	1,994						
G-110	Stage 2 crystallizer agitator	2,219						
G-111	Stage 3 crystallizer agitator	2,459						
G-112	Stage 4 crystallizer agitator	2,665						
G-113	Stage 5 crystallizer agitator	3,235						
	Compressors							
K-100	Flue gas blower	3,447						
	Total	26,541	247.3	274.8	(522.1)	393.5	21,183	395.7

Table 6-9. Hot-CAP-based PCC CO_2 compression section utilities

Item no.	Item name	Elec. power, kW	Steam, tonne/hr 0.8 MPa	Water condensate, kg/hr	Cooling water Load, MW	Cooling water Circ. rate, tonne/hr	Regeneration duty, MW
	Exchangers						
E-120	Stage 1 KO drum cooler				12.7	994	
E-121	Stage 2 KO drum cooler				11.7	916	
E-122	Stage 3 KO drum cooler				11.9	932	
E-123	Stage 4 KO drum cooler				13.9	1,088	
E-124	Stage 5 KO drum cooler				26.3	2,059	
	Compressors						
K-101	Stage 1 CO_2 compressor	9,717					
K-102	Stage 2 CO_2 compressor	9,444					
K-103	Stage 3 CO_2 compressor	8.956					
K-104	Stage 4 CO_2 compressor	7,007					
K-105	Stage 4 CO_2 compressor	2,849					
	Packaged equipment						
V-100	TEG dehydration package	1,334	0.37	(0.37)	0.80	62	0.21
	Total	39,307	0.37	(0.37)	77.3	6,052	0.21

6.4.4 Capital cost estimate for Hot-CAP PCC

The Hot-CAP-based process CO_2 capture and CO_2 compression section ME lists are provided in Tables 6-10 and 6-11, respectively. The estimated TFCs for the CO_2 capture section (totaling $232.9 million) and CO_2 compression section (totaling $36.5 million), which include the ME costs, freight, bulk materials, and construction indirect costs, are shown in Tables 6-12 and 6-13, respectively. The TFC for the overall Hot-CAP PCC plant, totaling $269.4 million, is listed in Table 6-14.

Table 6-10. Hot-CAP-based CO_2 capture section ME list

VESSELS & TANKS:

Item No.	Item Name	Type	Design Conditions kPa	Design Conditions °C	Material of Construction	Quantity per Lot	Units	Inside Diameter m	Ht or Tan/Tan Length m	Width m	Length m	Number of Lots	2007 Equip Cost $1,000
C-101	Absorption Column	Vert	108	70	Kill CS	1	Vessel	14.8	42.1			2	25,253
	- Sulzerpak	250.0 Sulzer			304 SS	2236	cu.m					2	
	- Pall Rings	3.5 inch			304 SS	211	cu.m					2	
	- Support Plates				304 SS	344	sq. m	2 @ 14.8				2	
	- WW Support Plates				304 SS	106	sq. m	1 @ 11.6				2	
	- Hold-Down Plates				304 SS	344	sq. m	2 @ 14.8				2	
	- WW Hold-Down Plates				304 SS	106	sq. m	1 @ 11.6				2	
	- Liq Distributors				304 SS	344	sq. m	2 @ 14.8				2	
	- WW Liq Distributors				304 SS	106	sq. m	1 @ 11.6				2	
	- Chimney Trays				304 SS	344	sq. m	2 @ 14.8				2	
	- WW Chimney Trays				304 SS	106	sq. m	1 @ 11.6				2	
	- WW Demister Pads				304 SS	211	sq. m	2 @ 11.6				2	
C-102	Stripping Column	Vert	600	190	Kill CS	1	Vessel	7.3	39.1			1	8,273
	- Sulzerpak	250.0 Sulzer			304 SS	419	cu.m					1	
	- Support Plates				304 SS	84	sq. m	2 @ 7.3				1	
	- Hold-Down Plates				304 SS	84	sq. m	2 @ 7.3				1	
	- Liq Distributors				304 SS	84	sq. m	2 @ 7.3				1	
	- Chimney Trays				304 SS	84	sq. m	2 @ 7.3				1	
C-103	CO2 Product Gas Separator	Horizont	600	75	304 SS	1	Vessel	2.3	2.6			1	119
C-104	Stg 1 Crystallizer	Horizont	101	60	Concrete	1	Tank	5.0	12.5			1	221
C-105	Stg 2 Crystallizer	Horizont	101	55	Concrete	1	Tank	5.0	12.8			1	230
C-106	Stg 3 Crystallizer	Horizont	101	50	Concrete	1	Tank	5.0	13.1			1	240
C-107	Stg 4 Crystallizer	Horizont	101	45	Concrete	1	Tank	5.0	13.3			1	248
C-108	Stg 5 Crystallizer	Horizont	101	38	Concrete	1	Tank	5.0	13.8			1	268
C-109	Stage 1 crystallizer hydrocyclone	Cyclone	1000	60	CS	8	Vessel	0.3	1.0			1	80
C-110	Stage 2 crystallizer hydrocyclone	Cyclone	1000	55	CS	6	Vessel	0.3	1.0			1	60
C-111	Stage 3 crystallizer hydrocyclone	Cyclone	1000	50	CS	4	Vessel	0.3	1.0			1	40
C-112	Stage 4 crystallizer hydrocyclone	Cyclone	1000	45	CS	4	Vessel	0.3	1.0			1	40
C-113	Stage 5 crystallizer hydrocyclone	Cyclone	1000	38	CS	5	Vessel	0.3	1.0			1	50
												Sum	35,121

SHELL & TUBE EXCHANGERS AND AIR COOLERS:

Item No.	Item Name	Type	Design P, kPa Shell	Design P, kPa Tube	Des Temp, °C Shell	Des Temp, °C Tube	Material Of Construction Shell	Material Of Construction Tube	Duty MW	Total Bare Tube Area, sq. m	Physical Arrangement In Series	Physical Arrangement In Parallel	Total # Req	Total Equip Cost $1,000
E-100	Absorber R/L HX #1	P&F	800	800	190	190		304SS	75.6	3086	1	3	3	370
E-101	Stripper bottom R/L HX #2	P&F	800	800	190	190		304SS	606.5	13433	1	10	10	1,610
E-102	CO2 product gas HX #3	P&F	800	800	190	190		304SS	64.6	1125	1	1	1	135
E-103	Stripper inflow heater	P&F	800	800	190	190		304SS	182.5	3408	1	3	3	409
E-104	Stripper reboiler	S&T	1300	800	190	190		304SS	213.2	13325	1	1	1	3,199
E-105	Stage 1 crystallizer cooler by CW	STE		400		190		304SS	14.1	283	1	1	1	34
E-106	Stage 2 crystallizer cooler by CW	STE		400		190		304SS	70.4	1632	1	2	2	196
E-107	Stage 3 crystallizer cooler by CW	STE		400		190		304SS	26.1	713	1	1	1	85
E-108	Stage 4 crystallizer cooler by CW	STE		400		190		304SS	123.6	4123	1	6	6	494
E-109	Stage 5 crystallizer cooler by CW	STE		400		190		304SS	159.3	7165	1	10	10	859
E-110	Stage 1 crystallizer cooler by Mother	STE		400		190		304SS	74.5	7962	1	10	10	954
E-111	Stage 2 crystallizer cooler by Mother	STE		400		190		304SS	73.4	7846	1	10	10	941
E-112	Stage 3 crystallizer cooler by Mother	STE		400		190		304SS	101.7	7109	1	10	10	852
												Sum	68	10,138

COMPRESSORS, BLOWERS & DRIVERS:

Item No.	Item Name	Type	Design Conditions kPa	Design Conditions °C	Material Of Construction Wheel or Impel'r	Material Of Construction Casing	Design Capacity Des Flow SCMH	Design Capacity Inlet kPa	Design Capacity Delta P kPa	Design Capacity Comp BHP	Driver HP	Driver Type	Total # Req	Total Equip Cost $1,000
K-100	Flue Gas Blower	Cent.	200	60	304SS	304SS	2504320	102	6.0	4559	4623	Motor	2	2,539
												Sum	2	2,539

PUMPS & DRIVERS:

Item No.	Item Name	Type	Design Conditions kPa	Design Conditions °C	Material Of Construction Wheel or Impel'r	Material Of Construction Casing	Design Capacity Des Flow LPS	Design Capacity Inlet kPa	Design Capacity Delta P kPa	Design Capacity Pump BHP	Driver HP	Driver Type	Total # Req	Total Equip Cost $1,000
G-101	Absorber bottom rich pump	Cent.	300	70	CS	CS	3543	130	100	932	945	Motor	3	774
G-102	Slurry pump	Cent.	1200	65	CS	CS	877	130	1000	3076	3119	Motor	3	851
G-104	Absorber ovhd wash water pump	Cent.	600	60	CS	CS	425	130	450	447	453	Motor	3	242
G-105	Stage 1 crystallizer outlet pump	Cent.	300	60	CS	CS	3663	130	100	1092	1107	Motor	3	800
G-106	Stage 2 crystallizer outlet pump	Cent.	300	55	CS	CS	3592	130	100	1040	1054	Motor	3	785
G-107	Stage 3 crystallizer outlet pump	Cent.	300	50	CS	CS	3560	130	100	749	759	Motor	3	778
G-108	Stage 4 crystallizer outlet pump	Cent.	300	45	CS	CS	3556	130	100	967	980	Motor	3	777
G-109	Stage 5 crystallizer outlet pump	Cent.	800	38	CS	CS	3557	130	600	5615	5693	Motor	3	2670
G-110	Stage 1 crystallizer agitator	Propeller	500	60	CS	CS	3663	400	10	2638	2674	Motor	1	398
G-111	Stage 2 crystallizer agitator	Propeller	500	55	CS	CS	3592	400	10	2935	2976	Motor	1	428
G-112	Stage 3 crystallizer agitator	Propeller	500	50	CS	CS	3560	400	10	3252	3297	Motor	1	460
G-113	Stage 4 crystallizer agitator	Propeller	500	45	CS	CS	3556	400	10	3525	3574	Motor	1	487
G-114	Stage 5 crystallizer agitator	Propeller	500	38	CS	CS	3557	400	10	4280	4339	Motor	1	558
												Sum	29	10008

DUCTING

Item No.	Item Name	Type	Tube Design Cond kPa	Tube Design Cond °C	Insulation Mat Of Constr	Insulation Thickness Inches	Duct Dimensions Ht, m	Duct Dimensions Width, m	Duct Dimensions Total Length, m	Total # Req	Total Equip Cost $1,000
L-100	Flue Gas Feed & Exhaust Ducts	Duct	103	60	CS	1	4.5	4.5	1262	1	16731
										Sum	16731
										TOTAL EQUIP COST	**74537**

Table 6-11. Hot-CAP-based CO_2 compression section ME list

VESSELS & TANKS:

Item No.	Item Name	Type	Design Conditions kPa	Design Conditions °C	Material of Construction	Quantity per Lot	Units	Inside Diameter m	Ht or Tan/Tan Length m	Width m	Length m	Number of Lots	Total Equip Cost $1000
C-120	Stg 1 CO2 KO Drum	Vert	1,000	40	304Clad	1	Vessel	2.7	2.6			1	109
C-121	Stg 2 CO2 KO Drum	Vert	1,500	40	304Clad	1	Vessel	2.7	2.6			1	150
C-122	Stg 3 CO2 KO Drum	Vert	3,000	40	304Clad	1	Vessel	2.7	2.6			1	185
C-123	Stg 4 CO2 KO Drum	Vert	6,000	40	304Clad	1	Vessel	2.7	2.6			1	234
												Sum	678

SHELL & TUBE EXCHANGERS AND AIR COOLERS:

Item No.	Item Name	Type	Design P, kPa Shell	Design P, kPa Tube	Des Temp, °C Shell	Des Temp, °C Tube	Material Of Construction Shell	Material Of Construction Tube	Duty MW	Total Bare Tube Area, sq. m	Physical Arrangement In Series	Physical Arrangement In Parallel	Total # Req	Total Equip Cost $1000
E-120	Stg 1 KO Drum Cooler	S&T	1,000	600	190	190	304SS	304SS	12.7	1100	1	1	1	302
E-121	Stg 2 KO Drum Cooler	S&T	1,500	600	190	190	304SS	304SS	11.7	866	1	1	1	286
E-122	Stg 3 KO Drum Cooler	S&T	3,000	600	190	190	304SS	304SS	11.9	737	1	1	1	290
E-123	Stg 4 KO Drum Cooler	S&T	6,000	600	190	190	304SS	304SS	13.9	774	1	1	1	285
E-124	Stg 5 KO Drum Cooler	S&T	10,000	600	190	190	304SS	304SS	26.3	456	1	1	1	206
													Sum	1,369

COMPRESSORS, BLOWERS & DRIVERS:

Item No.	Item Name	Type	Design Conditions kPa	Design Conditions °C	Material Of Construction Wheel or Impel'r	Material Of Construction Casing	Design Capacity Des Flow SCMH	Design Capacity Inlet kPa	Design Capacity Delta P kPa	Design Capacity Comp BHP	Driver HP	Driver Type	Total # Req	Total Equip Cost $1000
K-101	1st Stage CO2 Compressor	Cent.	2,000	40	CS	CS	308515	600	600.0	13025	13677	Motor	1	3,160
K-102	2nd Stage CO2 Compressor	Cent.	4,000	40	CS	CS	306589	1200	1200.0	12660	13292	Motor	1	2,120
K-103	3rd Stage CO2 Compressor	Cent.	6,000	40	CS	CS	305670	2400	2400.0	12005	12606	Motor	1	1,664
K-104	4th Stage CO2 Compressor	Cent.	9,500	40	CS	CS	305312	4800	4200.0	9393	9862	Motor	1	1,580
K-105	5th Stage CO2 Compressor	Cent.	16,600	40	CS	CS	305312	9000	6280.0	3819	4010	Motor	1	1,495
													Sum	10,020

PUMPS & DRIVERS:

Item No.	Item Name	Type	Design Conditions kPa	Design Conditions °C	Material Of Construction Wheel or Impel'r	Material Of Construction Casing	Design Capacity Des Flow LPS	Design Capacity Inlet kPa	Design Capacity Delta P kPa	Design Capacity Pump BHP	Driver HP	Driver Type	Total # Req	Total Equip Cost $1000
													Sum	

PACKAGED & MISC EQUIPMENT:

Item No.	Item Name	Type	Tube Design Cond kPa	Tube Design Cond °C	Mat Of Construct	Design Capacity	Remarks	Total # Req	Total Equip Cost $1000
V-100	TEG Dehydration Package	Pkg						1	1722
								Sum	1722
								TOTAL EQUIP COST	
									13788

Table 6-12. Hot-CAP-based PCC CO_2 capture section total field cost

COST CODE	DESCRIPTION	QTY	MEAS Unit	UNIT COSTS MATL	UNIT COSTS LABOR	UNIT COSTS SC/Other	D HIRE UNIT MH	TOTAL MHRS * S/C	TOTAL MHRS * D HIRE	COSTS IN U.S.$1000 Equipment	COSTS IN U.S.$1000 BULK	COSTS IN U.S.$1000 LABOR	COSTS IN U.S.$1000 SC/Other	COSTS IN U.S.$1000 TOTAL
	PROCESS EQUIPMENT & DUCTWORK													
C	COLUMNS & TOWERS	3	EA							16,461		17,065		33,526
G	PUMPS & DRIVERS	29	EA							9,207		801		10,008
C	VESSELS, TANKS & STORAGE FACILITIES	6	EA							1,472		124		1,596
E	HEAT EXCHANGERS	68	EA							9,959		178		10,138
K	COMPRESSORS, BLOWERS, FANS & DRIVERS	2	EA							2,387		152		2,539
V	PACKAGED EQUIPMENT		EA											
L	DUCTWORK		EA								8,588	8,143		16,731
	FREIGHT	5.00	%							1,974				1,974
	TOTAL PROCESS EQUIPMENT & DUCTWORK		EA							41,460	8,588	26,463		76,511
	INSTRUMENTS													11,176
	PIPING													38,601
	STEELWORK													6,096
	INSULATION													4,743
	ELECTRICAL													19,978
	CONCRETE													7,562
	BUILDING													
	SITEWORK													9,593
	PAINTING													474
	TOTAL OTHER DIRECT COSTS													98,223
	SUBTOTAL DIRECT COSTS													174,734
	SUBTOTAL CONSTRUCTION INDIRECT COSTS													58,187
	SUBTOTAL FIELD COSTS													232,921
	TOTAL (2007 BASIS)													232,921

Table 6-13. Hot-CAP-based PCC CO_2 compression section total field cost

COST CODE	DESCRIPTION	QTY	MEAS Unit	UNIT COSTS MATL	UNIT COSTS LABOR	UNIT COSTS SC/Other	D HIRE UNIT MH	TOTAL MHRS * S/C	TOTAL MHRS * D HIRE	COSTS IN U.S.$1000 Equipment	COSTS IN U.S.$1000 BULK	COSTS IN U.S.$1000 LABOR	COSTS IN U.S.$1000 SC/Other	COSTS IN U.S.$1000 TOTAL
	PROCESS EQUIPMENT & DUCTWORK													
C	COLUMNS & TOWERS		EA											
G	PUMPS & DRIVERS	1	EA											
C	VESSELS, TANKS & STORAGE FACILITIES	4	EA							639		38		678
E	HEAT EXCHANGERS	5	EA							1,343		26		1,369
K	COMPRESSORS, BLOWERS, FANS & DRIVERS	4	EA							9,226		794		10,020
V	PACKAGED EQUIPMENT	1	EA							1,108		614		1,722
L	DUCTWORK		EA											
	FREIGHT	5.00	%							616				616
	TOTAL PROCESS EQUIPMENT & DUCTWORK		EA							12,933		1,472		14,405
	INSTRUMENTS													1,200
	PIPING													4,775
	STEELWORK													661
	INSULATION													647
	ELECTRICAL													3,976
	CONCRETE													1,959
	BUILDING													906
	SITEWORK													1,357
	PAINTING													129
	TOTAL OTHER DIRECT COSTS													15,611
	SUBTOTAL DIRECT COSTS													30,016
	SUBTOTAL CONSTRUCTION INDIRECT COSTS													6,482
	SUBTOTAL FIELD COSTS													36,498
	TOTAL (2007 BASIS)													36,498

Table 6-14. Hot-CAP-based PCC total field cost

COST CODE	DESCRIPTION	QTY	MEAS Unit	UNIT COSTS MATL	UNIT COSTS LABOR	UNIT COSTS SC/Other	D HIRE UNIT MH	TOTAL MHRS * S/C	TOTAL MHRS * D HIRE	COSTS IN U.S.$1000 Equipment	COSTS IN U.S.$1000 BULK	COSTS IN U.S.$1000 LABOR	COSTS IN U.S.$1000 SC/Other	COSTS IN U.S.$1000 TOTAL
	PROCESS EQUIPMENT & DUCTWORK													
	Hot CAP-based CO2 CAPTURE TRAIN 1	1	Train							39,486	8,588	26,463		74,537
	Hot CAP-based CO2 COMPRESSION TRAIN 1	1	Train							12,317		1,472		13,789
	FREIGHT	5.00	%							2,590				2,590
	TOTAL PROCESS EQUIPMENT & DUCTWORK		EA							54,393	8,588	27,935		90,916
	INSTRUMENTS													12,377
	PIPING													43,377
	STEELWORK													6,756
	INSULATION													5,390
	ELECTRICAL													23,954
	CONCRETE													9,521
	BUILDING													906
	SITEWORK													10,950
	PAINTING													603
	TOTAL OTHER DIRECT COSTS													113,834
	SUBTOTAL DIRECT COSTS													204,750
	SUBTOTAL CONSTRUCTION INDIRECT COSTS													64,669
	SUBTOTAL FIELD COSTS (2007 BASIS)													269,419
	TOTAL (2007 BASIS)													269,419

6.4.5 Performance summary of subcritical PC plant with Hot-CAP PCC

According to the design of the Hot-CAP-based PCC process described in Section 3, steam flows are required as a heating source to meet the process needs. Given the 10°C temperature approach, two steam flows with temperatures of 161 and 181°C are designed to be extracted directly from the intermediate-pressure (IP) turbine of the subcritical PC plant (Case 10 in the DOE/NETL report). Because the steam requirement for this Hot-CAP-based PCC plant is different from that in the benchmark MEA-based PCC in Case 10, there are inherent differences related to integration with the steam cycle of the PC plant:

- The steam extraction rates for the PC plant with Hot-CAP-based PCC are 247 tonne/hr with 800 kPa of pressure and 275 tonne/hr with 1,300 kPa of pressure.
- The benchmark MEA-based PCC uses 876 tonne/hr with 507 kPa of steam extracted at the IP/LP crossover line of the Case 10 PC plant.

Therefore, the net power output and thermal efficiency of the subcritical PC plant with Hot-CAP-based CO_2 capture differs from those in Case 10. Table 6-15 summarizes the performance and thermal efficiency of the overall PC plant with Hot-CAP-based PCC and provides a direct comparison with the benchmark MEA-based PCC. The net power output and efficiency of the subcritical PC plant with Hot-CAP CO_2 capture are 609 MWe and 29.0%, respectively, as compared with 550 MWe and 26.2% for MEA-based CO_2 capture.

Table 6-15. Performance summary of the subcritical PC plant with Hot-CAP-based PCC

Plant performance summary*	**Case 10 with MEA-based PCC**	**Case 10 with Hot-CAP PCC**	
Consumables:			
As-received coal feed, kg/hr	278,956	278,956	
Limestone sorbent feed, kg/hr	28,404	28,404	
Thermal input, kWt	2,102,643	2,102,643	
PCC steam extraction:		Steam flow 1	Steam flow 2
Extraction pressure, kPa	507	*800*	*1300*
Extraction temperature, °C	296	*316*	*388*
Flow before de-superheating, 1,000 kg/hr	876	*247*	*275*
Reboiler condensate return temperature, °C	348	*170*	*191*
Power generation summary, kW:			
Steam turbine gross power	672,700	*722,695*	
Auxiliary load summary, kW:			
Coal handling and conveying	540	540	
Limestone handling & reagent preparation	1,370	1,370	
Pulverizers	4,180	4,180	
Ash handling	800	800	
Primary air fans	1,960	1,960	
Forced-draft fans	2,500	2,500	
Induced-draft fans	12,080	12,080	
SCR	70	70	
Baghouse	100	100	
FGD pumps and agitators	4,470	4,470	
Miscellaneous balance of plant	2,000	2,000	
Steam turbine auxiliaries	400	400	
Condensate pumps	700	700	
Ground water pumps	1,020	1,020	
Cooling water circulation pumps[1]	11,190	*8,693*	
Cooling tower fans[1]	5,820	*4,521*	
Transformer losses	2,350	*2,600*	
CO_2 capture plant auxiliaries[2]	22,400	*26,541*	
CO_2 compression	48,790	*39,307*	
Total auxiliaries, kW	**122,740**	**113,852**	
Net power export, kW	**549,960**	**608,843**	
Net plant efficiency, % HHV	**26.2**	***29.0***	
Net plant heat rate, kJ/kWh	**13,764**	***12,454***	
Cooling tower loads, GJ/hr:			
Surface condenser duty	2,034	*2,670*	
CO_2 capture plant cooling duty[3]	3,585	*1,417*	
CO_2 compression cooling duty	Incl. above	*278*	
Total cooling tower loads, GJ/hr	**5,619**	***4,365***	
Overall makeup water balance, m^3/min:			
FGD makeup	5.5	5.5	
BFW makeup	0.4	0.4	
CO_2 capture & compression makeup	0.2	*0.2*	
Cooling tower makeup	36.4	*28.3*	
Net raw water makeup, m^3/min	**42.5**	***34.4***	

Notes:

1. Both surface condenser cooling duty and CO_2 capture cooling duty are assumed to be provided by cooling water in the cooling tower. Thus, auxiliary power uses for cooling water circulation pumps and cooling tower fans are assumed proportional to the total cooling load in the cooling tower.

2. Power uses for cooling water circulation pumps and cooling tower fans are not included; details of other auxiliaries are provided in Table 6-8.
3. The value of cooling duty for the MEA-based PCC is referred to the DOE/NETL report.[2] The cooling duty for the Hot-CAP-based PCC is based on the process simulation.

6.4.6 Capital cost estimate for the subcritical PC plant with Hot-CAP PCC

Table 6-16 shows the total plant capital cost organized by cost account following the format of the DOE/NETL report, based on the cost estimation methodology for the overall subcritical PC plant with Hot-CAP-based PCC, as described in Section 4.1. The engineering, construction management, and home office fees, as well as project and process contingencies, are applied to the TFC (bare erected cost in the DOE/NETL report) to arrive at the total subcritical PC plant with PCC capital cost. The total plant cost for the 550-MWe PC plant equipped with Hot-CAP for 90% CO_2 capture and compression is $1,533 million.

Table 6-16. Capital cost estimate for the subcritical PC plant with Hot-CAP-based PCC

Hot CAP PCC Total Plant Cost Details in U.S.$1000											
Acct No.	Plant Description	Equip Cost	Material Cost	Direct Labor Cost	Indirect Labor Cost	Sales Tax	Bare Erect Cost	Eng'g CM H.O. & Fee	Contingency Process	Contingency Project	Total Plt Cost
1	COAL & SORBENT HANDLING	21,191	5,688	12,662	0	0	39,541	3,548	0	6,463	49,552
2	COAL & SORBENT PREP & FEED	14,465	844	3,675	0	0	18,984	1,664	0	3,097	23,745
3	FEEDWATER & MISC BOP SYSTEMS										
	Feedwater System	20,624	0	7,119	0	0	27,743	2,430	0	4,526	34,699
	Water Makeup & Pretreating	*7,889*	*0*	*2,539*	*0*	*0*	*10,428*	*991*	*0*	*2,284*	*13,703*
	Other Feedwater Subsystems	6,747	0	2,851	0	0	9,598	860	0	1,569	12,027
	Service Water Systems	1,471	0	800	0	0	2,271	214	0	497	2,982
	Other Boiler Plant Systems	8,081	0	7,979	0	0	16,060	1,526	0	2,638	20,224
	FO Supply & Nat Gas	278	0	348	0	0	626	59	0	103	788
	Waste Treatment Equipment	5,087	0	2,900	0	0	7,987	777	0	1,753	10,517
	Misc Equip (Cranes, Air Comp, etc)	2,955	0	903	0	0	3,858	371	0	846	5,075
4	PC BOILER	171,007	0	109,973	0	0	280,980	27,374	0	30,835	339,189
5	FLUE GAS CLEANUP	107,581	0	36,768	0	0	144,349	13,816	0	15,817	173,982
5B1	*Hot CAP CO2 REMOVAL SYSTEM*	*41,460*	*75,627*	*115,834*	*0*	*0*	*232,921*	*22,127*	*46,584*	*60,327*	*361,959*
5B2	*CO2 COMPRESSION & DRYING*	*12,933*	*10,793*	*12,772*	*0*	*0*	*36,498*	*3,467*	*0*	*7,993*	*47,958*
6	COMBUSTION TURBINE/ACCESSORIES	N/A	N/A	N/A	0	0	0	0	0	0	0
7	HRSG, DUCTING & STACK	19,509	1,069	13,214	0	0	33,792	3,095	0	4,848	41,735
8	STEAM TURBINE GENERATOR										
	Steam TG & Accessories	55,209	0	6,905	0	0	62,114	5,951	0	6,806	74,871
	Turbine Plant Auxiliaries	387	0	828	0	0	1,215	119	0	133	1,467
	Condenser & Auxiliaries	*6,471*	*0*	*2,680*	*0*	*0*	*9,151*	*869*	*0*	*1,002*	*11,022*
	Steam Piping	*21,345*	*0*	*10,524*	*0*	*0*	*31,869*	*2,659*	*0*	*5,179*	*39,707*
	TG Foundations	0	1,213	1,917	0	0	3,130	296	0	685	4,111
9	COOLING WATER SYSTEM										
	Cooling Tower	*13,961*	*0*	*4,347*	*0*	*0*	*18,309*	*1,739*	*0*	*2,005*	*22,053*
	Circulating CW Pump	*2,905*	*0*	*218*	*0*	*0*	*3,123*	*264*	*0*	*339*	*3,726*
	Circulating CW Syst Aux	*703*	*0*	*94*	*0*	*0*	*797*	*76*	*0*	*87*	*960*
	Circulating CW Piping	*0*	*5,575*	*5,403*	*0*	*0*	*10,978*	*1,043*	*0*	*1,803*	*13,824*
	Makeup Water System	*586*	*0*	*784*	*0*	*0*	*1,370*	*130*	*0*	*225*	*1,725*
	Closed CW System	*823*	*0*	*655*	*0*	*0*	*1,478*	*140*	*0*	*243*	*1,861*
	Circ CW Syst Foundations & Structures	*0*	*3,307*	*5,253*	*0*	*0*	*8,560*	*813*	*0*	*1,875*	*11,248*
10	ASH/SPENT SORBENT HANDLING SYS	5,525	176	7,387	0	0	13,088	1,258	0	1,477	15,823
11	*ACCESSORY ELECTRIC PLANT*	*27,283*	*11,626*	*32,922*	*0*	*0*	*71,832*	*6,393*	*0*	*9,966*	*88,190*
12	INSTRUMENTATION & CONTROL	9,942	0	10,082	0	0	20,024	1,816	1,001	2,805	25,646
13	IMPROVEMENT TO SITE	3,344	1,922	6,739	0	0	12,005	1,184	0	2,638	15,827
14	BUILDING & STRUCTURES	0	25,775	24,432	0	0	50,207	4,529	0	8,210	62,946
	TOTAL COST	**589,763**	**143,615**	**451,508**			**1,184,885**	**111,600**	**47,585**	**189,073**	**1,533,143**

6.4.7 O&M cost estimate for the subcritical PC plant with Hot-CAP PCC

According to Section 4.1, the annual O&M cost consists of two components: the fixed O&M, which is independent of the power generation, and the variable O&M, which is proportional to the power generation and is estimated based on an 85% annual capacity factor.

The costs of consumables are escalated to 2010, the year when construction would be completed. The annual escalation factor for all consumables, excluding fuel, is 1.87%. For the Illinois No 6 coal, the annual escalation factor is 2.35%.

The annual variable O&M costs, including consumables such as fuel, water, and chemicals, as well as waste disposal costs, are determined based on the rates of consumption, the unit cost of each commodity, and the total annual operating hours. Because half of the net raw water makeup comes from groundwater, the water expenditure was calculated based on one-half of the net raw water makeup from the overall plant water balance. PC plant-related chemical expenditures are independent of the PCC and follow the Case 10 consumptions in the NETL/DOE report.

PCC-dependent chemicals include the piperazine promoter, active carbon for the piperazine filter, and the K_2CO_3 solvent. Different from Case 10, no sulfur-polishing facility is used before CO_2 capture in the Hot-CAP. Instead, the remaining SO_2 in the flue gas from the FGD reacts directly with K_2CO_3 in the absorber, resulting in a degradation loss of K_2CO_3 solvent. The K_2CO_3 solvent replacement cost is thus estimated based on the total degradation rate caused by the reaction with SO_2, which was quantified by the assumption that the same amount of sulfur as that in Case 10 of the DOE/NETL report (i.e., 137 kg/hr) is removed in the Hot-CAP absorber. A corrosion inhibitor is not required because of the assumption that Hot-CAP is less corrosive than MEA.

The total estimated annual O&M cost for the subcritical PC plant with Hot-CAP-based PCC is $175 million. Table 6-17 shows a breakdown of the O&M costs in a format similar to that in the DOE/NETL Case 10 report.

Table 6-17. O&M costs of the subcritical PC plant with Hot-CAP-based PCC*

Fixed Operating Expenses:			**Expense**
Annual Operating Labor Cost			$6,134,700
Maintenance Labor Cost			$10,057,417
Administration & Support Labor			$4,048,029
Property Taxes and Insurance			$30,662,856
Total Fixed Operating Costs			**$50,903,001**
Variable Operating Expenses:			
Maintenance Material Cost			$15,086,125
Consumables	Consumption/day	Unit Cost	
Water (/1,000 gallons)	6539	1.08	$2,191,095
Chemicals:			
MU & WT Chemicals (lb)	39119	0.17	$2,100,447
Limestone (ton)	751	21.63	$5,043,346
Carbon for Mercury Removal (lb)	0	1.05	$0
Piperazine Promotor (lb)	500	4.54	$704,392
K_2CO_3 Solvent (ton)	15.60	544.20	$2,633,874
NaOH (ton)	0	433.68	$0
H_2SO_4 (ton)	0.67	138.78	$28,789
Corrosion Inhibitor	0	0	$0
Act Carbon (lb)	168	1.05	$54,728
Ammonia (19% NH_3)(ton)	110	129.8	$4,446,378
SCR Catalysts (m^3)	0.46	5775.94	$831,516
Waste Disposal:			
Flyash (ton)	572	16.23	$2,881,846
Bottom Ash (ton)	143	16.23	$720,462
Gypsum (ton)	1,159	0	$0
AR Coal Feed	7,380	38.18	$87,425,787
Total Variable Operating Costs			**$124,148,784**
TOTAL ANNUAL OPERATING COSTS			**$175,051,786**

* 1 lb = 0.454 kg, 1 gallon= 3.79 liter, and 1 ton (short ton) = 908 kg.

6.4.8 LCOE estimate for the subcritical PC plant with Hot-CAP PCC

The estimated LCOE for the subcritical PC plant with Hot-CAP-based PCC using the methodology described in Section 4.1, and a comparison with the corresponding values in Cases 9 and 10 of the DOE/NETL report are listed in Table 6-18. The LCOE of the Hot-CAP PCC-based PC plant is 120.3 mills/kWh, a 60% increase over the LCOE (75.3 mills/kWh) of the same PC plant without CO_2 capture. Compared with a 139.0 mills/kWh LCOE for the MEA PCC-based PC plant, the increase in LCOE caused by CO_2 capture with the Hot-CAP is 29% lower than that with the benchmark 30 wt% MEA.

Table 6-18. LCOE estimate for the subcritical PC plant with Hot-CAP-based PCC

Postcombustion Case Description	Subcritical PC w/o CO_2 Capture	Subcritical PC w/ CO_2 Capture	
Case Number	**Case 9**	**Case 10**	**This Study**
Type of CO_2 Capture Technology	**N/A**	**Econoamine**	**Hot CAP**
Capital Cost Year	2007	2007	2007
CO_2 Capture	0%	90%	90%
Power Production, MW			
Gross Power	583	673	723
Net Power	550	550	609
Cost			
Total Plant Cost, 2007$/kW	1,662	2,942	2,518
Total Overnight Cost, 2007$/kW	1,996	3,610	3,085
Bare Erected Cost	1,317	2,255	1,946
Home Office Expenses	124	213	183
Project Contingency	182	369	311
Process Contingency	0	105	78
Owner's Costs	374	667	567
Total Overnight Cost, 2007$ x 1000	1,098,124	1,985,432	1,878,100
Total As Spent Capital, 2007$/kW	2,264	4,115	3,517
COE (mills/kWh, 2007$)	59.4	109.6	94.8
CO_2 TS&M Costs	0.0	5.8	5.2
Fuel Costs	15.2	21.3	19.3
Variable costs	5.1	9.2	8.1
Fixed Costs	7.8	13.1	11.2
Capital Costs	31.2	60.2	51.0
LCOE (excld. CO_2 TS&M), mills/kWh	**75.3**	**139.0**	**120.3**
% of Case 9 LCOE - Compare to 2007	**100%**	**185%**	**160%**

6.4.9 LCOE sensitivity analysis

A sensitivity analysis was conducted to evaluate the uncertainties associated with equipment costs and chemical prices, and the effects of operation conditions or processing technologies on the LCOE of the PC power plant with Hot-CAP PCC. The Hot-CAP case described above was used as a baseline. The cost sensitivity to any changes in cost estimates is indicated by LCOE changes over the baseline. The following Hot-CAP cases were examined in the sensitivity analysis:

1) A deep level of desulfurization is achieved with a polishing scrubber before the flue gas enters the Hot-CAP absorber. This will require an additional capital cost for the new scrubber and incur a change in the O&M cost owing to the increased NaOH consumption and reduced K_2CO_3 consumption.

2) The stripping pressure is elevated from 6 to 8 bar (5.92 to 7.90 atm). A higher stripping pressure will affect both the energy consumption and the capital cost of the stripping column.
3) The capital cost of the crystallization system varies from –50 to +100% of that in the baseline. This will affect the overall cost performance of the Hot-CAP.
4) The power consumption for slurry agitation in the crystallization process varies from –50 to +100% of that in the baseline. A change in auxiliary load of the Hot-CAP is expected.
5) The absorber capital is varied by –50 to +100% of that in the baseline. This change will affect the capital cost of PCC CO_2 capture.
6) The price of K_2CO_3 varies from –50 to +100% of that in the baseline. A solvent price change will affect the O&M cost.

6.4.9.1 Sensitivity to use of a polishing scrubber for deep desulfurization

To be consistent with Case 10 in the DOE/NETL report, the subcritical PC plant with Hot-CAP-based PCC utilizes a polishing scrubber to reduce the SO_x level in the flue gas below 1 ppmv before it enters the Hot-CAP absorber. At such a low SO_x concentration, nominal losses of K_2CO_3 attributable to the reaction with SO_x are minimized. It is assumed that the rate of K_2CO_3 degradation is determined stoichiometrically via reaction with the remaining SO_x. The resultant differences between the baseline and the PCC with a new polishing scrubber include the following:

- The polishing scrubber is 14.8 m in diameter and 7.3 m in depth of the 3.5-in. (8.9 cm) Pall ring packing;
- A new circulation pump is required to convey 4,918 m^3/hr of a NaOH aqueous solution;
- The O&M cost has changed with an increased consumption of 7.89 ton/day (7.16 tonne/day) of NaOH and a reduced consumption of 15.26 ton/day (13.86 tonne/day) of K_2CO_3; and
- The auxiliary load for the PCC increases from 26.54 MWe (baseline) to 27.56 MWe.

With these changes applied to the baseline, the LCOE for the subcritical PC plant with PCC is 124.9 mills/kWh, which is a 3.8% increase over the baseline, or a 66% increase over the plant without CO_2 capture. This result indicates that using a polishing scrubber for a deep level of desulfurization will incur a significant increase in LCOE compared with the baseline Hot-CAP.

6.4.9.2 Sensitivity to stripping pressure

Elevating the stripping pressure will affect the overall CO_2 capture performance by affecting the required CO_2 compression work and the quantity and quality of steam use. In the sensitivity analysis, the operating pressure in the stripping column is increased from the baseline 6 bar (5.92 atm) to 8 bar (7.90 atm):

- Compared with the baseline, the pressure and temperature of steam required in the 8-bar (7.90-atm) stripping case are higher. The required steam to the heater prior to the stripper (Figure 6-13) is at 10.75 bar (10.61 atm) and amounts to 165 tonne/hr, compared with 8 bar (7.90 atm) and 247 tonne/hr in the baseline. The steam to the reboiler (Figure 6-13)

amounts to 306 tonne/hr at 16.30 bar (16.09 atm) compared with 275 tonne/hr at 13.00 bar (12.83 atm) in the baseline. The total amount of steam usage is reduced, but the steam quality is raised.

- The required CO_2 compression power is reduced from 39.3 MWe in the baseline to 35.0 MWe in the case of 8-bar (7.90-atm) stripping.
- The required slurry pump power slightly increases from 2.3 MWe in the baseline to 2.6 MWe owing to the pressure increase.
- The temperature of the feed solution entering the stripper is 173°C, higher than the baseline (161°C). The temperature of the regenerated lean solution exiting the stripper is increased to 192°C compared with 181°C in the baseline. The temperature of the feed slurry is the same (64°C) as the baseline. An increase in temperature difference between the hot regenerated solution and the cold feed solution in the case of 8-bar (7.90 atm) stripping leads to an increase in heat duty of the cross-heat exchangers. However, a fraction of CO_2 and water evaporates at high temperature during heat exchange; thus, the outlet temperature of the rich solvent will be brought down by the phase change. The higher the temperature, the higher the evaporation fraction. As a result, the temperature approach at the hot end of the heat exchanger increases with increasing temperature of the regenerated lean solution from the stripper, which will be beneficial for reducing the size of the heat exchanger. In sum, the temperature increase affects the capital cost of the heater prior to the stripper, cross-heat exchangers, and reboiler.

When these changes from the baseline are applied, the LCOE for the PC plant with Hot-CAP operating at an 8-bar (7.90 atm) stripping pressure is estimated to be 119.0 mills/kWh, which is a 1.1% decrease over the baseline, or a 58% increase over the subcritical PC plant without CO_2 capture. This result indicates that increasing the operating pressure of the stripping column will only slightly reduce the LCOE.

6.4.9.3 Sensitivity to the crystallization equipment cost

Uncertainties are associated with the construction cost for concrete crystallizers and accessories. To examine their effect on the LCOE, the capital costs for major crystallization equipment, including hydrocyclones and crystallizer agitators, but excluding low-risk commercial equipment such as pumps and coolers, are varied by –50 to +100% of those in the baseline.

The LCOE results from the sensitivity analysis are shown in Figure 6-14. It can be seen that the LCOE increases with the increase in capital cost of the crystallization system. However, such an effect is limited, because the LCOE increases by only 0.8% even when the capital cost of the major crystallization equipment doubles.

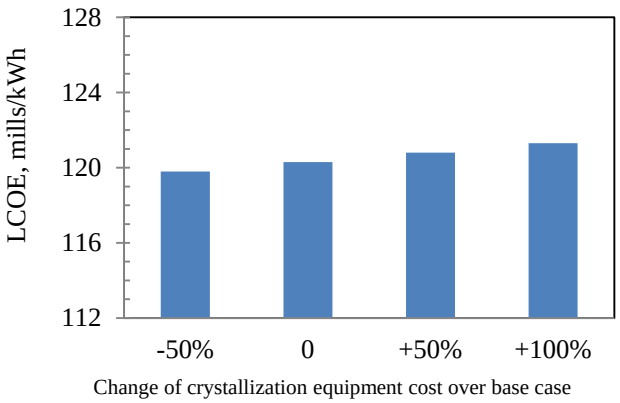

Figure 6-14. Effect of the major crystallization equipment cost on the LCOE.

6.4.9.4 Sensitivity to power consumption for crystallization

Uncertainties are also present in estimating the power consumption for agitating facilities used in the crystallization operation. The power use for slurry agitation can be optimized for the best crystallization performance. To examine its effect on the LCOE, the agitation power was varied by –50 to +100% from the baseline estimate. The auxiliary load and the net power production of the PC plant will vary with such variations in agitation power use.

As shown in Figure 6-15, the LCOE increases with an increase in power consumption for the crystallization process. The LCOE is increased by 2.1% (2.5 mills/kWh) when the power consumption for crystallization agitation doubles.

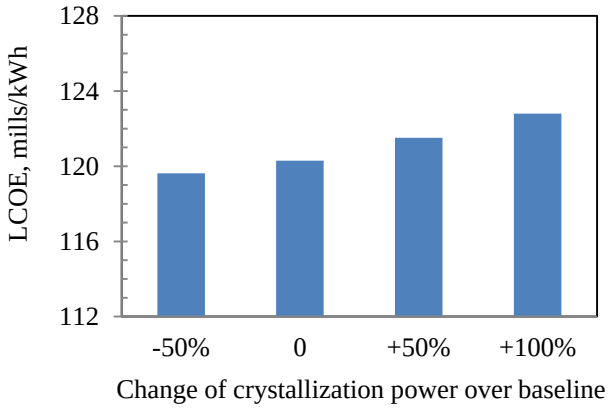

Figure 6-15. Effect of the crystallization agitation power use on the LCOE.

6.4.9.5 Sensitivity to the absorber capital cost

The absorption process may be further optimized for the best performance. For instance, a change in the lean/rich loading or the solvent circulation rate may affect the sizing of the absorber, which will eventually affect the capital cost of the absorber. To examine its effect on the LCOE, the capital cost of the absorber was varied by –50 to +100% of that in the baseline. The capital cost of PCC CO_2 capture will vary accordingly with the change in absorber capital.

The LCOE results from the sensitivity analysis are shown in Figure 6-16. The LCOE is very sensitive to the absorber capital, because of its large weight in the total PCC capital. The LCOE increases with an increase in the absorber capital cost. The LCOE is increased by 5.3% (6.4 mills/kWh) when the capital cost doubles.

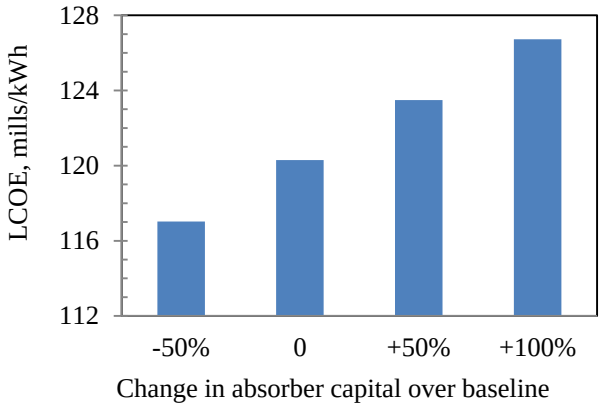

Figure 6-16. Effect of the absorber capital on the LCOE.

6.4.9.6 Sensitivity to the price of K_2CO_3

The range in market price of K_2CO_3 varies widely, from $200 to $1,200/tonne. An average K_2CO_3 price ($544/ton /$494/tonne) was adopted in the baseline. Assuming the K_2CO_3 price deviates by –50 to +100% of the price in the baseline, the annual O&M costs for the PC power plant with PCC will be affected.

Figure 6-17 shows that the LCOE increases only slightly with an increase in the K_2CO_3 price. However, the LCOE is not markedly affected by the K_2CO_3 price. The LCOE is increased by merely 0.6% (0.7 mills/kWh) when the K_2CO_3 price doubles.

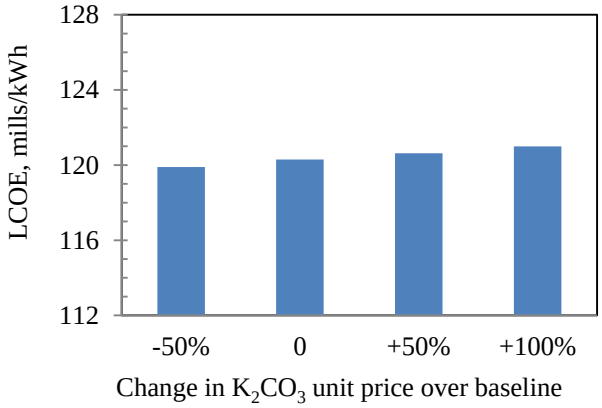

Figure 6-17. Effect of the unit price of K_2CO_3 on the LCOE.

6.5 Summary

A TEA was performed to compare the energy use and cost performance of a nominal 550-MWe subcritical PC plant without CO_2 capture (DOE/NETL Case 9) with the benchmark MEA-based

PCC (DOE/NETL Case 10) and the Hot-CAP-based PCC. The results show that the net power produced in the PC plant equipped with Hot-CAP is 609 MWe, greater than that with MEA (550 MWe) owing to the reduced steam demand for CO_2 stripping.

The Hot-CAP has a slightly lower capital cost ($48 million) for CO_2 compression compared with the MEA-based PCC ($50 million), because the stripped product gas has a higher pressure (6 bar/5.92 atm vs. 1.6 bar/1.58 atm). The Hot-CAP also has a lower capital cost in the CO_2 capture section ($362 million) compared with the MEA-based PCC ($443 million), because it requires a smaller stripping column and does not use an upstream polishing unit for deep sulfur removal prior to CO_2 capture.

O&M costs for the PC plant equipped with Hot-CAP are estimated to be $175 million annually, less than that for the PC plant with MEA ($178 million). The loss of K_2CO_3 solvent incurred by the reaction with SO_2 is included in the analysis.

The 20-year LCOE for the PC plant with Hot-CAP, including CO_2 transportation and storage, is 120.3 mills/kWh, a 60% increase over the base PC plant without CO_2 capture. The LCOE increase caused by CO_2 capture for the Hot-CAP is 29% lower than the benchmark MEA-based process.

Results of the sensitivity analysis indicate that the PC plant LCOE is quite sensitive to the capital cost of the absorber, the use of a new polishing scrubber for deep desulfurization, and the power consumption for crystallization. However, the LCOE is not markedly affected by the price of the K_2CO_3 solvent, the crystallization equipment cost, and the stripping pressure increase.

References

1. DOE/NETL DE-FOA-0000403. *Attachment 3—Basis for Technology Feasibility Study* (January 31, 2011).
2. DOE/NETL. *Cost and Performance Baseline for Fossil Energy Plants, Volume 1: Bituminous Coal and Natural Gas to Electricity* (Revision 2, November 2010), NETL Report No. DOE/NETL-2010/1397.
3. Chemstations, Inc. *ChemCad Version 6 User Guide*, 2012. http://www.chemstations.com/content/documents/CHEMCAD_6_User_Guide_2012.pdf
4. Otimeas Treating, Inc. *The Origins of ProTreat™. The Contactor*. Vol. 3 Supplement. October 2, 2009.
5. Nexant Inc. *Techno-Economic Study Results & Methodology for Post-Combustion Flue Gas CO_2 Capture Using Gas Pressurized Stripping Technology* (October 2012) [report].

Chapter 7. Conclusions and Recommendations

7.1 Conclusions

The Hot Carbonate Absorption Process with Crystallization-Enabled High-Pressure Stripping (Hot-CAP) developed in this project presents a unique approach that uses a concentrated carbonate salt solution (e.g., K_2CO_3) for CO_2 absorption and a bicarbonate slurry (e.g., $KHCO_3$) from a crystallization step for CO_2 stripping at an elevated pressure to overcome the energy use and other disadvantages associated with the benchmark monoethanolamine (MEA) process. The project was aimed at performing laboratory- and bench-scale experiments to prove its technical feasibility and generate process engineering and scale-up data, and conducting a techno-economic analysis (TEA) to demonstrate its energy use and cost competitiveness over MEA.

Accordingly, the proof-of-concept study sought technical solutions to the following questions or process risks:

- Is the overall rate of CO_2 absorption into a potassium carbonate/bicarbonate (PCB) solution under Hot-CAP operating conditions comparable with that into 5 M MEA?
- Is the crystallization rate fast enough (e.g., less than a 1-hr residence time in the crystallizer)?
- Can the CO_2 stripper operate at high pressure (e.g., ≥10 bar/9.9 atm)?
- Can SO_2 removal be combined with CO_2 capture by reclamation of the sulfate formed from the desulfurization reaction?
- Can fouling on the surfaces of the heat exchangers and crystallizer units caused by bicarbonate crystallization be prevented?
- Can the stripper be designed to handle slurry and operate at a high pressure?

A combination of experimental, modeling, process simulation, and cost analysis studies were performed to obtain detailed information to address the aforementioned questions. The major conclusions of the project are as follows: (1) major reactions and individual unit options involved in the Hot-CAP are thermodynamically- and kinetically-feasible, and (2) the Hot-CAP is energy-efficient and cost-effective compared with the benchmark MEA process. For integration of the Hot-CAP into a 550-MWe pulverized coal (PC)-fired power plant, the increase in cost of electricity (COE) is approximately 30% lower than that for MEA.

More detailed results and conclusions from those studies are summarized below.

Identification of promoters/catalysts for CO_2 absorption into PCB. Three Lewis base inorganic catalysts, five amines, and five amino acid salts were evaluated as promoters to accelerate the CO_2 absorption rates into a concentrated 40 wt% PCB solution at 60 to 80°C using a batch stirred tank reactor (STR).

- The addition of 4 wt% CAT1 or CAT2 Lewis base catalyst into a 40 wt% PCB with 20% CTB conversion (PCB40-20) approximately doubled the rates at 60, 70, and 80°C. However, the rates were still several times slower than those into a 3 M MEA solution at 50°C.

- The five amines tested increased the absorption rates into the PCB solution at 70°C by 3.5-to-50 times. Rates promoted with piperazine (PZ) and aminomethyl propanol (AMP) were the highest, followed by hexamethylenediamine (HDA). Rates into the lean PCB40-20 solution promoted with 1 M PZ, AMP, or HDA at 70°C were greater than or comparable with those into a lean 5 M MEA solution loaded with 0.2 mol of CO_2/mol of MEA at 50°C.

- Among the tested amino acid salts, the rates into both PCB40-20 and PCB40-40 promoted by K-sacrosine and K-glycine were more significant than those promoted by K-proline. Compared with the rate into the lean 5 M MEA, the promoted rates into the PCB40-20 were significantly lower. However, the rate difference between the promoted lean and rich PCB was much less substantial than that for MEA.

Performance of CO_2 absorption in a packed-bed column. A bench-scale packed-bed column of 3 m in height and 10 cm in internal diameter (I.D.) was fabricated to investigate the kinetic performance of CO_2 absorption into 40 wt% PCB solution without or with a promoter.

- Results confirmed that in the column, the CO_2 removal rate into PCB increased as the L/G ratio increased, as the promoter dosage increased, as the CO_2 loading decreased, or as the inlet CO_2 concentration decreased. The precipitation of $KHCO_3$ occurred when the CTB conversion in the feed PCB solution reached 40 to 45%. However, the accumulation of precipitates in the solution did not result in a pronounced decrease in CO_2 removal efficiency.

- The use of PZ, AMP, and diethanolamine (DEA) as promoters greatly increased the rate of CO_2 removal into the PCB solution. Among the promoters tested, the addition of PZ was the most effective. The 40 wt% PCB solution promoted with 0.5 M PZ at 70°C performed 1-to-3 times better than 5 M MEA at 50°C at the representative lean loading levels, and performed 3-to-5 times better at the rich CO_2 loading levels when all other conditions were the same.

- If desired, a sodium carbonate/bicarbonate (SCB) or a PCB/SCB mixture solution can potentially be used as an alternative to a PCB solution as the solvent. $NaHCO_3$ may be crystallized more easily than $KHCO_3$ from the CO_2-rich solution via cooling crystallization to form a $NaHCO_3$-based slurry that can be used for CO_2 stripping at a higher pressure than can a $KHCO_3$ slurry. A 15 wt% SCB solution (limited to its solubility) promoted with 0.5 M PZ exhibited a higher CO_2 removal efficiency at 70°C than 5 M MEA at 50°C within the corresponding CO_2 loading range.

- Promoted mixtures with similar total PCB/SCB concentrations revealed comparable CO_2 removal efficiencies, whereas at the same total concentration, the one with a higher PCB concentration showed slightly higher CO_2 removal efficiency. A mixture of 25 wt% PCB and 10 wt% SCB promoted with 0.5 M PZ had a CO_2 removal efficiency at 70°C comparable

with that of the promoted 40 wt% PCB, which was significantly higher than 5 M MEA at 50°C.

Kinetic behavior of bicarbonate crystallization. A kinetic study of the crystallization of $KHCO_3$ from the CO_2-rich PCB solution was performed using a continuous STR system under the mixed-suspension–mixed-product-removal (MSMPR) mode.

- The rate of $KHCO_3$ crystal growth was size dependent, increasing with increasing particle size and then leveling off when a certain critical size was reached (~600 μm). The crystallization of $KHCO_3$ was kinetically fast and could be completed within a residence time of as little as 15 min. A longer residence time decreased the overall rates of both nucleation and crystal growth but resulted in larger crystal particles. An increase in agitation speed enhanced the nucleation process but slowed crystal growth, which resulted in an overall reduction in crystal size. A higher level of supersaturation favored crystal growth and the formation of larger particles. The presence of PZ in the PCB solution accelerated crystallization.

- A three-parameter, size-dependent crystal growth model was developed for the PCB system to describe the rates of $KHCO_3$ crystal growth and nucleation and to predict the mean crystal size. The model was applied to perform a crystallizer sizing analysis based on a configuration of five crystallization units operating in sequence for the Hot-CAP equipped in a 609-MWe (net) power plant. A total crystallizer volume of approximately 3,200 m^3 (equivalent to a total residence time of 11 min) was found to be sufficient.

When a PCB/SCB mixture is used as a solvent, $NaHCO_3$ is preferentially crystallized out and used for CO_2 stripping. The feasibility of two process concepts for $NaHCO_3$ crystallization was investigated.

- The first process involves mixing the PCB-dominant mixture exiting the absorber with the SCB solution regenerated from the stripper to crystalize $NaHCO_3$ via cooling. X-ray diffraction (XRD) analyses indicated that the composition of the crystal particles depended on the composition of the PCB/SCB solution: the higher the total SCB concentration in the feed PCB/SCB mixture, the higher the content of nahcolite ($NaHCO_3$) in the crystal solids. The mass mean size of $NaHCO_3$ crystal particles (80 to 130 μm) was several times smaller than that of $KHCO_3$ particles (~400 μm).

- The second process involves the reactive crystallization of $NHCO_3$ in the regenerated SCB solution with the addition of $KHCO_3$ solids (formed from the cooling crystallization of the PCB-dominant mixture solution exiting the absorber). XRD analyses revealed that the crystal samples contained three crystallite phases: nahcolite, kalicinite, and trona. In all crystal products, nahcolite was dominant (>81 wt%) and kalicinite was insignificant (<5 wt%), indicating that it is feasible to crystalize $NaHCO_3$ through the reaction between solid $KHCO_3$ and aqueous Na_2CO_3 under the test conditions.

In addition, solubility data for the PCB, SCB, and PCB/SCB mixture solutions at various concentrations, CO_2 loading levels in solution, and temperatures were measured using a

turbidity-based approach. Such data are either unavailable or incomplete in the literature, but are required for identifying the design and operating conditions desired for the crystallization process.

Phase equilibrium behavior of PCB systems at high temperatures. The vapor–liquid equilibrium (VLE) data were measured for the 40, 50, and 60 wt% PCB solutions with CTB conversion levels ranging from approximately 20 to 85% at 140 to 200°C.

- The partial pressure of CO_2 increased substantially with increasing temperature and CTB conversion in the PCB solution, whereas the partial pressure of water vapor increased moderately with increasing temperature, but decreased slightly with increasing CTB conversion. The concentration of PCB solution (40 to 60 wt%) did not substantially affect the partial pressure of CO_2, but remarkably reduced the partial pressure of water vapor.

- A higher operating temperature, high PCB concentration, and higher CTB conversion level in solution were thus favored to obtain a higher total pressure and lower H_2O/CO_2 partial pressure ratio. For example, over the 60 wt% PCB with 83% CTB conversion at 200°C, the total pressure reached 507 psia (34.5 atm), and the ratio of H_2O/CO_2 partial pressure was 0.11:1. A high stripping pressure and a lower H_2O/CO_2 pressure ratio can result in a significant reduction in energy use, and the results indicated an energy use advantage by using a concentrated bicarbonate-dominant slurry for CO_2 stripping.

Performance of CO_2 stripping in a bench-scale stripping column. A bench-scale, packed-bed stripping column system with an I.D. of 1 in. (2.54 cm) and a height of 7 ft (2.1 m) rated at 200°C and 500 psia (34.0 atm) was fabricated in this study. Parametric tests were conducted to investigate the performance of CO_2 stripping under various conditions. The heat duty required for CO_2 stripping was determined based on heat usage for CO_2 desorption, water vaporization, and heating of the PCB solution.

- A higher stripping temperature favored a deeper level of $KHCO_3$ regeneration from the PCB solution/slurry. The change in CTB conversion through the 7-ft (2.1-m) column varied from 1 to 20 percentage points. As the stripping temperature was increased, both the partial pressure of CO_2 in the product gas stream and the total stripping pressure increased, whereas the CO_2/H_2O pressure ratio in the product gas decreased only slightly. A high CTB conversion in the feed or a high concentration of PCB, which is unique to the Hot-CAP, increased both the total stripping pressure and the CO_2/H_2O pressure ratio in the product gas. For example, the stripping pressure attained even with the PCB60-40 feed solution was 180 psia (12.2 atm) at 200°C.

- Increasing either the PCB concentration or CTB conversion in the PCB feed solution could significantly decrease the heat use for CO_2 stripping. Increasing the temperature was beneficial to reduce the total stripping heat use for the PCB system. The total heat use for CO_2 stripping from a rich 5 M MEA feed solution (loaded with 0.475 mol of CO_2/mol of MEA) varied from 4,300 to 6,200 kJ/kg of CO_2 when the obtained lean CO_2 loading varied from 0.37 to 0.2 mol of CO_2/mol of MEA. In comparison, the heat duty for CO_2 stripping

from the 30 to 50 wt% PCB feed solutions with 80% CTB conversion was two-to-three times lower.

- The presence of K_2SO_4 (1 wt%) and PZ (0.2 M) in the PCB solution did not noticeably affect the performance of CO_2 stripping. In comparison, a deeper level of $KHCO_3$ regeneration and a higher pressure were achieved in the presence of 0.5 M MDEA. The addition of MDEA in the PCB solution also decreased the heat use for CO_2 stripping. For example, the heat use was reduced by 69% for the PCB30-60 feed solution when 0.5 M MDEA was present. MDEA is regarded as a favorable additive for CO_2 stripping from the hot PCB solution.

Feasibility of sulfate reclamation for combining SO_2 removal with CO_2 capture. A process concept involving two reaction steps was initially proposed to reclaim the desulfurization product, K_2SO_4, from the PCB solution. The first step is to reduce the CO_3^{2-} concentration using a high-pressure CO_2 gas stream, and the second is to selectively precipitate $CaSO_4$ over $CaCO_3$ using lime. Batch and semi-continuous tests were performed to study the feasibility for K_2SO_4 reclamation.

- When the PCB concentration was above 0.2 M (2.7 wt%) or the reaction temperature was greater than 50°C, only $CaCO_3$ crystallite phases were formed. Improving the gas–liquid interface and mixing via CO_2 gas bubbling increased the $CaSO_4$ content from 1.5% gypsum + 42.3% syngenite to 8.6% gypsum + 91.4% syngenite in the precipitate particles obtained from the reactions of 0.2 M Ca^{2+} in the 0.2 M PCB + 0.4 M K_2SO_4 solution for 1 hr at room temperature. A reaction mechanism was suggested that explained well the competitive precipitation of $CaSO_4$ over $CaCO_3$.

- The precipitate particles obtained from the reactions of 0.4 M Ca^{2+} in either a 0.2 M $NaHCO_3$ + 0.4 M Na_2SO_4, or a 0.1 M $KHCO_3$ + 0.1 M $NaHCO_3$ + 0.2 M Na_2SO_4 + 0.2 M K_2SO_4 solution contained almost 100% gypsum phase, whereas those in a 0.2 M $KHCO_3$ + 0.4 M K_2SO_4 solution contained 8.6% gypsum and 91.4% syngenite under comparable operating conditions. This result suggests that the presence of sodium instead of potassium ions favored the competitive precipitation of $CaSO_4$ over $CaCO_3$ by prohibiting the formation of syngenite.

To overcome the limitation to the use of a low-concentration PCB and a low operating temperature and thus improve the compatibility of SO_2 removal with CO_2 capture, a modified process was proposed. The new process consists of SO_2 scrubbing using the CO_2-rich PCB solution from the Hot-CAP absorber, the oxidation of K_2SO_3 into K_2SO_4 in a forced-air unit, and the precipitation and separation of K_2SO_4 (because of its low solubility compared with other potassium salts) from the solution.

- Precipitate solids containing 100% K_2SO_4 were obtained from the oxidation of 10 wt% K_2SO_3 in PCB20-40 at 70°C, which was desirable for the modified process. Precipitate solids obtained from PCB40-40 contained approximately 70 wt% K_2SO_4 and 30 wt% $KHCO_3$, indicating that solvent loss might occur when the CO_2 loading in the 40 wt% PCB for SO_2 removal is too high.

- The rates of sulfite oxidation ranged from the order-of-magnitude of 10^{-6} to 10^{-5} mol/m^2·s under the investigated conditions (1 to 10 wt% sulfite concentrations, 50 to 70°C, and 3 to 13 psia/20.7 to 89.6 kPa of O_2 pressure). The rate depended considerably on the temperature and oxygen pressure (first-order), but did not vary appreciably with the sulfite concentration (almost zero-order).

- The results of the equilibrium composition and rate of the K_2SO_3 oxidation reaction indicated the feasibility of the modified process, but further investigation is needed.

Techno-economic performance of the Hot-CAP. In addition to the experimental studies, a technology-focused risk mitigation analysis was conducted to address the related technical questions mentioned.

- Discussions with vendors indicated that fouling of the cross-flow heat exchangers and the cooler inside the crystallizer, owing to possible $KHCO_3$ scaling on equipment surfaces, can be solved by a variety of available engineering solutions, such as pre-seeding and reducing the temperature difference between the inlet and outlet streams.

- The conventional crystallizer design requires a large temperature difference between the inlet solution (solution entering the crystallizer) and the mother liquor (solution leaving the crystallizer), jeopardizing the heat recovery from the incoming solution from the absorber. Thus, a configuration of five consecutive continuous STR-type crystallization tanks is used instead of a single crystallizer. This new configuration reduces the temperature difference between the inlet and outlet streams in each crystallizer to approximately 5°C, thereby facilitating the heat recovery desired in the Hot-CAP.

- Another challenge of the Hot-CAP is the need to modify the conventional stripper to handle slurry and operate at a high pressure. To attain a high stripping pressure, a combination of a high-concentration slurry and a high CO_2 loading in the regenerated lean solution is required, whereas a higher lean CO_2 loading would cause the risk of recrystallization in the cooling process. Thus, a reasonably high stripping pressure (e.g., 6 bar/5.92 atm) is selected as a trade-off between the high pressure requirement and the stripper design concern.

A TEA was performed to compare the energy use and cost performance of a nominal 550-MWe subcritical PC power plant without CO_2 capture (DOE/NETL Case 9) with the benchmark MEA-based post-combustion CO_2 capture (PCC; DOE/NETL Case 10) and the Hot-CAP-based PCC.

- The net power produced in the PC plant equipped with the baseline Hot-CAP is 609 MWe, greater than that with MEA (550 MWe) owing to the reduced steam demand for CO_2 stripping.

- The baseline Hot-CAP has a slightly lower capital cost ($48 million) for CO_2 compression compared with the MEA-based PCC ($50 million), because the stripped product gas has a higher pressure (6 bar/5.92 atm vs. 1.6 bar/1.58 atm). The Hot-CAP also has a lower capital cost in the CO_2 capture section ($362 million) compared with the MEA-based PCC ($443 million), because it requires a smaller stripping column and does not use an upstream

polishing unit for deep sulfur removal prior to CO_2 capture. Operating & maintenance (O&M) costs for the PC plant equipped with Hot-CAP are estimated to be $175 million annually, less than that for the PC plant with MEA ($178 million).

- The 20-year levelized COE (LCOE) for the PC plant with the baseline Hot-CAP, including CO_2 transportation and storage, is 120.3 mills/kWh, a 60% increase over the base PC plant without CO_2 capture. The LCOE increase caused by the Hot-CAP is 29% lower than that of the benchmark MEA-based process.

- A sensitivity analysis indicated that the increase in LCOE for the Hot-CAP is quite sensitive to the capital cost of the absorber, the addition of a new polishing scrubber for deep desulfurization, and the power consumption for crystallization. However, the LCOE is not markedly affected by the price of the K_2CO_3 solvent, the crystallization equipment cost, or the stripping pressure.

7.2 Recommendations

The following activities are recommended in future work:

- Scale-up testing of an integrated system. Operating issues, such as slurry handling and integration of individual unit operations, need to be investigated. The design and testing of an integrated Hot-CAP system at the bench-scale using a slipstream of actual flue gas are recommended.

- CO_2 absorption with precipitation and process improvement. Further investigation into the effect of PCB precipitation in the absorber is recommended. Such a study may lead to improvement in the current process or the development of new process concepts.

- Stripping additives and process improvement. An investigation into potential additives for PCB solutions or PCB-based composite solutions that can obtain VLE behavior desired to further improve the energy use for CO_2 stripping, as well as minimize the crystallization risk in the stripper and cross-heat exchanger is recommended.

- Combining SO_2 removal with CO_2 capture. Testing of the proposed process concept for combined SO_2 removal and CO_2 capture is recommended to generate engineering and design data and to evaluate its techno-economic performance.

Appendix A. Statement of Project Objectives

A. Objectives

For this three-year project, University of Illinois at Urbana-Champaign (UIUC) and Carbon Capture Scientific LLC will investigate a Hot Carbonate Absorption Process with Crystallization-Enabled High Pressure Stripping (Hot-CAP) to overcome the energy use disadvantage of the monoethanolamine (MEA)-based processes. Project objectives include performing a proof-of-concept study aimed at generating process engineering and scale-up data to help advance the Hot-CAP technology to a pilot-scale demonstration level within three years. The project tasks employ lab- and bench-scale test facilities to measure thermodynamics and reaction engineering data that can help evaluate technical feasibility and cost-effectiveness, performance for scale-up, and commercial competitiveness of the Hot-CAP with the MEA-based processes and other emerging post-combustion CO_2 capture technologies. The project aims to improve upon the current state-of-the-art by developing a post-combustion technology that can achieve ≥90% CO_2 removal from coal-fired power plants while meeting the DOE target of ≤ 35% increase in the cost of electricity (COE).

B. Scope of work

To meet the project objectives, a combination of experimental, modeling, process simulation, and techno-economic analysis studies will be used. The project will investigate the kinetics and thermodynamics data relevant to the four unit operations of the Hot-CAP, namely absorption, stripping, crystallization and SO_2 removal, using laboratory and bench-scale test facilities. The absorption tests will be conducted using both a stirred tank reactor for the kinetics measurement and an absorption column for the overall performance evaluation. An autoclave and a continuous high pressure distillation column will be used to measure the stripping kinetic and phase equilibrium performance of the bicarbonate slurry system at elevated temperatures and pressures. A modeling study will further evaluate the overall performance of the stripping unit. The crystallization kinetics of $KHCO_3$ at various process conditions (temperature, cooling rate, concentration, and impurity existence) will be evaluated using a stirred tank reactor. A similar approach will be used to investigate the crystallization kinetics of $CaSO_4$. The experimental and modeling studies will determine optimal operating conditions in each of the unit operations for CO_2 removal and regeneration. The experimental results will be used as a basis for performing process simulations and techno-economic studies to evaluate the overall performance, commercial feasibility, and cost-effectiveness of the Hot-CAP as a post-combustion CO_2 mitigation process for coal-fired power plants.

C. Tasks to be performed

The objectives of the project will be achieved by completing six tasks during a 39-month period. UIUC will lead Tasks 1-5, and Carbon Capture Scientific LLC will lead Task 6.

Task 1. Project planning and management

<u>Subtask 1.1 Project planning</u>

Project planning will include development of a test plan and a QA/QC plan. The test plan will specify all of the tasks to be carried out during the project. The DOE-NETL COR will be involved in all team discussions to ensure that objectives are clearly defined and that the proposed plan will meet project objectives. All team members will review the plan before it is submitted to the COR for the final review. Representatives from each participating team will attend a kick-off meeting at DOE-NETL's headquarter.

Subtask 1.2 Laboratory preparations

This subtask will ensure that laboratory testing begins on schedule. Preparation activities include organizing laboratory space, equipment setup and checkout, ordering parts, reagents, and supplies, procurement, staff hiring and scheduling, and safety training. A project-specific laboratory plan will be developed, outlining procedures for testing and health & safety related issues.

Subtask 1.3 Project management

The Recipient shall finalize the Project Management Plan within 30 days after award and manage project activities in accordance with the plan. The PMP will be used and modified throughout the project to track technical, schedule, and budget status. Results of internal monthly review meetings to discuss the status of all aspects of the PMP will be provided to the COR in each quarterly update report. Any known deviations to schedule or budget will be communicated directly to the COR at the time they are determined. Included in this effort will be all communications, briefings, and meetings with the DOE/NETL as well as the preparation of all topical, periodic, and final reports required by the project's Federal Assistance Check List. The PI will also be responsible for coordinating project activities between UIUC and its sub-contractor (Carbon Capture Scientific LLC). Consultation will be provided by Carbon Capture Scientific LLC during preparation of the final technical report.

Task 2. Kinetics of CO_2 absorption

This task is aimed at measuring the kinetics of the CO_2 absorption into high concentration $K_2CO_3/HKCO_3$ solutions with low carbonate-to-bicarbonate conversion levels at elevated temperatures. Test objectives will also include determining the impacts of major impurities and potassium and sodium mixture on the absorption kinetics.

Subtask 2.1 CO_2 absorption into $K_2CO_3/HKCO_3$ solution

An existing lab/bench-scale continuous stirred tank reactor (CSTR) system, Figure 1, will be modified to measure the CO_2 absorption rate into $K_2CO_3/HKCO_3$ solutions. The reactor is 4-inch in internal diameter and 7-inch in height. The temperature of the reactor is maintained by a water jacket and an internal heating coil. Two separate magnetic-coupled stirrers are used for gas- and liquid-phase mixing. The reactor can be operated at both a batch mode and a semi-continuous mode with respect to the gas phase. The amount of CO_2 absorbed in the reactor is measured either by the change of the CO_2 partial pressure under the batch mode operation, or by

measuring the CO_2 concentrations at the gas (N_2/CO_2 simulated gas) inlet and outlet under the semi-continuous mode operation.

The planned parametric tests are aimed at evaluating the impacts of temperature (60-80°C), K_2CO_3/$HKCO_3$ concentration (40-50 wt%), carbonate-to-bicarbonate conversion in the solution (15-50%), and addition of a catalyst/promoter on the rate of CO_2 absorption.

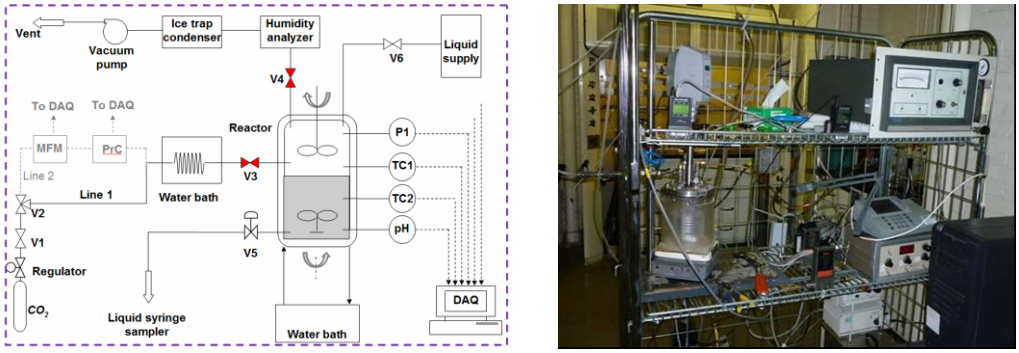

Figure A-1. CSTR experimental system for absorption kinetics measurement.

Subtask 2.2 Absorption in K_2CO_3/$HKCO_3$/K_2SO_4 solution

Impurities present in the solvent impact the rate of absorption of CO_2 into the K_2CO_3/$HKCO_3$ solution because they change the ionic strength and potentially other properties (CO_2 solubility and diffusivity, viscosity, surface tension, etc.) of the solvent. The major impurity of concern is sulfate salts, others include chloride and nitrate salts. The reactor system described in Subtask 2.1 will be used to investigate the impacts of the K_2SO_4 concentrations based on the solubility limitation in the K_2CO_3/$HKCO_3$ solution on the rate of CO_2 absorption without and with the addition of a catalyst/promoter.

2.3 Absorption column test

A bench-scale packed-bed absorption column or a membrane contactor system operated at atmospheric pressure will be designed and fabricated to measure the performance of the CO_2 absorption into K_2CO_3/$HKCO_3$ solutions in a continuous flow system. The column/contactor will be designed based on the reaction rate data obtained in Subtasks 2.1 and 2.2. The column will be up to ten liters in volume. A survey of the commercial packing materials or membrane systems will be conducted to select a suitable material or membrane system for this application. Tests will be performed, under unsteady test conditions with the liquid circulating and/or under steady-state test conditions with the liquid passing once through, to evaluate the overall performance of the absorption column. A simulated flue gas (10-15vol% CO_2, 1000-3000ppm SO_2, balanced with N_2) will be employed. Other operating parameters, including temperature, concentration of the solution, carbonate-to-bicarbonate conversion level, and use of a catalyst/promoter will also be examined. A mathematical model which incorporates mass transfer, hydrodynamics, and reaction kinetics considerations will be developed to evaluate the overall performance of the absorption column. Consultation will be provided by Carbon Capture

Scientific LLC for selection of column configuration, column design, selection of packing materials and other parts, and development of a test matrix.

2.4 Absorption in $K_2CO_3/HKCO_3/Na_2CO_3/NaHCO_3$ solution

This subtask is aimed at evaluating the CO_2 absorption rate into a mixture of potassium and sodium carbonate/bicarbonate solution ($K_2CO_3/HKCO_3/Na_2CO_3/NaHCO_3$) in comparison with that into the potassium solution, without and with the addition of a catalyst/promoter. The results from the competitive crystallization performances of $HKCO_3$ and $NaHCO_3$ (see Subtask 3.3) will aid in determining the concentration levels of K_2CO_3, $HKCO_3$, Na_2CO_3 and $NaHCO_3$ to be employed in the test. The reactor system and testing approach outlined in Subtask 2.1 will be employed in this subtask.

Task 3. Crystallization kinetics and solubility of bicarbonate

This task is aimed at measuring the crystallization kinetics and morphology of $KHCO_3$ crystals formed at various operating conditions. Such data are critical for the design and scale-up of the crystallization tank. Slow crystallization kinetics and unfavorable crystal particle size and particle size distribution will impact the crystallization operation and solid-liquid filtration processes. Slow crystallization kinetics will also require a larger tank, increasing the capital cost of the plant. In this task, conditions that can generate fast crystallization kinetics will be explored. The impact of process conditions including temperature, carbonate/ bicarbonate concentration, rate of cooling, and addition of additives to promote crystal formation and growth will be evaluated.

Subtask 3.1 $KHCO_3$ crystallization

A batch-type crystallizer will be designed and fabricated to measure the crystallization kinetics of $KHCO_3$ in $K_2CO_3/KHCO_3$ mixture solutions. Parametric tests will be performed to evaluate the impacts of temperature (20-40°C), cooling rate (1-25°C/min), initial total bicarbonate/carbonate concentration (40-50 wt%), and carbonate-to-bicarbonate conversion level (30-50%) on the crystallization kinetics, and physical and chemical properties and morphology of crystals formed. Crystal characterization methods will include X-ray diffraction (XRD), scanning electron microscope (SEM) and energy-dispersive X-ray spectroscopy (EDX).

Subtask 3.2 Impact of sulfate on $KHCO_3$ crystallization

In this subtask, the kinetics of $KHCO_3$ in the $K_2CO_3/KHCO_3/K_2SO_4$ mixture will be measured. The operating parameters to be investigated will be those described in Subtask 3.1. The results will aid in identifying acceptable K_2SO_4 concentrations in the process.

Subtask 3.3 $NaHCO_3$ crystallization

The feasibility of using $NaHCO_3$ as an alternative solvent to $KHCO_3$ will be examined in this subtask. $NaHCO_3$ has a lower solubility in water than $KHCO_3$ at the same temperature. A lower solubility results in lowering the bicarbonate concentration in the lean solution exiting the

stripper, thus, enhancing the working capacity of the bicarbonate slurry during stripping. $NaHCO_3$ also has a smaller heat of regeneration than $KHCO_3$ which helps reduce the energy use of the Hot-CAP. The kinetics of $NaHCO_3$ crystallization in the $K_2CO_3/KHCO_3/Na_2CO_3/NaHCO_3$ mixture will be measured following the approaches described in Subtask 3.1.

Subtask 3.4 Solubility of $K_2CO_3/KHCO_3$ system

This subtask is aimed at measuring solubility data of the $K_2CO_3/KHCO_3$ system. Such data are required for the design, scale-up, and operation of a crystallizer. Existing literature data for the $K_2CO_3/KHCO_3$ system do not cover the entire range of operating conditions employed in the Hot-CAP. Solubility data will be measured for a system containing multiple solutes. The conventional measurement technique involves dissolution of solutes, separation of precipitates, and evaporation of remaining solution until the solution is fully evaporated. Chemical properties of the precipitates at each processing step will be determined by wet titration or XRD, and the ion concentration in the liquid phase will be measured by titration, ion chromatography (IC), or atomic absorption spectrometry (AAS). The parametric tests will cover temperatures between 20 and 40°C.

Task 4. Phase equilibrium and desorption kinetics of high pressure CO_2 stripping

This task is aimed at measuring the phase equilibrium and desorption kinetics of CO_2-$K_2CO_3/KHCO_3$ slurry systems at elevated pressures and temperatures. High pressure stripping is one of the key innovations of the Hot-CAP, which can both reduce stripping heat and save CO_2 compression work. However, in order to achieve a higher stripping pressure, an elevated regeneration temperature may have to be employed. Both equilibrium data and desorption kinetics are required for the design, scale-up, and overall performance evaluation of the high pressure stripper. The optimal stripping pressure and temperature will be determined from the experimental measurements as well as from process simulations. Consultation will be provided by Carbon Capture Scientific LLC for: (1) selection of column configuration, column design, and test matrix development; (2) column test planning; and (3) analysis of experimental results to evaluate the overall performance of high pressure stripping and identification of the optimal stripping conditions.

Subtask 4.1 Vapor-liquid-equilibrium (VLE) of $K_2CO_3/KHCO_3$ slurry

The phase equilibrium data of the CO_2-H_2O-K_2CO_3-$KHCO_3$ slurry systems will be measured using a high-pressure autoclave. Conventional measurement methods will be followed to obtain VLE data for concentrations of the bicarbonate in the slurry between 50 and 90 wt%, temperatures between 120 and 200°C, and pressures between 1 to 40 atm.

Subtask 4.2 VLE of $K_2CO_3/KHCO_3/K_2SO_4$ slurry

Phase equilibrium data of the CO_2-H_2O-K_2CO_3-$KHCO_3$-K_2SO_4 system will be measured. A range of K_2SO_4 concentrations, based on the solubility limitation, will be examined. Other operating parameters examined will include those described in Subtask 4.1. The experimental

data obtained in this subtask, along with operating cost data, will help determine acceptable K_2SO_4 concentration levels used in the Hot-CAP.

Subtask 4.3 Stripping column test of $K_2CO_3/KHCO_3$ system

A high-pressure stripping column will be designed and fabricated to investigate carbonate regeneration kinetics of the CO_2-$K_2CO_3/KHCO_3$ system. The column will be equipped with an electrically-heated reboiler to simulate the steam reboiler used in practice. Process modeling and calculations will be performed to provide optimal process conditions as input for the designs of the stripper and major accessories (i.e., preheater, reboiler, reflux condenser, etc.) of the system, and the selection of common system auxiliaries (i.e., pump, valves, etc.).

Shakedown tests will be performed and necessary modifications, if any, will be made to ensure the experimental system functions reliably and safely. Tests will be conducted at the optimal temperature and pressure conditions identified in Subtask 4.1 using bicarbonate slurry concentrations ranging from 50 to 90 wt%. Parametric tests will also be performed to investigate the CO_2 stripping performance at various conditions (e.g., slurry flow rate, CO_2 lean loading, reboiler temperature, etc.). The data generated in this subtask will aid in evaluating the regeneration kinetics of the K_2CO_3-$KHCO_3$ system.

Subtask 4.4 Stripping column test of $K_2CO_3/KHCO_3/ K_2SO_4$ system

The regeneration kinetics of the CO_2-$K_2CO_3/KHCO_3/K_2SO_4$ systems will be measured in this subtask. The concentration of the bicarbonate slurry and the operating temperature/pressure of the stripper will be those identified in the Subtasks 4.2 and 4.1, respectively.

Task 5. Kinetics of sulfate removal

This task is aimed at measuring the kinetics of competitive crystallization of $CaSO_4$ (by-product of the SO_2 removal reaction during CO_2 absorption) and $CaCO_3$ when hydrated lime reagent and high-pressure CO_2 are introduced into the $K_2CO_3/KHCO_3/K_2SO_4$ solution. The kinetic data are required to properly design a sulfate reclaimer to recover the carbonate solvent for reuse. The experiments will be performed using 40 to 50 wt% total carbonate/bicarbonate concentration, temperatures between 20 and 80°C, and CO_2 partial pressures between 10 and 60 atm. Consultation will be provided by Carbon Capture Scientific LLC to assist in analysis of experimental results, identification of the optimal process conditions, and assessment of the combined SO_2/CO_2 removal process options.

Subtask 5.1 $CaSO_4$ precipitation in $K_2CO_3/KHCO_3/K_2SO_4$ solution

An existing semi-continuous, high-pressure autoclave system (continuous gas flow) will be modified to measure the crystallization kinetics of $CaSO_4$ in the $K_2CO_3/KHCO_3/K_2SO_4$ solution, Figure 2. The two-liter autoclave is equipped with a magnetic-coupled stirrer and can be operated at 345 bar (340.5 atm) and 500°C. Tests will be conducted using K_2SO_4 concentrations based on the solubility limitation, and $K_2CO_3/KHCO_3$ concentrations between 40 and 50 wt% to simulate the solutions used in the Hot-CAP. Hydrated lime, $Ca(OH)_2$, will be used as the reagent

to precipitate SO_4^{2-} while bubbling pure CO_2 (10-60atm) into the solution. The liquid and crystals in the autoclave will be sampled during the test period for ion analysis (such as IC, AAS, and FTIR) and crystal characterization (such as XRD, SEM, and EDX).

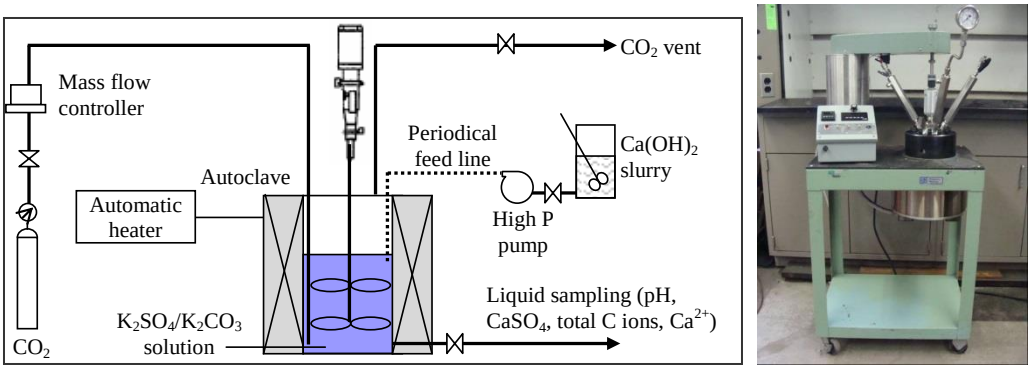

Figure A-2. Experimental system for kinetic measurement of sulfate removal

Subtask 5.2 $CaSO_4$ precipitation in $K_2CO_3/KHCO_3/Na_2CO_3/NaHCO_3/K_2SO_4$ solution

As previously mentioned, $NaHCO_3$ slurry may be considered as an alternative solvent in the Hot-CAP. In this case, a mixture of the potassium and sodium carbonate/bicarbonate will be used. The tests in this subtask are aimed at investigating the impact of the coexistence of $Na_2CO_3/NaHCO_3$ in the $K_2CO_3/KHCO_3/K_2SO_4$ solution on the crystallization kinetics of $CaSO_4$. The approaches and process conditions described in Subtask 5.1 will be followed in this subtask.

Subtask 5.3 Solubility of $K_2CO_3/KHCO_3/K_2SO_4$ system

The solubility data of the $K_2CO_3/KHCO_3/K_2SO_4$ system is required for the design, scale-up, and performance evaluation of a crystallizer when a large amount of K_2SO_4 is present. The solubility data for this multi-component system are not available in the literature. The solubility measurement approach and testing conditions will follow those described in Subtask 3.4.

Task 6. Techno-economic evaluation

This task is aimed at conducting process simulation and techno-economic studies to evaluate the cost-effectiveness and suitability of the Hot-CAP as a post-combustion CO_2 capture technology for coal-fired power plants. Mitigation studies of technical risks associated with the process will also be performed to develop the related risk mitigation strategies. Thermo-chemical modeling simulations will be employed by Carbon Capture Scientific LLC to size equipment, optimize process configurations, and examine the effects of key parameters (temperature, pressure, composition etc.) on the CO_2 absorption efficiency and process energy use. A conceptual 550 MWe (net) high-sulfur bituminous (such as Illinois No.6) coal-fired power plant will be considered for the cost evaluation.

Subtask 6.1 Literature review, flowcharting and data preparation

A thorough review of literature regarding all major unit operations involved in the Hot-CAP will be conducted to collect relevant technical and cost information. Technical information

includes process design, operating conditions, and requisite material properties. Cost information includes cost data of related materials and process units, and guidelines for chemical equipment scale-up and cost estimation. A detailed process flow diagram that includes all major materials and equipment will be developed for the Hot-CAP.

As part of the risk mitigation strategy study, five major technical risks were identified for the Hot-CAP. Risk A is related to CO_2 absorption kinetics into the potassium carbonate solution at elevated temperatures, while Risk B is associated with potential pressure limitations in the CO_2 stripping column. The mitigation measures for Risks A and B will be addressed through work activities proposed in Tasks 2 and 4. Risks C and D are related to the designs of the heat exchanger and crystallizer, respectively, while Risk E is related to the design of the high-pressure stripping column and its related accessories.

The risk mitigation analysis study requires literature search, extensive discussion with equipment vendors, and evaluation/analysis of potential equipment options. Initially, the risks associated with fouling of the heat exchanger and the required heat recovery from the crystallizer will be investigated and improvements/enhancements to the Hot-CAP design will be pursued. In addition, work will be performed to determine the optimal crystallization process configuration for the Hot-CAP, and to better define the modifications required to commercial strippers to handle high-pressure slurries.

Subtask 6.2 Process modeling simulations

Process simulations will be performed for material and energy balance calculations, solubility properties, and process evaluation and optimization. A process simulation software package (such as Aspen Plus®, Pro-Treat™, CHEMCAD or similar simulation software packages) will be selected and used to perform steady state simulations of the thermo-chemical processes. The testing results obtained in this project will be used as inputs for process simulations and equipment sizing. These will include the performance of the absorption, stripping and crystallization processes at various temperatures, pressures, and composition conditions. Literature data will be referred to for determining any other technical data of major equipment and other process components required in the process simulations.

Subtask 6.3 Process and economic evaluations

After identifying the optimum process conditions, the material and energy in- and out-flows, and sizing the major equipment in Subtask 6.3, cost estimation will be conducted. The cost of major chemicals and equipment that employs standard industrial designs and materials will be referred to available commercial practices and literature information. For non-conventional equipment, such as the slurry vessels, the guidelines/handbooks of chemical equipment scale-up and cost estimation will be referenced. Both capital cost and operating & maintenance cost will be included in the economic assessment, and the standard methodology for the engineering economic analysis will be followed. A conceptual 550 MWe (net) high-sulfur bituminous (such as Illinois #6) coal-fired power plant would be considered for the economic evaluations

Subtask 6.4 Process sensitivity analysis

The sensitivity of the economic performance to a few important process and cost variables used in the process design and economic evaluation will be examined. These include the technical factors, such as temperature and pressure variations, effects of additives and impurities, and the economic factors such as carbon credit and oil price.

D. Deliverables

The Recipient shall provide reports in accordance with the enclosed Federal Assistance Reporting Checklist and the instructions accompanying the Checklist. In addition to the reports identified on the Reporting Checklist, the Recipient shall provide the following:

- Final process flow diagrams (PFDs) will be provided when complete
- Detailed process simulation model for UIUC carbon capture system for power plant flue gas

Additional project deliverables may be provided subject to mutual agreement by UIUC and the DOE.

E. Briefings/technical presentations

UIUC will prepare detailed briefings for presentation to the Project Officer at the Project Officer's facility located in Pittsburgh, PA or Morgantown, WV. Briefings will be given by UIUC in order to explain plans, progress and results of the technical effort. UIUC will make presentations at a project kick-off meeting, annual briefings, and a final project briefing.

UIUC will provide and present a technical paper regarding the project at the DOE/NETL Annual Contractor's Review Meeting to be held in Pittsburgh, PA or Morgantown, WV and one other technical conference each year during the project duration. If requested, the Recipient shall also prepare a detailed briefing for external project/merit reviews.